Design, Synthesis and Evaluation of Solution Processable Small Organic Molecules for Applications in Organic Electronics

Thesis Submitted to AcSIR for the Award of

the Degree of

DOCTOR OF PHILOSOPHY

In Chemical Sciences

By

Durgaprasad B. Shinde

(AcSIR Reg. No.: 10CC13J26007)

Under the Guidance of

Dr. Prakash P. Wadgaonkar

Polymer Science and Engineering Division

CSIR-NATIONAL CHEMICAL LABORATORY

PUNE - 411008, INDIA

2018

Dedicated

To

My Beloved Parents

सीएसआईआर - राष्ट्रीय रासायनिक प्रयोगशाला
(वैज्ञानिक तथा औद्योगिक अनुसंधान परिषद)
डॉ. होमी भाभा मार्ग, पुणे - 411 008, भारत

CSIR - NATIONAL CHEMICAL LABORATORY
(Council of Scientific & Industrial Research)
Dr. Homi Bhabha Road, Pune - 411 008, India

Certificate

This is to certify that the work incorporated in this Ph.D. thesis entitled **"Design, Synthesis and Evaluation of Solution Processable Small Organic Molecules for Applications in Organic Electronics"** submitted by **Mr. Durgaprasad B. Shinde** to Academy of Scientific and Innovative Research (AcSIR) in fulfillment of the requirements for the award of the Degree of **Doctor of Philosophy in Chemical Sciences,** embodies original research work under my supervision. I further certify that this work has not been submitted to any other University or Institution in part or full for the award of any degree or diploma. Research material obtained from other sources has been duly acknowledged in the thesis. Any text, illustration, table etc., used in the thesis from other sources, have been duly cited and acknowledged.

Durgaprasad B. Shinde
(Student)

Prakash P. Wadgaonkar
(Supervisor)

Communication Channels
NCL Level DID : 2590
NCL Board No. : +91-20-25902000
EPABX : +91-20-25893300
: +91-20-25893400
FAX
Director's Office : +91-20-25902601
COA's Office : +91-20-25902660
SPO's Office : +91-20-25902664
WEBSITE
www.ncl-india.org

Declaration

I hereby declare that the original research work embodied in the thesis entitled "**Design, Synthesis and Evaluation of Solution Processable Small Organic Molecules for Applications in Organic Electronics**" submitted to the Academy of Scientific and Innovative Research (AcSIR) for award of degree of Doctor of Philosophy is the outcome of experimental investigations carried out by me under the supervision of Dr. Prakash P. Wadgaonkar, Chief Scientist, CSIR-National Chemical Laboratory, Pune. I further affirm that to the best of my knowledge, the work incorporated is original and has not been submitted to any other Academy, Institute and University for the award of any degree.

December, 2018

CSIR- National Chemical Laboratory,

Pune- 411008

Durgaaprasad B. Shinde

(Research student)

Acknowledgement

Completion of this doctoral dissertation is not the symbol of individual efforts but this journey was possible with the support of several people. I would like to express my sincere gratitude to all of them.

Firstly and most importantly, I feel extremely humbled and delighted to express my gratitude and respect to my supervisor, Dr. Prakash P. Wadgaonkar for his profound guidance, freedom of work ,consistent encouragement to explore new ideas, understanding and limitless patience. His knowledge, constructive advices and invaluable supervision motivat ed me during the entire study period. Learning from him was an experience of paramount importance to develop my thought process and scientific skills. His support during all the ups and downs throughout the journey was remarkable and I will be obliged forever for his generous support.

I would also like to express my gratitude to Prof. Ashwini Kumar Nangia (Director, CSIR-NCL), Dr. Vijayamohanan Pillai and, Dr. Sourav Pal (former Directors of CSIR-NCL) for giving me the opportunity to work at CSIR-NCL. It is my pleasure to thank Dr. U. K. Kharul (Chair, PSE Division), Dr. Ashish Lele (former Chair, PSE Division) and Dr. A. J. Varma (former Chair, PSE Division) for allowing me to work in Polymer Science and Engineering Division and for providing instrumental facilities along with the infrastructure to perform the research work.

I am thankful to my Doctoral Advisory Committee (DAC) members, Dr. P. R. Rajamohanan, Dr S. K. Asha and Dr. K. Krishnamoorthy, for the regular assessment of research work, suggestions, valuable advices and fruitful discussions during the DAC meetings which, in turn, helped me to build and improve upon my research skills. I am also thankful to Dr. J. Nithyanandhan for scientific discussions and valuable suggestions.

I am thankful to Dr. Prashanat Sonar (Queensland University of Technology, Australia) for his help. I am highly delighted to express my gratitude to Jagdish Salunke (Tampere University of Technology, Finland) and Nitin Valsange for their consistent and immense support. Working with them was a great learning experience.

I owe gratitude to Dr. C. V. Avadhani, Dr. A.V. Ambade, Mr. Shamal Menon, Mr. Anandrao Patil, Dr. Nilakshi V. Sadavarte, Dr. Satish Ogale, Dr. Samir Chikkali, Dr. S. P. Chavan, Dr. Sayam Sen Gupta, Dr. B. Punji, Dr. D. Srinivas, Dr. B. B. Idage, Dr (Mrs.) S. B. Idage, Dr. D.

S. Reddy, Dr. A. T Biju, Dr. Rahul Banerjee, Dr. M. Jayakannan (IISER, Pune) and Dr. Vaishali Shinde (SPPU, Pune) for their kind support and help throughout the PhD. tenure.

I am sincerely thankful to Dr. Arri Priimagi (TUT, Finland), Nadia Camioni (Istituto per la Sintesi Organica e la Fotoreattività, Italy), Paola Vivo (TUT, Finland), Dr. V.A.L. Roy (University of Honk Kong, HK.), F.L. Wong (University of Hong Kong) Krishna Feron (CSIRO Energy Centre, Australia), Sergi Manzhos (National University of Singapore), C.S Lee (University of Hong Kong) and Samual Chang (Nihan University, Japan).

I am thankful to Mrs. Santhakumari for HRMS facility, Dr. Asha's group for IR facility. I am also thankful to Mrs. Dhoble and Mrs. Poorvi for different characterizations.

I appreciate Student Academic Office (SAO) Chairman Dr. B.L.V. Prasad, former chairman Dr. M. S. Shashidhar and Dr. C. G.Suresh. I am also thankful to all the staff members including Mrs. Kolhe and Mr. S. Iyer for their kind help and co-operation throughout the PhD tenure.

I would like to express my sincere thanks to my seniors Dr. Pandurang Honkhambe, Dr. Ankush Mane, Dr. Sushilkumar Jadhav, Dr. Rahul Shingte, Dr. Arvind More, Dr. Arun Kulkarni, Dr. Anjana Sarkar, Dr. Snehalata Bapat, Dr. Dnyaneshwar Palaskar, Dr. Prakash Sane, Dr. Sharad Pasale, Dr. Savita Kumari, Dr. Bhausaheb Tawade, Dr. Shraddha Chhatre, Dr. Sayali Shaligram, Dr. Indravadan Parmar, Dr. Nagendra Kalva, Dr. Naganath Patil, Dr. Sachin Patil, Dr. Kavita Garg, Dr. Dilip Raut, Dr. Shyambo Mukherjee, Dr. Murugesan, Dr. Aarti Shedge, Dr. Prakash Babu, Dr. Ravindra Patil and Dr. Namdev Ghule for their valuable suggestions and help during my PhD tenure.

I am fortunate to have an opportunity to work with fantastic lab mates in PPW group. I take this opportunity to express my deep sense of gratitude to lab mates Dr. Vikas Garg, Dr. Samadhan Nagane, Dr. Sachin Kuhire, Dr. Bharat Shrimant, Nitin Basutkar, Amol Ichake, Ketan Makwana, Uday Jadhav, Deepak Maher, Geethika, Deepshikha Chatterjee, Sachin Basutkar, Ashwini Deshpande, Sagar Joshi, Rupali Jadhav, Abhijeet Patil, Dr. Ikhlas Gadwal, Yogesh Nevare, and Shakib who made my life in the lab easier and enjoyable.

I take this opportunity to express my gratitude to my friends Satej Deshmukh, Dr. Balasaheb Jawale,Pralhad Burate, Rahul Jagtap, Pravin Shinde, Nilesh Mote, Shahaji Gaikwad, Ulhas Patel, Swechchha Pandey, Dilip Pandey, Dr. Shrikant Khake, Dr.Vijay Koshti, Dr. Neeta Karjule, Dr. Sachin Bhojgude, Arjun Haldar, Dr. Sandeep Sharma, Dr. Nagesh Kolhe, Dr. Swapnil Sonawane, Navnath, Shrikant Nikam, Shrikant Karegaonkar, Dr. Viswanadh Nalla,

Gunvant Deshmukh, Anup, Pravin Shinde, Arun Nikam, Gajanan Kale (C-MET, Pune), Avinash , Ashok Jadhav, Sainath Shinde and Vikas Wankhede. Thanks to all !

The words are hardly sufficient to express gratitude towards my friends Nagesh Gattuwar (C-MET, Pune) and Nilesh Deshpande (IISER, Pune) for their consistent help and strong support in the good and bad times during the tenure of PhD. I am highly obliged for their generous help and motivation. I would also like to thank Mr. Ravi Chillappan and Mr. Shankar Mane (Electrical section, CSIR-NCL) for their invaluable help during harsh time.

I am grateful to Dr. Sachin Nagapurkar (Hardikar hospital) for his efforts to make me literally stand on my feet. I'd also like to express my sincere gratitude to Dr. Shubhangi Wadgaonkar Madam for her moral support.

I would like to thank all my teachers in the entire academic journey from Mamata Primary School (Gangakhed) to DSM college, Parbhani for nurturing values and knowledge.

I would like to express my sincere thankfulness to University Grants Commission (UGC), New Delhi for fellowship.

Eventually, I dedicate this thesis to the people who unambiguously have most important place in my life, my father Late Shri. Babanrao Rustumrao Shinde and my mother Smt. Vidyadevi B. Shinde. Their consistent support and encouragement for my studies, their sacrifices and hard work have been great source of inspiration for me and it will remain so forever inspiring me to face challenges and achieve new goals in life. I would like to thank my dear brother Krushna whose endurance and sacrifices are highly adorable. Without his strong support my higher studies would have not been possible. My sister, Sonali, from whom I learnt the passion to pursue goals with hard work, sincerity and excellence….Thanks dear! I would also like to thank my sister-in-law Sharayu for her patience and efforts for the family. I am thankful to my nephews Advait and Nachiket whose presence has made my life beautiful and happy.

Finally, I am grateful to the God for giving me a beautiful life and a great opportunity to work in NCL. I pray to God for the energy and endurance for life ahead.

Durgaprasad B. Shinde

Table of Contents

Chapter 3: Pyrene-Cored Small Organic Molecule with Flexible Alkyl Spacer for Solution Processable Blue Emitter with Bright Photoluminescence.

Chapter 4: Phenothiazine and Carbazole Substituted Pyrene-Based Electroluminescent Organic Semiconductors for OLED Devices

Chapter 5: Crystallization-Enhanced Bulk Hole Mobility in Phenothiazine-Based Organic Semiconductors

Introduction:

Organic electronics deals with design and synthesis of organic materials and their applications in the field of electronics e.g. organic light emitting diodes (OLEDs),[1] organic field effect transistors (OFETs) and organic photovoltaics (OPVs). Compared to their inorganic counterparts, organic materials enjoy advantages such as light weight, mechanical flexibility, possibility of chemical modifications and easy and cost effective processing e.g. ink jet, spin coating, etc. However, lower performance and stability issues are required to be addressed in order to further improve the performance of organic electronic devices.[2,3] Additionally, charge transport properties of organic molecules have major impact on overall performance of the devices such as switching of OFETs, turn-on voltage in OLEDs and charge separation and extraction in case of OPVs. Thus, organic materials with optimum charge mobility are important for optoelectronic applications.[4-7]

Statement of the problem:

Although tremendous advancements have been made in the field of OLEDs, current OLEDs face some problems such as obtainment of pure strong emission with low power consumption which is determined by the low driving voltage and efficiency of the device. Additionally, the electroluminescent properties of emitting materials remain challenging. Pyrene which is used to derive different organic molecules useful as emissive layer in OLEDs, is a primary chromophore. Due to its high quantum yield, pyrene is a good candidate to design functional materials for fluorescent probe and labeling experiments.[8] However, the intermolecular π-π stacking between the pyrene core in the solid state causes excimer formation and fluorescence quenching of the emission that hampers the overall performance of OLEDs.[9,10]

Phenothiazine is an electron rich molecule with butterfly shape which is useful to suppress the molecular aggregation.[11] However, most of the phenothiazine-based molecules exhibit low charge carrier mobility resulting into inferior results in different applications. Therefore, it is highly desirable to synthesize phenothiazine-based molecules with high mobility, film forming nature and good light harvesting properties. The introduction of substituents at C-3 and C-7 position in phenothiaine molecule helps to extend pi-conjugation, intramolecular charge transfer (due to D-A type structure) which eventually contributes to improve the charge carrier mobility.

Aims and objectives: The overall aim of the present work was to design and synthesize solution processable small organic molecules and evaluate their applications in the field of organic electronics e.g. OLEDs. Also charge carrier mobility of organic compounds was studied for their potential application in OFETs. Following specific objectives were chosen for the work.

i) To synthesize pyrene-based small molecule with carbazole as the substituent attached to the core with alkyl chain linker and study its structure- property relationship and performance in OLED.

ii) To synthesize carbazole and phenothiazine substituted pyrene-based small molecules and study their performance in OLEDs.

iii) To synthesize phenothiazine-based small organic molecules with donor- acceptor (D-A) structure and study their charge carrier mobility characteristics.

Methodology used:

1) A pyrene cored 1,3,6,8- tetrasubstituted molecule, namely, 1,3,6,8-tetrakis(4-((5-(9H-carbazol-9-yl)pentyl)oxy)phenyl)pyrene **PY-II** with carbazole as the substituent attached to core with alkyl chain linker was synthesized. The site isolation effect over the fluorescence properties was studied.
2) Synthesized 1,3,6,8-tetrasubstituted pyrene-based small molecules with carbazole and phenothiazine, namely, 1,3,6,8-tetrakis(9-(4-methoxyphenyl)-9H-carbazol-3yl)pyrene (**PY-CA**) and 1,3,6,8-tetrakis(10-(4-methoxyphenyl)-10Hphenothiazin-3-yl)pyrene (**PY-PH**), respectively and their OLED device performance was studied.
3) Three phenothiazine-based small molecules with D-A type structure namely, 2-((10-(4-methoxyphenyl)-10H-phenothiazin-3-yl) methylene) malononitrile (**O-1**), 2-((7, 10-bis (4-methoxyphenyl)-10H-phenothiazin-3-) methylene) malononitrile (**O-2**) and 2-((7-(6-butoxynaphthalen-2-yl)-10-(4-methoxyphenyl)-10H-phenothiazin-3-yl) methylene) malononitrile (**O-3**) were synthesized and their charge carrier mobility was studied with the help of impedance spectroscopy. Also the structure – properly relationship study was performed.

Sample results:

Scheme 1: *Pyrene cored small organic molecule with flexible alkyl spacer for solution processable blue emitter with bright photoluminescence*

A new pyrene cored small organic molecule *viz* 1,3,6,8-tetrakis(4-((5-(9H-carbazol-9-yl)pentyl)oxy)phenyl)pyrene (**PY-II**) with flexible alkyl spacer was synthesized. Carbazole moiety was linked by alkyl chain in order to improve solution processability. **PY-II** was soluble in different organic solvents e.g. dichloromethane, chloroform, tetrahydrofuran, toluene, etc. **PY-II** exhibited wide band gap nature with absorption in the range 300-500 nm. **PY-II** showed PLQY of 0.9 in solution and a bright blue emission at 450 nm. A solution processed non-doped OLED device was fabricated using **PY-II** in emissive layer. OLED showed blue emission with CIE coordinates at (0.16, 0.16), turn on voltage at 4.5 V, current efficiency of 0.41 cdA^{-1}, power efficiency of 0.17 lmW^{-1}, EL maxima at 470 nm and maximum brightness of 202 cdm^{-2}

Scheme 2: *Phenothiazine and carbazole substituted pyrene -based electroluminescent organic semiconductors for OLEDs*

Two new solution processable 1,3,6,8 tetrasubstituted pyrene-based compounds with carbazole and phenothiazine as the substituents were synthesized by Suzuki coupling reaction. These compounds, namely, 1,3,6,8-tetrakis(9-(4-methoxyphenyl)-9H-carbazol-3yl)pyrene(**PY-CA)** and 1,3,6,8-tetrakis(10-(4-methoxyphenyl)-10Hphenothiazin-3-yl)pyrene (**PY-PH)** were characterized by IR, ^{1}H NMR, and MALDI-TOF and their optical and electrochemical properties were studied. The electroluminescent compounds were used as emissive layers in the OLED device fabrication. **PY-CA** -based device showed turn-on voltage of 3.3V, current efficiency of 1.6 cdA^{-1}, power efficiency of 1.5 lmW^{-1}, EL maxima at 493nm and maximum brightness of 2500 cdm^{-2} whereas **PY-PH** based device exhibited turn-on voltage of 3.8V, current efficiency of 1.1 cdA^{-1} power efficiency of 0.45 lmW^{-1}, EL maxima at 540nm, and maximum brightness of 2116 cdm^{-2}

Scheme 3: *Crystallization enhanced bulk hole mobility in phenothiazine based organic semiconductors*

Three new phenothiazine-based D-A type molecules namely, 2-((10-(4-methoxyphenyl)-10H-phenothiazin-3-yl) methylene) malononitrile **(O-1),** 2-((7,10-bis(4-methoxyphenyl)-10H-

phenothiazin-3-) methylene) malononitrile**(O-2)** and 2-((7-(6-butoxynaphthalen-2-yl)-10-(4-methoxyphenyl)-10H-phenothiazin-3-yl) methylene) malononitrile **(O-3)** were synthesized by a sequence of Ullmann coupling, Vilsmier-Haack formylation, Suzuki coupling and Knoevenagel condensation. Their spectral, electrochemical and thermal characterizations were performed. The introduction of electron donor substituents at C-7 position in case of **O-2** and **O-3** had little impact over their optical and electrochemical properties, but it affected their film forming properties. Highly ordered films were formed in case of unsubstituted **O-1** molecule. Charge carrier mobility of these molecules was studied using impedance spectroscopy method. **O-1** showed good hole mobility in the order of 10^{-3} $cm^2V^{-1}S^{-1}$ while **O-2** and **O-3** showed mobility in the order of 10^{-6} $cm^2V^{-1}S^{-1}$

References:

1. A. C. Grimsdale, K. L. Chan, R. E. Martin, P. G. Jokisz and A. B. Holmes, *Chem. Rev*., 2009, **109**, 897.
2. Z.Ma, P.Sonar , Z.K. Chen,,*Curr. Org. Chem*., 2011, **14**, 2034.
3. N. J. Jeon, J. Lee, J. H. Noh, M. K. Nazeeruddin, M. Gratzel, S. Seok, *J. Am. Chem. Soc.*, 2013, **135**, 19087.
4. D. Curiel, M. Mas Montoya, C.H. Chang, P.Y. Chen, C.W. Tai and A. Tarraga, J. Mater. Chem. C, 2013, **1**, 3421.
5. Bazan, M. R. Bryce and M. R. Bryce, *J. Mater. Chem. C*, 2016, **4**, 3675.
6. Ma, Z., Geng, H., Wang, D. & Shuai, Z. *J. Mater. Chem. C*, 2016, **4**, 4546.
7. K. Konidena, K. R. J. Thomas, S. Sahoo, D. K. Dubey, J. H. Joub, *J. Mater. Chem. C*, 2017, **5**, 709.
8. T.M.F. Durate and K. Mullen, *Chem. Rev.* 2011, **111**, 7260.
9. M. R. Pokhrel and S. H. Bossmann, *J. Phys. Chem. B*, 2000, **104**, 2215.
10. K. Sun, Y. Sun, W. Tian, D. Liu, Y. Feng, Y. Sun and W. Jiang, *J. Mater. Chem. C*, 2018, **6**, 43.
11. W. Wu, J. Yang, J. Hua, J. Tang, L. Zhang, Y. Long and H. Tian, *J. Mater. Chem.*, 2010, **20**, 1772.

List of abbreviations

A	Ampere
AFM	Atomic force microscopy
CE	Current efficiency
Cd	Candela
$CHCl_3$	Chloroform
CV	Cyclic voltammetry
DCM	Dichloromethane
DFT	Density functional theory
DMF	N,N-Dimethylformamide
DMSO	Dimethylsulfoxide
DSC	Differential scanning calorimetry
EL	Electroluminescence
Eg	Band gap
eV	Electron-volt
FWHM	Full width at half maximum
HOMO	Highest occupied molecular orbital
IR	Infrared
ITO	Indium tin oxide
Kcal	Kilo calorie
K_2CO_3	Potassium carbonate
KOAc	Potassium acetate
lm	Lumens
LUMO	Lowest unoccupied molecular orbital
MHz	Mega hertz

NMR	Nuclear magnetic resonance
OLED	Organic light emitting diode
OFET	Organic field effect transistor
OPV	Organic photovoltaics
PCM	Polarizable continuum model
PE	Power efficiency
PEDOT:PSS	Poly(3,4-ethylenedioxythiophene): polystyrene sulfonate
PESA	Photoelectron spectroscopy in air
PL	Photoluminesccence
TEGDME	Triethylene glycol dimethyl ether
THF	Tetrahydrofuran
TGA	Thermogravimetric analysis
UV-vis	Ultraviolet-visible
V_{on}	Turn-on voltage
W	Watt
XRD	X-Ray diffraction

List of schemes

List of tables

List of figures

Chapter-1

Introduction and Literature Survey

1.1) Organic electronics

Depending upon the ability to conduct electricity, the materials are categorized as conductors, insulators and semiconductors.[1] Conductors, such as metals, have a continuous electronic density of states meaning that an electron can easily be promoted to an effectively infinitesimally higher energy state with a different momentum allowing conduction even at very small applied fields. An insulator is a material which does not allow the flow of electric current through it under influence of electric field. Semiconductors are extremely useful materials that are named for their capacity to function as either conductors or insulators depending on the conditions they are placed under. This property arises because they have a band gap, an energy gap where there are no allowed electronic states. For semiconductors to conduct, either sufficient energy must be put in (in the form of heat or light) to excite carriers across the energy gap, or the carrier density must be changed by moving the Fermi level away from the centre of the band gap by doping or injecting carriers from the electrodes. Depending on the type of material used the semiconductors are categorized as inorganic and organic semiconductors. Organic semiconductors[2] (OSCs) are a class of carbon-based (organic) materials that exhibit optical and electronic properties similar to their inorganic counterparts.

Organic chemistry refers to the chemistry of carbon-based compounds. Carbon atom exhibits tetravalent nature which means it requires four electrons to fulfill its octet. With electronic configuration $1s^2\ 2s^2\ 2p^2$ carbon is unable to complete its octet, hence it undergoes the process of redistribution of orbitals to form new ones with equivalent energy levels. The process is known as hybridization and new orbitals are known as 'hybrid orbitals'.[3] Two electrons in 1s orbital are closest to the nucleus and have lowest energy; hence do not participate in the hybridization process. Four electrons in the valence shell ($2s^2\ 2p^2$) undergo hybridization to form four sp^3 orbitals of equivalent energy and tetrahedral geometry (bond angel $109^o.28'$), each containing one electron and form four sigma bonds with other atoms through atomic overlap. In case of sp^2 carbon, 2s orbital is mixed with two out of three 2p orbitals in carbon to form three sp^2 orbitals of equivalent energy with one electron in each sp^2 orbital and leaving one electron in an unhybridized 2p orbital. Three sp^2 orbitals are coplanar with bond angle of 120^o and overlap with another sp^2 orbital to form C-C sigma bond while the unhybridized 2p orbital which is perpendicular to plane of sp^2 hybrid orbitals overlap with unhybridized 2p orbital of another carbon atom to form a π bond i.e. a C=C double bond. Thus, when two p orbitals overlap in

phase they form a π bond and the bonding orbital contains two electrons in it. This orbital is known as highest occupied molecular orbital (HOMO). When two p orbitals overlap out of phase then it forms a higher energy π* antibonding orbital known as lowest unoccupied molecular orbital (LUMO). These HOMO- LUMO energy levels in organic semiconductors are analogous to valence band and conduction band in inorganic semiconductors, respectively. The tetrahedral arrangement for sp^3 carbon and planar arrangement for sp^2 carbon is shown in **Figure.1.1**

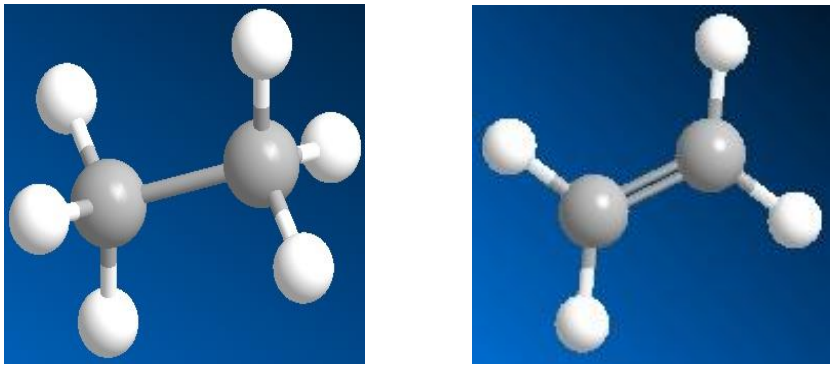

Figure 1.1: Arrangement of sp^3 and sp^2 hybridized carbon atom

When the two C=C bonds are separated by a C-C bond, the conjugated system is formed. By adopting such a configuration of alternating single and double bonds, carbon atoms can form conjugated chains (such as polyacetylene) or rings (such as benzene, or larger systems like perylene, pyrene, etc). In fact the single and double bonds in conjugated systems are not fixed but are delocalized over the whole conjugated system leading to formation of HOMO and LUMO energy levels as shown in **Figure 1.2.** The energy gap between the HOMO and LUMO, known as band gap, is about 1.5- 3.5 eV for most of the organic materials.[4] In conjugated systems, as the conjugation length increases, it leads to reduction in the energy gap between HOMO and LUMO i.e smaller band gap is obtained. Also, in case of polycyclic aromatic compounds, as the number of benzene rings are increased, it leads to extended conjugation and eventually the HOMO-LUMO band gap values are decreased.[5] The reducing value of band gap for benzene, naphthalene, anthracene, tetracene and pentacene is shown in **Figure 1.3.** The extended conjugation also helps to stabilize the charged states by spreading the charges over the system through conjugation. These overall phenomena result into organic material functioning

like semiconductor as observed in perylene[6] and polyacetylene.[7] With the potential ability to replace the inorganic materials in the electronics technology, the organic semiconductors have opened a channel of new technologies such as organic light emitting diodes (OLEDs),[8] organic photovoltaics,[9] organic field effect transistors (OFETs),[10] organic lasers[11] and memory cells.[12] With their flexible nature, the organic electronics has introduced entirely new concept of consumer electronics.

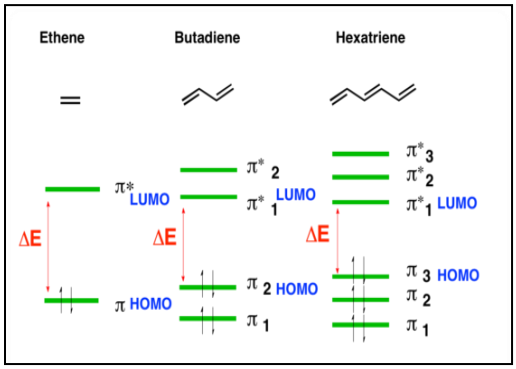

Figure 1.2: The effect of conjugation length on HOMO-LUMO energy gap (adapted from ref [5])

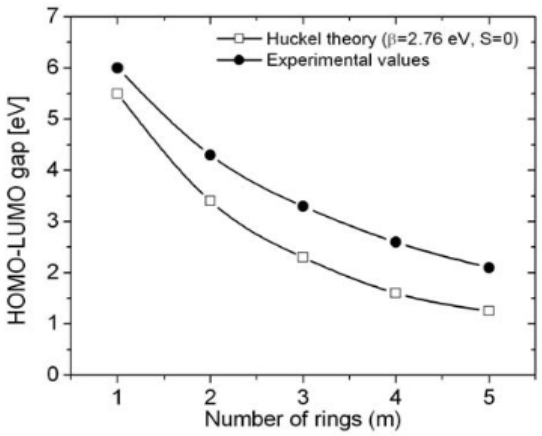

Figure 1.3: HOMO-LUMO band gap from experiment (solid) and calculated from Huckel theory (squares) for organic molecules (adapted from ref [13])

1.2) Organic light emitting diodes (OLEDs)

Organic light emitting diode is basically a light emitting diode in which emissive layer is composed of electroluminescent organic material sandwiched between the electrodes (anode and cathode). OLEDs have promising application in flat panel displays and lightning. In the OLED device opposite charge carriers (electron and hole) are injected through electrode, migrate through organic material under forward bias voltage with positive terminal connected to anode and negative terminal connected to cathode. The charge carriers recombine in the emissive layer to form exciton (electron-hole pair) which undergoes radiative decay to release the energy in the form of photon and thus light is emitted through transparent electrode. Depending on the type of organic material used as emissive layer i.e. small molecule /polymers the OLEDs are known as small molecule OLEDs (SMOLED) or polymer light emitting diodes (PLED).

Electroluminescence (EL) was observed by H. J. Round using a piece of carborundum (SiC) crystal in 1907.[14] After 55 years, in 1962, Holonyak and his coworkers commercialized these researches by producing the first inorganic LED. [15]. Acridine orange and quinacridone were the pioneer organic compounds from which electroluminescence was observed by Bernanose in 1950 using high voltage alternating current (AC).[16,17] [**Figure 1.4**]

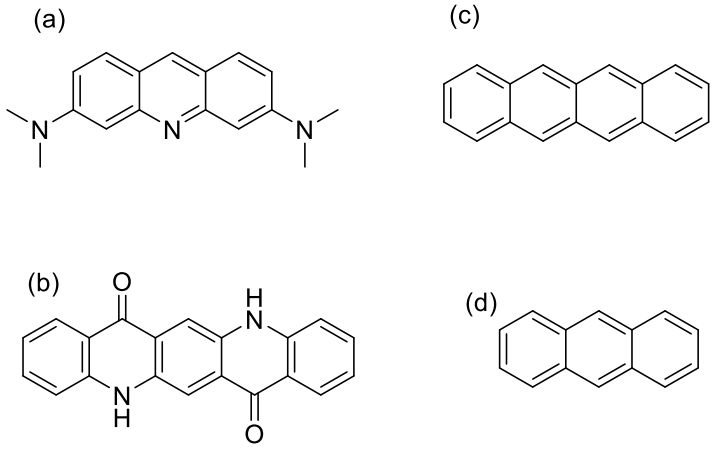

Figure 1.4. Chemical structures of (a) acridine orange, (b) quinacridone (c) tetracene and (d) anthracene.

After that, Pope *et al.*[18] chose to apply direct current (DC) rather than AC current and the electroluminescence was shown by using single crystals of anthracene. However, the device gave an emission only above 400 V and had 10-20 µm thickness.[19] Schneider and Helfrich used

electron and hole injecting electrodes and produced the double injection recombination electroluminescence into a single crystal of anthracene and succeeded to lower the turn-on voltage to around 60 V for visible emission.[20] The organic electroluminescence of a polymer, polyvinyl carbazole (PVK), was firstly observed by R H. Patridge.[21] Until 1980s, all attempts for developing organic electroluminescence had some significant drawbacks, that is, in order to obtain a sizeable light output there had to be applied very high driving voltages (> 100V).[22,23] By using the deposition technique of organic materials, in 1982 Vincett *et al*. used anthracene and had a success to achieve an operating voltage below 30 V, still the external quantum efficiency was quite low with a value of about 0.05%.[24]

Till the beginning of 80's all attempts to improve organic electroluminescence had to face setbacks due to high operating voltage (> 100V) with limited efficiency.[22] Hence the field was limited more to academic interest rather than industrial applications. In the late 80's, the first important breakthrough in the field of OLED was achieved by Tang and Van Slyke from Kodak.[25] They achieved record external quantum efficiency (EQE) of about 1% with luminescence greater than 1000 cdm^{-2} and power efficiency of about 1.5 lmW^{-1} at a voltage operating below 10 V. They used a diode with heterolayer structure [**Figure 1.5**] with a separate hole transporting layer (N,N'-diphenyl-N,N'-bis (3-methylphenyl) 1,1'-biphenyl-4, 4' diamine (TPD)) and an electron transporting layer *viz,* tris(8-hydroxyquinoline) aluminum (Alq3) so that charge recombination and light emission occurred in the middle of organic layer.

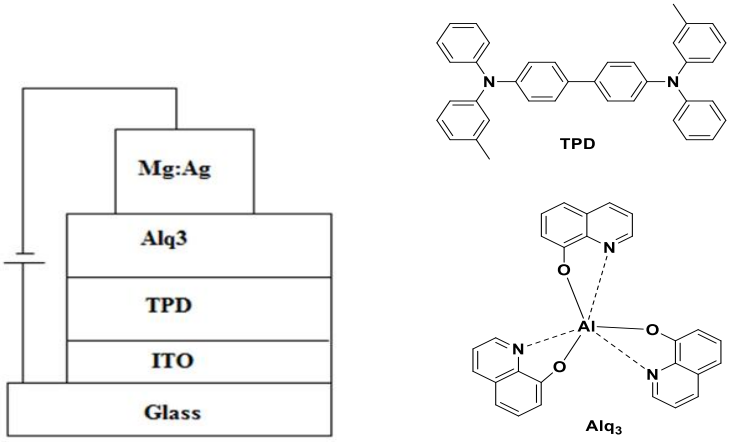

Figure 1.5: Device structure of the first heterojunction OLED and molecular structures of Alq3 and TPD.[25]

This helped to reduce the operating voltage with improved device efficiency and boosted the research in the field of OLEDs. Motivated form these results, the researchers started to focus on the synthesis of new materials with good efficiency and easy processing abilities. In 1990, Friend *et al* [26] reported single layer polymer light emitting diode (PLED) with poly(p-phenylene vinylene) (PPV) as an emissive layer exhibiting highly fluorescent yellow green color and 0.05% efficiency.

Until late 90's fluorescent materials had dominated the field of organic electroluminescent materials. However fluorescence is generated only by singlet excitons which contribute to 25% of total exciton population and rest of the 75% triplet excitons are almost entirely lost through non radiative decay. In order to break the 25% efficiency barrier and utilize 75 % triplet excitons to achieve theoretical 100 % internal quantum efficiency, Forest and co workers reported phosphorescent OLEDs in 1998.[27] The phosphorescent OLED [PHOLED] was having platinum based phosphorescent dopant material i.e. platinum octaethylporphyrin which helped to increase the efficiency by utilizing both singlet and triplet excitons and EQE of 4% was reported. Soon after, Adachi and coworkers achieved an EQE value of about 22% using a phosphorescent dopant in a high band-gap host.[13]

1.2.1) Commercial applications of OLEDs

The massive growth of the consumer electronics industry over the past decades boosted OLED technology grow from a research lab concept to a commercially viable technology. OLED technology is realized in commercial applications such as flat-panel displays (FPDs) and solid-state lighting (SSL). The liquid crystal display (LCD) technology in flat panel displays (FSL) was rapidly replaced by OLED. In the case of small screen applications such as small screens in mobile phones, portable digital media players, car radios, digital cameras, as well as large screen applications such as TV screens, hoardings, etc, OLEDs are used in place of LCDs.[28]

The most basic difference between LCD and OLED TVs is that in OLEDs, each pixel provides its own illumination while in case of LCDs, all the pixels are illuminated by back LED light.[29] The OLED displays have different advantages over conventional LCDs[30] such as higher resolutions, wide view angle, wide color gamut, ultra high contrast ratios, fast response time, semi transparent OLED screens, etc. The most important advantage of OLEDs over LCD is their

low energy consumption. As the pixels in OLEDs are self illuminated, they consume about 40-50% less power as compared to LCD displays. [31]

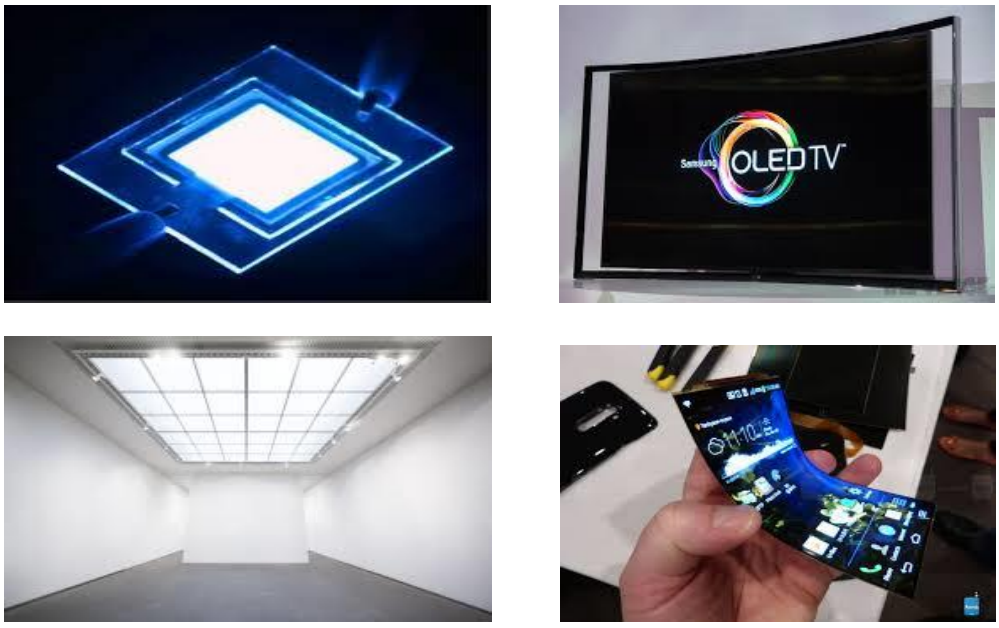

Figure 1.6: Different commercial applications of OLEDs in displays and lightning

Applications in solid state lighting are also being developed. OLEDs have advantage over incandescent lightning in terms of power efficiency. However, compared to OLED displays, OLED lighting is still gaining momentum and attempts for the full-level commercialization are underway. Compared to its strongest competitor i.e. inorganic LED lighting, OLEDs offer the advantages of low heat generation, color tuning and flexible form factors. Several companies have already offered OLED lighting panels-including Philips/OLED works, Osram, LG, Konica, Minolta and others. Attempts are underway to increase lightning performance, lifetime, light quality and reduce the price to make it an affordable technology. Overall, with these efforts, the OLEDs have bright future in lightning application.

1.2.2) Structure of device

The simplest structure of OLED contains an organic electroluminescent material sandwiched between electrodes. The charge carriers are injected from electrodes into organic material where they undergo recombination to emit the light. The structure of corresponding single layer device is shown in **Figure 1.7**. However, single layer device reported by Burroughes *et al* [26] exhibited low quantum efficiency of 0.05%. The low efficiency of single layer OLED could be attributed

to the imbalanced charge transport in the organic material resulting into loss of charge carriers near opposite electrode without formation of excition. As discussed earlier, in the heterolayer (multilayer) OLED device reported by Tang and Van Slyke,[25] they used TPD as hole transporting layer and Alq3 as electron transporting and emissive layer. By introducing separate hole transporting layer, the efficiency of SMOLEDs was improved to 1% as compared to earlier reports.[19-21] A polymer light emitting diode with heterolayer structure developed in 1992 also exhibited quantum efficiency of 0.08%. With such inspiring results the researchers started to develop different heterolayer OLEDs with multiple layers for attaining higher efficiencies. **Figure 1.8** shows the typical multi-layer OLED structure, which consists of hole transport layer (HTL), electron transport layer (ETL) and emissive layer (EML).

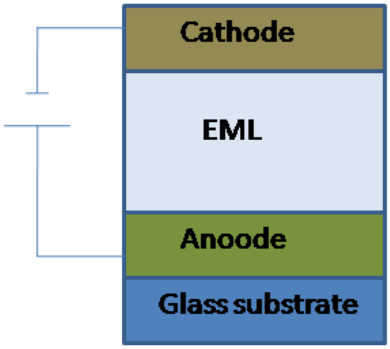

Figure 1.7: Structure of single layer OLED device

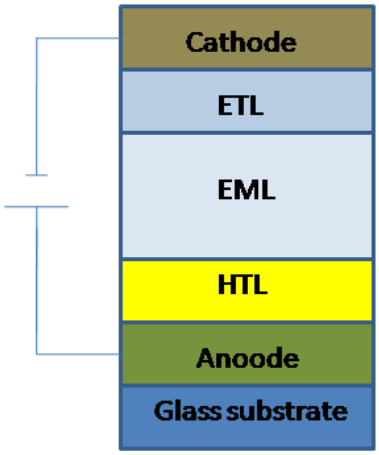

Figure1.8: Structure of heterolayer (multilayer) OLED device

In OLED device charge carriers i.e. holes and electrons are injected from anode and cathode, respectively. The anodes are generally coated on the transparent substrate like glass. The anode material[32] should possess high conductivity in order to decrease the contact resistance, good film forming properties and wettability to have good contact with neighboring organic layers, high thermal and chemical stability and high work function (>4.1 eV)[33] to support hole injection into the organic material. Also the anode should be adequately transparent so that light photons generated into emissive layer can effectively leave the device. Indium Tin Oxide (ITO)[34] is widely used anode in the OLED devices. It consists of indium oxide and an about 10% amount of tin oxide. It has a high work function varying between 4.5 to 4.8 eV. Also, it is transparent in the visible region due to its high band gap (>4.0 eV). The cathode in OLEDs is normally made up of metal alloy or pure metal. The cathode materials should have high conductivity. In order to promote injection of electrons into the organic layers, the cathode materials should have low work function. Also to have good contact with neighboring organic layers, the cathode materials should possess good film forming properties and wettability.[35] The metals such as calcium (Ca), magnesium (Mg), aluminum (Al) and their alloys are used as cathode. The problem with low work function metals is that they are very susceptible to air and moisture. Cathode materials degrade by formation and enlargement of non-emissive dark spots. In order to get rid of this unwanted issue, a very thin layer of LiF or CsF can be added.[36]

Sometimes, OLED devices also require introduction of buffer layers between electrode and transporting layers to facilitate the injection of holes or electrons from electrodes into the adjacent transport layers and they are called as electron injection layer (EIL) and hole injection layer (HIL).[4] The HIL and EIL create a dipole layer at the interface and facilitate better charge injection by lowering injection energy barrier.[37] Injection layers also help to protect the excitons from the process of metal quenching caused by field exposure and gap states at the interface.[38] Poly(3,4- ethylenedioxythiophene):poly(4-styrenesulfonate) (PEDOT:PSS) and MoO_3 are two typical hole injection materials (HIM).[39,40] LiF and CsF are two widely-used electron injection materials (EIM). [41,42]

The hole transport materials (HTM) are crucial elements for multi-layer small organic OLED devices. The functions of HTMs are to help positive charge carriers drift from anode into the emissive layer by acting as a hole conductive pathway. Generally, HTMs need to have properties such as it should have low ionization potential and should easily get oxidized. The material needs

to have low electron affinity to prevent negative charge carriers reaching the anode i.e. act as an electron blocking layer. The HTMs should be stable in one electron oxidized state and should exhibit low HOMO level.[43] The most common hole transport layer compounds are triarylamines because of their electron rich moieties. N,N '-bis(3-methylphenyl)-N,N '-diphenyl-[1,1 'biphenyl]-4,4' –diamine (TPD), N,N'-di-[(1-naphthyl)-N,N'-diphenyl]-1,1'biphenyl)-4,4'-diamine (NPD) and 4,4',4''-tris(N-3-methylphenyl-Nphenylamino)triphenyl amine are used as a HTMs. (**Figure 1.9**)[44,45]

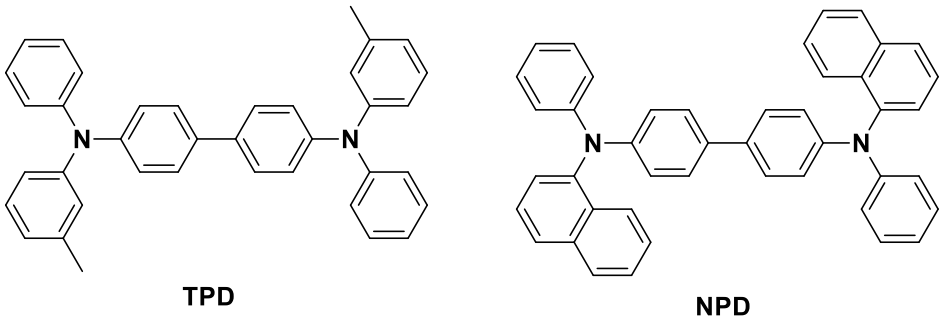

Figure 1.9: Hole transport materials with high thermal stabilities

Electron transport layer materials are important compounds in OLEDs. The function of ETL layer is to serve as a conducting material and assist electrons moving from cathode to organic layers. Materials used in ETL need to posses properties such as high electron affinity, matching the work function with cathode and decrease the potential between cathode and the emitter. [46] The material should be stable in one electron reduced form and should have high electron transport ability. ETMs should exhibit good film forming properties in order to form uniform films for minimizing pin-hole defects. ETM should exhibit low lying HOMO level so that it can act as hole blocking layer and prevent the holes from reaching to the cathode by crossing emissive layer. Different metal chelates and electron deficient heterocyclic compounds *viz.* 2-(4-*tert*-Butylphenyl)-5-(4-biphenylyl)-1,3,4-oxadiazole (PBD)**,** 2,2′,2''-(1,3,5-benzinetriyl)-tris(1-phenyl-1-H-benzimidazole) (TPBi), tris-(8-hydroxyquinoline)aluminum (Alq_3), etc are used as ETMs.[47] (**Figure 1.10**)

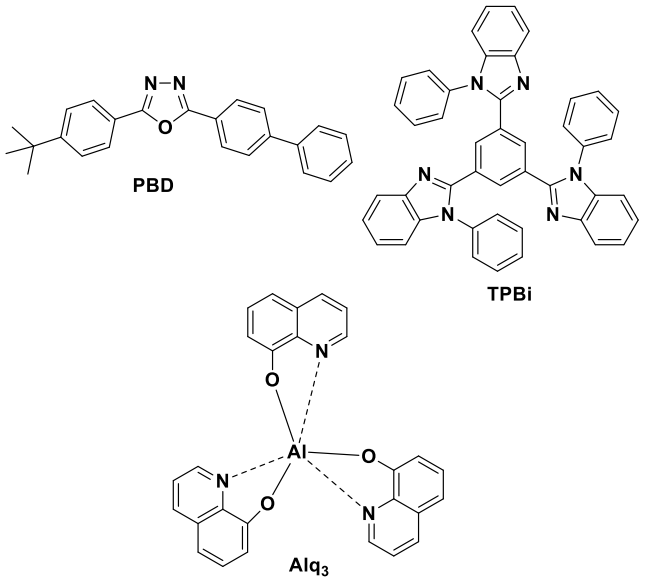

Figure 1.10: Common electron transport materials

1.2.3) Device fabrication

Since the discovery of electroluminesce many techniques were used to fabricate the electroluminescent devices.[48] Generally, organic light emitting devices could be fabricated by means of two main techniques *viz.* dry and wet techniques. The dry techniques involve thermal evaporation under high vacuum and wet techniques involve spin coating and ink jet printing. Low molecular weight small organic molecules could be deposited under high vacuum by thermal evaporation and polymeric type molecules could be deposited by solution processed procedures.

The thermal vacuum deposition techniques are useful for depositing an extensive range of materials; from inorganic LEDs to low molecular weight organic compounds in SMOLEDs. It is also suitable for fabrication of OLEDs, based on the small organic molecules.[49] The deposition is generated in a high vacuum chamber ($<10^{-6}$ mbar).[50] Thermal evaporation yields even and high-density thin films as well as enables the fabrication of multi-layered devices which have proven to be reliably highly efficient.[51] However, thermal evaporation can't be easily transferred to large-scale production and it is also energy consuming. The requirement of vacuum environment increases production cost. Solution processing is much more viable for large-scale production, as various solution processing techniques can be used such as roll-to-roll printing, dip-coating, screen printing, doctor blade, spray coating, ink-jet printing and spin coating [52] Polymers are

generally used as the primary material for solution-based methods, due to high solubility and good film formability.[53] However, small molecules have proven quite well in solution-processed devices.[54] Due to benefits of small molecules over polymers such as high purity, monodisperse nature, batch to batch reproducibility, etc, it is desirable to develop solution processable small molecules for application in OLEDs. In fact, utilization of small molecules to create efficient solution processed OLEDs is one of the main aims of the work reported in the present thesis. The solution processing technique used for device fabrication in this thesis is spin-coating.[55] In spin coating, the material is first dissolved into an appropriate solvent and dispensed onto a substrate, typically glass or plastic. The substrate is then spun at high speeds (1000–4000 rpm) so that excess material is thrown off, leaving a thin film (thickness approx. 30–60 nm),[56] film thickness is determined mainly by the spin speed and the solution concentration. Increasing the spin speed will decrease the film thickness, while increasing the solution concentration will increase the thickness. The final thickness is reached after approximately 20 seconds, but the substrate is usually spun for 40–60 seconds to further dry the film before baking. The films are then baked to evaporate the residual solvent from the film so as to avoid solvent-induced trapping and material degradation. The baking temperature is typically below the glass transition temperature of the materials, so that the film remains amorphous. (**Figure 1.11**)

Spin coated systems do not require high vacuum therefore the coating expenses are reduced. An important criterion for spin coating systems is that the molecule to be studied must dissolve in desirable solvent. Although solution processed techniques are easy and low-priced, re-dissolving the previously deposited layers are the major drawbacks.[57] Additionally, the film thicknesses can be controlled by choosing proper solution concentration.

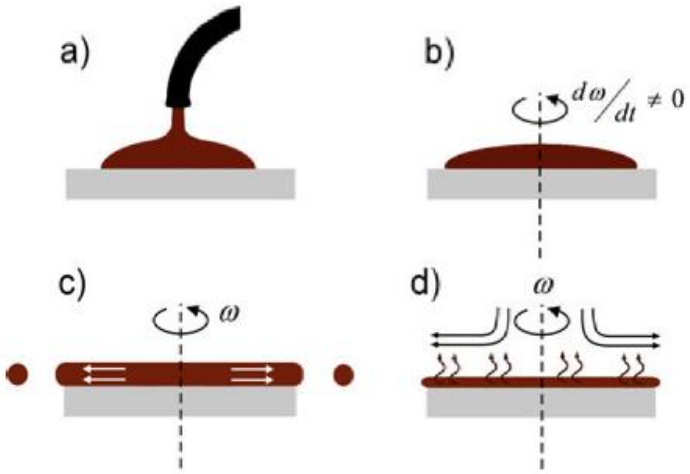

Figure 1.11: Spin-coating process (a) dispersion (b) acceleration (c) flow dominated (d) evaporation dominated (adapted from ref 56)

1.2.4) Functioning of OLEDs

OLEDs can function only when an electric field is applied between the two metallic electrodes. The voltage around which OLED starts to emit any detectable color is called as turn-on voltage. The energy barriers between the layers are related with the turn on-voltage of the device. Lower turn on voltage is better than higher ones since at higher voltage, the organic materials start to degrade eventually.[58] The light generation process taking place in an OLED device is depicted in **Figure 1.12**.

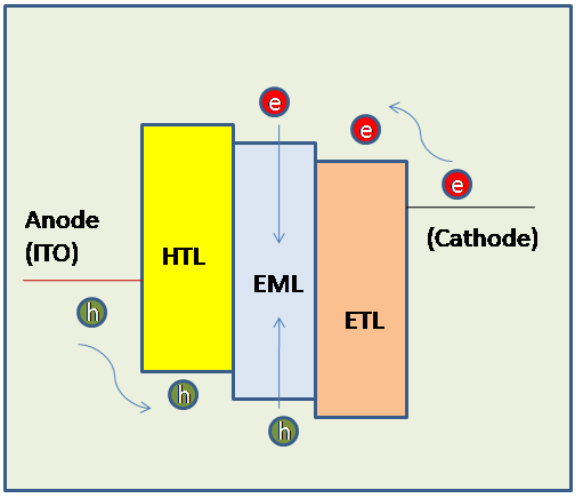

Figure 1.12: Light generation process in OLED device.

Holes and electrons are injected due to an applied voltage higher than the built-in voltage from anode into the HOMO and from cathode into the LUMO of organic material, respectively. Due to the applied electrical field charge carriers travel from the electrodes towards each other and then recombine resulting into formation of an exciton inside the organic layer. The energy levels for both charge carriers are shifted within the energy gap of the organic material due to the binding energy of the exciton. Finally, the excitons undergo radiative decay and electroluminescence from the organic material is observed. The color of light emitted depends upon energy levels (band gap) of emissive material. Into a single layer OLED device, holes and electrons are injected from the electrodes due to an applied voltage higher than the built-in voltage. Due to the applied electrical field charge carriers travel from the electrodes towards each other. However, a huge amount of injected electrons and holes reach the opposite electrode without recombining with each other in the organic layer. Hence, these charge carriers are lost and do not contribute towards light emission from the organic light-emitting diode, and therefore result into reduced device efficiency. Furthermore, the emission zone is not fixed in such devices and it can spread over the whole device, especially near both contact interfaces resulting in quenching of excitons near the electrodes.[59,60] Moreover, the recombination zone can shift inside the organic layer with the applied voltage due to different injection barriers at the electrodes followed by variation of the emitted color and efficiency of the device.[61] Thus, it is necessary to use different layers that are tailored for their special function in modern OLEDs. Hence as discussed earlier, HTM and ETM are introduced into a multilayer OLED near anode and cathode, respectively. It is important to use wide energy gap materials as transport layers to avoid absorption of light that is created inside the emission layer of the OLED. Due to perfect energy alignment of the work function of the anode and the HOMO level of the HTL, under forward bias holes are injected instantly from the anode into the HTL under forward bias. The same process happens for electron injection from the metallic cathode into the LUMO of the ETL. Additionally, both transport layers also act as charge carrier blocking layers for the opposite charges.[62] Thus, charge carriers that travel in the EML of the device cannot reach the opposite charged electrode and remain in the EML until they recombine under the formation of an exciton (electron-hole pair). The excitons formed undergo radiative decay and result into light emission.

1.2.5) Jablonski diagram

In OLEDs, the luminescence is generated from radiative decay of excitons which are basically of two types i.e. singlet and triplet.[63] Singlet excitons undergo radiative decay rapidly at room temperature, producing the luminescence known as fluorescence, while radiative decay of triplet excitons is known as phosphorescence. However, phosphorescence is forbidden at room temperature. The luminescence can be illustrated by Jablonski diagram[64] as shown in **Figure 1.13.** Ground state, first and second electronic states are represented as S_0, S_1 and S_2, respectively. Absorption of energy excites molecules from ground state S_0 to excited state S_1 or S_2. The molecule in higher excited state S_2 is rapidly relaxed to the S_1 by internal conversion. Molecule in the excited state S_1 undergoes rapid decay to generate fluorescence.

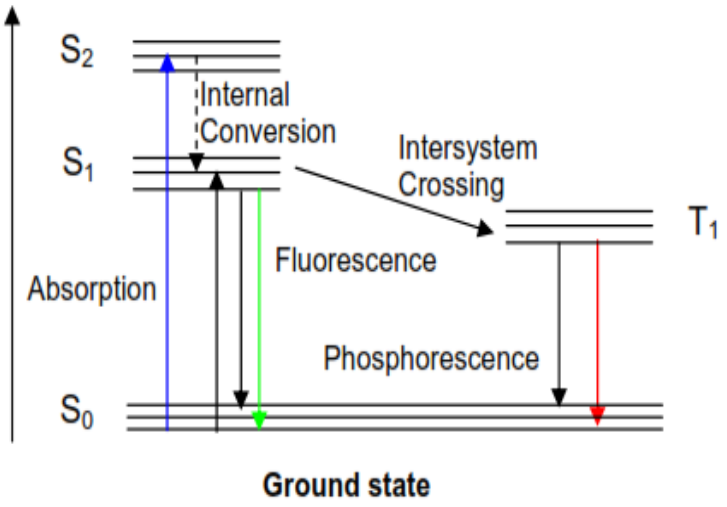

Figure 1.13: Jablonski diagram (adapted from ref [61])

In other possibility, molecule in the S_1 state undergoes inter system crossing to generate triplet state T_1. Emission from T_1 is termed as phosphorescence and is generally shifted to longer wavelengths (lower energy) relative to fluorescence. The lifetimes of singlet and triplet excitons are different; fluorescence lifetime is fast and it is of the order of subnanoseconds,[65] while the triplet exciton has a considerably longer lifetime as compared to the singlet, with typical lifetimes of the order of 10 - 100 µs.[66] Due to the long lifetime of triplet excitons, they tend to undergo deactivated process, decay nonradiatively or quench emission. Since the radiative decay of triplet excitons is forbidden at room temperature, the early research of organic light-emitting

materials was mainly concentrated on fluorescent materials. The inclusion of heavy transition metal atoms in the molecular structure can give strong spin-orbit coupling which leads to singlet-triplet state mixing, realizing phosphorescence at room temperature. Depending upon the nature of exciton formed and mechanism of luminescence production, the electroluminescent organic materials can be categorized as fluorescent[67] and phosphorescent[68] materials.

1.2.6) Characterization terminologies

Different types of OLEDs with varying color and efficiencies are being developed in academia as well as industries. In order to compare the performance of an OLED with another OLED or inorganic light emitting diode, there should be a set of characterization parameters. These different parameters are needed to be considered while designing different materials for OLEDs and device fabrication for having good quality of light source in domestic lightning and display technology.

Device efficiency of OLED is categorized as current efficiency (CE), luminous efficiency or power efficiency (PE) and external quantum efficiency (EQE). The current efficiency is determined by measuring luminescence obtained from the device at a given current density and it is expressed as cdA^{-1}. Luminous efficiency is a measure of how well a device produces the light. It is the ratio of luminous flux emitted to the input power and it is expressed as lmW^{-1}. External quantum efficiency of a device is the ratio of number of photons ejected to the number of electrons injected into the device. Brightness of an OLED device is also important property to be considered. The brightness of a device being viewed directly is measured in the number of lumens they radiate per steradian in the viewing direction. One lumen per steradian is known as candela. The brightness is best described in candela using all the light emitted for the device and the brightness is expressed in units of cdm^{-2}.

The usual method for representing the colour output of an OLED is to compare it to a Commission Internationale de l'Eclairage (CIE) 1931 chromaticity diagram.[69] A CIE color diagram shown in **Figure 1.14** accounts for the properties of color perceivable by human eye i.e. hue, saturation and brightness of light.

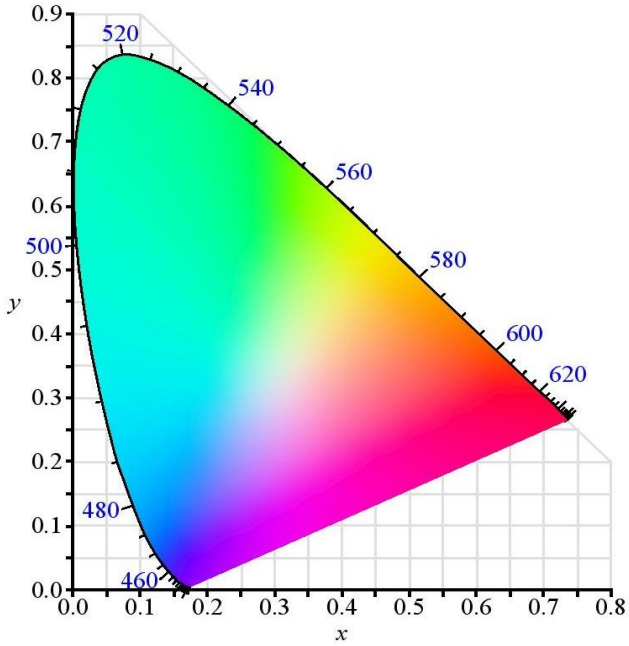

Figure 1.14: CIE 1931 color diagram

Whilst individual wavelengths in the visible spectrum are related to individual colors, combinations of different wavelengths can lead to the same perception of color. The outer edges of the CIE diagram represent the limit of human colour perception, and the fully saturated spectral colors (i.e. containing no white light) make up the horseshoe shaped boundary. Any point within the diagram shows a unique and perceivable color hue, but equally any hue may be produced by a combination of different colors. The color of light is plotted on the CIE diagram as a function of the two color coordinates *x* and *y*, which map the color in relation to hue and saturation. The value of the *x* and *y* coordinates are determined from the spectral power density of light measured with a spectrophotometer after factoring with sensitivity curves determined for the average human eye. In this way, the emission of light from an OLED consisting of a range of different wavelengths at different intensities is simplified into two coordinates relevant to the perception of color, allowing for effective and quantitative comparisons of color emission.

1.2.7) Advantages and challenges of OLEDs

Compared to the conventional LCD display technology or inorganic LEDs, the OLEDs have different advantages as follows.

Flexibility: OLEDs can be fabricated on the flexible substrates such as plastic layers which accord them flexibility as well as displays become lightweight.

Easy manufacturing: Apart from inorganic LEDs, OLEDs fabricated by solution processing methods like roll-to-roll, inkjet printing and screen printing are cost effective and consume less energy for fabrication.

Self Emitting: The luminous efficiency of OLEDs is higher than the other display technologies. OLEDs do not require a backlight, polarizers and diffusers. Therefore much thinner display panels could be made that give OLEDs lightweight ability.[70]

Picture quality: OLED displays have high resolution, high brightness and high contrast values. As well as they have large viewing angle (up to 170°) and fast switching times (1000 fold faster) compared to traditional displays

Energy efficient: OLEDs consume about 40% less energy compared to LCD display,[71] hence they are energy efficient.

Apart from these exceptional properties, the field of OLEDs face different challenges as follows

Lifespan: The biggest technical problem for OLEDs was the limited lifetime of the devices[72] In particular, blue OLEDs have achieved a lifetime of ~14,000 hours to half original brightness (five years at 8 hours a day) when used for flat-panel displays. The lifetime of OLEDs is lower than the average lifetime of LCDs or plasma displays—each currently rated for 25,000–40,000 hours to half brightness, depending on manufacturer and model[73,74]

Color balance issue: As blue emitters degrade significantly more rapidly than green or red emitters, then blue light output decreases relative to the other colors. This variation in the differential color output changes the color balance of the display and is much more noticeable than a decrease in overall luminance.[75] Hence, improvement to the efficiency and lifetime of blue OLEDs is vital to the success of OLEDs as replacements for LCD technology.

Water damage: Moisture and oxygen present in the environment rapidly damage the organic materials of OLEDs. Therefore, improved sealing processes are critical for practical manufacturing. Water damage may especially limit the longevity of more flexible displays.[76]

Outdoor performance: As an emissive display technology, OLEDs rely completely upon converting electricity to light. The metallic cathode in OLED acts as a mirror, with reflectance approaching 80%, leading to poor readability in bright ambient light such as outdoor application.

1.2.8) Materials used in OLEDs

Different types of small molecules based on the chromophores such as anthracene, pyrene, carbazole, phenothiazine, naphthalene, diphenylamine, fluorene, etc are used as electroluminescent materials in OLEDs. Among these different molecules, the work in this dissertation is focused on pyrene based molecules.

Pyrene is a polycyclic aromatic hydrocarbon (PAH) consisting of four fused benzene rings, resulting in a large, flat aromatic system. Pyrene is a colorless or pale yellow solid. Since the pioneering work of Laurent[77] in 1837, who discovered pyrene as the residue of the destructive distillation of coal tar, pyrene has remained the subject of immense investigations. Later on, in 1871, Grabe reported the isolation of pyrene *via* extraction with carbon disulfide, which left the accompanying chrysene undissolved.[78] With its extended conjugation pyrene shows good thermal and chemical stability, good solubility, high photoluminescence efficiency[79] and high charge carrier mobility. Pyrene also exhibits excellent hole injection ability when compared to other chromophores.[80] The fluorescence properties of pyrene have been utilized over the last 50 years in the investigations of water-soluble polymers, making pyrene, by far, the most frequently applied dye in fluorescence labeled polymers.[81] The pyrene chromophore is also frequently employed as a probe to measure properties of surfactant micelles, phospholipid vesicles, and surfactant/polymer aggregates. The tendency of pyrene and its derivatives to form excimers has been widely employed for supramolecular design and for probing the structural properties of macromolecular systems. Pyrene labels have been extensively used in structural studies of proteins and peptides,[82,83] DNA recognition[84,85] and investigation of lipid membranes.[86,87] The excimer fluorescence properties of pyrene and its derivatives have been also utilized to sense environmental parameters such as temperature,[88] pressure,[89] or pH. [90]

Thus, pyrene, as a blue-light-emitting chromophore with good chemical stability and high charge carrier mobility, appears to be a very attractive building block for light-emitting devices. However, the use of pyrene is limited. As the intermolecular π-π interactions between pyrene molecules easily form π-aggregates/excimers which leads to an appearance of additional emission band in longer wavelength and the quenching of fluorescence, resulting into low solid-state fluorescence quantum yields. This effect of fluorescence quenching limits the use of pyrene as an emissive material in OLEDs. Nevertheless, several efforts in the structural modifications of

pyrene containing organic semiconductors have been made in order to avoid aggregation and improve the fluorescence quantum yield for applications in OLEDs.[91] One such attempt of structural modification is to design the molecules using the core-side group concept[92] in which the core group plays a fundamental role in determining the emission wavelength and luminous efficiency of the emitter. The side group is attached to the core group to control the structure, arrangement, and polarity of the emitter in order to prevent excimer formation, fine-tune the emission wavelength and increase the luminous efficiency. The electronic and photophysical properties of pyrene are very attractive for the design of new organic light-emitting semiconductors. In the case of pyrene, modification of the chemical structure by varying the substitutents at different positions on pyrene ring allows control of the molecular architecture and thus the molecular packing, which renders handling of pyrene substitution a key factor in pyrene-based semiconductors. Molecules having substituents at different positions on pyrene core have been reported earlier such as 1-substituted pyrenes, 1,3,6,8- tetrasusbstituted pyrenes, 1,6- and 1,8-disubstituted pyrenes, 1,3-disubstituted pyrenes, 2,7-disubstituted pyrenes, 4,5,9,10-tetrasubstituted pyrenes, etc.[91] Among these different types of pyrene derivatives, 1,3,6,8-tetrasusbstituted pyrene compounds have been investigated in the thesis.

General structure of 1,3,6,8-tetrasubstituted pyrenes is shown in **Figure 1.15.** The electrophilic substitution of pyrene is known to take place preferentially at the 1-, 3-, 6-, and 8-positions, based both on experimental results[93,94] and on consideration of calculations of molecular orbitals,[95,96] the only exception being the *tert*-butylation.[97] Thus, 1,3,6,8-tetrasubstituted pyrenes can be easily accessible by direct electrophilic substitution of pyrene.

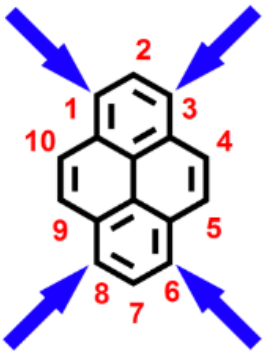

Figure 1.15: 1,3,6,8-Tetrasubstituted pyrene

Most of the reported pyrene derivatives are monosubstituted, but a practical precursor to tetrafunctional compounds is 1,3,6,8-tetrabromopyrene, which has been produced easily on the gram scale since 1937, by the bromination of pyrene at high temperatures [94] Thus, 1,3,6,8-tetrabromopyrene [98]can be obtained in high yield (90%) *via* bromination with Br_2 in nitrobenzene at 160 ^oC.[99] This straightforward access to 1,3,6,8-tetrabromopyrene has opened up new routes to a broad family of C-functionalized pyrenes obtained by Suzuki or Sonogashira coupling reactions. 1,3,6,8- Tetrasusbstituted pyrene compounds bearing carbazole and phenothiazine as the substituents have been studied in the present thesis.

Carbazole is an aromatic heterocyclic compound. It has a tricyclic structure, consisting of two six-membered benzene rings fused on either side of a five-membered nitrogen-containing ring.[100] Carbazole is a conjugated unit that has interesting optical and electronic properties such as its photoconductivity and photorefractivity[101,102] Carbazole derivatives are widely used as the materials for hole-transporting layers of OLEDs, utilizing their high charge mobility.[101] Carbazole derivatives are also used as light emitting layers because they are thermally stable and show blue photo- and electroluminescence due to the large bang gap of the biphenyl unit. [101]

Carbazole compounds are known for intense luminescence and are widely used as blue, green, red, and white emitters.[102] Similarly, phenothiazine is an electron rich heterocyclic compound containing nitrogen and sulphur heteroatoms due to which phenothiazine exhibits stronger electron donating properties compared to triphenylamine, carbazole, tetrahydroquinoline and many other N-heterocycles.[103] Phenothiazine has a non-planar butterfly conformation which helps to suppress the molecular aggregation and the formation of molecular excimers [104]

1.2.9) 1, 3, 6, 8-Tetrasubstituted pyrene derivatives for applications in organic electronics

1,3,6,8-Tetrasubstituted pyrene based small organic molecules for applications in organic electronics are compiled in **Table 1.1**.

Table 1.1: 1, 3, 6, 8-Tetrasubstituted pyrene derivatives for applications in organic electronics

Sr . No.	Pyrene-based small organic molecules	Ref. No.
1	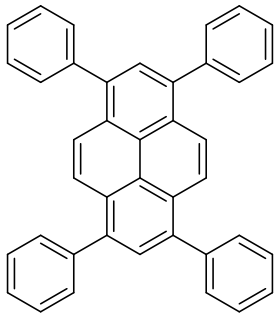 **TPPy** In 1970, Berlman and coworkers reported 1,3,6,6-tetraphenyl pyrene (**TPPy**) which exhibited high luminescence (0.9) in cyclohexane solution.[105] Sotoyam and coworkers investigated the effect of different phenyl group substitutions of 1, 3, 6, 8-tetrasubstituted pyrene by molecular orbital method and fabricated the OLED devices using TPPy which exhibited EQE of 2.1%, current efficiency of 1.87 cdA^{-1} with CIE of (0.17, 0.09).[106] A light emitting diode with transistor characteristics was fabricated *via* vacuum deposition by Oyamada and coworkers using 1% rubrene doped TPPy as the active layer. An EQE of 0.8% was observed in a short channel device.[107]	105, 106, 107
2	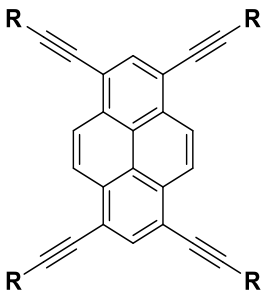 a. R= $SiMe_3$ b. R= $C(Me)_2OH$ c. R= CH_2OH d. R= $CH(OEt)_2$ e. R= C_6H_5 f. R= 4-$CF_3C_6H_4$ 1, 3, 6, 8-Tetraethynylpyrene and its derivatives were reported in 2005 and effect of extended acetylenic conjugation on their optical properties were studied.[108] It was found that extension of conjugation of the pyrene chromophore by acetylenic substituents effectively shifted the wavelength	108

	of absorption and fluorescence emission of derivatives into the visible region of the electromagnetic spectrum in comparison to the unsubstituted pyrene molecule. The quantum efficiencies of fluorescence of the tetraethynyl derivatives were comparable to that of pyrene (0.6), except in the case of the phenyl-substituted derivatives whose fluorescence quantum efficiencies were observed to be low due to the deactivation of the excited state resulting from the free rotation of the terminal phenyl groups.	
3	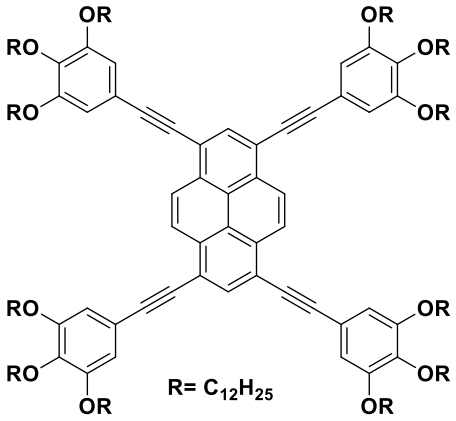 1,3,6,8-Ttetrakis(trisalkoxy- phenylethynyl)pyrene was reported by Hayer and coworkers.[109] The molecule exhibited hexagonal and rectangular columnar mesophases. The material was highly fluorescent in solution and, most remarkably, in the condensed state, with a fluorescence quantum yields of 0.7 in dichloromethane solution and 0.62 in the solid state. The high luminescence efficiency in the solid state was ascribed to rotated chromophores resulting into formation of cofacial stacks, which eventually led to an optically allowed lowest optical transition.	109
4	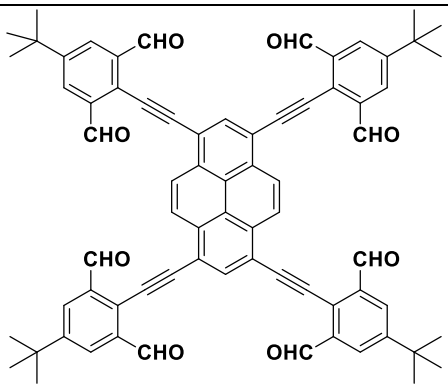	110

	Venkataraman and co workers[110] synthesized a pyrene octaaldehyde derivative and systematically investigated the effect of solvent, concentration, and temperature on the aggregation of a pyrene derivative. They observed that in the solid state as well as in non polar solvents, the molecules of pyrene derivative exhibited intermolecular π-π and C-H---O interactions, bringing the two molecules closer that resulted into excimer formation. This eventually led to appearance of longer wavelength band in emission spectra.	
5	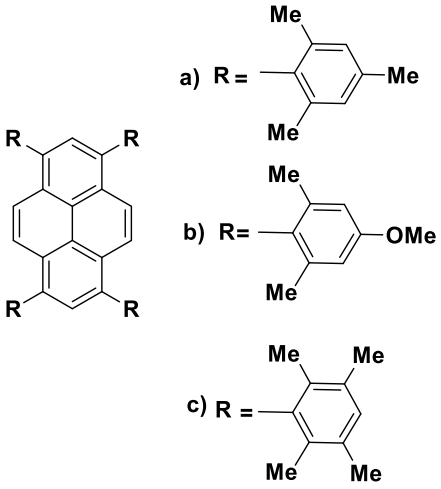 Moorthy and co-workers[111] developed a series of sterically congested 1, 3, 6, 8-tetraarylpyrene derivatives by introducing sterically crowded groups on the periphery of pyrene core. Due to presence of these bulky groups, pyrene derivatives did not show molecular aggregation due to π stacking in both solution and solid state. OLED devices fabricated *via* vacuum deposition of pyrene derivatives exhibited blue electroluminescence. The maximum luminous efficiency of 2.7 cdA^{-1} and maximum EQE of 3.3% was obtained.	111

6	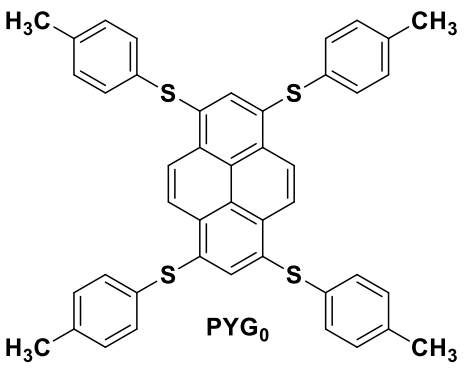 **PYG$_0$** In 2008, Gingras and co workers[112] synthesized polysulfurated pyrene cored dendrimers PYG$_0$, with thiophenylene dendron appended on the pyrene core and its luminescence and electrochromic properties were studied. 1,3,6,8-tetrasubstituted pyrene derivative, namely, PYG$_O$ was synthesized by nucleophilic aromatic substitution with thiolate anions in a polar solvent that exhibited interesting redox properties, such as the change of the color emission upon reversible one-electron oxidation, which could be useful for optoelectronic devices.	112
7	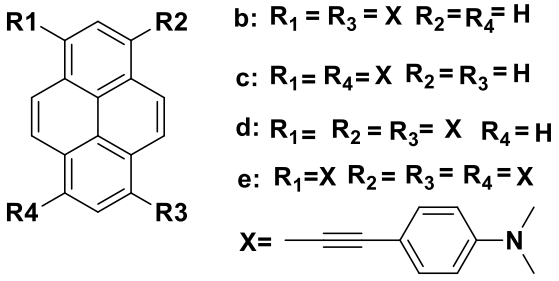 A series of pyrene derivatives having 4-(*N*,*N*-dimethylamino)phenylethynyl groups as the substituent were synthesized by Kim and coworkers.[113] They thoroughly investigated the effect of number of substituents and their positions on pyrene derivatives. The results strongly indicated that substituents can be used to tune the photophysical properties of the pyrene chromophore, as well as to improve the solubility or prevent aggregation. In other words, the	113

	substituents can be used to develop new photofunctional materials of desired properties.	
8	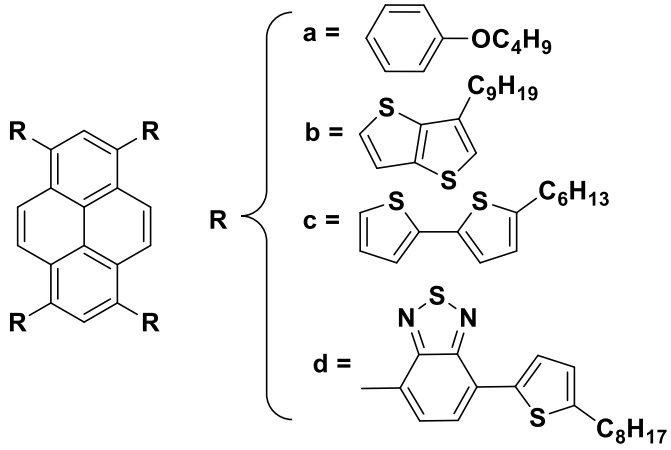 Sonar and coworkers[114] reported a series of star shaped organic semiconductors in 2010, derived from 1,3,6,8-tetrabromopyrene bearing different conjugated moieties on the periphery of pyrene. The materials were soluble in common organic solvents allowing for solution processing of OLED device. OLED devices were fabricated by solution processing of the pyrene derivatives.One of the derivatives in the series i.e. 1, 3, 6, 8-tetrakis(4-butoxyphenyl)pyrene, was used as the active emitting layer in simple solution-processed OLEDs. It exhibited deep blue emission with CIE coordinates of (0.15,0.18), maximum current efficiency of 2.56 cdA^{-1}, low turn of voltage of 3.0 V and maximum brightness of 5015 lmW^{-1}.	114
9	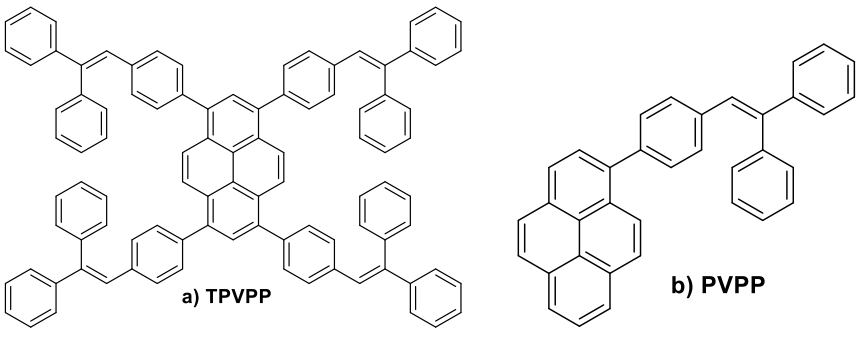 Two pyrene-based fluorophores, namely, 1,3,6,8-tetrakis[4-(2,2-	115

	diphenylvinyl)phenyl] pyrene (TPVPP) and 1-[4-(2,2-diphenylvinyl) phenyl] pyrene (PVPP) were synthesized and characterized by Liang and coworkers.[115] It was observed that in case of PVPP, aggregation induced fluorescence quenching of pyrene units in the solid state was suppressed and bright blue emission was observed while same phenomenon was not observed in case of TPVPP despite the presence of same substituent. PVPP exhibited aggregation induced enhanced emission while a distinct fluorescent behavior was observed in case of TPVPP due to intermolecular C-H---π bond interaction.	
10	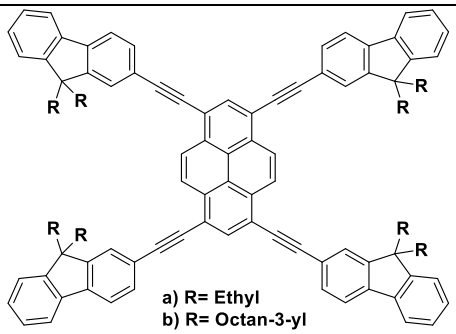 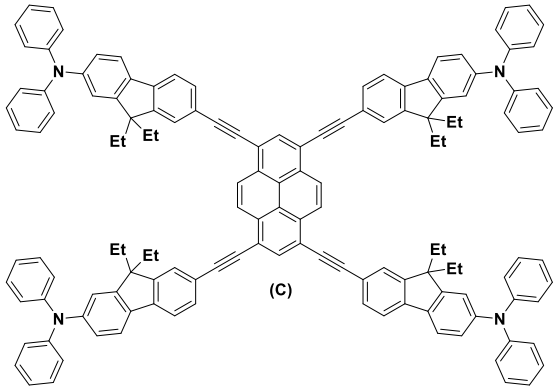 Thomas and coworkers[116] developed blue to yellow-emitting materials by incorporating fluorene-based chromophores on pyrene core with acetylene linkage (**a-c**). Both mono and 1, 3, 6, 8-tetrasubstituted derivatives were synthesized and characterized. The tetrasubstituted derivatives displayed red-shifted emission when compared to the monosubstituted derivative indicative of an extended conjugation in the former. End-capping with a diphenylamine unit further red-shifted the absorption and emission profiles and imparted a weak dipolar character to the molecules. Amine-	116

	containing derivatives exhibited positive solvatochromism in the fluorescence spectra indicating a more polar excited state due to an efficient charge migration from the diphenylamine donor to the pyrene acceptor. All of the derivatives were tested as emitting dopants with host material 4,4'-bis(9H-carbazol-9-yl)biphenyl (CBP) in a multilayered OLED and found to exhibit bright blue or yellow electroluminescence. The device utilizing 1,3,6,8-tetrasubstituted pyrene derivative as a dopant emitter displayed highest maximum luminescence 4630 cdm^{-2} with power efficiency 3.8 lmW^{-1} and current efficiency 7.1 cdA^{-1} at 100 cdm^{-2} attributable to the proper alignment of energy levels that led to the efficient harvesting of excitons. All of the devices exhibited color purity over a wide range of operating voltages.	
11	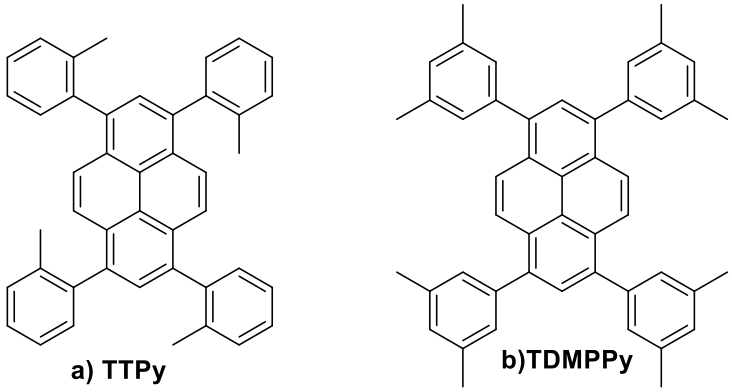 **a) TTPy** **b)TDMPPy** Two methyl-substituted tetraphenylpyrenes, namely, 1,3,6, 8-tetra-o-tolylpyrene (TTPy) (**a**) and 1, 3, 6, 8-tetrakis(3,5-dimethylphenyl)pyrene (TDMPPy), (**b**) were synthesized through Suzuki coupling reactions by Chang and coworkers[117] and the effect of methyl substitution on the PL and EL properties of chromophores were investigated. TTPy with methyl substituents at the 2-position of the phenyl rings absorbed and emitted blue-shifted light as compared to TDMPPy, bearing methyl substituents at the 3 and 5-positions of phenyl rings. In the study, a nondoped OLED device was fabricated using TDMPPy as light emitting layer. The device exhibited a low turn-on voltage of 3.7V, CIE chromaticity coordinates of	117

	(0.19, 0.48), emitted green light with a high maximum luminance of 26670 cdm^{-2} and displayed a high maximum current efficiency of 10.8 cdA^{-1}.	
12	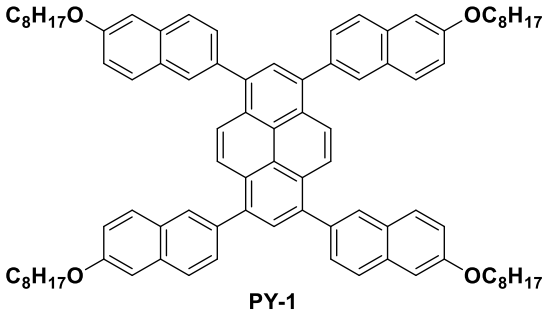 PY-1 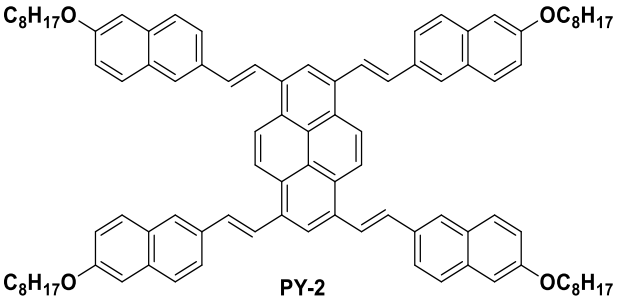 PY-2 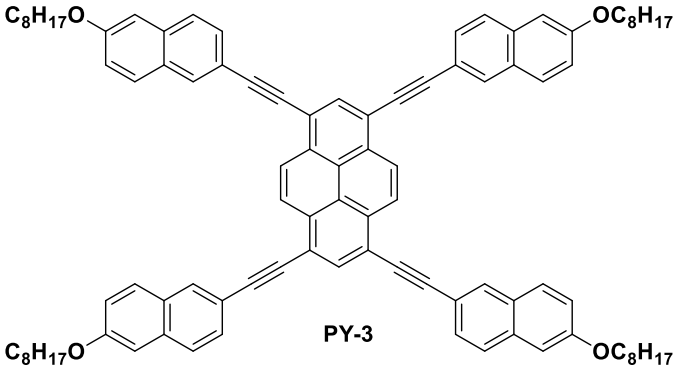 PY-3 A series of 1,3,6,8-tetrasubstituted pyrene derivatives bearing alkoxy naphthalene unit were synthesized.[118] In the pyrene derivatives PY-1, PY-2 and PY-3 the substituent and pyrene core were linked *via* single, double and triple bonds, respectively. The effects of bond alteration were studied. OLED device was fabricated by solution processing of pyrene derivatives. The PY-1 device exhibited low turn-on voltage of 4V, C.I.E. coordinates were maintained at (0.17, 0.15) to (0.17, 0.16), respectively, as the voltage changed from 5 V to 11 V. PY-1 device exhibited power efficiency of 1.1 lmW^{-1}. The PY-2 device exhibited a power efficiency of	118

	0.06 lmW^{-1} at 8 V, with turn-on voltage of 5 V and C.I.E. coordinates of (0.31, 0.54) at 7 V. Whereas, the PY-3 device exhibited a power efficiency of 0.27 lmW^{-1}, turn-on voltage of 3 V and C.I.E. coordinates of (0.36, 0.56) at 7 V.	
13	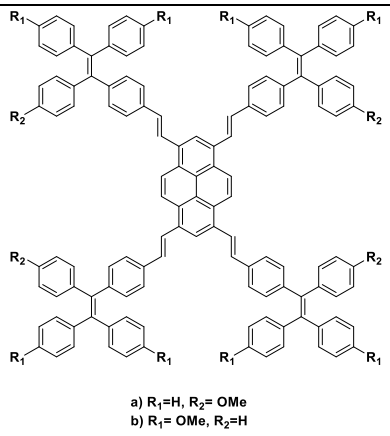 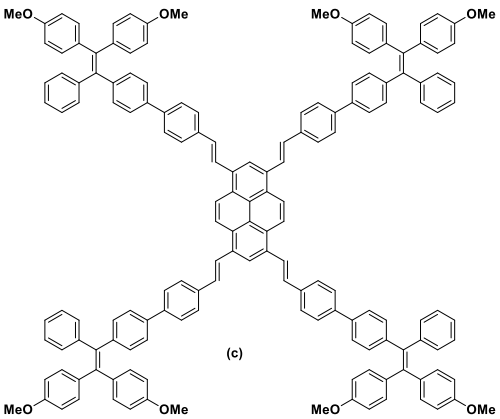 A series of planar–vinyl–rotor configured molecules employing two different chromophoric units, such as, pyrene and tetraphenylethylene linked *via* vinyl/phenylvinyl bonds was reported by Jana and coworkers.[119] The vinyl spacer mono-branched compound was found to be aggregation induced emission (AIE) active. Vinyl spacer incorporated compounds were found to be AIE inactive, but their fluorescence quantum yield was good in both solution (0. 63) phase and in the aggregated state (0.43). Phenylvinyl spacer incorporated compounds emitted light strongly in solution (0.92), but not in the aggregated state (0.8).	119
14	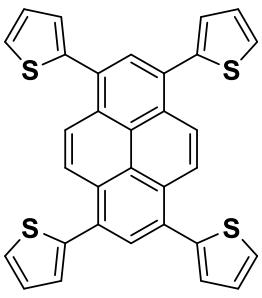 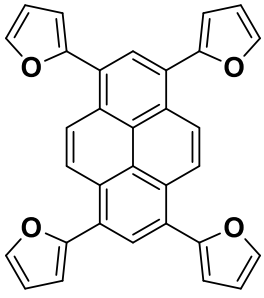 In 2015, two 1,3,6,8-tetrasubstituted pyrene derivatives bearing thienyl and furyl substituents were synthesized.[120] The fluorescence quantum yield of tetrathienyl and tetrafuryl derivative was found to be 0.22 and	120

	0.68, respectively. Replacement of the thiophene by furan increased the fluorescence quantum yield, most likely due to the more planar structure of the former allowing for an efficient contribution of the π-electrons. OLED devices fabricated by using thienyl and furyl derivatives of pyrene exhibited blue light at 12 V and yellow light at 24 V, respectively.	
15	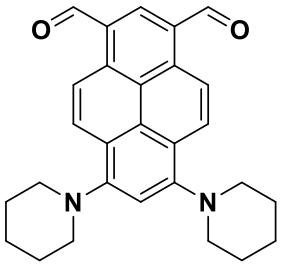 1, 3, 6, 8- Tetrasubstituted asymmetric pyrene derivatives bearing electron donor and acceptor moieties as substituents were . reported, together with examination of their photophysical properties by Niko and coworkers.[121] Pyrene derivative with two formyl groups at the 1- and 3-positions and two piperidyl groups at the 6- and 8 positions exhibited less pronounced solvatochromism, but displayed a narrow fluorescent band with high fluorescence yield in different organic solvents (> 0.75) with highest value (0.94) in toluene with their promising application in non linear optical materials such as two photon active fluorophore.	121
16	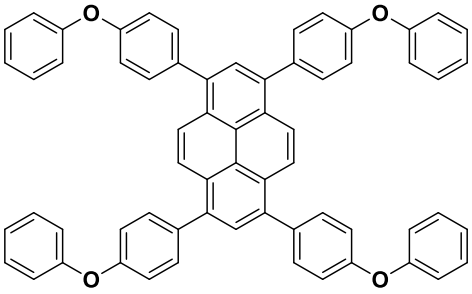 In 2016, Assad and co workers[122] reported a 1,3,6,8-tetrasubstituted pyrene derivative and its optical properties, emission lifetime and solvatochromatism was studied. The substituted pyrene derivative exhibited positive solvatochromic behavior. OLED device was fabricated using the pyrene derivative as the emissive layer. 1,3,6,8-Tetrakis(4-	122

	phenoxyphenyl)pyrene based OLED device exhibited blue electroluminescence coupled with impressively low turn-on voltage of 2.8 V and maximum luminescence of 13,542 cdm^{-2} at 8.2 V.	
17	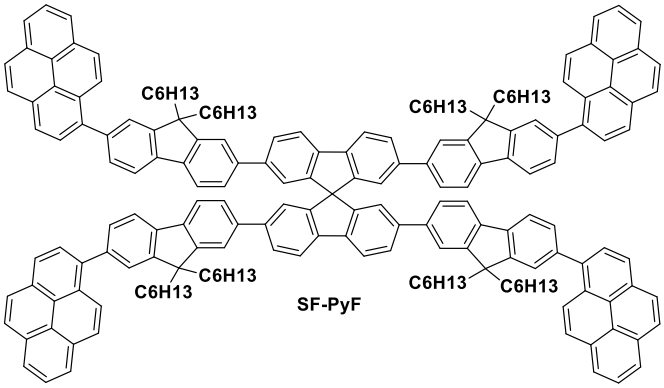 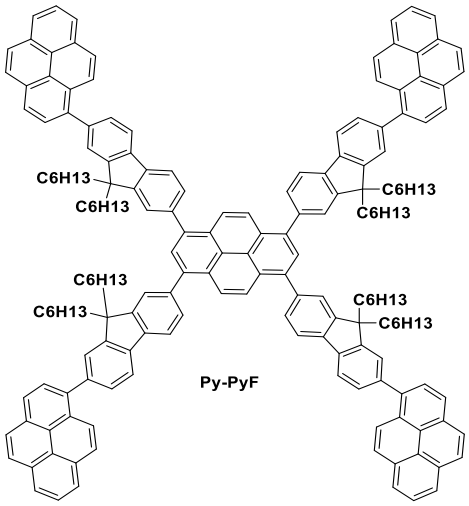 A set of pyrene-capped starburst organic emitters composed of non-planar cross-shaped spirofluorene core (SF-PyF) and a large rigid planar pyrene core (Py-PyF) were reported by Yi and coworkers.[123] The PL quantum yields (PLQY) were observed to be 0.71 and 0.85 for SF-PyF and Py-PyF, respectively, in dilute solutions. In the film state, the PLQY values of 0.62 (SF-PyF) and 0.74 (Py-PyF) still remained quite high, suggesting efficient emissive properties in the condensed state for both the samples.The molecules were found to be promising for the application in organic lasers.	123

18	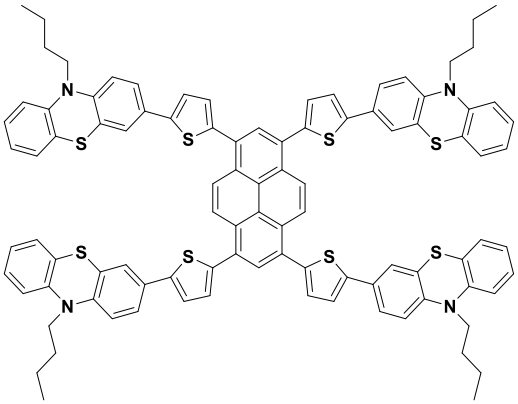 A series of thienylphenothiazine-integrated pyrene was prepared *via* Stille coupling reactions by Konidena and coworkers.[124] All the molecules exhibited positive solvatochromism in the emission spectra, whereas their absorption profiles were insensitive to solvent polarity, indicating more polarized excited state of the molecules. Solution processable multilayer OLED device was fabricated by using 1,3,6,8- tetrasubstituted pyrene derivative either as host emitters or dopants in the CBP host matrix and found to exhibit decent device performances. The OLED device exhibited power efficiency of 1.5 lmW^{-1} at driving voltage of 7.1 V, current efficiency 3.4 cdA^{-1}, CIE chromaticity coordinates of (0.37, 0.50) and maximum luminescence of 2402 cdm^{-2}. The device exhibited external quantum efficiency of 1.1%.	124
19	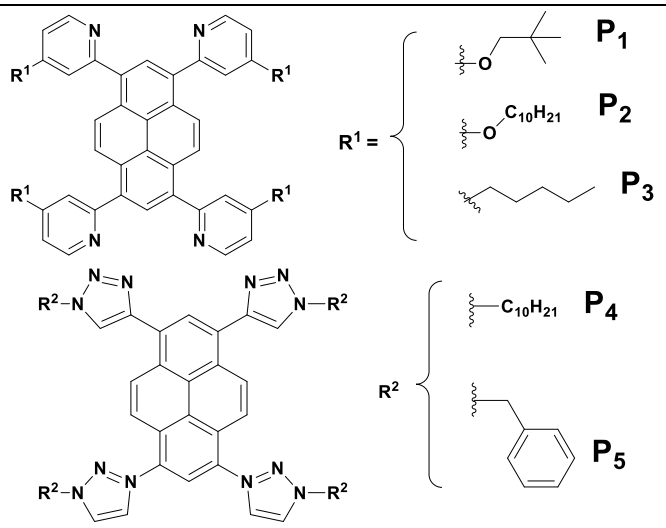	125

	Zych and coworkers reported five pyrene derivatives substituted at 1,3,6,8 positions containing different moieties attached to pyrene core.[125] All the derivatives exhibited high photoluminescence quantum yield (approximately 0.75) in solution; however very low PLQY in the range 0.03-0.09 was observed in thin films. Effect of different substitutions over the electroluminescenct properties was studied. Diodes prepared with single-layer and guest–host configurations emitted light with λ_{EL} ranging from 468 to 642 nm, depending on the compound and device structure. Preliminary electroluminescence tests indicated that (**P4**) was the most promising for potential applications in OLED technology.	
20	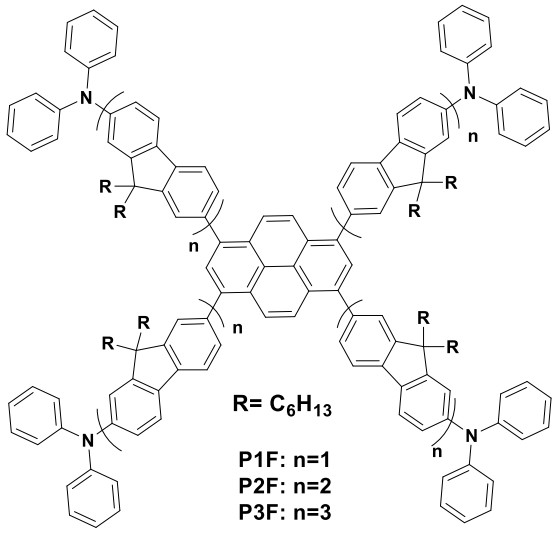 A series of starburst conjugated molecules composed of a pyrene core and diphenylamine end-cappers with various oligofluorene bridge lengths attached at 1,3,6,8-positions namely, P1F, P2F and P3F, were reported by Zhang and coworkers in 2017.[126] The effects of diphenylamine moieties as end cappers on the optoelectronic properties were studied. The PL spectra were found to be blue shifted along with increase in conjugation length. The non doped blue OLEDs were fabricated by solution processing of pyrene derivatives as emissive layer in the device. P1F based device exhibited a maximum luminescence (L_{max}) of 45l6 cdm^{-2} at 9.0 V, a maximum luminescence efficiency (LE_{max}) of 3.9 cdA^{-1}, a	126

	maximum power efficiency (PE_{max}) of 1.8 lm W^{-1} and EQE of 1.52% The performance of P2F device was much better with an L_{max} of 8923 cdm^{-2} at 10.3 V, an LE of 4.1 cdA^{-1} ,a PE_{max} of 2.1 lmW^{-1} and an EQE of 2.27%, whereas the best EL performance was observed for P3F device with a L_{max} of 12057cdm^{-2} at 8.7 V, an LE_{max} of 5.7 cd A^{-1}, a PE_{max} of 4.8 lmW^{-1}, and EQE of 3.36%.	
21	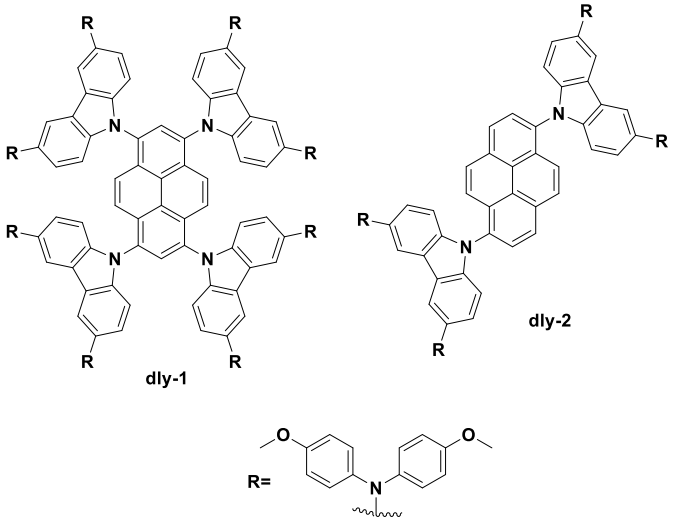 Recently, Li and coworkers reported 1,3,6,8-tetrasubstituted pyrene with carbazole and triphenylamine substituents.[127] The pyrene derivatives dly-1 and dly-2 were used as HTMs for perovskite solar cell. The perovskite solar cell with dly-1 as HTM exhibited power conversion efficiency of 17.19% whereas the solar cell with dly-2 exhibited PCE of 18.23%. Both materials exhibited the PCEs comparable to that of spiro-OMeTAD based solar cell (19.59%)	127

1.3) Charge transport in organic semiconductors

As discussed in the section 1.1, depending upon the conductivity, the materials can be categorized as conductors, semiconductors and insulators. The differences in their conduction properties arise due to the energy gap between conduction band and valence band of material.[1] In case of conjugated organic compounds, the HOMO-LUMO energy levels are similar to the valence band- conduction band in inorganic materials. In insulators, there exists a large energy gap (Eg > 4) between the energies of the valance band (HOMO) and conduction band (LUMO), so that insulators are unable to conduct charges or electricity. On the other hand, there is no band

gap existing in conductors (metal) due to overlapping of the VB and CB, so that a fraction of electrons/charges can easily move through the material (e.g. copper). The semiconductors have properties between conductor and insulator due to accessible energy gap (Eg < 3) between VB and CB and which enables transport of charges under certain conditions. [128]

In the crystalline inorganic semiconductors, atoms are perfectly aligned in a lattice allowing for good orbital overlap between neighboring atoms and an associated delocalization of the electronic states throughout the material.[129,130] In such materials charges are transported by band-like motion and the mobility is very high. In case of inorganic semiconductors like Si or Ge the charge carrier mobility of the order of 10^3 is observed. However, in case of organic semiconductors, the molecules interact through Van der Waals forces [131] which limit their charge carrier mobility. Since organic conjugated materials are typically disordered, unlike the band transport in inorganic materials, the charge carriers in organic compounds are mostly localized over a single molecule and charge transport between the molecules occur *via* a hopping mechanism. [132] The transfer rate is dependent mainly on the energy barrier, electric field applied and the distance between the sites. [4] [133] The phenomenon of hopping transport is usually observed in amorphous organic solids and is the dominant model for the intermolecular transport in organic semiconductors. In hopping model, the charge carriers need to overcome an energy barrier to move from one molecule to the next and the mobility values of the charge carriers are just of the order of $10^{-6} \sim 10^{-3}$ $cm^2V^{-1}s^{-1}$ [134,135]

Intrinsic charge carrier mobility of organic compounds is one of the most important parameters which plays crucial role to decide high efficiency of optoelectronic devices. Hence the performance of organic semiconductors is often evaluated by their charge carrier mobility. For example, lower turn on voltage is required for the OLEDs based on the materials with high mobility [136] Also if the hole and electron mobilities of emissive layer are similar then it prevents the formation of space charges near the electrodes and helps to improve the external quantum efficiency of device. In OFETs, the source and drain current is directly proportional to charge carrier mobility, as well as the charge carrier mobility directly affects the switching of OFETs [137] In organic solar cell, higher charge carrier mobility of organic material facilitates better charge carrier extraction at electrodes and reduces the charge carrier recombination which eventually leads to increase in current.[136,138] Hence, it is highly essential to study the charge carrier mobility as well as nature of charge transport (holes and electrons) in the organic semiconductors. Charge

carrier mobility of organic semiconductor can be measured by using instrumental techniques such as OFET,[139] time of flight (TOF),[140] space-charge limited current (SCLC),[141] pulse-radiolysis time resolved microwave conductivity (PR-TRMC)[142] and impedance spectroscopy.[143]

In this dissertation, the charge carrier properties of organic semiconductors have been studied by using the method of impedance spectroscopy. The impedance spectroscopy is mainly categorized as electrochemical impedance spectroscopy (EIS) and non electrochemical impedance spectroscopy (IS).[143] EIS is useful for the measurements and analysis of the materials in which ionic conduction predominates e.g. liquid electrolytes in fuel cells, rechargeable batteries, etc. The other type of impedance spectroscopy i.e. 'IS' is applied for the study of dielectric materials i.e. the materials whose electrical characteristics involve dipolar rotation and the materials with predominant electric conduction e.g. single crystal or amorphous semiconductors. In this method, normally impedance is measured directly in the frequency domain by applying a modulation signal (single-frequency voltage) to the interface and measuring the phase shift and amplitude, or real and imaginary parts of the resulting current at that frequency. In the impedance spectroscopy, if capacitance is measured as the function of frequency under a specific bias voltage, the measurement is called capacitance-frequency (C-f) spectroscopy, whereas it is called capacitance-voltage (C-V) measurement when capacitance is measured as the function of bias voltage at a specific frequency. To fit the C-f curve well, distributed impedance elements e.g. constant phase elements (CPEs), are always used to replace the ideal circuit elements (capacitors, resistors, etc.) in the circuit model due to a distribution of energy states or a spatially distributed conductivity of organic materials.

Phenothiazine-based small organic molecules along with their hole mobility values are compiled in **Table 1.2**

Table 1.2: Phenothiazine-based small molecules and their mobility

Sr. No.	Phenothiazine-based small organic molecules	Ref. No.
1.	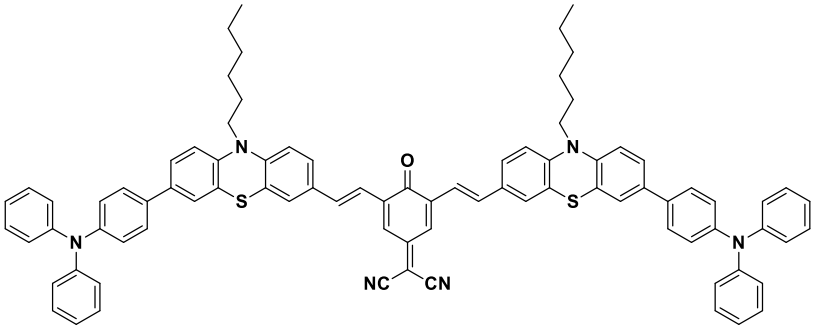 **APPM** A phenothiazine-based small organic molecule containing triphenylamine and 2-pyran-4-ylidenemalononitrile entities was synthesized by Li and coworkers.[144] The small molecule, namely, APPM exhibited hole mobility of the order of 7.91×10^{-6} $cm^2V^{-1}S^{-1}$ (by SCLC method). The bulk heterojunction (BHJ) solar cell fabricated by using APPM:PCBM as the blend exhibited fairly low power conversion efficiency of 0.65% which was attributed to the low charge carrier mobility of APPM.	144
2	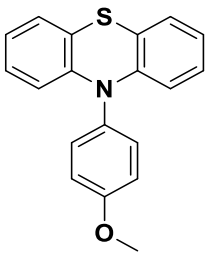 **APS** A phenothiazine based solution processable small molecule, namely, 4-phenothiazin-10-yl-anisole (APS) was reported by Huang and coworkers.[145] Hole mobility of APS was measured by SCLC method and was found to be 7.6×10^{-5} $cm^2V^{-1}S^{-1}$ for spin coated film (sAPS) while mobility of 3.1×10^{-4} $cm^2V^{-1}S^{-1}$ was exhibited by thermally annealed film (tAPS). APS was used as an efficient hole collection layer in OSCs and the device exhibited power conversion efficiency of 3.56%. APS based device also exhibited much better stability under ambient conditions in comparison to the conventional devices.	145

	The APS containing OSC exhibited efficiency of 2.83% after 2400 h of durability in air without encapsulation as compared to PEDOT: PSS based device which almost lost its efficiency after 2400 h under atmospheric exposure.	
3	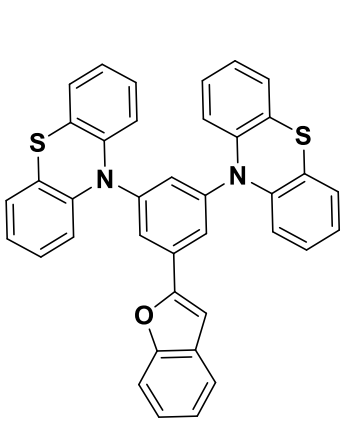 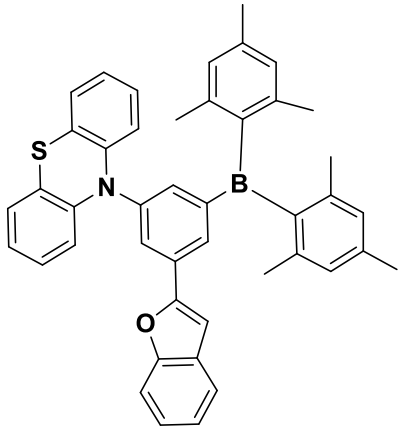 **C-PhOL** **C-PhMesOL** In 2016, Tsai and coworkers[146] synthesized benzofuranyl benzene-based small molecules incorporating phenothiazinyl entity. The compounds exhibited bipolar transport characteristics. C-phOL exhibited hole mobility of 7.5×10^{-5} $cm^2V^{-1}S^{-1}$ and electron mobility of 19×10^{-5} $cm^2V^{-1}S^{-1}$ whereas C-PhMesOL showed hole mobility of 25×10^{-5} $cm^2V^{-1}S^{-1}$ and electron mobility of 36×10^{-5} cm^2 $V^{-1}S^{-1}$. An OLED device was fabricated using C-PhMesOL as an emissive layer. The device exhibited turn-on voltage of 3.4 V, maximum brightness 1340 cd m^{-2}, CIE coordinates (0.48, 0.49), power efficiency 5.19 lmW^{-1}, current efficiency 7.36 cdA^{-1} and external quantum efficiency of 3.14%.	146

1.4) Summary

This chapter highlighted the versatility of organic semiconductor technology, its importance to the modern world as well as utility of organic semiconductors as a class of materials that offer much of the same functionality as conventional inorganic semiconductors, together with many advantages in terms of flexibility and low cost processing. Evolution of field of organic electronics, in particular the OLEDs has been discussed in detail. The development of OLEDs from the pioneering work of Tang and Van Slyke to the state- of- the- art multilayer OLEDs along with their advantages and shortcomings have been briefed. In the array of different chromophores, pyrene is the most promising due to its high luminescence, charge carrier mobility and thermal stability. However, excimer formation tendency of pyrene hampers the overall performance of pyrene based OLEDs. Introduction of substituents on pyrene core helps to overcome this problem along with improvement in the luminescence properties. Earlier reports on pyrene based molecules with this strategy have been discussed.

The charge carrier mobility of organic semiconductors is of paramount importance for improving the overall performance of organic materials for optoelectronic applications. The method of impedance spectroscopy for evaluation of charge carrier mobility of organic materials has been discussed.

1.5) References

1. M. Grundmann, *The Physics of Semiconductors: An Introduction Including Nanophysics and Applications*, Springer, New York, 3rd edn, 2015.
2. W. Brutting, *Physics of Organic Semiconductors*, John Wiley & Sons, New Jersey, 2006.
3. R. T. Morrison and R. N. Boyd, *Study Guide to Organic Chemistry*, Allyn and Bacon, Harvard,18th ed., 1975.
4. J. Shinar and V. Savvateev, in *Organic Light-Emitting Devices*, Springer, New York, 2004, pp. 1-41.
5. J.I. Aihara, *J. Phys. Chem. A*, 1999, **103**, 7487.
6. H. Akamatu, H. Inokuchi and Y. Matsunaga, *Nature*, 1954, **173**, 168.
7. H. Shirakawa, E. I. Louis, A. G. MacDiarmid and C. K. Chiang, *Chem. Commun.*, 1977, **16**, 578.
8. N. T. Kalyani and S. J. Dhoble, *Renew. Sust. Energ. Rev.*, 2012, **16**, 2696.
9. B. Kippelen and J.-L. Bredas, *Energ. Environ. Sci.*, 2009, **2**, 251.

10. W. Wu, Y. Liu and D. Zhu, *Chem. Soc. Rev.*, 2010, **39**, 1489.
11. S. Chenais and S. Forget, *Polym. Int.*, 2012, **61**, 390.
12. J.T. Wang, S. Takashima, H.C. Wu, Y.C. Chiu, Y. Chen, T.Isono, T. Kakuchi, T. Satoh and W.C. Chen, *Adv. Funct. Mater*. 2016, **26**, 2695.
13. C. Adachi, M. A. Baldo, M. E. Thompson and S. R. Forrest, *J. Appl. Phys.*, 2001, **90**, 5048.
14. H. J. Round, *Elect.World*, 1907, **49**, 309.
15. N. Holonyak Jr and S. F. Bevacqua, *Appl. Phys. Lett.*, 1962, **1**, 82.
16. A. Bernanose, M. Comte and P. Vouaux, *J. Chim. Phys*, 1953, **50**, 64.
17. A. Bernanose, *J. Chem. Phys.*, 1955, **52**, 396.
18. H. Kallmann and M. Pope, *Nature*, 1960, **186**, 31.
19. M. Pope, H. P. Kallmann and P. Magnante, *J. Chem. Phys.*, 1963, **38**, 2042.
20. W. Helfrich and W. G. Schneider, *Phys. Rev. Lett.*, 1965, **14**, 229.
21. R.H.Partridge, *Polymer,* 1983, **24**,733.
22. U. Mitschke and P. Bauerle, *J. Mater. Chem.,* 2000, **10**, 1471.
23. D. F. Williams and M. Schadt, *J. Chem. Phys.*, 1970, **53**, 3480.
24. P. S. Vincett, W. A. Barlow, R. A. Hann and G. G. Roberts, *Thin solid films*, 1982, **94**, 171.
25. C. W. Tang and S. A. VanSlyke, *Appl. Phys. Lett.*, 1987, **51**, 913.
26. J. H. Burroughes, D. D. C. Bradley, A. R. Brown, R. N. Marks, K. Mackay, R. H. Friend, P. L. Burns and A. B. Holmes, *Nature,* 1990, **347**, 539.
27. M. A. Baldo, D. F. O'Brien, Y. You, A. Shoustikov, S. Sibley, M. E. Thompson and S. R. Forrest, *Nature*, 1998, **395**, 151.
28. H.-W. Chen, J. H. Lee, B.Y. Lin, S. Chen and S.T. Wu, *Light: Sci. Appl.*, 2017, **7**, 17168.
29. H.W. Chen, J.H. Lee, B.Y. Lin and S. Chen, *Light Sci. Appl.*, 2018, **7**, 17168
30. M. Koden, *OLED Displays and Lighting*, John Wiley and Sons, 2016.
31. S. R. Forrest, *Org. Electro.*, 2003, **4**, 45.
32. T.L. Wu, C.-H. Yeh, W.-T. Hsiao, P.Y. Huang, M.-J. Huang, Y.H. Chiang, C.H. Cheng, R.-S. Liu and P.-W. Chiu, *ACS Appl. Mater. Interfaces*, 2017, **9**, 14998.
33. H.Kim, J.S.Horwitz, W.H.Kim, A.J.Makinen, Z.H.Kafafi and D.B.Chrisey, *Thin Solid Films,* 2002, **420**,539.

34. T. Nagatomo, Y. Maruta and O. Omoto, *Thin solid films*, 1990, **192**, 17-25.
35. S. E. Shaheen, G. E. Jabbour, M. M. Morrell, Y. Kawabe, B. Kippelen, and N. Peyghambarian, *J. Appl. Phys.*,1998, **84**, 2324.
36. L. Niu and Y. Guan, P*hys. Status Solidi A*, 2010, **207**, 993-997.
37. H. Ishii, K. Sugiyama, E. Ito and K. Seki, *Adv. Mater.*, 1999, **11**, 605-625.
38. V. E. Choong, Y. Park, Y. Gao, B. R. Hsieh and C. W. Tang, *Macromol. Symp.*, 1998.
39. S. A. Choulis, V.-E. Choong, M. K. Mathai and F. So, *Appl. Phys. Lett.*, 2005, **87**, 113503.
40. Z. B. Wang, M. G. Helander, J. Qiu, D. P. Puzzo, M. T. Greiner, Z. W. Liu and Z. H. Lu, *Appl. Phys. Lett.*, 2011, **98**, 39.
41. Z. T. Xie, W. H. Zhang, B. F. Ding, X. D. Gao, Y. T. You, Z. Y. Sun, X. M. Ding and X. Y. Hou, *Appl. Phys. Lett.*, 2009, **94**, 40.
42. P. Piromreun, H. Oh, Y. Shen, G. G. Malliaras, J. C. Scott and P. J. Brock, *Appl. Phys. Lett.*, 2000, **77**, 2403-2405.
43. N. Peyghambarian and R. A. Norwood, *Opt. Photonics News*, 2005, **16**, 28-33.
44. C. Adachi, K. Nagai and N. Tamoto, *Appl. Phys. Lett.*, 1995, **66**, 2679.
45. D. Mutaguchi, K. Okumoto, Y. Ohsedo, K. Moriwaki and Y. Shirota, *Org. Electron.*, 2003, **4**, 49.
46. A. P. Kulkarni, C. J. Tonzola, A. Babel and S. A. Jenekhe, *Chem. Mater.*, 2004, **16**, 4556.
47. C. H. Chen and J. Shi, *Coord.Chem. Rev.*, 1998, **171**, 161.
48. Junji Kido *and* Yasuhiro Iizumi, *Appl. Phys. Lett.* 1998, **73**, 2721.
49. A. B. Chwang, M. A. Rothman, S. Y. Mao, R. H. Hewitt, M. S. Weaver, J. A. Silvernail, K. Rajan, M. Hack, J. J. Brown and X. Chu, *Appl. Phys. Lett.*, 2003, **83**, 413.
50. P. Broms, J. Birgersson, N. Johansson, M. Logdlund and W. R. Salaneck, *Synth. Met.*, 1995, **74**, 179.
51. J. Eccher, W. Zajaczkowski, G. r. C. Faria, H. Bock, H. Von Seggern, W. Pisula and I. H. Bechtold, *ACS Appl. Mater. Interfaces*, 2015, **7**, 16374.
52. T. Tsujimura, *OLED Display Fundamentals and Applications*, John Wiley & Sons, 2017.
53. M. Granstrom and O. Inganas, *Appl.Phys. Lett.*, 1996, **68**, 147.
54. K.-H. Kim, S.-Y. Huh, S.-m. Seo and H. H. Lee, *Appl. Phys. Lett*, 2008, **92**, 76.

55. C. D. Muller, A. Falcou, N. Reckefuss, M. Rojahn, V. R. Wiederhirn, P. Rudati, H. Frohne, O. Nuyken, H. Becker and K. Meerholz, *Nature*, 2003, **421**, 829.
56. Z.Teruaki, H. S. Ando, M. Ueda , T. Akiike, H. Miyamoto, T. Kajita and M. Kakimoto, *Adv. Funct. Mater.*, 2008, 18, 584.
57. V. A. Montes, G. Li, R. Pohl, J. Shinar and P. Anzenbacher Jr, *Adv.Mater.*, 2004, **16**, 2001.
58. M. C. Gather, A. Kohnen and K. Meerholz, *Adv. Mater.*, 2011, **23**, 233.
59. W. L. Barnes, *J. Mod. Opt.*, 1998, **45**, 661.
60. J. A. E. Wasey and W. L. Barnes, *J. Mod. Opt.*, 2000, **47**, 725.
61. H. Becker, S. E. Burns and R. H. Friend, *Phys. Rev. B*, 1997, **56**, 1893.
62. C. Adachi, T. Tsutsui and S. Saito, *Appl. Phys. Lett.*, 1990, **57**, 531.
63. R. Shediac, M. H. B. Gray, H. T. Uyeda, R. C. Johnson, J. T. Hupp, P. J. Angiolillo and M. J. Therien, *J. Am. Chem. Soc.*, 2000, **122**, 7017.
64. D. Frackowiak, *J. Photochem. Photobiol. B: Biology*, 1988, **2**, 399.
65. M. A. Baldo, M. E. Thompson and S. R. Forrest, *Pure Appl. Chem.*, 1999, **71**, 2095.
66. K. Haskins-Glusac, M. R. Pinto, C. Tan and K. S. Schanze, *J. Am. Chem. Soc.*, 2004, **126**, 14964.
67. L. Basabe-Desmonts, D. N. Reinhoudt and M. Crego-Calama, *Chem. Soc. Rev.*, 2007, **36**, 993-1017.
68. Y. Tao , C. Yang and Jingui Qin, *Chem. Soc. Rev.*, 2011, **40**, 2943.
69. T. Smith and J. Guild, *Trans.Opt. Soc.*, 1931, **33**, 73.
70. J. N. Bardsley, *IEEE J. Sel.Top.Quantum Electron.*, 2004, **10**, 3.
71. B. Geffroy, P. Le Roy and C. Prat, *Polym. Int.*, 2006, **55**, 572.
72. W. Song and J. Y. Lee, *Adv. Opt. Mater.*, 2017, **5**, 1600901
73. Y. Liu, X. Tao, F. Wang, X. Dang, D. Zou, Y. Ren and M. Jiang, *J.Phys. Chem. C*, 2008, **112**, 3975.
74. G. Qian, B. Dai, M. Luo, D. Yu, J. Zhan, Z. Zhang, D. Ma and Z. Y. Wang, *Chem. Mater.*, 2008, **20**, 6208.
75. H. Li, X. Zhang, Z. Chi, B. Xu, W. Zhou, S. Liu, Y. Zhang and J. Xu, *Org. Lett.*, 2011, **13**, 556.
76. M. Wang, X. Gu, G. Zhang, D. Zhang and D. Zhu, *Anal. Chem.*, 2009, **81**, 4444.

77. A. Laurent, *Ann. Chim*, 1837, **66**, 136.
78. C. Graebe, *Justus Liebigs Ann. Chem.*, 1871, **158**, 285.
79. P. C. Bevilacqua, R. Kierzek, K. A. Johnson and D. H. Turner, *Science*, 1992, **258**, 1355.
80. W.L. Jia, T. McCormick, Q.D. Liu, H. Fukutani, M. Motala, R.Y. Wang, Y. Tao and S. Wang, *J. Mater. Chem.*, 2004, **14**, 3344.
81. F. M. Winnik, *Chem.Rev.*, 1993, **93**, 587-614.
82. M. Goedeweeck, M. Van der Auweraer and F. C. De Schryver, *J. Am. Chem. Soc.*, 1985, **107**, 2334.
83. D. Sahoo, V. Narayanaswami, C. M. Kay and R. O. Ryan, *Biochemistry*, 2000, **39**, 6594.
84. P. L. Paris, J. M. Langenhan and E. T. Kool, *Nucleic Acids Res.*, 1998, **26**, 3789.
85. G. Tong, J. M. Lawlor, G. W. Tregear and J. Haralambidis, *J. Am. Chem. Soc.*, 1995, **117**, 12151.
86. M. Ollmann, G. Schwarzmann, K. Sandhoff and H. J. Galla, *Biochemistry*, 1987, **26**, 5943.
87. T. V. Kurzchalia and R. G. Partan, *Curr .Opin. Cell Biol.*, 1999, **11**, 424-431.
88. J. B. Birks, M. D. Lumb, I. H. Munro and B. H. Flowers, *Proc. R. Soc. Lond. A*, 1964, **280**, 289.
89. R. H. Templer, S. J. Castle, A. R. Curran, G. Rumbles and D. R. Klug, *Faraday Discuss.*, 1999, **111**, 41.
90. M. R. Pokhrel and S. H. Bossmann, *J. Phys. Chem. B*, 2000, **104**, 2215.
91. T. M. Figueira-Duarte and K. Mullen, *Chem.Rev.*, 2011, **111**, 7260.
92. H. Jung, S. Kang, H. Lee, Y.-J. Yu, J. H. Jeong, J. Song, Y. Jeon and J. Park, *ACS Appl. Mater. Interfaces*, 2018, **10**, 30022.
93. H. Vollmann, H. Becker, M. Corell and H. Streeck, *Justus Liebigs Ann. Chem.*, 1937, **531**, 1.
94. L. Altschuler and E. Berliner, *J. Am. Chem. Soc.*, 1966, **88**, 5837.
95. M. J. S. Dewar and R. D. Dennington, *J. Am. Chem. Soc.*, 1989, **111**, 3804.
96. M. J. S. Dewar and R. D. Dennington, *J. Am. Chem. Soc*. 1989, **111**, 3804.
97. A. Miyazawa, T. Yamato and M. Tashiro, *Chem. Express.*, 1990, **5**, 381.
98. B. Bodenant, T. Weil, M. Businelli-Pourcel, F. Fages, B. Barbe, I. Pianet and M. Laguerre, *J.Org. Chem.*, 1999, **64**, 7034.

99. S. Bernhardt, M. Kastler, V. Enkelmann, M. Baumgarten and K. Mullen, *Chem. Eur. J.*, 2006, **12**, 6117.

100. G. Sathiyan, E. K. T. Sivakumar, R. Ganesamoorthy, R. Thangamuthu and P. Sakthivel, *Tetrahedron Lett.*, 2016, **57**, 243.

101. J.-X. Yang, X.-T. Tao, C. X. Yuan, Y. X. Yan, L. Wang, Z. Liu, Y. Ren and M. H. Jiang, *J. Am. Chem. Soc.*, 2005, **127**, 3278.

102. R. M. Adhikari, R. Mondal, B. K. Shah and D. C. Neckers, *J. Org. Chem.*, 2007, **72**, 4727.

103. B. Basheer, D. Mathew, B. K. George and C. P. R. Nair, *Solar Energy*, 2014, **108**, 479.

104. W. Wu, J. Yang, J. Hua, J. Tang, L. Zhang, Y. Long and H. Tian, *J. Mater. Chem.*, 2010, **20**, 1772.

105. I. B. Berlman, *J. Phys. Chem.*, 1970, **74**, 3085.

106. W. Sotoyama, H. Sato, M. Kinoshita, T. Takahashi, A. Matsuura, J. Kodama, N. Sawatari and H. Inoue, SID Symposium Digest of Technical Papers, 2003.

107. T. Oyamada, H. Uchiuzou, S. Akiyama, Y. Oku, N. Shimoji, K. Matsushige, H. Sasabe and C. Adachi, *J. Appl. Phys.*, 2005, **98**, 074506.

108. G. Venkataramana and S. Sankararaman, *Eur. J. Org. Chem.*, 2005, **2005**, 4162.

109. A. Hayer, V. r. De Halleux, A. Kohler, A. El-Garoughy, E. W. Meijer, J. Barbera, J. Tant, J. Levin, M. Lehmann and J. Gierschner, *J.Phys. Chem. B*, 2006, **110**, 7653.

110. G. Venkataramana and S. Sankararaman, *Org. Lett.*, 2006, **8**, 2739.

111. J. N. Moorthy, P. Natarajan, P. Venkatakrishnan, D.-F. Huang and T. J. Chow, *Org. Lett.*, 2007, **9**, 5215.

112. M. Gingras, V. Placide, J. M. Raimundo, G. Bergamini, P. Ceroni and V. Balzani, *Chem. Eur. J.*, 2008, **14**, 10357.

113. H. M. Kim, Y. O. Lee, C. S. Lim, J. S. Kim and B. R. Cho, *J. Org. Chem.*, 2008, **73**, 5127.

114. P. Sonar, M. S. Soh, Y. H. Cheng, J. T. Henssler and A. Sellinger, *Org. Lett.*, 2010, **12**, 3292.

115. Z.-Q. Liang, Y.-X. Li, J.-X. Yang, Y. Ren and X.-T. Tao, *Tetrahedron Lett.*, 2011, **52**, 1329.

116. K. R. J. Thomas, N. Kapoor, M. N. K. P. Bolisetty, J.-H. Jou, Y.-L. Chen and Y.-C. Jou, *J. Org. Chem.*, 2012, **77**, 3921.

117. Z. Chang, S. Ye, B. He, Z. Bei, L. Lin, P. Lu, B. Chen, Z. Zhao and H. Qiu, *Chem. Asian J.*, 2013, **8**, 444.

118. J. K. Salunke, P. Sonar, F. L. Wong, V. A. L. Roy, C. S. Lee and P. P. Wadgaonkar, *Phys. Chem. Chem. Phys.*, 2014, **16**, 23320.

119. D. Jana, S. Boxi, P. P. Parui and B. K. Ghorai, *Org. Biomo. Chem.*, 2015, **13**, 10663.

120. K. R. Idzik, W. Kuznik, J. Frydel, T. Licha and T. Ratajczyk, *Phys. Chem. Chem. Phys.*, 2015, **17**, 22758.

121. Y. Niko, S. Sasaki, K. Narushima, D. K. Sharma, M. Vacha and G.I. Konishi, *J.Org. Chem.*, 2015, **80**, 10794.

122. T. H. El-Assaad, M. Auer, K. M. Hallal, F. M. Jradi, L. Mosca, R. S. Khnayzer, D. Patra, T. V. Timofeeva and J.-L. Bredas, *J. Mater. Chem. C*, 2016, **4**, 3041.

123. J.-P. Yi, L. Zhao, W. Xu, C.-F. Liu, W.-Y. Lai and W. Huang, *J. Mater. Chem. C*, 2016, **4**, 7546.

124. R. K. Konidena, K. R. J. Thomas, M. Singh and J.-H. Jou, *J. Mater. Chem. C*, 2016, **4**, 4246.

125. D. Zych, A. Kurpanik, A. Slodek, M. Matussek, S. A. Krompiec, E. Schab□Balcerzak and S. Kotowicz, *Chem.Eur.J.*, 2017, **23**, 15746.

126. H. Zhang, T.-T. Lu, W.-Y. Lai, X.-W. Zhang, M.-K. Zhang, P. Lv, C.-F. Liu and W. Huang, *J. Phys. Chem. C*, 2017, **121**, 27569.

127. D. Li, J.-Y. Shao, Y. Li, Y. Li, L.-Y. Deng, Y.-W. Zhong and Q. Meng, *Chem. Commun.*, 2018, **54**, 1651.

128. F. Capasso, *Science*, 1987, **235**, 172.

129. N. W. Ashcroft and N. D. Mermin, *Stamford, CT*, 1976.

130. S. M. Sze and K. K. Ng, *Physics of Semiconductor Devices*, John wiley & sons, 2006.

131. N. Nerngchamnong, L. Yuan, D.C. Qi, J. Li, D. Thompson and C. A. Nijhuis, *Nature Nanotechnology*, 2013, **8**, 113.

132. A. J. Campbell, D. D. C. Bradley and H. Antoniadis, *Appl. Phys. Lett.*, 2001, **79**, 2133-2135.

133. J. D. Wright, *Molecular Crystals.*, Cambridge University Press, 2 nd ed., 1995.

134. P. W. M. Blom, M. J. M. De Jong and M. G. Van Munster, *Phys. Rev. B*, 1997, **55**, R656.

135. H. Sirringhaus, N. Tessler and R. H. Friend, *Science*, 1998, **280**, 1741-1744.

136. V. Coropceanu, J. r. m. Cornil, D. A. da Silva Filho, Y. Olivier, R. Silbey and J.-L. Bredas, *Chem. Rev.*, 2007, **107**, 926-952.

137. M. M. Mandoc, L. J. A. Koster and P. W. M. Blom, *Appl. Phys. Lett.*, 2007, **90**, 133504.

138. S. Yoshikawa, A. Saeki, M. Saito, I. Osaka and S. Seki, *Phys. Chem. Chem. Phys.*, 2015, **17**, 17778.

139. S. Allard, M. Forster, B. Souharce, H. Thiem and U. Scherf, *Angew. Chem. Int. Ed.*, 2008, **47**, 4070.

140. Z. B. Wang, M. G. Helander, M. T. Greiner, J. Qiu and Z.-H. Lu, *J. Appl. Phys.*, 2010, **107**, 034506.

141. C. W. Struijk, A. B. Sieval, J. E. J. Dakhorst, M. van Dijk, P. Kimkes, R. B. M. Koehorst, H. Donker, T. J. Schaafsma, S. J. Picken and A. M. van de Craats, *J. Am. Chem. Soc.*, 2000, **122**, 11057.

142. A. M. Van de Craats, J. M. Warman, P. Schlichting, U. Rohr, Y. Geerts and K. Mullen, *Synth. Met.*, 1999, **102**, 1550.

143. J.R. MacDonald, *Ann. Biomed. Engg.*, 1992, **20**, 289.

144. Z. Li, Q. Dong, Y. Li, B. Xu, M. Deng, J.Pei and W. Tian, *J. Mater. Chem.*, 2011, **21**, 2159.

145 J.H. Huang and K.C. Lee, *ACS Appl. Mater. Interfaces*, 2014, **6**, 7680.

146 (a)Y.W. Tsai, J.S. Ni, F.L. Wu, M.C.P. Yeh, Y.J. Cheng, L.Z. Tsai and J.T. Lin, *Organic Electronics*, 2016, **30**, 265. (b) J. R. Macdonald and E. Barsoukov, *Impedance Spectroscopy: Theory, Experiment and Applications*, John Wiley, New York, 3rd ed., 2018

Chapter-2

Scope and Objectives

2.1) Scope and Objectives

Organic electronics is the field of material science related to design, synthesis, characterization and applications of organic materials (small molecules or polymers) in the field of electronics technology.[1] Much of the interest towards organic electronics developed due to the opportunity of gaining low-cost products.[2] Materials and processing costs were reduced in comparison to conventional silicon-based technology.[3,4] In addition, methods such as standard printing techniques can be applied for their fabrication. For these reasons the costs are reduced for organic electronics, but besides the low-cost, it is also possible to achieve new kinds of device properties that are hard to achieve with inorganic electronics e.g. flexibility, light weight, thin and large device area.[5] Also, wide scope of structural variation in organic molecules offers possibility of tuning the desirable properties of optoelectronic devices which is hardly possible in case of inorganic semiconductors. However, organic electronics also faces many challenges that limit device performance, and hence, commercialization of applications. These challanges include low charge carrier mobility and life-time problems. Also the fabrication process. although simpler, is less robust than for inorganic semiconductors. By and large, organic electronics currently competes with silicon-based electronics above all on price instead of quality. Therefore, active research work is needed to bridge the gap and to bring out the advantages of organic electronics.

The appeal of new technologies based on organic semiconductors has notably promoted the advancement of devices such as organic light emitting diodes (OLEDs),[6] organic photovoltaic cells (OPVs),[7] organic field-effect transistors (OFETs),[8] organic lasers,[9] and memory cells[10] [**Figure 2.1**] These devices were tailored for applications in flat-panel displays, lighting, RFID (radio frequency identification tags),[11] electronic skin,[12] and solar modules. Furthermore, flexible organic electronic devices have generated entirely new design concepts for consumer electronics, since they are fully adaptable to complex surface shapes. The field of OLEDs which was initially confined to the level of academic research has now evolved to the field of commercial applications for e.g. OLED televisions, OLED mobile screens, OLED lighting, etc. Depending upon the type of organic materials used, the OLEDs are of two types i.e. small molecule organic light emitting diodes (SM-OLEDs) and polymeric light emitting diodes (PLEDs).[13]

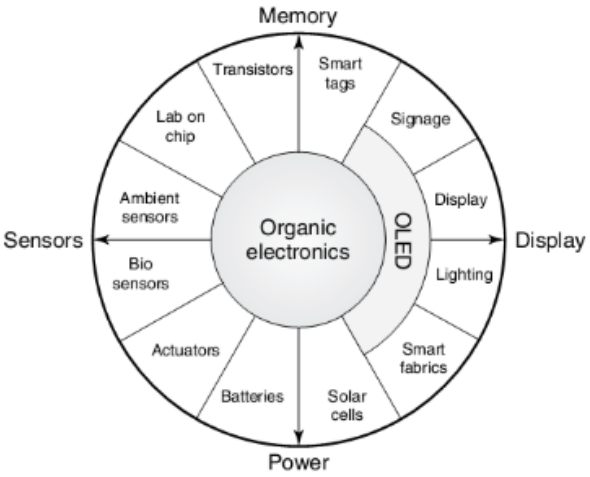

Figure 2.1: Different applications based on organic electronics (adapted from ref [14])

The active layer in SMOLEDs is normally composed of molecules derived from different fluorophores such as anthracene, pyrene, diphenylamine, fluorene, phenothiazine, carbazole, naphthalene, etc. Among these, pyrene is a polycyclic aromatic hydrocarbon with four fused benzene rings and flat aromatic system.[15] Along with its chemical and thermal stability, it exhibits high fluorescence and good charge carrier mobility making pyrene and its derivatives potentially useful for different optoelectronic applications such as OLEDs. However, due to its highly fused nature, supramolecular π-π stacking between the pyrene cores results into excimer formation[16] that leads to fluorescence quenching which eventually results into low fluorescence quantum yield and hampers the overall performance of OLEDs. In order to overcome this problem, rigid and bulky groups were introduced at the periphery of pyrene core which reduced intermolecular π-π interaction between the emissive cores and helped to lower the fluorescence quenching. [15]

The charge carrier mobility of organic semiconductors is highly important while designing organic molecules for optoelectronic applications. Compared to the band like motion of charges in inorganic materials, organic materials exhibit charge transport through hopping mechanism[17] due to weak Van der Waals interactions between the molecules. Hence the charge carrier mobility values are just of the order of 10^{-6} to 10^{-3} $cm^2V^{-1}S^{-1}$. As the performance of organic semiconductors is highly influenced by charge carrier mobility, it is highly important to design organic semiconductors with optimum charge carrier mobility to improve the efficiency of optoelectronic devices e.g. OLEDs, OFTEs, OPVs, etc.

The overall objective of the present work was to design, synthesize and evaluate the solution-processable small organic molecule for applications in the field of organic electronics. **Figure 2.2** represents the theme of the thesis.

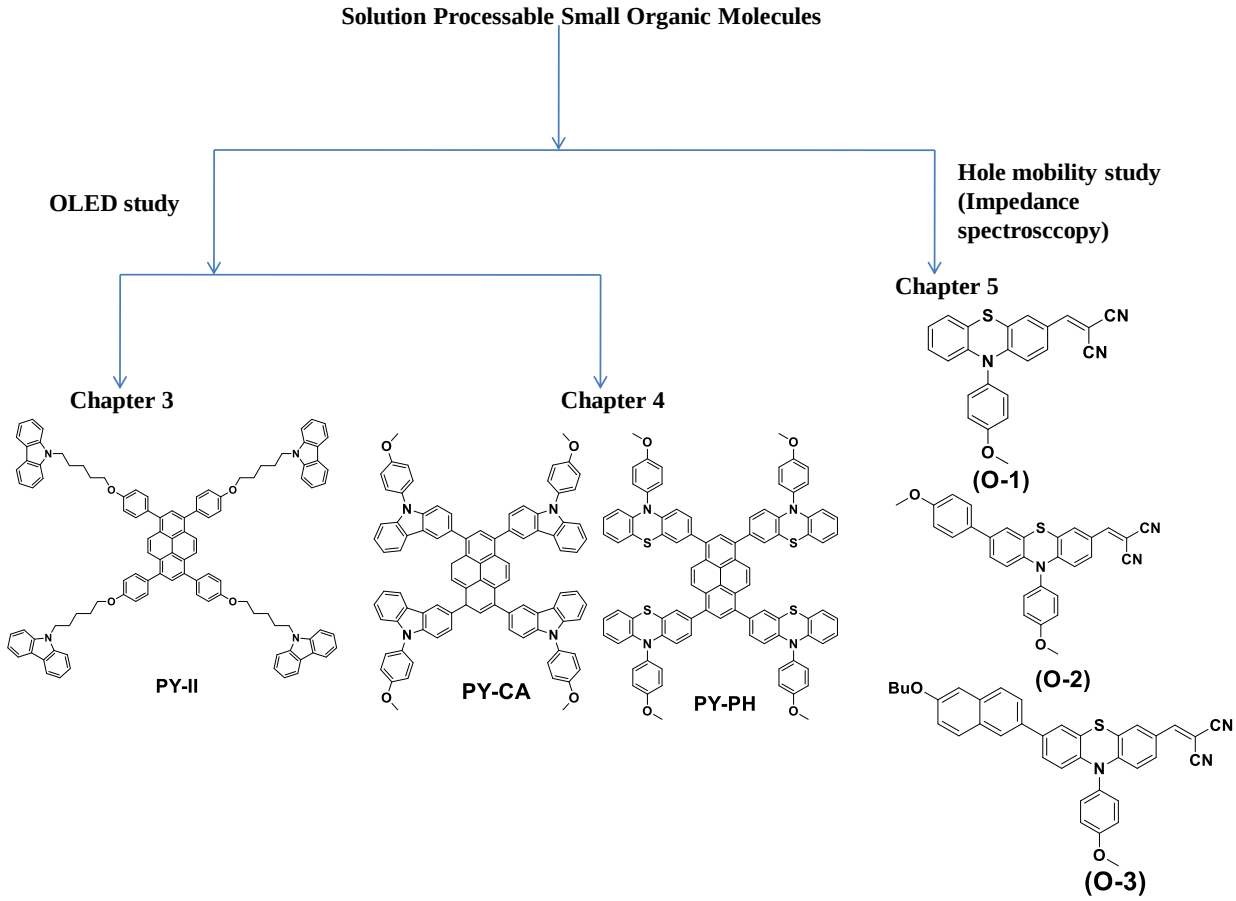

Figure 2.2: Theme of the thesis

a) Synthesis of pyrene-based 1,3,6,8-tetrasubstituted small molecule bearing carbazole substituent attached to the core *via* alkyl chain linker and study of the structure –property relationship and performance in OLED device.

The introduction of bulky groups with charge transporting properties attached to pyrene core through alkyl chain linkers helps to enhance the solubility, increase in charge transport properties and reduction of intermolecular interaction between the emissive cores. Carbazole is reported to be the moiety with good hole transporting ability as well as energy harvesting

property.[18,19,20] Considering the inspiring properties of carbazole and pyrene, following objectives were chosen for the study.

I. To synthesize 1,3,6,8-tetrasubstituted pyrene-based small molecule with carbazole attached to pyrene core *via* alkyl chain linker namely, 1,3,6,8-tetrakis(4-((5-(9H-carbazol-9-yl)pentyl)oxy)phenyl)pyrene (**PY-II**)

II. To study optoelectronic properties (UV-vis and photoluminescence) and evaluate the site isolation effect over fluorescence properties by introduction of substituents on pyrene core.

III. To study thermal and electrochemical properties of **PY-II**.

IV. To fabricate OLED device using **PY-II** as the emissive layer and evaluate its device performance.

b) Synthesis of pyrene-based 1,3,6,8- tetrasubstituted small molecules bearing N-substituted carbazole and phenothiazine attached to pyrene core and study their OLED performance.

Carbazole and phenothiazine have been reported as the deep blue and green emitting materials.[21] [22] Direct attachment of these substituents to pyrene core (without any aliphanic linker) is anticipated not only to reduce the fluorescence quenching by site isolation effect but also to enhance the optical properties by extended conjugation between pyrene core and the attached substituent. Considering these properties of pyrene, carbazole and phenothiazine following objectives were chosen for the study.

I. To synthesize 1,3,6,8-tetrasubstituted pyrene-based small molecules bearing carbazole and phenothiazine as the substituents attached directly to pyrene core, namely, 1,3,6,8-tetrakis(9-(4-methoxyphenyl)-9H-carbazol-3-yl)pyrene (**PY-CA**) and 1,3,6,8-tetrakis(10-(4-methoxyphenyl)-10H-phenothiazin-3-yl)pyrene (**PY-PH**), respectively.

II. To study the optical and electrochemical properties of **PY-CA** and **PY-PH.**

III. To fabricate OLED devices using **PY-CA** and **PY-PH** as the emissive layer in the device and to study their OLED performance.

c) Synthesis of phenothiazine-based small organic molecules with donor- acceptor structure and study of their charge carrier mobility properties.

Phenothiazine is an electron rich heterocyclic compound due to the presence of sulphur and nitrogen as the heteroatoms. Due to its non planar butterfly conformation, phenothiazine exhibits reduced molecular aggregation and excimer formation.[23] The introduction of substituents on phenothiazine ring helps to improve the intramolecular charge transfer (ICT).[24] It was reported that extension of π system of phenothiazine helps to increase ICT and consequently improves its charge transport properties.[25,26] Inspired from the above reports, following objectives were chosen for the study.

I. To synthesize phenothiazine-based small organic molecules with donor- acceptor structure bearing methoxy phenyl and butoxy napthyl as the electron donating and malononitrile as the electron withdrawing substituents. The molecules namely, 2-((10-(4-methoxyphenyl)-10H-phenothiazin-3-yl) methylene) malononitrile (**O-1**), 2-((7,10-bis(4-methoxyphenyl)-10H-phenothiazin-3-) methylene) malononitrile (**O-2**) and 2-((7-(6-butoxynaphthalen-2-yl)-10-(4-methoxyphenyl)-10H-phenothiazin-3-yl)methylene) malononitrile (**O-3**) were designed and synthesized.

II. To study optical, electrochemical and thermal properties of the synthesized molecules.

III. To evaluate the hole mobility characteristics of small molecules using impedance spectroscopy and to study relation between structure of molecules and their hole mobility characteristics using differential field theory (DFT) and XRD characterization.

2.2) References

1. H. Klauk, *Organic Electronics: Materials, Manufacturing, and Applications*, John Wiley & Sons, New Jersey, 2006.
2. A. Facchetti, *Chem. Mater.*, 2010, **23**, 733.
3. S. E. Shaheen, D. S. Ginley and G. E. Jabbour, *MRS Bull.*, 2005, **30**, 10.
4. D. J. Gaspar and E. Polikarpov, *OLED Fundamentals: Materials, Devices, and Processing of Organic Light-Emitting Diodes*, CRC Press, 2015.
5. T. Sekitani and T. Someya, *Adv.Mater.*, 2010, **22**, 2228.
6. N. T. Kalyani and S. J. Dhoble, *Renew. Sust. Energ. Rev.*, 2012, **16**, 2696.

7. B. Kippelen and J.L. Bredas, *Energy Environ. Sci.*, 2009, **2**, 251.
8. L. Torsi, M. Magliulo, K. Manoli and G. Palazzo, *Chem. Soc. Rev.*, 2013, **42**, 8612.
9. S. Chenais and S. Forget, *Polym. Int.*, 2012, **61**, 390.
10. J. Ouyang, C.W. Chu, D. Sieves and Y. Yang, *Appl. Phys. Lett.*, 2005, **86**, 123507.
11. C. M. Roberts, *Comput. Secur.*, 2006, **25**, 18.
12. S. J. Benight, C. Wang, J. B. H. Tok and Z. Bao, *Prog. Polym. Sci.*, 2013, **38**, 1961.
13. T. Tsujimura, *OLED Display Fundamentals and Applications*, John Wiley & Sons, New Jersey, 2017.
14. F. Li, A. Nathan, Y. Wu and B. S. Ong, *Organic Thin Film Transistor Integration: A Hybrid Hpproach*, John Wiley & Sons, New Jersey, 2011.
15. T. M. F. Duarte and K. Mullen, *Chem. Rev.*, 2011, **111**, 7260.
16. I. Yamazaki, F. M. Winnik, M. A. Winnik and S. Tazuke, *J.Phys. Chem.*, 1987, **91**, 4213.
17. R. M. Hill, *Philos.Mag.*, 1971, **24**, 1307.
18. T. Keawin, N. Prachumrak, S. Namuangruk, S. Pansay, N. Kungwan, S. Maensiri, S. Jungsuttiwong, T. Sudyoadsuk and V. Promarak, *RSC Adv.*, 2015, **5**, 73481.
19. P. Moonsin, N. Prachumrak, S. Namuangruk, S. Jungsuttiwong, T. Keawin, T. Sudyoadsuk and V. Promarak, *J. Mater. Chem. C*, 2014, **2**, 5540.
20. S. J. Kim, Y. J. Kim, Y. H. Son, J. A. Hur, H. A. Um, J. Shin, T. W. Lee, M. J. Cho, J. K. Kim and S. Joo, *Chem. Commun.*, 2013, **49**, 6788.
21. S. J. Lee, J. S. Park, K. J. Yoon, Y. I. Kim, S. H. Jin, S. K. Kang, Y. S. Gal, S. Kang, J. Y. Lee and J. W. Kang, *Adv. Funct. Mater.*, 2008, **18**, 3922.
22. G. B. Bodedla, K. R. J. Thomas, S. Kumar, J.H. Jou and C.-J. Li, *RSC Adv.*, 2015, **5**, 87416.
23. W. Wu, J. Yang, J. Hua, J. Tang, L. Zhang, Y. Long and H. Tian, *J. Mater. Chem.* 2010, **20**, 1772.
24. Z.S. Huang, H. Meier and D. Cao, *J. Mater. Chem. C*, 2016, **4**, 2404.
25. A. A. Bakulin, A. Rao, V. G. Pavelyev, P. H. M. van Loosdrecht, M. S. Pshenichnikov, D. Niedzialek, J. R. M. Cornil, D. Beljonne and R. H. Friend, *Science*, 2012, **335**, 1340.
26. S. Shoaee, T. M. Clarke, C. Huang, S. Barlow, S. R. Marder, M. Heeney, I. McCulloch and J. R. Durrant, *J. Am. Chem. Soc.*, 2010, **132**, 12919.

Chapter-3

Pyrene-Cored Small Organic Molecule with Flexible Alkyl Spacer for Solution Processable Blue Emitter with Bright Photoluminescence

3.1) Introduction

Over the past three decades, organic light emitting diodes (OLEDs) have attracted great attention because of their applications in flat panel displays and solid-state lighting devices.[1-5] Generally, small molecule organic light emitting diodes (SMOLEDs) are fabricated by high-vacuum thermal evaporation whereas polymer light emitting diodes (PLEDs) are fabricated by the solution processing method. The vacuum evaporation results in complicated architectures, it is expensive and not well suited for large area fabrication.[6 7] On the other hand, solution processing of organic molecules for device fabrication is an attractive method with low cost and large area manufacturability.[8-11] To date, both small molecules and polymers have been extensively used as emitting materials in OLEDs.[12-14] Recently, OLEDs based on organic and organometallic compounds have drawn intense interest due to their inherent features such as excellent solution processability, tunable emission properties, thin film forming ability and high chemical and thermal stability.

A variety of solution processable fluorescent and phosphorescent light emitting materials have been reported to date.[15-18] Among the various fluorescent chromophores used for OLEDs, pyrene stands out as a promising chromophore because of its strong emission efficiency and high charge carrier mobility.[19-22] These features make pyrene a potential candidate to develop an interesting class of materials for OLEDs. However, supramolecular π–π stacking between pyrene cores in the solid state leads to a red shift and fluorescence quenching of the emission.[23,24] To overcome these problems, rigid and bulky groups with alkyl chains were introduced at the periphery of the pyrene core which helps to prevent intermolecular aggregation and leads to enhanced emission efficiency [25] A number of light emitting materials based on pyrene have been reported in the literature.[26,28] Pyrene has been successfully utilized for the synthesis of materials with pure blue and green emission.[29-31] Blue light-emitting materials can facilitate white light emission in the presence of suitable dopants.[32-35] Thus, it is important to develop new class of blue light emitting materials with good solution processability and high fluorescence efficiency. It is reported that moieties with charge transporting ability and aliphatic chain linkers offer several advantages such as enhancement in the solubility, facilitated charge transport and reduction of intermolecular interaction between the emissive cores.[36-40] Such molecules provide a

pathway to reduce or eliminate aggregation induced fluorescence quenching by the site isolation effect.

Inspired from the above considerations, in the present work a new pyrene cored solution processable blue light emitting material, namely, 1,3,6,8-tetrakis(4-((5-(9H-carbazol-9-yl)pentyl)oxy)phenyl)-pyrene (**PY-II**) was synthesized. The carbazole moiety with an alkyl spacer was introduced at 1, 3, 6, 8-positions of the pyrene core. Carbazole was employed due to its high hole transporting and energy harvesting ability,[41-45] and its property to enhance the emission of the core.[46] The flexible alkyl chain was introduced to further improve the solution processability and glass-like properties. **PY-II** was characterized by IR, ^{1}H and ^{13}C NMR spectroscopy, MALDI-TOF, DSC and TGA. Optical and electrochemical properties of **PY-II** were studied. An OLED device fabricated using **PY-II** as an emitting material showed blue emission with a maximum brightness of 202 cdm^{-2} and a maximum current efficiency of 0.41 cd A^{-1}.

3.2) Experimental

3.2.1) Materials

All the chemicals namely, carbazole, 1,3,6,8- tetrabromopyrene, 1, 5-dibromopentane, 4-iodoanisole, bis(pinacolato)diboron, [1,1′- is(diphenylphosphino)ferrocene]dichloropalladium(II) [$Pd(dppf)Cl_2$], tetrakis (triphenylphosphine) palladium [$Pd(PPh_3)_4$], potassium acetate and potassium carbonate were purchased from Sigma-Aldrich and were used without further purification. The solvents namely, N,N-dimethylformamide (DMF), dimethyl sulfoxide (DMSO), 1,4-dioxane, toluene, etc. were purchased from Sigma-Aldrich and were purified according to the standard procedures.[47] All the reactions were carried out under argon or nitrogen atmosphere.

3.2.2) Instrumentation

Melting points were recorded on Electrothermal MEL-TEMP apparatus and are uncorrected. IR spectra were recorded on Perkin Elmer GX spectrophotometer in the range of 4000-500 cm^{-1} using ATR mode. NMR spectra were recorded using chlroform-d ($CDCl_3$) as a solvent on a Bruker AC spectrometer operating at 400 MHz for ^{1}H and 100 MHz for ^{13}C. HR-MS characterization was performed on Thermo Scientific Q-Exacative with Accela 1250 pump.

Matrix assisted laser desorption/ionization time-of-flight (MALDI-TOF) spectra were obtained on a Bruker Autoflex TOF/TOF instrument using dithranol as a matrix. UV-vis absorbance and photoluminescence (PL) spectra were recorded on a Jasco V-570 and a Cary Eclipse Fluorescence spectrometer, respectively, using chloroform as a solvent. Thermogravimetric and DSC analyses were performed on a Perkin Elmer STA 6000 and TA Instrument DSC Q10, respectively, at a heating rate of 10 ^{o}C min^{-1} under nitrogen atmosphere. The cyclic voltammogram was recorded on Autolab using a conventional three-electrode assembly with a Pt wire as a working electrode, a Pt foil as a counter electrode and Ag/AgCl as a reference electrode. Cyclic voltammetry was carried out in freshly distilled dichloromethane (DCM) using 0.1 M tetrabutyl ammonium hexafluoro phosphate (TBAPF6) as a supporting electrolyte and a scan rate of 50 mV s^{-1} was used. The cyclic voltammogram was calibrated with a ferrocene/ferrocinium (Fc/Fc^{+}) redox couple. The HOMO energy level of **PY-II** was calculated by photoelectron spectroscopy in air (PESA) using a spin coated thin film of **PY-II** on the ITO coated glass substrate. The surface of **PY-II** thin film was irradiated with UV energy that emits photoelectrons of certain energy level known as the photoelectron work function. The photoelectron output was plotted with a horizontal X-axis as the UV energy applied and the vertical Y-axis as the standardized photoelectron yield ratio, the result was a line with a specific slope of degree (Y/eV). The HOMO value of **PY-II** was calculated from the onset energy level recorded in PESA. Solution and thin film (solid state) photoluminescence quantum yield (PLQY) measurements were carried out using an Absolute PL Quantum Yield Spectrometer (Hamamatsu, C11347) using an integrating sphere equipped with a multichannel spectrometer.[48] The roughness measurement was conducted by atomic force microscopy (AFM). **PY-II** solution prepared in chloroform (5 mg/mL) was spin-coated on an ITO substrate. The film coated ITO substrate was baked at 70 ^{o}C for 20 min. The scan dimension was typically set as 5 mm × 5 mm.

3.2.3) Synthesis

3.2.3.1) Synthesis of 9-(5-bromopentyl)-9H-carbazole (2)

Into a 100 mL round bottom flask equipped with a magnetic stirring bar and a dropping funnel were added carbazole (2 g, 11.96 mmol), KOH (0.671 g, 11.96 mmol) and DMF (40 mL). The reaction mixture was stirred at room temperature for 1 h. 1,5-Dibromopentane (8.25 g, 35.88 mmol) was added drop wise into the reaction mixture at 0 ^{o}C. After the addition, the reaction

mixture was allowed to stir at room temperature for 12 h. After completion of reaction, the mixture was quenched with water (50 mL) and extracted with dichloromethane (2×100 mL). The organic layer was separated and washed with water (50 mL), brine solution (50 mL) and again with water (50 mL). The dichloromethane solution was dried over anhydrous sodium sulfate and filtered. Removal of the solvent on a rotary evaporator yielded a crude product which was purified by column chromatography using petroleum ether: dichloromethane (9:1, v/v) as an eluent to obtain the title compound **2** as a white powder.

Yield: 2.95 g (78%)

Melting point: 137 ^{0}C

IR (ATR, cm^{-1}): 1311 (C-N, amine), 723 (C-Br) [**Figure S 3.7**]

^{1}H NMR (400 MHz, $CDCl_3$) δ ppm = 8.12 (d, 2H), 7.54-7.46 (m, 2 H), 7.44 - 7.36 (m, 2 H), 7.30 - 7.21 (m, 2 H), 4.34 (t, 2 H), 3.37 (t, 2 H), 1.94 - 1.86 (m, 4 H), 1.59 - 1.51 (m, 2 H). [**Figure S 3.1**]

^{13}C NMR (100 MHz, $CDCl_3$) δ= 140.27, 125.61, 122.80, 120.34, 118.80, 108.51, 42.72, 33.28, 32.40, 28.11, 25.83.[**Figure S 3.2**]

HRMS: calculated for $C_{17}H_{18}BrN$ 315.0623, found 315.0619

3.2.3.2) Synthesis of 9-(5-(4-iodophenoxy)pentyl)-9H-carbazole (3)

Into a 100 mL round bottom flask equipped with a magnetic stirring bar and a dropping funnel were placed 4-iodophenol (2 g, 9.09 mmol), KOH (2.04 g, 36.36 mmol) and DMSO (30 mL). After stirring for 10 minutes, the solution of 9-(5-bromopentyl)-9H-carbazole (3.16 g, 10 mmol) (**2**) in DMSO (20 mL) was added drop wise into the reaction mixture. The reaction mixture was stirred at room temperature for 24 h. After completion of reaction, the reaction mixture was quenched with water (50 mL) and extracted with dichloromethane (100 mL). The organic layer was separated and washed with water (50 mL), brine solution (50 mL) and again with water (50 mL). The dichloromethane solution was dried over anhydrous sodium sulfate and filtered. Removal of solvent on a rotary evaporator yielded a crude product which was purified by column chromatography using petroleum ether: dichloromethane (8:2, v/v) as an eluent to give compound **3** as colorless crystals.

Yield: 3.72 g (82%)

Melting point: 153 ^{0}C

IR (ATR, cm^{-1}): 1321 (C-N, amine), 1232 (C-O-C), 523 (C-I). [**Figure S 3.8**]

^{1}H NMR (400 MHz, $CDCl_3$) δ ppm= 8.14 (d, 2H), 7.55-7.48 (m, 4H), 7.44-7.37 (m, 2H), 7.27 (t, 2H), 6.65-6.57 (m, 2H), 4.33 (t, 2H), 3.84 (t, 2H), 1.99-1.92 (m, 2H), 1.82-1.74 (m, 2H), 1.59-1.48 (m, 2H). [**Figure S 3.3**]

^{13}C NMR (100 MHz, $CDCl_3$) δ= 158.75, 140.30, 138.09, 125.59, 122.77, 120.33, 118.76, 116.83, 108.55, 82.53, 67.59, 42.81, 28.89, 28.71, 23.77. [**Figure S 3.4**]

HRMS: Calculated for $C_{23}H_{22}INO$ 455.3395, found 455.3391

3.2.3.3) Synthesis of 9-(5-(4-(4, 4, 5, 5-tetramethyl-1,3,2-dioxaborolan-2-yl) phenoxy) pentyl)-9H-carbazole (4)

Into a 50 mL Schlenk tube equipped with a magnetic stirring bar were added 9-(5-(4-iodophenoxy)pentyl)-9H-carbazole (**3**) (1 g, 2.20 mmol), bis (pinacolato) diboron (0.669 g, 2.60 mmol), $PdCl_2$(dppf) (161 mg, 0.2 mmol) and potassium acetate (646 mg, 6.60 mmol) under argon flow. After addition of reactants, the tube was evacuated for 30 minutes. Subsequently, under an argon flow, anhydrous 1,4-dioxane (10 mL) was added to the reaction mixture. The reaction mixture was stirred at room temperature for 1 h and subsequently at 80 °C for 24 h. After completion of reaction, the reaction mixture was quenched by addition of ice-cold water (100 mL) and extracted with dichloromethane (200 mL). The organic layer was separated and washed with water (50 mL), brine solution (50 mL), and again with water (50 mL). The dichloromethane solution was dried over anhydrous sodium sulfate and filtered. Removal of the solvent on a rotary evaporator yielded a crude product, which was chromatographed over neutral alumina using 2% ethyl acetate in petroleum ether as an eluent to give compound **4** as a white solid.

Yield: 0.64 g (64%).

Melting point: 161 ^{0}C

IR (ATR, cm^{-1}): 1370 (B-O, boronic ester). [**Figure S 3.9**]

^{1}H NMR (400 MHz, $CDCl_3$) δ= 8.11 (d, *J* =7.71 Hz, 2H), 7.75 (d, *J*=8.46 Hz, 2H), 7.51-7.37

(m, 4H), 7.27-7.19 (m, 2H), 6.85 (d, *J*=8.59 Hz, 2H), 4.31 (t, J=6.95 Hz, 2H), 3.91 (t, J=6.32 Hz, 2H), 1.98-1.90 (m, 2H), 1.84-1.73 (m, 2H), 1.62-1.51 (m, 2H), 1.34 (s, 12H). [**Figure S 3.5**]

^{13}C NMR (100 MHz, $CDCl_3$) δ= 161.52, 140.33, 136.47, 125.59, 122.78, 120.32, 118.75, 113.80, 108.57, 83.49, 67.30, 42.85, 28.97, 28.73, 24.82, 23.82.

HRMS: Calculated for $C_{29}H_{34}NO_3B$ 455.2632, found 455.2630 [**Figure S 3.6**]

3.2.3.4) Synthesis of 1, 3, 6, 8-tetrakis (4-((5-(9H-carbazol-9-yl) pentyl) oxy) phenyl) pyrene (PY-II)

Into a 50 mL Schlenk tube were placed 1,3,6,8-tetrabromopyrene (0.1 g, 0.19 mmol), 9-(5-(4-(4,4,5,5-tetramethyl-1,3,2-dioxaborolan-2-yl)phenoxy)pentyl)-9H-carbazole (0.528 g, 1.16 mmol), 2M aqueous solution of K_2CO_3 (2 mL) and $Pd(PPh_3)_4$ (0.022 g, 0.019 mmol) under argon flow. The tube was evacuated and refilled with argon three times and then toluene (10 mL) was added into the flask. The reaction mixture was stirred at 80 ^oC for 48 h and the reaction progress was monitored by TLC. After completion of reaction, it was quenched by addition of ice-cold water (50 mL) and extracted with dichloromethane (3x50 mL). The combined organic layer was washed with water (50 mL), brine solution (50 mL) and again with water (50 mL). The dichloromethane solution was dried over sodium sulfate and filtered. Removal of the solvent on a rotary evaporator yielded a crude product, which was purified by column chromatography using petroleum ether: dichloromethane (6:4, v/v) as an eluent to give title compound **PY-II** as a yellow solid.

Yield: 0.18 g (62%)

Melting point: 216 ^oC

IR (ATR, cm^{-1}): 1330 (C-N, amine), 1242(C-O-C). [**Figure 3.1**]

^{1}H NMR (400 MHz ,$CDCl_3$) δ ppm= 8.16 - 8.12 (m, 12 H), 7.95 (s, 2 H), 7.59 (d, 8 H), 7.51 - 7.44 (m, 16 H), 7.27-7.20 (m, 8 H), 7.05 (d, 8 H), 4.39 (t, 8 H), 4.04 (t, 8 H), 2.07 – 1.97 (m, 8 H), 1.95 - 1.86 (m, 8 H), 1.70 - 1.61 (m, 8 H) [**Figure 3.2**]

^{13}C NMR (100 MHz, $CDCl_3$) δ = 158.37, 140.39, 136.74, 133.47, 131.67, 129.6, 127.99, 126.13, 125.6, 125.1, 122.84, 120.36, 118.78, 114.39, 108.62, 67.71, 42.94, 29.13, 28.81, 23.94. [**Figure 3.3**]

MALDI-TOF: Calculated for $C_{108}H_{96}N_4O_4$ 1510.7275, found 1511.4016.

3.3) Results and discussion

3.3.1) Synthesis and characterization

Initially, commercially available carbazole was converted into 9-(5-bromopentyl)-9H-carbazole **(2)** *via* alkylation reaction of carbazole with excess 1,5-dibromopentane. Compound **2** was subsequently reacted with 4-iodophenol to afford 9-(5-(4-iodophenoxy) pentyl)9H-carbazole **(3)**. The transformation of compound **3** into the boronic ester analogue 9-(5-(4-(4, 4, 5, 5-tetramethyl-1,3,2-dioxaborolan-2-yl)phenoxy)pentyl)-9H-carbazole (**4**) was carried out *via* Miyaura borylation reaction. The target compound 1,3,6,8-tetrakis(4-((5-(9H-carbazol-9-yl)pentyl)oxy)phenyl)pyrene (**PY-II**) was prepared *via* the Suzuki coupling[49] using 1,3,6,8-tetrabromopyrene and monoboronic ester analogue **(4)**. The synthesis of **PY-II** is depicted in **Scheme 3.1**.

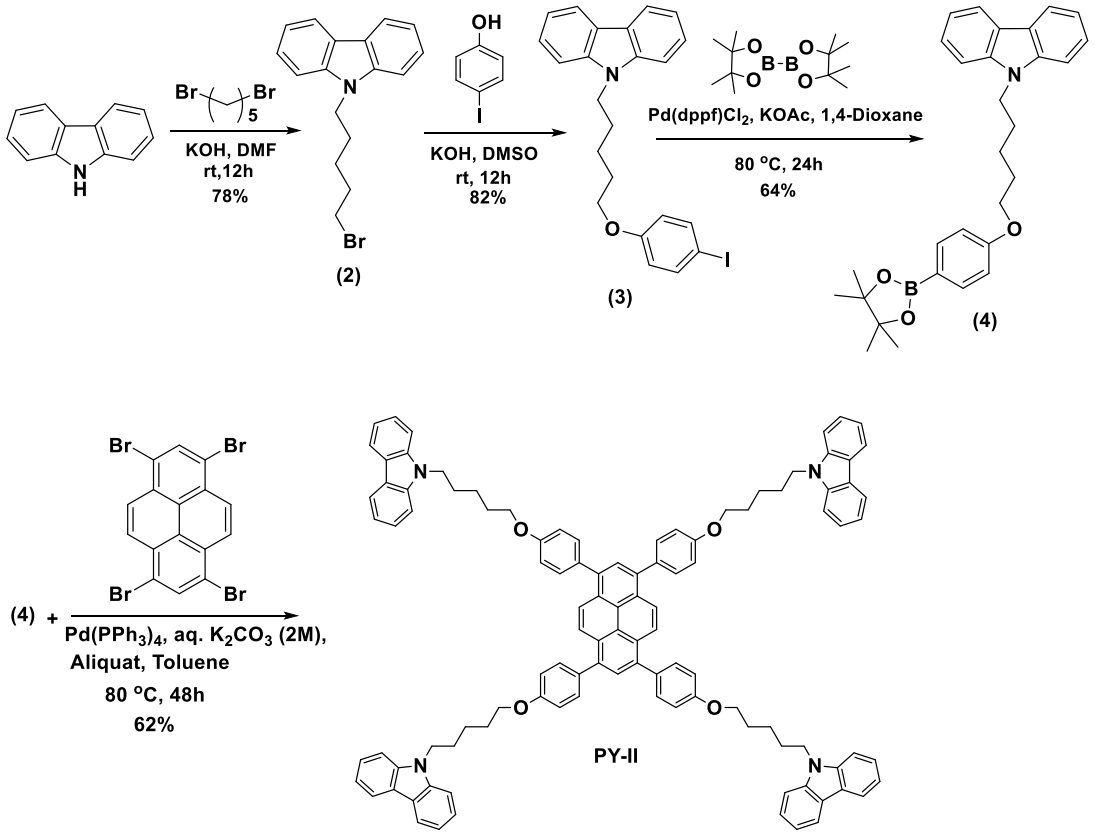

Scheme 3.1: Synthesis of 1, 3, 6, 8-tetrakis (4-((5-(9H-carbazol-9-yl)pentyl)oxy)phenyl)pyrene **(PY-II)**

The IR spectrum of **PY-II** is as shown in **Figure 3.1**. In the spectrum, band at 1330 cm^{-1} is due to C-N stretching whereas the band observed at 1242 cm^{-1} is attributed to C-O-C stretching.

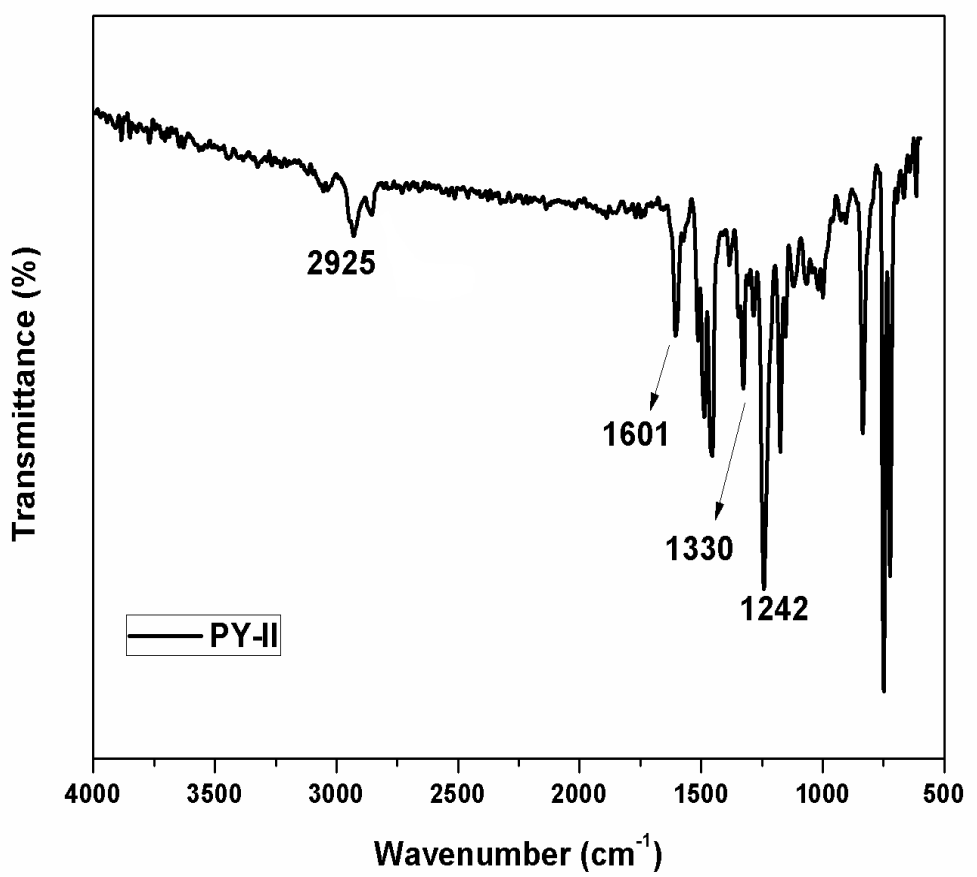

Figure 3.1: IR spectrum of 1, 3, 6, 8-tetrakis (4-((5-(9H-carbazol-9-yl)pentyl) oxy) phenyl) pyrene (**PY-II**)

^{1}H NMR spectrum of **PY-II** along with assignments is depicted in **Figure 3.2** Methylene protons 'e' and 'a' were observed as separate triplets at 4.39 δ ppm and 4.04 δ ppm, respectively. The signals for methylene protons'd', 'b' and 'c' were observed at 2.02 δ ppm, 1.91 δ ppm and 1.66 δ ppm, respectively. Aromatic protons 'j' were observed as a doublet at 7.05 δ ppm, whereas signal for protons 'k' was observed as a doublet at 7.59 δ ppm. The signals for protons 'n' and 'm' on pyrene core were observed at 8.12 δ ppm and 7.95 δ ppm, respectively. The protons on carbazole moiety were observed over the range 8.16-8.14 δ ppm and 7.49-7.23 δ ppm.

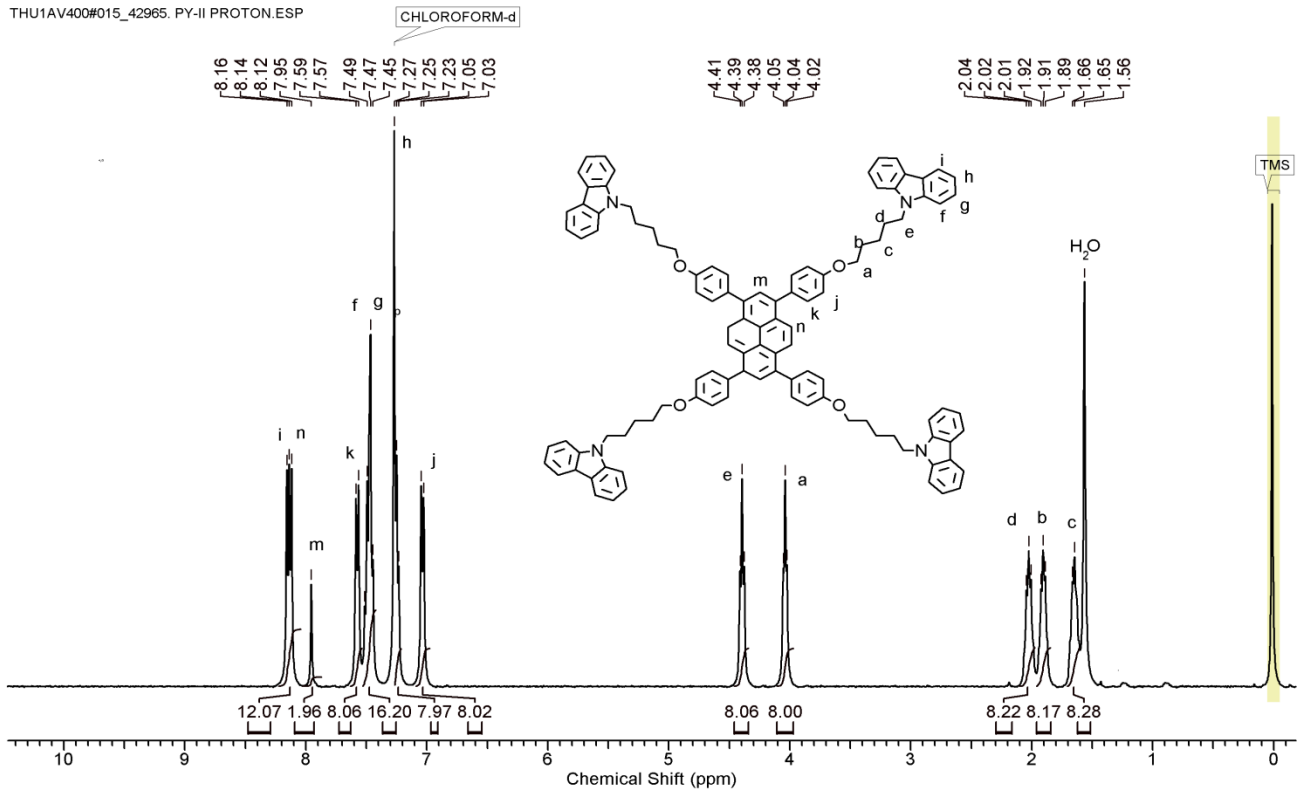

Figure 3.2: ^{1}H NMR spectrum (in $CDCl_3$) of 1,3,6,8-tetrakis(4-((5-(9H-carbazol-9-yl)pentyl)oxy)phenyl)pyrene (**PY-II**)

^{13}C NMR spectrum of **PY-II** along with assignments is represented in **Figure 3.3.** The signals for carbon atoms 'a' and 'e' were observed at 66.71 δ ppm and 42.91 δ ppm , respectively. The carbon atoms 'b', 'c' and 'd' exhibited signals at 29.13 δ ppm, 28.81 δ ppm and 23.94 δ ppm, respectively. The carbon atom 'm' of aromatic unit exhibited a signal in the downfiled region at 158.37 δ ppm due to inductive effect of oxygen. The signals exhibited by the carbon atoms of central pyrene core, carbazole and phenylene moiety were observed over the range 140.39-108.32 δ ppm

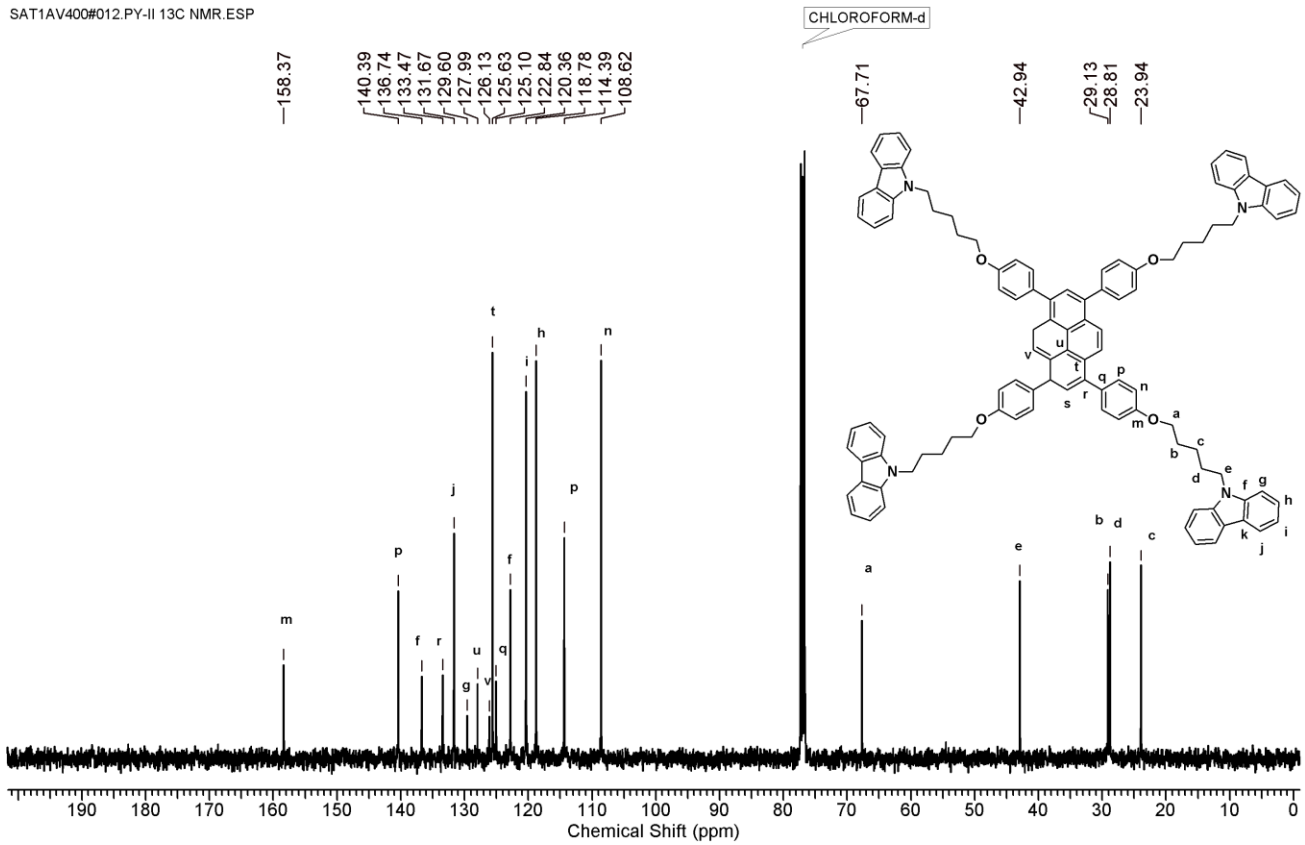

Figure 3.3: ^{13}C NMR spectrum (in $CDCl_3$) of 1,3,6,8-tetrakis (4-((5-(9H-carbazol-9-yl)pentyl)oxy)phenyl)pyrene (**PY-II**)

2D NMR spectrum of **PY-II** is shown in **Figure 3.4** In the spectrum, proton labeled as 'i' is coupled with proton 'h' due to *ortho* coupling, whereas proton labeled as 'k' is coupled with proton 'i' due to *ortho* coupling. Proton 'g' is coupled with proton 'f' due to *ortho* coupling. In the upfield region, the methylene proton labeled as 'e' is coupled with proton'd', whereas proton 'a' is coupled with proton 'b'. Methylene proton 'c' showed coupling with protons'd' and 'b'.

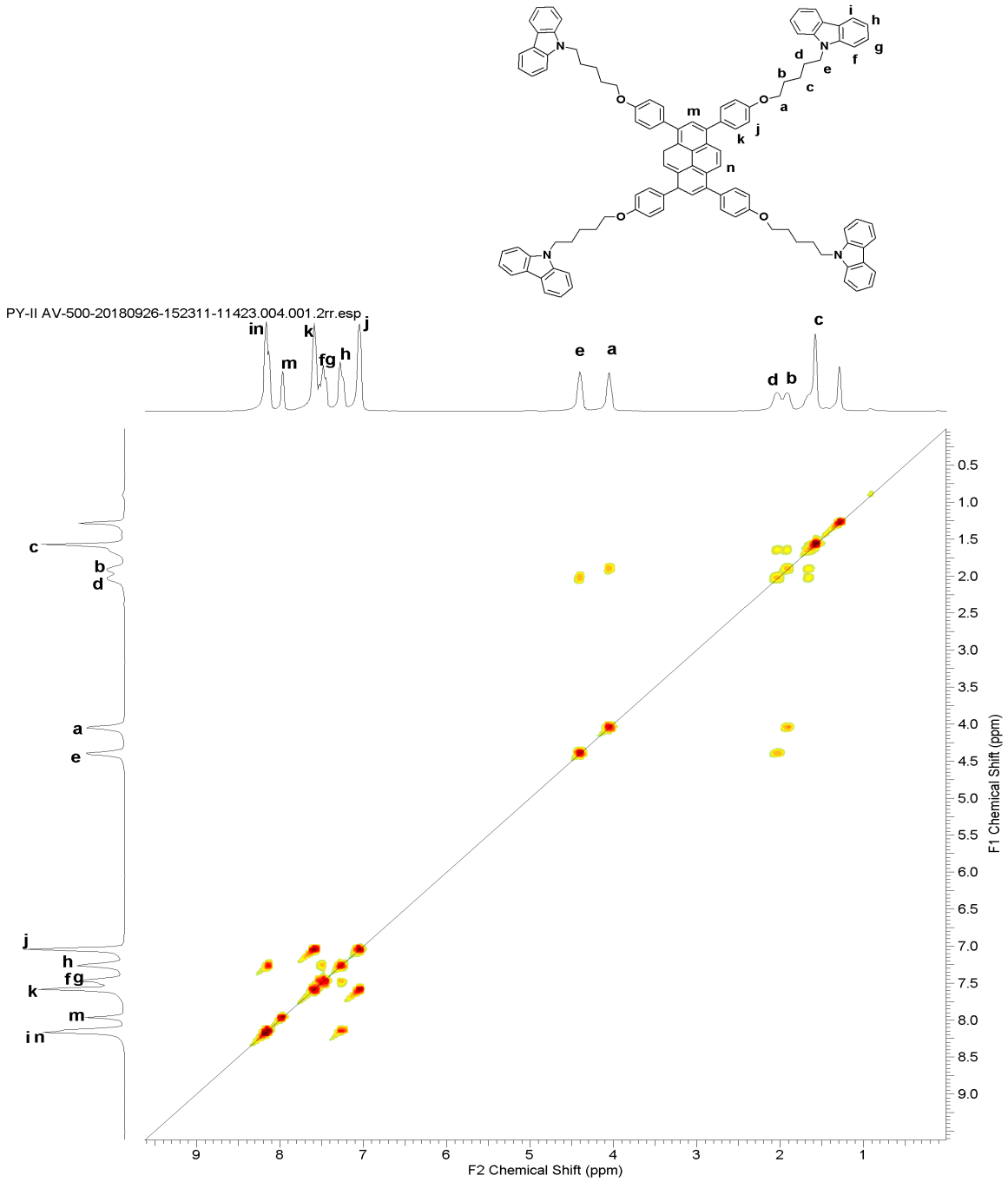

Figure 3.4: ^{1}H-^{1}H NMR spectrum (in $CDCl_3$) of 1,3,6,8-tetrakis(4-((5-(9H-carbazol-9-yl)pentyl)oxy)phenyl)pyrene (**PY-II**)

MALDI-TOF of **PY-II** was recorded using dithranol as a matrix and the spectrum is shown in **Figure 3.5 MALDI**-TOF spectrum for **PY-II** showed a signal at 1511.4016 (calculated for $C_{108}H_{94}N_4O_4$ = 1510.73)

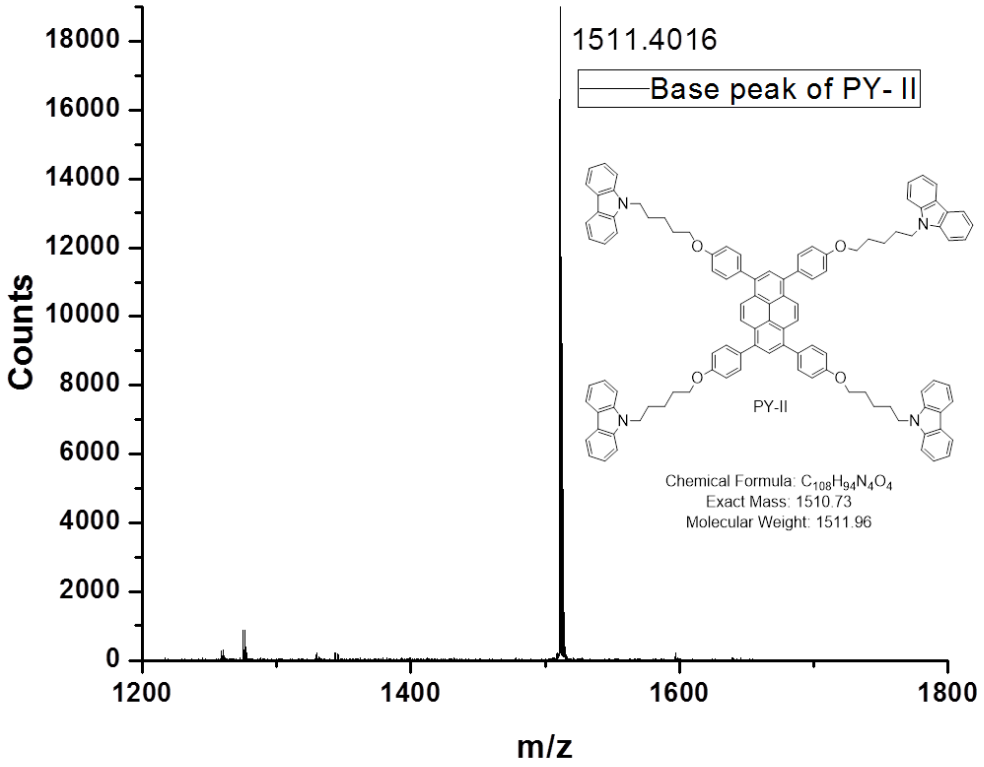

Figure 3.5: MALDI-TOF spectrum of 1, 3, 6, 8-tetrakis (4-((5-(9H-carbazol-9-yl) pentyl) oxy) phenyl) pyrene (**PY-II**)

Thermal properties of **PY-II** were studied by TGA and DSC. TG and DSC curves are shown in **Figure 3.6** and **Figure 3.7**, respectively**. PY-II** showed good thermal stability with 5% weight loss at 435 ^{o}C. In DSC analysis, **PY-II** exhibited a sharp melting peak at 215 ^{o}C during the first heating scan. However, after cooling and reheating of the sample during second heating scan, it demonstrated molecular glass behavior up to a glass transition temperature of 82 ^{o}C. Further heating up to 250 ^{o}C did not result in any other thermal transitions indicating the formation of stable amorphous glass.

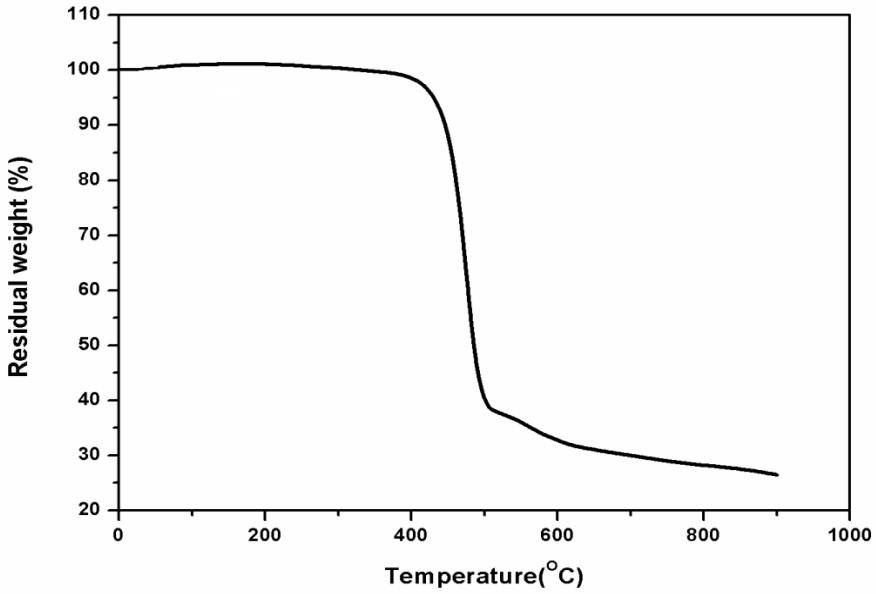

Figure 3.6: TG curve of **PY-II**

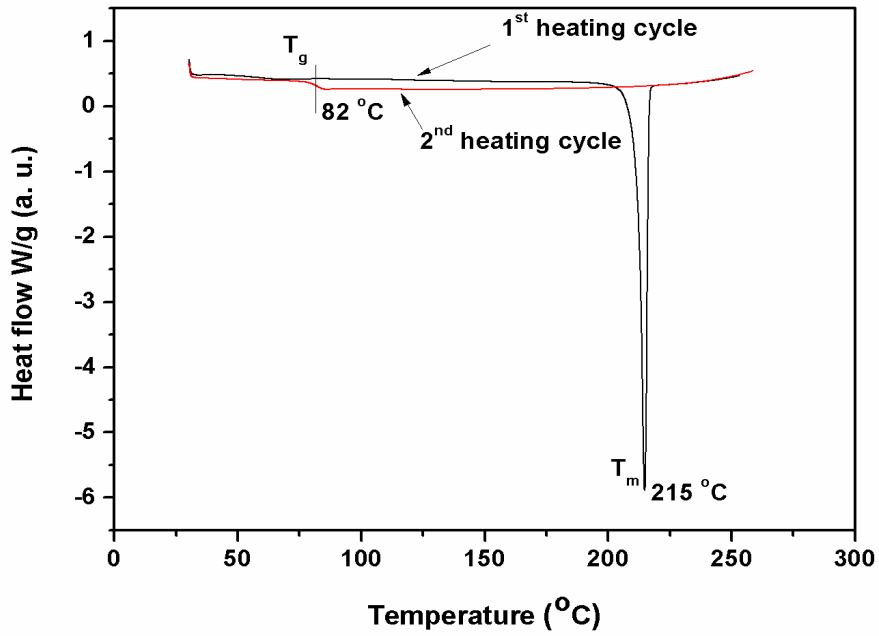

Figure 3.7: DSC curve of **PY-II**

3.3.2) Optical and electrochemical properties

The optical properties of **PY-II** were characterized by UV-vis absorption and photoluminescence spectroscopy. UV-absorption spectra of **PY-II** in chloroform solution and in the solid state are shown in **Figure 3.8**. The absorption in the range of 275-500 nm clearly indicated wide band gap nature of **PY-II**. In solution, **PY-II** exhibited absorption peaks at 297 nm and 394 nm which originated from π–π* transition of carbazole moieties and the pyrene core, respectively. When compared with the absorbance peak of molecular pyrene (338 nm), the absorption peak at 394 nm exhibited a red shift of 56 nm, which could be attributed to the extended conjugation length between the pyrene core and the attached oxyphenylene moiety. The absorption spectrum in the solid state was nearly identical to that in solution with red shifted absorption peaks at 298 nm and 408 nm. The optical band gap calculated from the absorption onset value from the thin film spectrum was found to be 2.76 eV. This higher band gap value of **PY-II** is a clear indication of a blue emitter. [50]

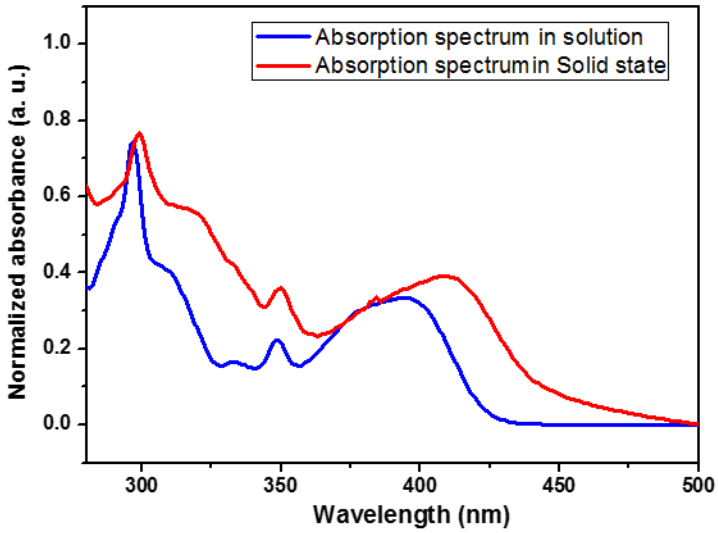

Figure 3.8: UV-vis absorption spectrum of **PY-II** in solution ($CHCl_3$) and thin film

The photoluminescence (PL) spectra of **PY-II** in both solution and the solid state are shown in **Figure 3.9**. The emission peaks at 434 nm and 450 nm were observed in solution and the thin film of **PY-II**, respectively. The thin film emission at 450 nm is the most suitable blue emission color for human eye[51]. The shape of the emission spectrum in thin film is almost similar to that in solution with a slight red shift of 16 nm. This result of small value of red shift clearly

indicated little intermolecular interaction between the emissive cores which could be attributed to the encapsulation effect of the alkyl separated carbazole moiety. The optical properties of PY-II are summarized in **Table 3.1**.

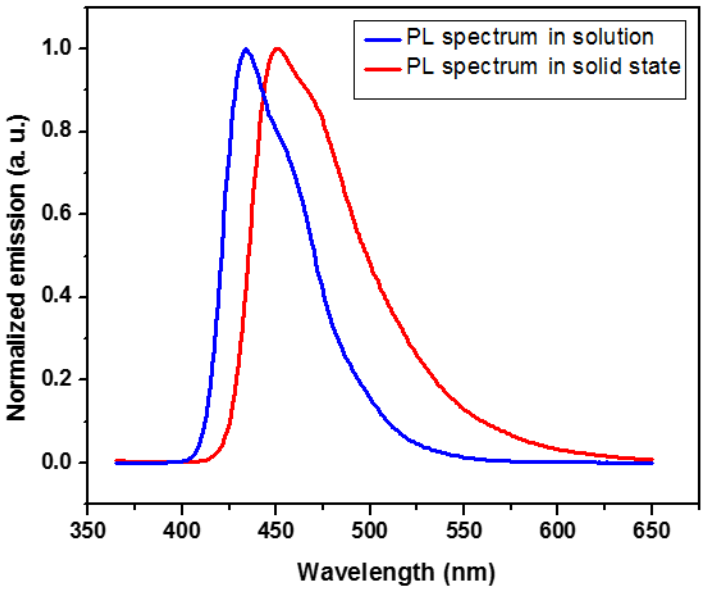

Figure 3.9: Photoluminescence spectrum of **PY-II** in solution ($CHCl_3$) and thin film

Table 3.1: Optical properties of **PY-II**

PY-II	**UV-vis (λ_{max} in nm)**	**PL (λ_{max} in nm)**
Solution ($CHCl_3$)	297,394	434
Solid	298,408	450

The PL quantum yield (PLQY) of **PY-II** in chloroform solution and thin film was measured by using an integrating sphere technique after argon gas bubbling through the solution sample and under an ambient atmosphere for film sample. In solution **PY-II** exhibited a very high PLQY of almost 0.9. In **PY-II** sample, there are two fluorophores namely pyrene and carbazole. The absorption band of carbazole is located higher than that of pyrene. If there is no energy transfer occurring between pyrne and carbazole fluorophores, then they will emit fluorescence

independently. In such a scenario, the carbazole moiety can be preferably excited by shorter wavelength light and the pyrene moiety can be preferably excited by longer wavelength light. If PLQY of pyrene moiety is higher than that of carbazole moiety, then PLQY under shorter wavelength excitation is smaller than PLQY under longer wavelength excitation because fraction of excited pyrene (or carbazole) moiety is different. This was not observed in the present study, which is why PLQY values were not sensitive to the excitation wavelength between 300 nm and 400 nm. In this excitation wavelength range, absorption due to pyrene and carbazole moieties coexists. Since absorption due to pyrene moiety is found to be located in the longer wavelength range, fluorescence spectra shown in **Figure 3.9** are assigned to pyrene fluorescence. Accordingly, a change in PLQY and spectral shape are expected to be observed, if carbazole moiety is excited preferably in shorter wavelength range. As mentioned above, no change in PLQY and spectral shape was observed in this excitation wavelength range. This clearly shows that energy transfer from excited carbazole moiety to pyrene part occurs efficiently and subsequently fluorescence emission occurs with a high PLQY. In other words, all excitation energy obtained by light absorption is converted to the excitation energy of pyrene.

Thus, PLQY value of **PY-II** is determined by PLQY of pyrene moiety. It was also observed that spectral shape is not sensitive to excitation wavelength. This again indicates the presence of energy transfer from carbazole to pyrene because only pyrene gives fluorescence. However, PLQY value in the film was smaller than that in solution with a value of 0.33, suggesting that some deactivation processes are induced. For further insight into excited-state relaxation processes, time-resolved PL decay measurements were carried out in chloroform solution and thin film. PL decay for both conditions is depicted in **Figure 3.10**

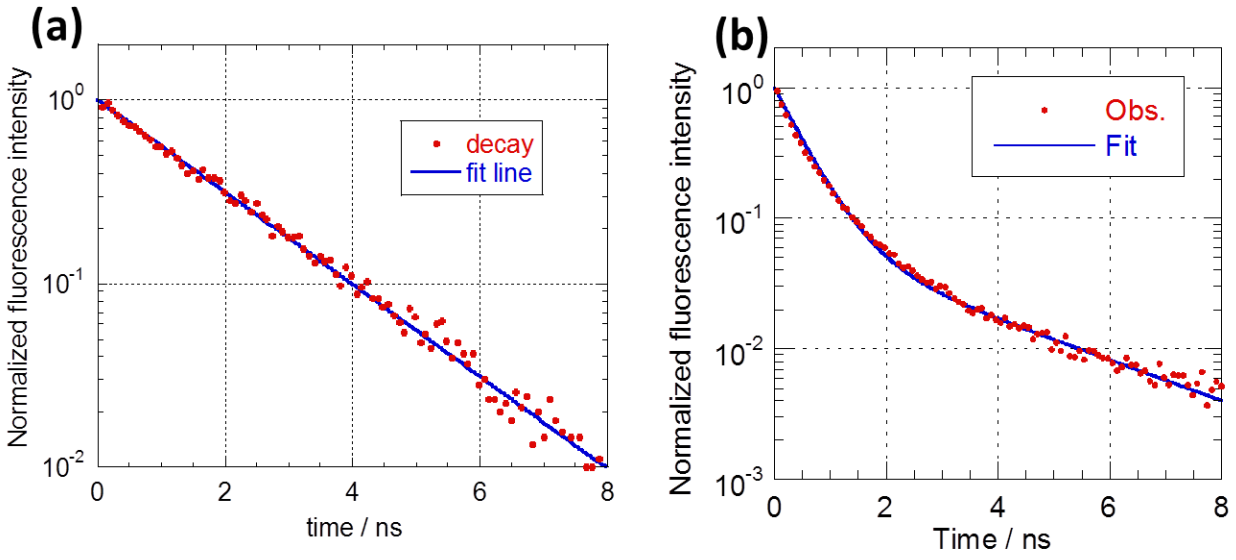

Figure 3.10: Transient PL decay curves of **PY-II** in solution (a) and thin film (b)

In solution, **PY-II** exhibited a simple exponential decay with a fluorescence lifetime (t) of 1.75 ns, while in thin films a double exponential decay profile was observed with a lifetime of 0.5 ns (93%) and 2.8 ns (7%) for fast and slow components, respectively [**Figure 3.10(b)** and **Figure 3.11**]. The fast component spectrum of thin film sample was similar to that in solution. This suggests that the fast component originated from the pyrene moiety and quenched through some decay process, judging from the shorter lifetime. After decay of the fast component fluorescence, the slow component fluorescence was observed (**Figure 3.11)** in the longer wavelength range.

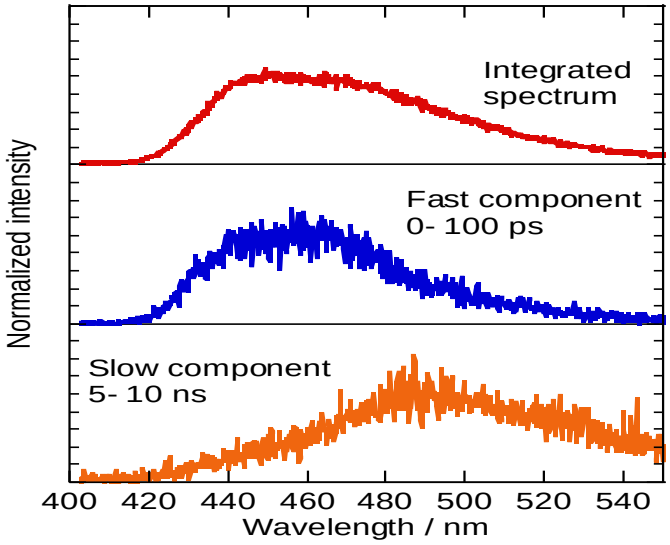

Figure 3.11: Photoluminescence (PL) decay spectrum of **PY-II**

This could be the possible reason for the slight difference of spectral shape between the solution and the film, which suggests that energy transfer takes place from the pyrene moiety to some defect sites, presumably due to the aggregates of carbazole moieties. The high photoluminescence in solution of **PY-II** is an attractive signature to use this fluorescent material with high brightness not only in photonic applications but also in other applications such as bioimaging or chemical sensing where a high solution quantum yield is desired.[52]

The HOMO level of **PY-II** was characterized by photoelectron spectroscopy in air (PESA) as shown in **Figure 3.12**. The thin film of **PY-II** was spin coated on an ITO substrate, which was used for the determination of ionization potential. The photoelectron yield ratio was measured with respect to the applied UV- energy. The onset value calculated from this graph gave a HOMO value of -5.71 eV.

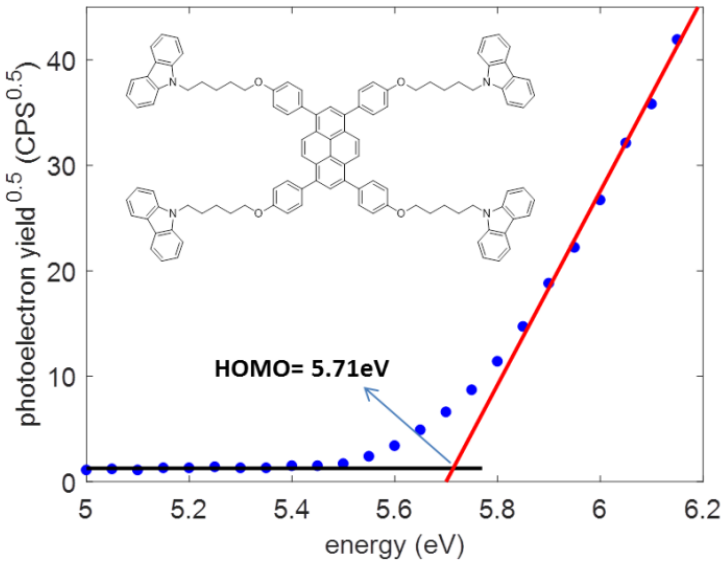

Figure 3.12: Photoelectron spectroscopy in air (PESA) analysis of **PY-II** in thin film

Additionally, HOMO level of **PY-II** was investigated using cyclic voltammetry and the voltammogram is shown in **Figure 3.13.** HOMO level calculated from onset oxidation potential (-0.84 eV) was found to be -5.64 eV, which is in good agreement with HOMO level (-5.71 eV) calculated by PESA. Such a low HOMO value could be attributed to presence of a non-conjugated aliphatic spacer in the structure, which is important for obtaining air stable organic electronic devices.[53]

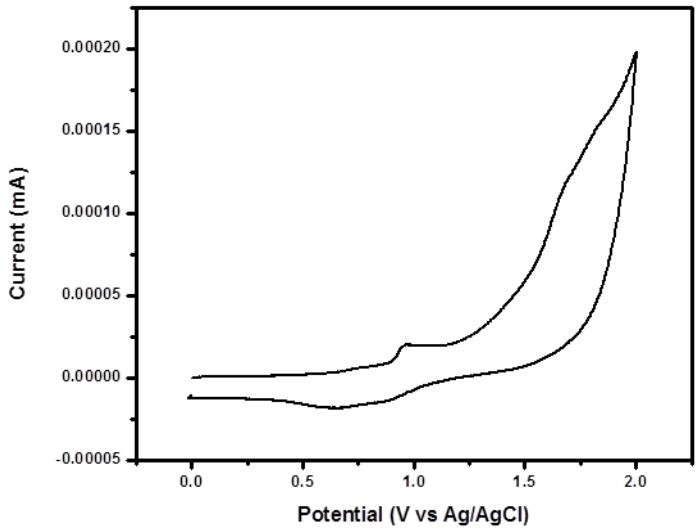

Figure 3.13: Cyclic voltammogram of **PY-II**

3.3.3 Density functional theory (DFT) studies

Density functional theory (DFT)[54] calculations were performed to compute molecular structures, the energies of the frontier orbitals and their localization as well as absorption and photoluminescence spectra. The calculations were carried out using B3LYP[55] (for frontier orbital energies and optical properties) and CAM-B3LYP.[56] (for the oxidation potential) with the LANL2DZ basic set. The absorption and PL spectra were computed with time dependent DFT (TD-DFT) considering the lowest six excited states.[57] The PL spectrum was computed by optimizing the first excited state. The calculations were performed with polarizable continuum model (PCM) of chloroform solvent.[58] The calculations were performed using Gaussian 09.[59] Highest occupied molecular orbital (HOMO) and lowest unoccupied molecular orbital (LUMO) of **PY-II** are shown in **Figure 3.14**

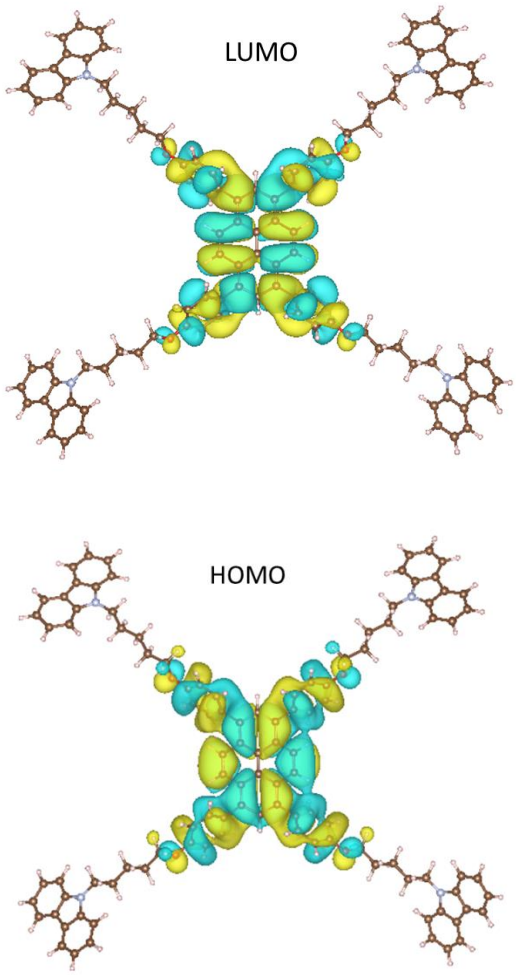

Figure 3.14: Distributions of the HOMO and LUMO of **PY-II** obtained with DFT

The HOMO and LUMO energy levels are centered on pyrene core. HOMO is only slightly more delocalized than LUMO and has appreciable amplitude on the oxyphenylene moieties, while the LUMO is localized on central pyrene core and partially on oxyphenylene moieties. Theoretically predicted HOMO and LUMO values were found to be -5.18 eV and -1.96 eV, respectively. The HOMO–LUMO band gap for **PY-II** was calculated to be 3.22 eV. Absorption and photoluminescence peak maximum of **PY-II** computed by B3LYP were 424 nm and 523 nm, respectively. The absorption and PL spectra are shown in **Figure 3.15** It was previously shown that a functional with a significant fraction of exact exchange is required to accurately estimate the oxidation potential.[60,61] The oxidation potential was, therefore, estimated using range-separated hybrid functional CAM-B3LYP from the difference in energies of (respectively

optimized) neutral and cationic states,[60,61] giving a value of 5.44 eV, which is in good agreement with the experimental value (5.71 eV) calculated by PESA study.

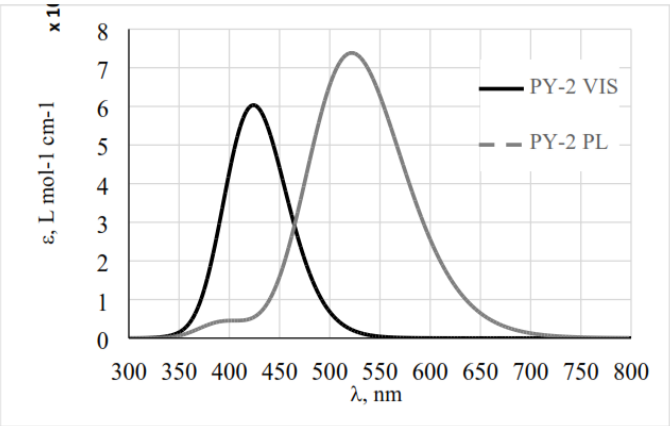

Figure 3.15: Visible absorption (VIS) and photoluminescence (PL) spectra of **PY-II** in chloroform solution computed with DFT.

3.3.4) OLED Device Fabrication and Studies

PY-II was used as emissive layer in the OLED device in order to evaluate its electroluminescence properties. The device configuration using **PY-II** as an active emissive layer is shown in **Figure 3.16** with an ITO/PEDOT:PSS (50 nm)/**PY-II** (35 nm)/TPBi(20 nm)/LiF(1nm)/Al (200 nm) device architecture. ITO coated glass and LiF/Al act as an anode and cathode, respectively, whereas TPBi namely, 2,2',2''-(1,3,5-benzinetriyl)-tris(1-phenyl-1-H-benzimidazole) is an electron transporting layer.

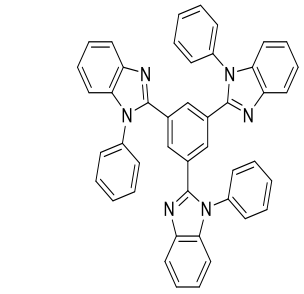

2,2',2"-(1,3,5-Benzinetriyl)-tris(1-phenyl-1-H-benzimidazole)
(TPBi)

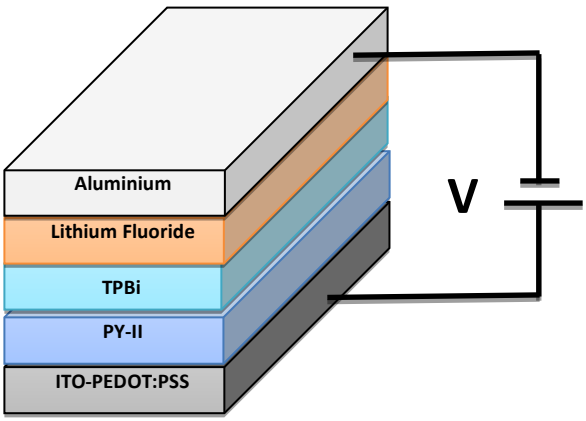

Figure 3.16: The OLED device architecture of **PY-II**

When a potential is applied, holes are injected from the anode and electrons are injected from the cathode, respectively. Due to the recombination of holes and electrons in the active emissive layer, blue photon emission was observed in OLED devices. The obtained OLED device performance parameters such as the turn-on voltage, current efficiency, power efficiency, CIE co-ordinates, electroluminescent peak and maximum brightness and their values are given in **Table 3.1**

Table 3.2: EL performance summary of **PY-II-**based OLED device

Turn-on voltage (V_{on}) @ 1Cdm^{-2}	**Current Efficiency (Cd A^{-1})**	**Power efficiency (lm W^{-1})**	**CIE coordinates**	**EL Peak (nm)**	**Maximum brightness (cd m^{-2})**
4.5	**0.41**	**0.17**	**(0.16,0.16)**	**445,470**	**202**

The observed electroluminescence (EL) spectrum is shown in **Figure 3.17. PY-II** device exhibited EL maxima of 445 nm and 470 nm emission peaks in the visible blue region with a full wave half maximum (FWHM) of 70 nm and CIE coordinates of (0.16,0.16). It was noticed that **PY-II** exhibited a different EL spectrum than the PL spectrum. EL spectrum of the **PY-II** device was measured from 5V to 11V and it was observed that the spectrum contained two emission peaks, one at 445 nm and other at 470 nm.

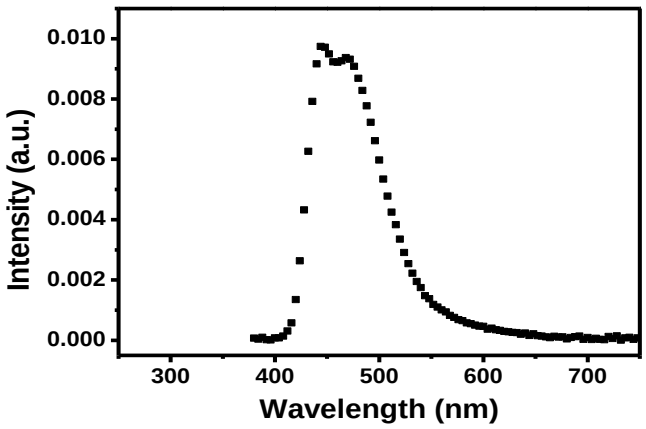

Figure 3.17: Electroluminescence spectrum of **PY-II-**based OLED device

The difference between PL and EL spectra is attributed to the voltage effect and this can be clearly seen in the applied voltage–EL graph (**Figure S 3.10**).

The details of J–V–B, CE and PE characteristics of **PY-II** device are shown in **Figure 3.18**. The **PY-II** device showed turn-on voltage (V_{on}), maximum current efficiency (CE_{max}), maximum power efficiency (PE_{max}), and maximum brightness (B_{max}) of 4.5 V, 0.41 cd A^{-1}, 0.17 lm $W^{-1}$and 202 cd m^{-2}, respectively. As the voltage was increased from 4.5 V to 7 V and 8.5 V, the CE and PE of **PY-II** device increased rapidly to CE_{max} and PE_{max} of 0.41 cd A^{-1} and 0.17 lm W^{-1}, respectively. As the drive voltage was further increased, CE and PE curves of **PY-II** device typically roll-off. However, CE and PE of **PY-II** device still remained at higher than one-half of CE_{max} and PE_{max} even as drive voltage was further increased beyond 10 V. The stable blue colour output additionally proved that **PY-II** is a promising candidate to be a blue emitter in OLED applications. A turn on voltage of 4.5 V also makes the **PY-II**-based OLED device energy efficient.

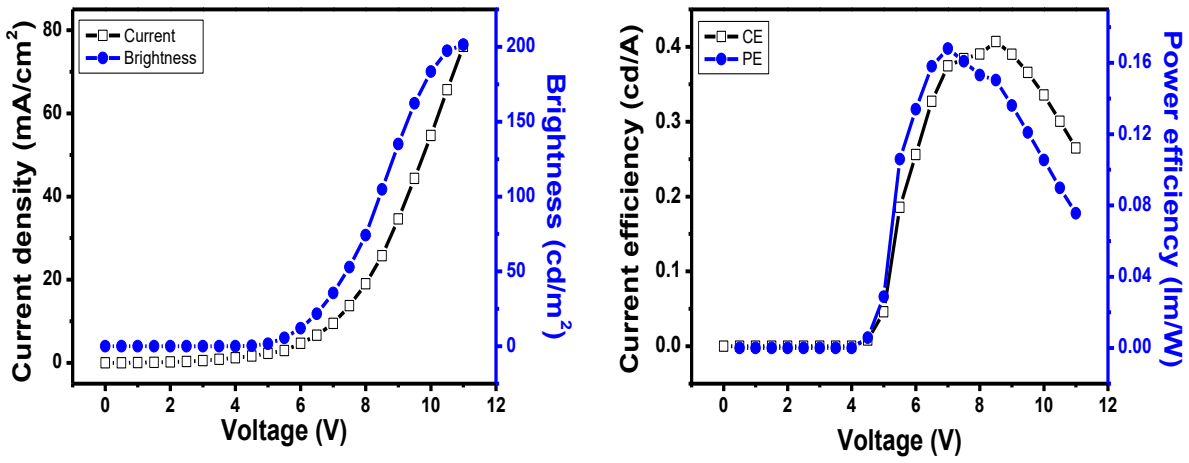

Figure 3.18: Current-Voltage-Brightness (J-V-B) and (left) and CE and PE (right) characteristics of **PY-II** -based OLED device

3.3.5) Atomic force microscopy (AFM) studies

The morphological behaviour of **PY-II** active layer thin film was characterized by AFM as shown in **Figure 3.19.** The measured root mean square (RMS) roughness of film samples is 3.46 nm. Pristine ITO coated glass showed surface roughness with an RMS of 3.25 nm. **PY-II** exhibited a low roughness value, which is desirable for transportation of holes and electrons in the recombination zone.

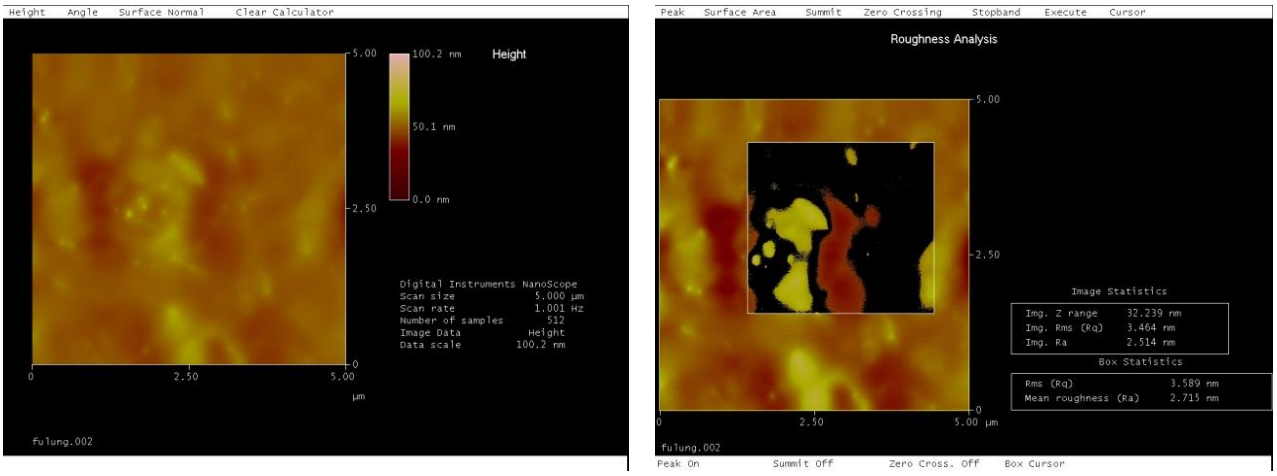

Figure 3.19: Atomic force microscopy image of **PY-II** spin coated thin film on ITO coated glass

3.4) Conclusions

In summary, the work in this chapter demonstrated the design strategy and synthesis of a new 1,3,6,8- tetrasubstituted pyrene cored small organic molecule namely, 1, 3, 6, 8-tetrakis (4-((5-(9H-carbazol-9-yl) pentyl) oxy) phenyl) pyrene (**PY-II)**, containing a carbazole moiety with an alkyl spacer for solution processable OLEDs. **PY-II** exhibited excellent solution processability and high thermal stability. **PY-II** showed wide absorption in the range of 275 nm to 500 nm with an optical band gap of 2.76 eV. The PLQY of PY-II was found to be 0.90 and 0.33 in solution and the solid state, respectively. The HOMO level calculated using PESA was found to be -5.71 eV. The solution processed non-doped OLED device using **PY-II** as EML exhibited a turn-on voltage of 4.5 V, blue emission with EL peaks at 445 nm and 470 nm, a maximum brightness of 202 cd m^{-2} and a power efficiency of 0.17 lm W^{-1}. These results support that this class of functional materials hold high potential for future cost effective and efficient light emitting materials for OLED devices. Further improvements with introduction of a larger number of conjugated moieties on pyrene core would greatly improve the performance of electroluminescent molecules in OLEDs. The higher PLQY and higher brightness of **PY-II** in solution are important attributes for bioimaging and sensor applications. Overall, the present study pinpoints a useful strategy to design new solution processable pyrene-based materials as blue emitters with bright photoluminescence.

3.5) References

1. C. W. Tang and S. A. Van Slyke, *Appl. Phys. Lett.*, 1987, **51**, 913.
2. C. W. Tang, S. A. VanSlyke and C. H. Chen, *J. Appl. Phys.*, 1989, **65**, 3610.
3. J. H. Burroughes, D. D. C. Bradley, A. R. Brown, R. N. Marks, K. Mackay, R. H. Friend, P. L. Burns and A. B. Holmes, *Nature*, 1990, **347**, 539.
4. L. S. Hung and C. H. Chen, *Mater. Sci. Eng. R. Rep.*, 2002, **39**, 143.
5. R.-P. Xu, Y.-Q. Li and J.-X. Tang, *J. Mater. Chem. C*, 2016, **4**, 9116.
6. S. Feng, L. Duan, L. Hou, J. Qiao, D. Zhang, G. Dong, L. Wang and Y. Qiu, *J. Phys. Chem. C*, 2011, **115**, 14278.
7. M. Zhang, S. Xue, W. Dong, Q. Wang, T. Fei, C. Gu and Y. Ma, *Chem. Commun.*, 2010, **46**, 3923.
8. M. Cai, T. Xiao, E. Hellerich, Y. Chen, R. Shinar and J. Shinar, *Adv. Mater.*, 2011, **23**, 3590.
9. Y. R. Cho, H. S. Kim, Y.J. Yu and M. C. Suh, Sci. *Rep.*, 2015, **5**, 15903.
10. H. Wu, G. Zhou, J. Zou, C. L. Ho, W. Y. Wong, W. Yang, J. Peng and Y. Cao, *Adv. Mater.*, 2009, **21**, 4181.
11. L. Duan, L. Hou, T.W. Lee, J. Qiao, D. Zhang, G. Dong, L. Wang and Y. Qiu, *J. Mater. Chem.*, 2010, **20**, 6392.
12. J.-H. Jou, S. Kumar, A. Agrawal, T.-H. Li and S. Sahoo, J. *Mater. Chem. C*, 2015, **3**, 2974.
13. A. C. Grimsdale, K. Leok Chan, R. E. Martin, P. G. Jokisz and A. B. Holmes, *Chem. Rev.*, 2009, **109**, 897.
14. X.-H. Zhu, J. Peng, Y. Cao and J. Roncali, *Chem. Soc. Rev.*, 2011, **40**, 3509.
15. E. Kozma, W. Mrez, F. Villafiorita-Monteleone, F. Galeotti, A. M. Catellani and C. Botta, *RSC Adv.*, 2016, **6**, 61175.
16. R. K. Konidena, K. R. J. Thomas, S. Sahoo, D. K. Dubey and J.-H. Jou, *J. Mater. .Chem. C*, 2017, **5**, 709.
17. K. S. Yook and J. Y. Lee, *Adv. Mater.*, 2014, **26**, 4218.
18. Y.L. Deng, L.-S. Cui, Y. Liu, Z.-K. Wang, Z.Q. Jiang and L.-S. Liao, *J. Mater. Chem. C*, 2016, **4**, 1250.

19. J. N. Moorthy, P. Natarajan, P. Venkatakrishnan, D.F. Huang and T. J. Chow, *Org. Lett*, 2007, **9**, 5215.
20. M. Y. Lo, C. Zhen, M. Lauters, G. E. Jabbour and A. Sellinger, *J. Am. Chem. Soc.*, 2007, **129**, 5808.
21. R. Xia, W. Y. Lai, P. A. Levermore, W. Huang and D. D. C. Bradley, *Advanced Functional Materials*, 2009, **19**, 2844.
22. Z. Zhao, J.H. Li, X. Chen, X. Wang, P. Lu and Y. Yang, J.Org. *Chem.*, 2008, **74**, 383.
23. J. B. Birks, Photophysics of Aromatic Molecules, Wiley-Interscience, London, 1970.
24. J. R. Lackowicz, Principles of Fluorescence Spectroscopy, Kluwer Academic/Plenum Publishers, New York, 2nd Ed.,1999, p. 595.
25. T. M. Figueira Duarte and K. Mullen, *Chem. Rev.*, 2011, **111**, 7260.
26. J. K. Salunke, P. Sonar, F. L. Wong, V. A. L. Roy, C. S. Lee and P. P. Wadgaonkar, *Phys. Chem. Chem. Phys.*, 2014, **16**, 23320.
27. P. Sonar, M. S. Soh, Y. H. Cheng, J. T. Henssler and A. Sellinger, *Org. Lett.*, 2010, **12**, 3292.
28. R. K. Konidena, K. R. J. Thomas, M. Singh and J.-H. Jou, *J.Mater. Chem. C*, 2016, **4**, 4246.
29. T. H. El-Assaad, M. Auer, R. Castada, K. M. Hallal, F. M. Jradi, L. Mosca, R. S. Khnayzer, D. Patra, T. V. Timofeeva and J.L. Bredas, *J. Mater. Chem. C*, 2016, **4**, 3041.
30. R. Zhang, Y. Zhao, T. Zhang, L. Xu and Z. Ni, *Dyes Pigm.*, 2016, **130**, 106.
31. D. G. Vanga, M. Santra, A. Keerthi and S. Valiyaveettil, *Org. Biom. Chem.*, 2014, **12**, 7914.
32. C. H. Chang, C.L. Ho, Y.S. Chang, I. C. Lien, C.-H. Lin, Y.W. Yang, J.L. Liao and Y. Chi, *J. Mater. Chem. C*, 2013, **1**, 2639.
33. F. Zhao, L. Zhu, Y. Liu, Y. Wang and D. Ma, *Org. Electron.*, 2015, **27**, 207.
34. M.Y. Chang, C.H. Wang, S.C. Lin and Y.F. Chen, *J. Appl. Phys.*, 2009, **105**, 064318.
35. J. Liang, L. Ying, F. Huang and Y. Cao, *J. Mater. Chem. C*, 2015, **4**, 10993.
36. L. Chen, Z. Ma, J. Ding, L. Wang, X. Jing and F. Wang, *Chem. Commun.*, 2011, **47**, 9519.
37. J.X. Cai, T.L. Ye, X.F. Fan, C.M. Han, H. Xu, L.L. Wang, D.G. Ma, Y. Lin and P. F. Yan, *J. Mater. Chem.*, 2011, **21**, 15405.

38. H. Xu, D.H. Yu, L.L. Liu, P.F. Yan, L.W. Jia, G.M. Li and Z.Y. Yue, *J. Phys. Chem. B*, 2009, **114**, 141.
39. X. Ban, W. Jiang, T. Lu, X. Jing, Q. Tang, S. Huang, K. Sun, B. Huang, B. Lin and Y. Sun, *J. Mater. Chem. C*, 2016, **4**, 8810.
40. D. Xia, B. Wang, B. Chen, S. Wang, B. Zhang, J. Ding, L. Wang, X. Jing and F. Wang, *Angew. Chem.*, 2014, **126**, 1066.
41. T. Keawin, C. Sooksai, N. Prachumrak, T. Kaewpuang, D. Muenmart, S. Namuangruk, S. Jungsuttiwong, T. Sudyoadsuk and V. Promarak, *RSC Adv.*, 2015, **5**, 16422.
42. P. Moonsin, N. Prachumrak, S. Namuangruk, S. Jungsuttiwong, T. Keawin, T. Sudyoadsuk and V. Promarak, *J.Mater. Chem. C*, 2014, **2**, 5540.
43. J. Li, D. Liu, Y. Li, C.-S. Lee, H.-L. Kwong and S. Lee, *Chem. Mater.*, 2005, **17**, 1208.
44. D. Curiel, M. Mas-Montoya, C.H. Chang, P.Y. Chen, C.W. Tai and A. Tarraga, *J. Mater. Chem. C*, 2013, **1**, 3421.
45. S. J. Kim, Y. J. Kim, Y. H. Son, J. A. Hur, H. A. Um, J. Shin, T. W. Lee, M. J. Cho, J. K. Kim and S. Joo, *Chem. Commun.*, 2013, **49**, 6788.
46. X. Wang, S. Wang, Z. Ma, J. Ding, L. Wang, X. Jing and F. Wang, *Adv. Funct. Mater.* 2014, **24**, 3413.
47. K. N. Armarego and D. D. Perrin, *Purification of Laboratory Chemicals*, Butterworth-Heinemann, Oxford, 4th Edition, Butterworth Heinemann, 1996.
48. H. Ishida, S. Tobita, Y. Hasegawa, R. Katoh and K. Nozaki, *Coord. Chem. Rev.*, 2010, **254**, 2449.
49. A. Suzuki, *J. Organomet. Chem.*, 1999, **576**, 147.
50. L. Zhang, Y.X. Zhang, Y. Hu, X.B. Shi, Z.Q. Jiang, Z.K. Wang and L.S. Liao, *ACS Appl. Mater. Interfaces*, 2016, **8**, 16186.
51. G. Wyszecki and W. S. Stiles, *Color Science*, Wiley New York, **1982**.
52. J.-C. Hsiang, A. E. Jablonski and R. M. Dickson, *Acc. Chem . Res.*, 2014, **47**, 1545.
53. H. Nakanotani, K. Masui, J. Nishide, T. Shibata and C. Adachi, *Sci. Rep.*, 2013, **3**, 2127.
54. W. Kohn and L. J. Sham, *Phys. Rev.*, 1965, **140**, A1133.
55. A. D. Becke, *J. Chem. Phys.*, 1993, **98**, 5648.
56. T. Yanai, D. P. Tew and N. C. Handy, *Chem. Phys. Lett.*, 2004, **393**, 51.
57. M. A. L. Marques and E. K. U. Gross, *Annu. Rev. Phys. Chem.*, 2004, **55**, 427.

58. J. Tomasi, B. Mennucci and R. Cammi, *Chem. Rev.*, 2005, **105**, 2999.

59. M. J. Frisch, G. W. Trucks, H. B. Schlegel, G. E. Scuseria, M. A. Robb, J. R. Cheeseman, G. Scalmani, V. Barone, B. Mennucci and G. A. Petersson, *Gaussian Inc. Wallingford CT*, 2009, **27**, 34.

60. M. A. Sk, Y. Chen and S. Manzhos, *Chem. Phys. Lett.*, 2016, **659**, 270.

61. Y. Chen and S. Manzhos, *J. Power Sources*, 2016, **336**, 126.

Supporting Information

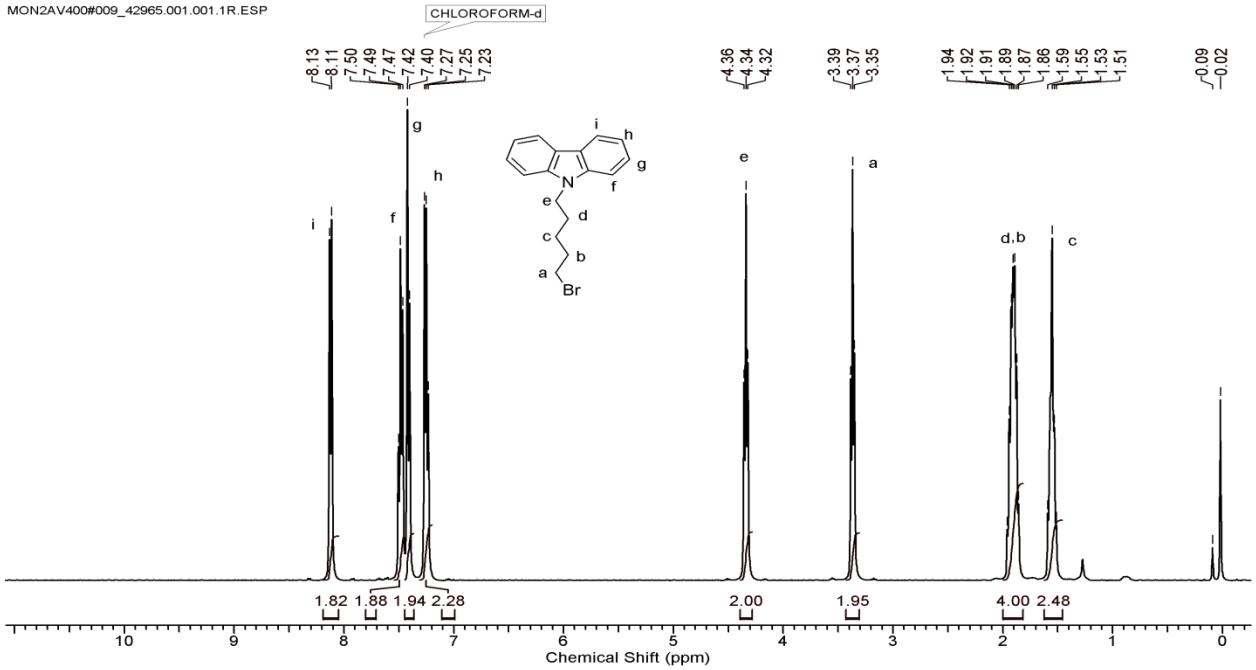

Figure S 3.1: ^{1}H NMR spectrum (in $CDCl_3$) of 9-(5-bromopentyl)-9H-carbazole (**2**)

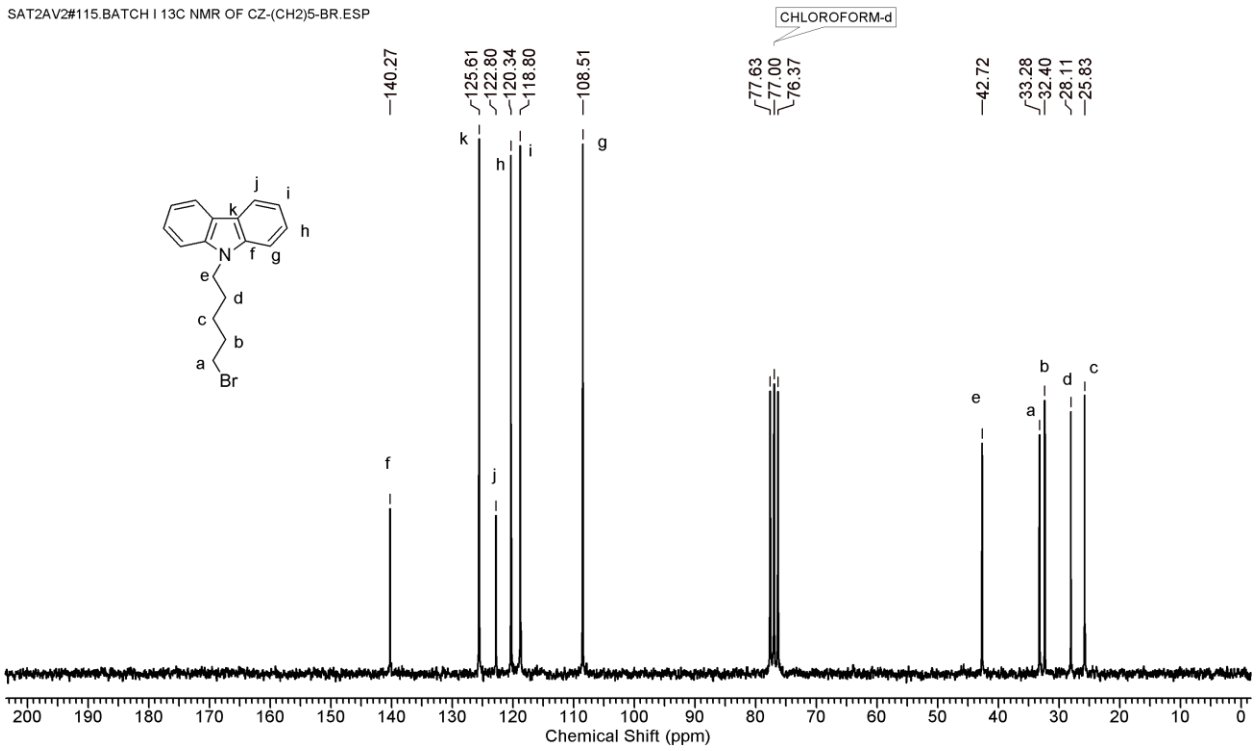

Figure S 3.2: ^{13}C NMR spectrum (in $CDCl_3$) of 9-(5-bromopentyl)-9H-carbazole (**2**)

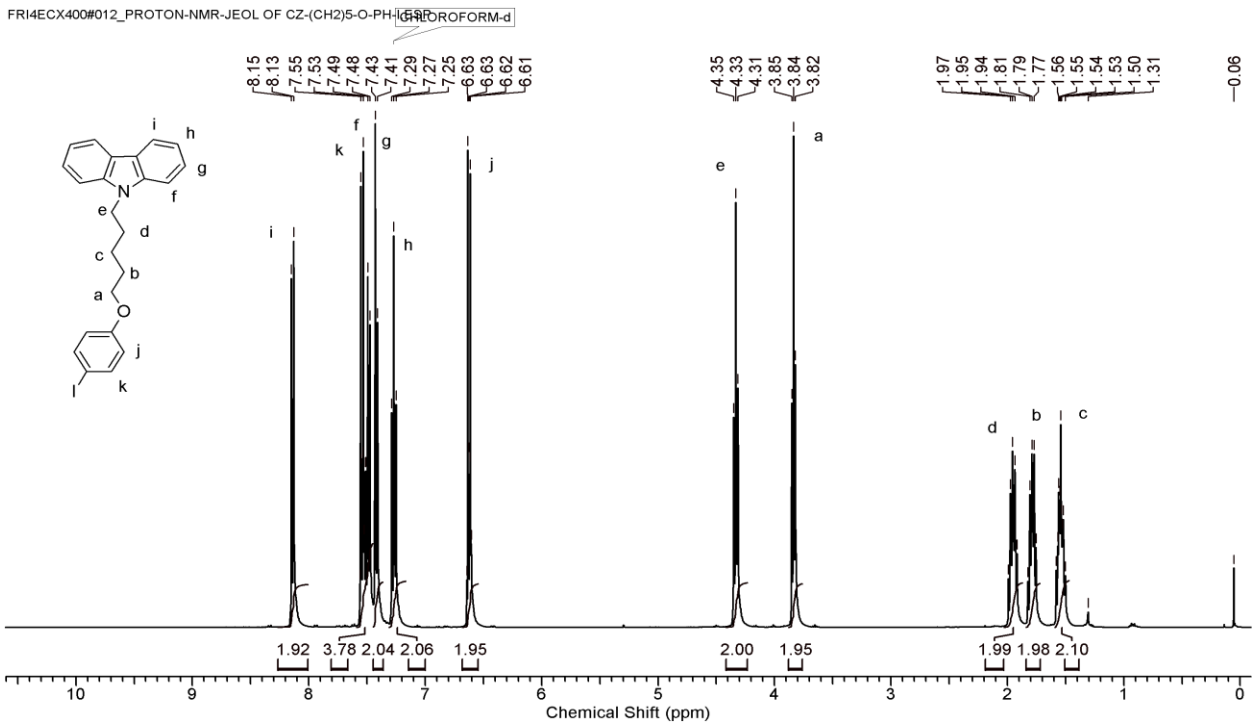

Figure S 3.3: ^{1}H NMR spectrum (in $CDCl_3$) of 9-(5-(4-iodophenoxy)pentyl)-9H-carbazole (**3**)

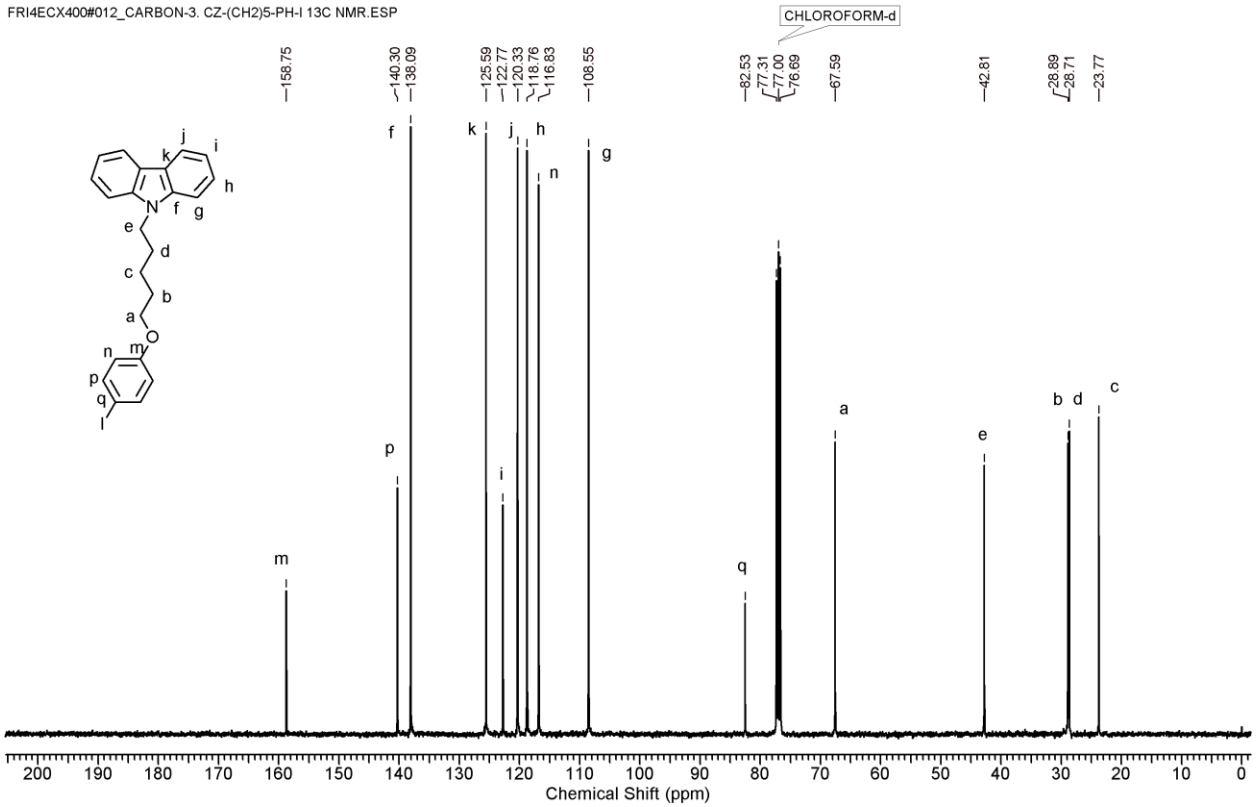

Figure S 3.4: ^{13}C NMR spectrum (in $CDCl_3$) of 9-(5-(4-iodophenoxy)pentyl)-9H-carbazole (**3**)

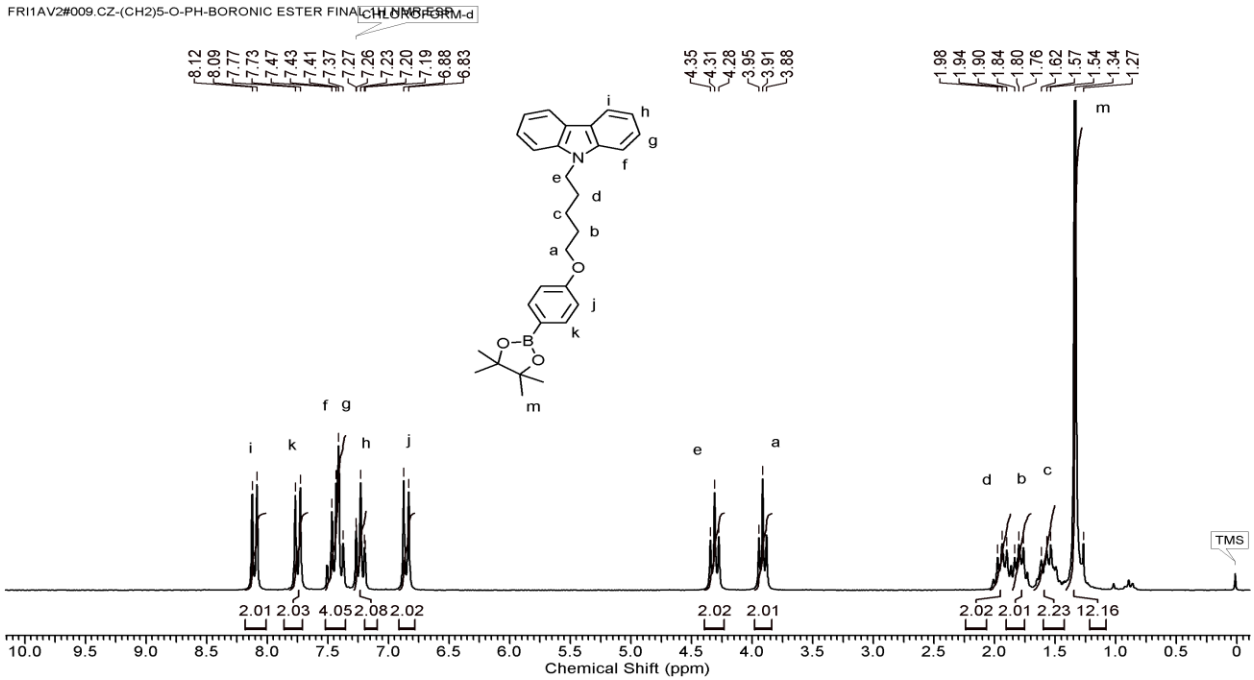

Figure S 3.5: ^{1}H NMR spectrum (in $CDCl_3$) of 9-(5-(4-(4,4,5,5-tetramethyl-1,3,2-dioxaborolan-2-yl)phenoxy)pentyl)-9H-carbazole (**4**)

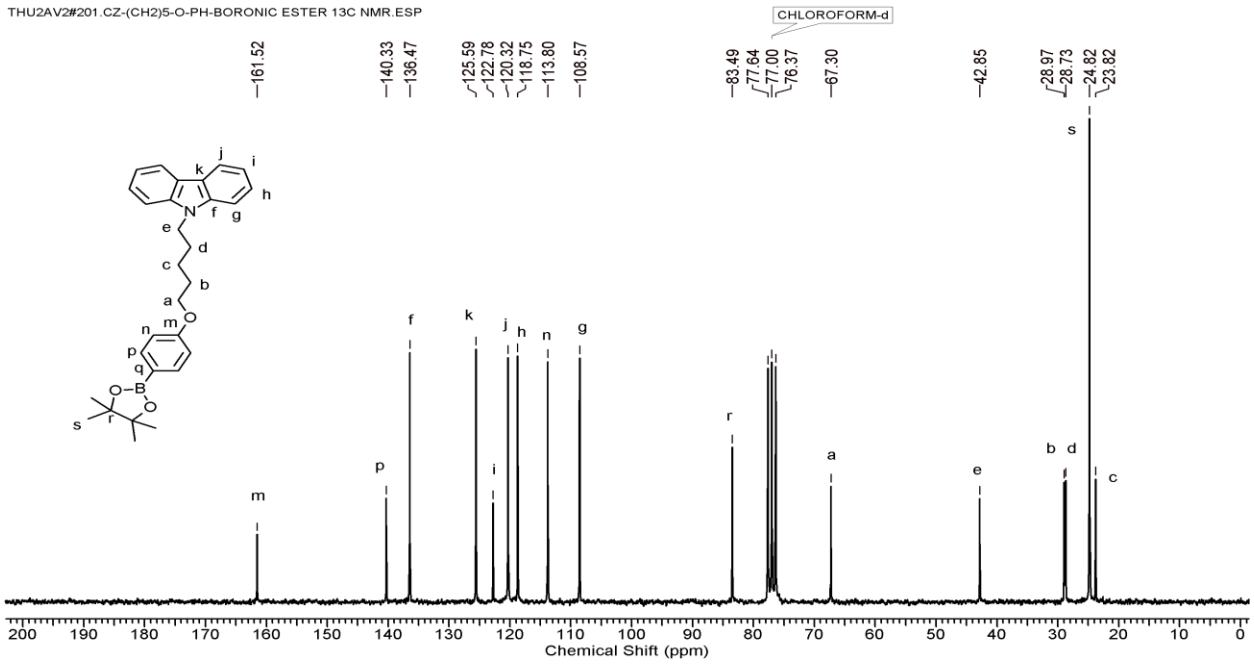

Figure S 3.6: ^{13}C NMR spectrum (in $CDCl_3$) of 9-(5-(4-(4,4,5,5-tetramethyl-1,3,2-dioxaborolan-2-yl)phenoxy)pentyl)-9H-carbazole (**4**)

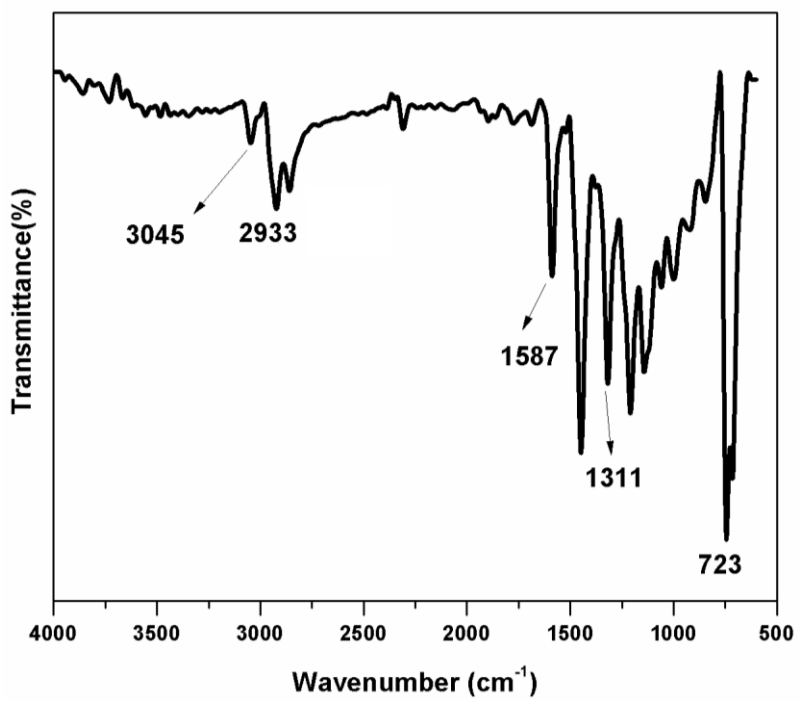

Figure S 3.7: IR spectrum of 9-(5-bromopentyl)-9H-carbazole

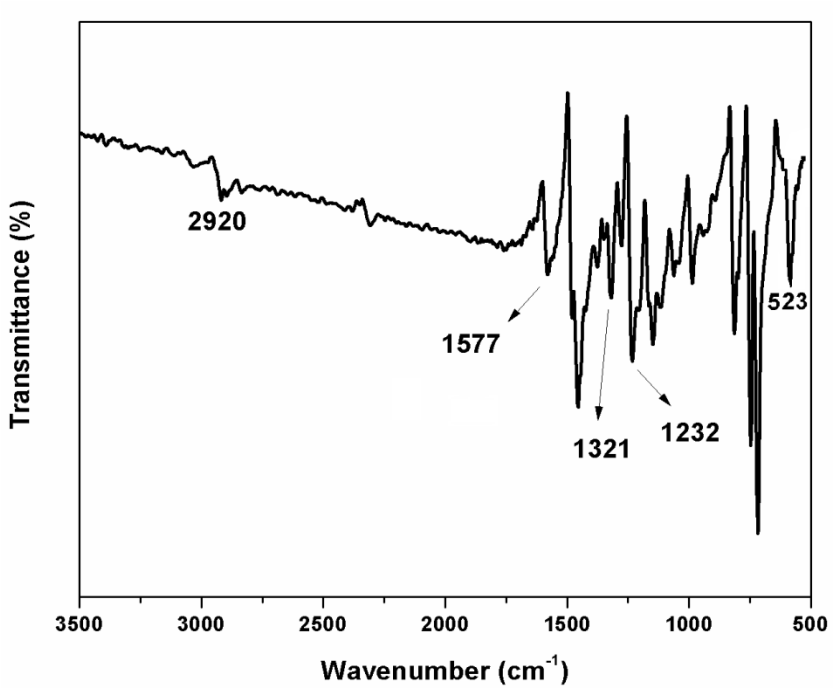

Figure S3.8: IR spectrum of 9-(5-(4-iodophenoxy)pentyl)-9H-carbazole

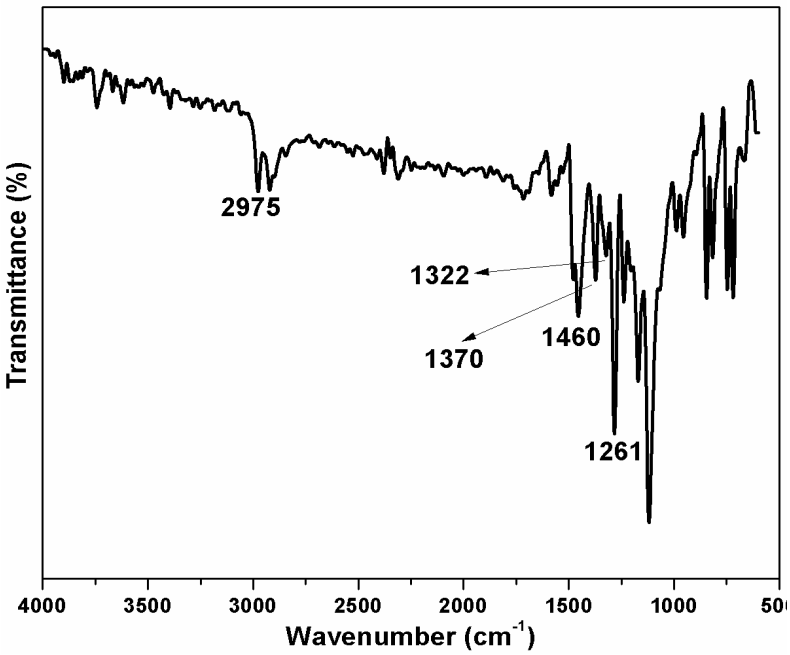

Figure S 3.9: IR spectrum of 9-(5-(4-(4,4,5,5-tetramethyl-1,3,2-dioxaborolan-2-yl)phenoxy)pentyl)-9H-carbazole

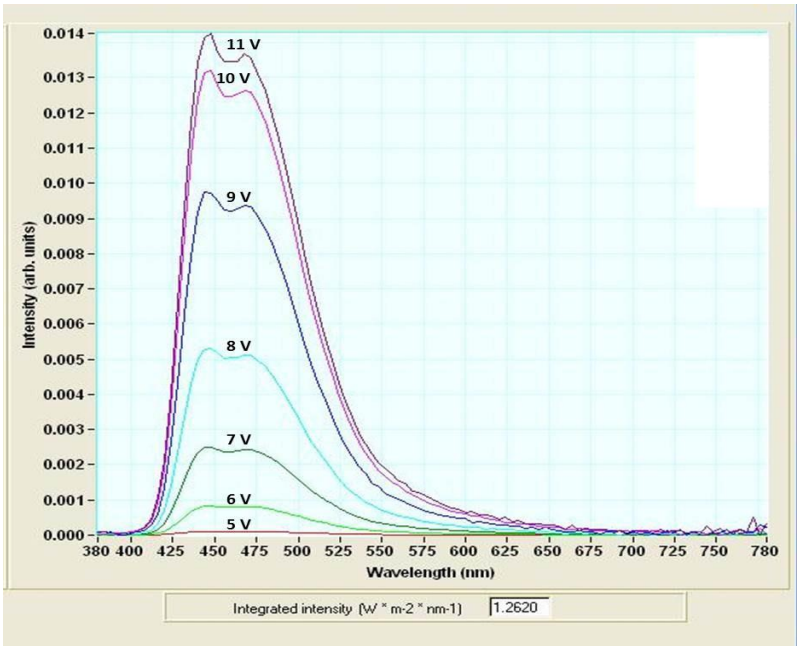

Figure S 3.10: Electroluminescent (EL) peak variation with respect to different applied bias using **PY-II -**based OLED devices.

Table S 3.1: Atomic coordinates of **PY-II**

opt B3LYP/6-31g(d,p) scrf-(solvent-chloroform)

C	-4.14325152	-4.26874240	-0.00100104
C	-2.74056333	-4.26031318	-0.00084069
C	-2.04892783	-3.04147873	-0.00067431
C	-2.76065934	-1.83850984	-0.00063619
C	-4.15840191	-1.84137154	-0.00077470
C	-4.85271971	-3.05867693	-0.00095287
C	-0.64526334	-3.02353227	-0.00055125
C	-2.07234038	-0.62862114	-0.00045438
C	-0.67460005	-0.62575706	-0.00034556
C	0.02719390	-1.84152129	-0.00040109
C	0.01971906	0.59154808	-0.00017497
C	-0.68975054	1.80161882	-0.00007923
C	-2.09244304	1.79318145	-0.00016375
C	-2.78407097	0.57434547	-0.00037674
C	-4.18773520	0.55640104	-0.00051852
C	-4.86019434	-0.62560749	-0.00072471
H	-5.93018872	-0.62896317	-0.00084439
H	-4.73157566	1.47788731	-0.00046714
H	-0.10142088	-3.94501723	-0.00057903
H	-4.67235651	-5.19876801	-0.00115486
H	1.09718833	-1.83816353	-0.00032089
H	-0.16064768	2.73164585	0.00006082
C	1.55969231	0.60070118	-0.00008826
C	2.26036201	0.60007042	1.21357695
C	2.26039830	0.60966486	-1.21369987
C	3.66173957	0.60839757	1.21362581
H	1.72535967	0.59322677	2.14019723
C	3.66177162	0.61800608	-1.21365107
H	1.72541960	0.61014344	-2.14035932
C	4.36244332	0.61736794	0.00001168
H	4.19671974	0.60790426	2.14028414
H	4.19677242	0.62486240	-2.14027263
C	-2.87144238	3.12162559	-0.00001916
C	-3.22594600	3.72587816	1.21370638
C	-3.22582512	3.72625929	-1.21358939
C	-3.93481645	4.93477043	1.21386562
H	-2.95537245	3.26422244	2.14029373
C	-3.93471255	4.93514598	-1.21343010
H	-2.95515691	3.26490034	-2.14029645
C	-4.28920182	5.53940417	0.00029748
H	-4.20547140	5.39613614	2.14057384
H	-4.20530368	5.39679326	-2.14001630
C	-6.39269135	-3.06785821	-0.00108143
C	-7.09327251	-3.07191539	-1.21479115
C	-7.09348407	-3.07214786	1.21250455
C	-8.49464699	-3.08024682	-1.21491581
H	-6.55820019	-3.06865581	-2.14139089

C	-8.49485982	-3.08045881	1.21238034
H	-6.55857420	-3.06907025	2.13919857
C	-9.19544113	-3.08450800	-0.00133006
H	-9.02955550	-3.08335203	-2.14161065
H	-9.02993191	-3.08370983	2.13898003
C	-1.96160367	-5.58877940	-0.00084058
C	-1.60731990	-6.19331718	1.21280684
C	-1.60703962	-6.19314916	-1.21448892
C	-0.89849725	-7.40223944	1.21280512
H	-1.87802438	-5.73186008	2.13945474
C	-0.89819732	-7.40205978	-1.21449079
H	-1.87753524	-5.73156634	-2.14113515
C	-0.54393492	-8.00661012	-0.00084369
H	-0.62801441	-7.86382948	2.13945162
H	-0.62746807	-7.86350232	-2.14113873
N	5.83241733	0.62610911	0.00006312
C	6.77018906	-0.11637110	-0.91175596
C	6.76123716	1.37969557	0.91195556
C	6.48423332	-0.97474173	-1.95612362
C	8.12513833	0.17636320	-0.56466469
C	6.46500422	2.23461721	1.95628822
C	8.11959605	1.10307984	0.56497751
C	7.54918284	-1.55015430	-2.66542327
H	5.44597394	-1.20660487	-2.23138325
C	9.17011599	-0.39623988	-1.27036168
C	7.52299790	2.82263859	2.66564386
H	5.42404624	2.45416634	2.23143877
C	9.15767852	1.68821768	1.27059572
C	8.86903391	-1.26554023	-2.32807634
H	7.33308304	-2.23498506	-3.49871921
H	10.21476507	-0.17612367	-1.00942753
C	8.84616424	2.55403826	2.32815254
H	7.29871488	3.50467691	3.49907129
H	10.20491008	1.48055490	1.00979922
H	9.69029206	-1.72665585	-2.89640875
H	9.66184140	3.02518610	2.89629129
N	-5.03277788	6.80747144	0.00046435
C	-5.77505718	7.45399247	1.13762692
C	-5.23469850	7.77115968	-1.13649638
C	-5.93718351	7.02130647	2.43984523
C	-6.35850436	8.68464620	0.70503703
C	-4.77806078	7.70163198	-2.43877267
C	-6.02377828	8.88111926	-0.70360867
C	-6.68415661	7.81369578	3.32442055
H	-5.49277610	6.07667068	2.78288484
C	-7.09433798	9.46043577	1.58512809
C	-5.10496919	8.74058790	-3.32308411
H	-4.17065864	6.85266997	-2.78203543
C	-6.34147678	9.90237354	-1.58338473
C	-7.25264831	9.01237455	2.90394301
H	-6.81962819	7.47885788	4.36346119

H	-7.54621221	10.40801633	1.25996621
C	-5.87311305	9.82208514	-2.90221074
H	-4.74692092	8.69541993	-4.36223844
H	-6.94777723	10.75933892	-1.25805001
H	-7.83485777	9.61970269	3.61265944
H	-6.11861377	10.62704369	-3.61063314
N	0.19958717	-9.27470905	-0.00084549
C	0.74825336	-10.03491765	1.17523062
C	0.59505407	-10.12474892	-1.17693427
C	0.68868903	-9.73240610	2.52215805
C	1.40532310	-11.22234096	0.72763874
C	0.36012733	-9.92503486	-2.52385645
C	1.31041300	-11.27799658	-0.72935146
C	1.28505089	-10.61323271	3.43693677
H	0.18589997	-8.82205142	2.87707836
C	1.99130889	-12.08611958	1.63778598
C	0.83756512	-10.87560147	-3.43861406
H	-0.18881798	-9.04174763	-2.87877320
C	1.77787298	-12.21131245	-1.63946200
C	1.92510474	-11.76989091	3.00186452
H	1.24363502	-10.38226128	4.51165131
H	2.49852064	-13.00120650	1.30136118
C	1.53403982	-11.99918205	-3.00352173
H	0.65642754	-10.72655342	-4.51334858
H	2.32876961	-13.10081035	-1.30310063
H	2.38664759	-12.44807320	3.73476375
H	1.90013512	-12.73332870	-3.73638877
N	-10.66541527	-3.09322650	-0.00146060
C	-11.59885127	-3.05679443	-1.18022124
C	-11.59857103	-3.14072980	1.17714468
C	-11.30792974	-3.00707381	-2.53009797
C	-12.95545080	-3.08079144	-0.73176266
C	-11.30730379	-3.18701662	2.52706934
C	-12.95527995	-3.13280173	0.72844994
C	-12.36950672	-2.98086096	-3.44698962
H	-10.26836173	-2.98831715	-2.88570651
C	-13.99707301	-3.05460395	-1.64401165
C	-12.36867012	-3.22581976	3.44374869
H	-10.26765419	-3.19350311	2.88286397
C	-13.99671768	-3.17155354	1.64048300
C	-13.69096183	-3.00426586	-3.01107267
H	-12.14944473	-2.94125082	-4.52405887
H	-15.04296258	-3.07271288	-1.30694109
C	-13.69023215	-3.21847063	3.00758881
H	-12.14834957	-3.26259075	4.52086855
H	-15.04270920	-3.16582382	1.30328648
H	-14.50951787	-2.98317457	-3.74565791
H	-14.50861103	-3.24965997	3.74200994

Chapter-4

Phenothiazine and Carbazole Substituted Pyrene-Based Electroluminescent Organic Semiconductors for OLED Devices

4.1) Introduction

Since the discovery of organic light emitting diodes (OLEDs), numerous classes of light emitting organic semiconductors have been designed and developed and these efforts are still continuing in order to find materials that are easy to synthesize and exhibit improved solution processability and high efficiency.[1-3] The OLED technology has been used successfully for flat panel display and solid-state lighting applications.[4,5] Still there is a demand for the development of efficient pure red, blue, and green light emitting materials for OLEDs. Blue light emitting materials are also one of the important key elements for fabricating white OLED devices. Conjugated building blocks such as anthracene,[6] pyrene,[7] phenothiazine[8] and carbazole[9,10] have been successfully used for designing and synthesizing light emitting active layers for OLED devices. However, current OLEDs still have some problems to get pure strong emission with lower power consumption which is determined by driving voltage and efficiency of the devices. Low driving voltage and high efficiency are required to reduce the power consumption of OLEDs[10] In addition to the above issues, the electroluminescence properties of blue light emitting materials remain challenging,[11] particularly in terms of easy availability, lower cost, efficiency, stability and color purity.

Thus, it is very important to explore the new class of blue light emitting materials using various synthetic methodologies and promising chromophores as building blocks of organic semiconductors. Among such potential building blocks, a pyrene conjugated system has attracted considerable interest in designing small organic molecules for different applications including OLEDs[12-15] and organic field effect transistors (OFETs)[16-19] due to its fused four aromatic condensed planar structure. Pyrene is a promising chromophore with a higher fluorescent quantum yield which makes it an attractive candidate for designing functional materials for fluorescent probes [20] and labeling experiments.[21] Recently, N,N-di-*para*-methoxyphenylamine-substituted pyrene has been successfully used as a hole transporting material for perovskite based solar cells with high efficiency.[22] These examples clearly reveal that pyrene is a versatile conjugated building block and can be used for designing a variety of conjugated functional materials. Pyrene possesses excellent thermal and chemical stability, however, despite these excellent properties pyrene itself is not a good candidate for light emitting devices due to its excimer emission tendency which diminishes the fluorescence efficiency.[23,24]

Nonetheless, this limitation of pyrene has been overcome by introducing bulky groups with long alkyl chains which enhances fluorescence quantum efficiency in OLEDs and also reduces the aggregation of the final material[25] In 2010, Sonar *et al* reported a series of star shaped organic semiconductors using bithiophene, phenylene, thienothiophene and benzothiadiazole-thiophene chromophores.[26] Among them, 1,3,6,8-tetrakis(4-butoxyphenyl)pyrene was used as the active emitting layer in simple solution-processed OLEDs with deep blue emission (CIE = 0.15, 0.18) and maximum efficiencies and brightness levels of 2.56 cd/A and 5000 cd/m^2, respectively. In 2014, synthesis of single, double and triple bond incorporated three pyrene cored small conjugated organic molecules were reported.[27] The molecules, namely PY-1, PY-2 and PY-3 were having an octyloxy naphthalene conjugated substituent decorated at 1, 3, 6, and 8 positions of pyrene *via* Suzuki, Heck and Sonogashira coupling reactions, respectively. The effects of single, double and triple bonds on their optical, electrochemical, and thermal properties were studied in detail and all these materials were used successfully in OLEDs.[27]

In the present work, two new pyrene based molecules, namely, 1,3,6,8-tetrakis(9-(4-methoxyphenyl)-9H-carbazol-3yl)pyrene (**PY-CA**) and 1,3,6,8-tetrakis(10-(4-methoxyphenyl)-10Hphenothiazin-3-yl)pyrene (**PY-PH**) were synthesized. The introduction of carbazole and phenothiazine units on 1, 3, 6, 8-tetrabromopyrene core is the effective way to design wide band gap electroluminescent materials. **PY-CA** and **PY-PH** were characterized by IR, ^{1}H and ^{13}C NMR spectra and MALDI-TOF. Optical properties were determined by UV-Vis absorption and photoluminescence spectroscopy. HOMO-LUMO energy levels of **PY-CA** and **PY-PH** were characterized by photoelectron spectroscoscopy in air (PESA). To evaluate their optoelectronic properties, **PY-CA** and **PY-PH** were used as an active layer in OLED devices and electroluminescence studies were performed. The highest brightness for carbazole and phenothiazine substituted pyrene derivatives were measured in OLED devices and were observed at 2500 cd m^{-2} and 2116 cd m^{-2}, respectively.

4.2) Experimental

4.2.1) Materials

All the chemicals namely, carbazole, phenothiazine, 1,3,6,8-tetrabromopyrene, 4-iodoanisole, N-bromosuccinimide, bis(pinacolato)diboron, tetrakis(triphenylphosphine) palladium [$Pd(PPh_3)_4$], [1,1′-bis(diphenylphosphino)ferrocene]dichloropalladium(II) [$Pd(dppf)Cl_2$], copper powder,

potassium acetate and potassium carbonate were purchased from Sigma-Aldrich and were used without further purification. The solvents namely, triethylene glycol dimethyl ether, chloroform, 1,4- dioxane and tetrahydrofuran (THF) were purchased from Sigma Aldrich and were purified according to the standard procedures.[28] All reactions were carried out under argon or nitrogen atmosphere.

4.2.2) Instrumentation

Melting points were recorded on Electrothermal MEL-TEMP apparatus and are uncorrected. IR spectra were recorded on Perkin Elmer GX spectrophotometer in the range of 4000-500 cm^{-1} using ATR mode. ^{1}H and ^{13}C NMR spectra were recorded in chloroform-d ($CDCl_3$) on a Bruker AC spectrometer operating at 400 MHz for ^{1}H and 100 MHz for ^{13}C. HR-MS characterization was performed on Thermo Scientific Q-Exacative with Accela 1250 pump. Matrix assisted laser desorption/ionization time-of flight (MALDI-TOF) mass spectra were obtained on a Bruker Auto flex TOF/TOF instrument using dithranol as a matrix. UV-vis and photoluminescence (PL) spectra were recorded on a Jasco V-570 and a Cary Eclipse Fluorescence spectrofluorometer, respectively using chloroform as a solvent.

4.2.3) Synthesis

4.2.3.1) Synthesis of 9H-carbazole-9-(4-methoxyphenyl) (2)

Into a 100 mL round bottom flask equipped with a magnetic stirring bar were added carbazole (2 g, 50 mmol), 4-iodoanisole (2.8 g, 60 mmol), copper powder (0.53 g, 50 mmol), potassium carbonate (2.7 g, 100 mmol) and triethylene glycol dimethyl ether (30 mL) and the mixture was stirred under argon atmosphere at 180 °C for 24 h. The reaction mixture was cooled to room temperature, filtered and poured into ice cold water (500 mL). The white precipitate was collected by filtration. Recrystallization of product from methanol gave compound **2** as white crystalline solid.

Yield: 2.27 g (70%)

Melting point: 153-154 °C

IR (ATR, cm^{-1}): 1314 (C-N, amine), 1223 (C-O-C) [**Figure S 4.13**]

^{1}H NMR (400 MHz, CDCl3) δ = 8.21 (d, *J* = 7.6 Hz, 2 H), 7.56 - 7.49 (m, 2 H), 7.48 - 7.42 (m, 2 H), 7.41 - 7.30 (m, 4 H), 7.22 - 7.14 (m, 2 H), 3.97 (s, 3 H). [**Figure S 4.1**]

^{13}C NMR (100 MHz, $CDCl_3$) δ = 158.89, 141.41, 130.33, 128.61, 125.88, 123.13, 120.3, 119.68, 115.1, 109.73, 55.64. [**Figure S 4.2**]

HRMS: Calculated for $C_{19}H_{15}NO$ 273.1154, found 273.1146

4.2.3.2) Synthesis of 3-bromo-9-(4-methoxyphenyl)-9H-carbazole (3)

Into a 100 mL two necked round bottom flask equipped with a magnetic stirring bar were added 9H-carbazole-9-(4-methoxyphenyl) (5 g, 10 mmol) and chloroform (150 mL). Nitrogen gas was bubbled through the reaction mixture at ice cold temperature for 30 minutes. Subsequently N-bromosuccinimide (3.58 g, 12 mmol) was added and the reaction mixture was stirred for 12 h at room temperature. After completion of reaction, the reaction mixture was poured into ice cold water (250 mL) and extracted with dichloromethane (3×100 mL). The dichloromethane layer was separated and washed with water (50 mL), brine solution (50 mL) and again with water (50 mL). Dichloromethane solution was dried over anhydrous sodium sulfate and filtered. Removal of solvent on a rotary evaporator afforded a crude product which was then purified by column chromatography using petroleum ether: dichloromethane (8:2, v/v) as an eluent to give compound **3** as a white solid.

Yield: 5.51 g (80%)

Melting point: 177 °C

IR (ATR, cm^{-1}): 732 (C-Br). [**Figure S 4.14**]

^{1}H NMR (400 MHz, $CDCl_3$) δ = 8.33 (d, J = 1.5 Hz, 1 H), 8.16 (d, J = 7.8 Hz, 1 H), 7.56 - 7.46 (m, 4 H), 7.40 - 7.34 (m, 2 H), 7.26 (d, 1H), 7.18 (d, 2H), 3.98 (s, 3 H). [**Figure S 4.3**]

^{13}C NMR (100 MHz, $CDCl_3$) δ = 159.02, 141.64, 139.97, 129.72, 129.25, 128.40, 126.54, 124.79, 122.92, 121.98, 120.38, 120.02, 115.11, 112.37, 111.14, 109.90, 55.55. [**Figure S 4.4**]

HRMS: Calculated for $C_{19}H_{14}BrNO$ 351.0259, found 351.0249.

4.2.3.3) Synthesis of 9-(4-methoxyphenyl)-3-(4,4,5,5-tetramethyl-1,3,2-dioxaborolan-2-yl)-9H-carbazole (4)

Into a Schlenk tube equipped with a magnetic stirring bar were added 3-bromo-9-(4-methoxyphenyl)-9H-carbazole (2 g, 1 mmol), bis(pinacolato)diboron (1.4 g, 1.2 mmol), $PdCl_2$(dppf) (418 mg, 0.1 mmol) and potassium acetate (1.6 g, 3 mmol) under argon flow and then evacuated for 20 minutes. Under an argon flow, dry 1, 4-dioxane (25 mL) was added to the reaction mixture. The solution was stirred at room temperature for 30 min, and then at 80 °C for 24 h. After completion of reaction, the mixture was quenched by addition of ice-cold water (100 mL) and then extracted with dichloromethane (250 mL). The dichloromethane layer was separated and washed with water (50 mL), brine solution (50 mL) and again with water (50 mL). The dichloromethane solution was dried over anhydrous sodium sulfate and filtered. Removal of solvent on a rotary evaporator afforded a crude product which was purified by column chromatography on neutral alumina suing 2% dichloromethane in petroleum ether as an eluent to obtain title compound **4** as a white solid.

Yield: 1.71 g, (76%)

Melting point: 165 °C

IR (ATR, cm^{-1}): 1340 (B-O). [**Figure S 4.15**]

^{1}H NMR (400 MHz, $CDCl_3$) δ= 8.63 (s, 1 H), 8.16 (d, 1 H), 7.84 (d, 1H), 7.42 (d, 2 H), 7.35-7.24 (m, 4 H), 7.10 (d, 2H), 3.90 (s, 3 H), 1.39 (s, 12 H). [**Figure S 4.5**]

^{13}C NMR (100 MHz, $CDCl_3$) δ = 158.93, 143.43, 141.49, 132.31, 130.03, 128.54, 127.69, 125.83, 123.28, 122.82, 120.45, 120.03, 115.07, 109.70, 109.05, 83.61, 55.57, 24.91 [**Figure S 4.6**]

HRMS: Calculated for $C_{25}H_{26}NO_3B$, 400.2079, found 400.2070

4.2.3.4 Synthesis of 1, 3, 6, 8-tetrakis (9-(4-methoxyphenyl)-9H-carbazol-3-yl) pyrene (PY-CA)

Into a Schlenk tube equipped with a magnetic stirring bar were added 1,3,6,8-tetrabromopyrene (0.5 g, 1 mmol), 9-(4-methoxyphenyl)-3-(4,4,5,5-tetramethyl-1,3,2-dioxaborolan-2-yl)-9H-carbazole (2.31 g, 6 mmol), 2M K_2CO_3 (5 mL) and $Pd(PPh_3)_4$ (0.11 g, 0.1 mmol) under argon

flow. The tube containing reaction mixture was evacuated and refilled with argon three times, THF (25 mL) was added into Schlenk tube and reaction mixture was stirred at 80 °C for 48 h. After completion of reaction, the reaction mixture was poured into water (100 mL) and extracted with dichloromethane (250 mL). The dichloromethane layer was separated and washed with water(50 mL), brine solution (50 mL) and again with water (50 mL). The dichloromethane solution was dried over anhydrous sodium sulfate and filtered. Removal of dichloromethane on rotary evaporator afforded a crude product which was then purified using silica gel column chromatography with 2% dichloromethane in petroleum ether as an eluent to obtain title compound **PY-CA** as a green solid.

Yield: 0.969 g, (78%)

Melting point: 211 °C

IR (ATR, cm^{-1}): 1316 (C-N), 1225 (C-O-C). [**Figure 4.1**]

^{1}H NMR (400 MHz, $CDCl_3$) δ ppm = 8.53 (s, 4 H), 8.35 (d, 6 H), 8.19 (d, 4H), 7.83-7.76 (m, 4 H), 7.59 - 7.50 (m, 12 H), 7.46 - 7.39 (m, 8 H), 7.32-7.26 (m, 4 H), 7.16 (d, 8 H), 3.95 (s, 12 H).[**Figure 4.3**]

^{13}C NMR (100 MHz, $CDCl_3$) δ ppm = 158.9, 141.84, 140.70, 137.76, 132.95, 130.68, 130.32, 128.89, 128. 56, 128.34, 126.01, 125.45, 123.37, 123.20, 122.34, 120.45, 119.82, 115.12, 109.81, 109.49, 55.59. [**Figure 4.4**]

MALDI-TOF: Calculated for $C_{92}H_{64}N_4O_4$ 1288.0, found 1287.73.

4.2.3.5) Synthesis of 10-(4-methoxyphenyl)-10H-phenothiazine (6)

Into a Schlenk tube equipped with a magnetic stirring bar were added phenothiazine (2 g, 50 mmol), 4-iodoanisole (3.36 g, 60 mmol), copper powder (0.754 g, 50 mmol), potassium carbonate (3.30 g, 100 mmol) and triethylene glycol dimethyl ether (30 mL). The reaction mixture was stirred under argon atmosphere at 180 °C for 24 h and progress of reaction was monitored by TLC. After completion of reaction, the reaction mixture was cooled to room temperature, filtered and poured into ice cold water (250 mL). The brown precipitate was collected by filtration. The product was purified by recrystallization from ethyl acetate to afford title compound **6** as yellowish crystalline solid.

Yield: 1.83 g (60%)

Melting point: 170 °C

IR (ATR, cm^{-1}): 1300 (C-N), 1230 (C-O-C), 807 (C-S-C) [**Figure S 4.16**]

^{1}H NMR (400 MHz, $CDCl_3$) δ ppm = 7.34 (d, 2 H), 7.15 (d, 2 H), 7.03 (d, 2 H), 6.89-6.80 (m, 4 H), 6.23 (d, J = 7.5 Hz, 2 H), 3.93(s, 3 H). [**Figure S 4.7**]

^{13}C NMR (100 MHz, $CDCl_3$) δ ppm = 159.17, 144.60, 133.21, 132.22, 126.77, 126.56, 122.19, 119.58, 115.83, 115.57, 55.48 [**Figure S 4.8**]

HRMS: Calculated for $C_{19}H_{15}NOS$ 305.0869, found 305.0867

4.2.3.6) Synthesis of 3-bromo-10-(4-methoxyphenyl)-10H-phenothiazine (7)

Into a 250 mL two necked round bottom flask equipped with a magnetic stirring bar was added chloroform (30 mL), nitrogen gas was bubbled through it for 15 minutes and subsequently 4-phenothiazine-10-yl-anisole (2 g, 10 mmol) was added. The mixture was cooled to 0 ^{o}C, N-bromosuccinimide (1.28, 12 mmol) was added and reaction mixture was stirred for 12 h at room temperature. After completion of reaction, the reaction mixture was poured into ice cold water (250 mL) and extracted with dichloromethane (3×100 mL). The dichloromethane layer was separated and washed with water (50 mL), brine solution (50 mL) and with water (50 mL). The dichloromethane solution was dried over anhydrous sodium sulfate and filtered. Removal of solvent on rotary evaporator afforded a crude product which was purified by silica gel column chromatography using 2% ethyl acetate in petroleum ether as an eluent to obtain title compound **7** as a green solid

Yield: 2.14 g (85%)

Melting point: 192°C

IR (ATR, cm^{-1}): 790 (C-Br). [**Figure S 4.17**]

^{1}H NMR (400 MHz, $CDCl_3$) δ ppm = 7.33 (d, 1H), 7.30 (d, 1H), 7.18 - 7.11 (m, 3H),7.02-6.86 (m, 3H), 6.22 (d, 1 H), 6.09-6.04 (m, 1 H), 3.94 (s, 3 H). [**Figure S 4.9**]

^{13}C NMR (100 MHz, $CDCl_3$) δ ppm = 159.36, 132.01, 131.77, 129.64, 129.35, 128.66, 128.60, 127.03, 126.73, 126.58, 122.51, 116.87, 116.74, 116.16, 116.0, 115.70, 55.5. [**Figure S 4.10**]

HRMS: Calculated for $C_{19}H_{14}BrNOS$, 382.9979, found 382.9976

4.2.3.7) Synthesis of 10-(4-methoxyphenyl)-3-(4,4,5,5-tetramethyl-1,3,2-dioxaborolan-2-yl)-10H-phenothiazine (8)

Into a Schlenk tube equipped with a magnetic stirring bar were added 3-bromo-10-(4-methoxyphenyl)-10H-phenothiazine (2 g, 1 mmol), bis(pinacolato)diboron (1.59 g, 1.2 mmol), $PdCl_2$(dppf) (383 mg, 0.1 mmol) and potassium acetate (1.5 g, 3 mmol) under argon flow and then Schlenk tube was evacuated for 30 minutes. Dry 1,4- dioxane (25 mL) was added to the reaction mixture under an argon flow. The solution was first stirred for 30 minutes at room temperature, and then at 80 °C for 24 h. After completion of reaction, the reaction mixture was quenched by addition of water (250 mL) and then extracted into dichloromethane (2×250 mL). The dichloromethane layer was separated and washed with water (50 mL), brine solution (50 mL) and again with water (50 mL). The dichloromethane solution was dried over anhydrous sodium sulphate and filtered. Removal of solvent on rotary evaporator afforded a crude product which was purified by column chromatography on neutral alumina using petroleum ether : dichloromethane (8:2, v/v) as an eluent to obtain title compound **8** as a green solid

Yield: 1.21 g (68%)

Melting point: 189°C

IR (ATR, cm^{-1}): 1350 (B-O, boronic ester). [**Figure S 4.18**]

^{1}H NMR (400 MHz , $CDCl_3$) δ = 7.40 (d, J = 1.4 Hz, 1 H), 7.30 (d, 1 H), 7.24 (d, 2H), 7.10 (d, 2 H), 6.98-6.93 (m, 1 H), 6.83-6.76 (m, 2 H), 6.12 (d, J = 8.0 Hz, 2 H), 3.89 (s, 3 H), 1.30 (s, 12 H). [**Figure S 4.11**]

^{13}C NMR (100 MHz, $CDCl_3$) δ = 159.2, 133.7, 133.56, 132.9, 132.10, 131.94, 126.74, 126.61, 122.45, 119.79, 115.88, 115.68, 114.88, 114.73, 83.5, 55.5, 24.7. [**Figure S 4.12**]

HRMS: Calculated for $C_{25}H_{26}NO_3SB$ 431.1726, found 431.1720

4.2.3.8) Synthesis of 1, 3, 6, 8-tetrakis (10-(4-methoxyphenyl)-10H-phenothiazin-3-yl)pyrene (PY-PH)

Into a Schlenk tube equipped with a magnetic bar were added 1,3,6,8-tetrabromopyrene (0.5 g, 1 mmol),10-(4-methoxyphenyl)-3-(4,4,5,5-tetramethyl-1,3,2-dioxaborolan-2-yl)-10H-phenothiazine (2.49 g, 6 mmol), 2M aqueous solution of K_2CO_3 (5 mL) and $Pd(PPh_3)_4$ (0.11 g,

0.1 mmol) under argon flow. The Schlenk tube containing reaction mixture was evacuated and refilled with argon three times and dry THF (25 mL) was subsequently added into the flask. The reaction mixture was stirred at 80 °C for 48 h. After completion of reaction, the reaction mixture was poured into water (100 mL) and extracted with dichloromethane (250 mL). The dichloromethane layer was separated and washed with water (50 mL), brine solution (50 mL) and again with water (50 mL). The dichloromethane solution was dried over anhydrous sodium sulfate and filtered. Removal of solvent on rotary evaporator afforded a crude product which was then purified using silica gel column chromatography with petroleum ether: dichloromethane (8:2, v/v) as an eluent to obtain title compound **PY-PH** as a yellow solid.

Yield: 0.82 g (60%)

Melting point: 231°C

IR (ATR, cm^{-1}): 1295 (C-N. amine), 1234 (C-O-C), 812 (C-S-C) [**Figure 4.2**]

^{1}H NMR (400 MHz, $CDCl_3$) δ = 8.13 (s, 4 H), 7.83 (s, 2 H), 7.41 - 7.27 (m, 12 H), 7.17-7.01 (m, 16 H), 6.89 - 6.80 (m, 8 H), 6.35 - 6.24 (m, 8 H), 3.92 (s, 12 H) [**Figure S 4.5**]

^{13}C NMR (100 MHz, $CDCl_3$) δ = 159.32, 144.49, 143.86, 135.89, 135.02, 133.25, 132.25, 129.16, 128.72, 128.39, 127.87, 126.87, 126.69, 126.03, 125.06, 122.34, 119.78,119.41, 115.99, 115.67,115.44, 55.54 [**Figure S 4.6**]

MALDI-TOF: Calculated for $C_{92}H_{62}N_4O_4S_4$ 1415.04, found 1415.37

4.3) Results and discussion

4.3.1) Synthesis and characterization

In this work, two conjugated small molecules, namely 1,3,6,8-tetrakis(9-(4-methoxyphenyl)-9H-carbazol-3-yl)pyrene **(PY-CA)** and 1,3,6,8-tetrakis(10-(4-methoxyphenyl)-10H-phenothiazin-3-yl)pyrene **(PY-PH)** were synthesized by attaching two conjugated segments *viz* carbazole and phenothiazine to the central pyrene chromophore. Initially, commercially available compounds *viz,* carbazole (**1**) and phenothiazine (**5**) were converted into 9H-carbazole-9-(4-methoxyphenyl) (**2**) and 10-(4-methoxyphenyl)10H-phenothiazine (**6**), respectively in 70% and 60% yield through Ullmann coupling using 4-iodoanisole in the presence of K_2CO_3 as a base. Compounds **2** and **6** were then converted into their monobromo derivatives *viz* 3-bromo-9-(4-methoxyphenyl)-9H-carbazole (**3**) and 3-bromo10-(4-methoxyphenyl)-10H-phenothiazine (**7**). The subsequent

transformation of mono bromo compounds (**3**) and (**7**) to their respective bisboronic ester analogs 9-(4-methoxyphenyl)-3-(4,4,5,5-tetramethyl-1,3,2dioxaborolan-2-yl)-9H-carbazole (**4**) and 10-(4-methoxyphenyl)-3(4,4,5,5-tetramethyl-1,3,2-dioxaborolan-2-yl)-10H-phenothiazine (**8**) was carried out *via* Miyaura borylation[29] reaction using bis(pinacolato) diboron reagent. The target compounds 1,3,6,8-tetrakis(9-(4-methoxyphenyl)-9H-carbazol3-yl) pyrene (**PY-CA**) and 1,3,6,8-tetrakis(10-(4-methoxyphenyl)-10Hphenothiazin-3-yl)pyrene (**PY-PH**) were prepared in 78% and 60% yield, respectively through C-C bond formation *via* classical Suzuki coupling conditions [30] using 1,3,6,8 tetrabromopyrene and monoboronic ester analogs (**4**) and (**8**), respectively. Synthesis of both pyrene compounds i.e. **PY-CA** and **PY-PH** are shown in **Scheme 4.1** and **Scheme 4.2**, respectively. Both **PY-CA** and **PY-PH** derivatives were soluble in different organic solvents such as dichloromethane, chloroform, toluene, tetrahydrofuran, etc. This allowed solution processing of organic material during device fabrication.

The structure of **PY-CA** and **PY-PH** were confirmed by FT-IR, ^{1}H NMR, ^{13}C NMR and MALDI-TOF spectroscopy.

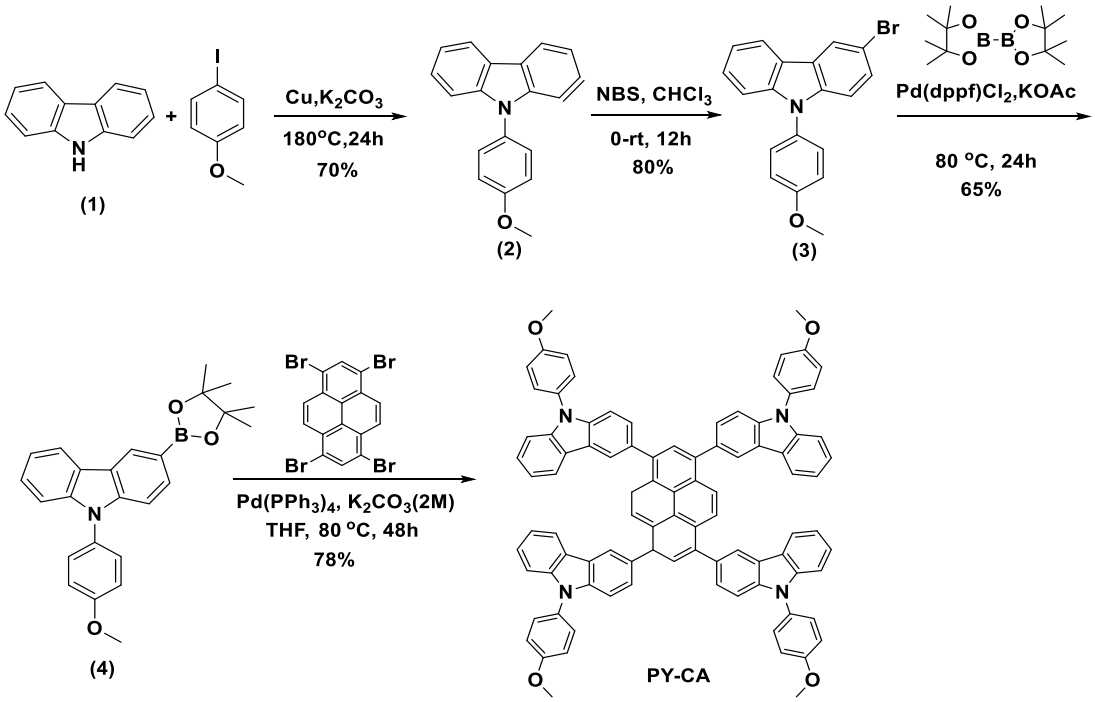

Scheme 4.1: Synthesis of 1,3,6,8-tetrakis(9-(4-methoxyphenyl)-9H-carbazol-3-yl)pyrene **(PY-CA**)

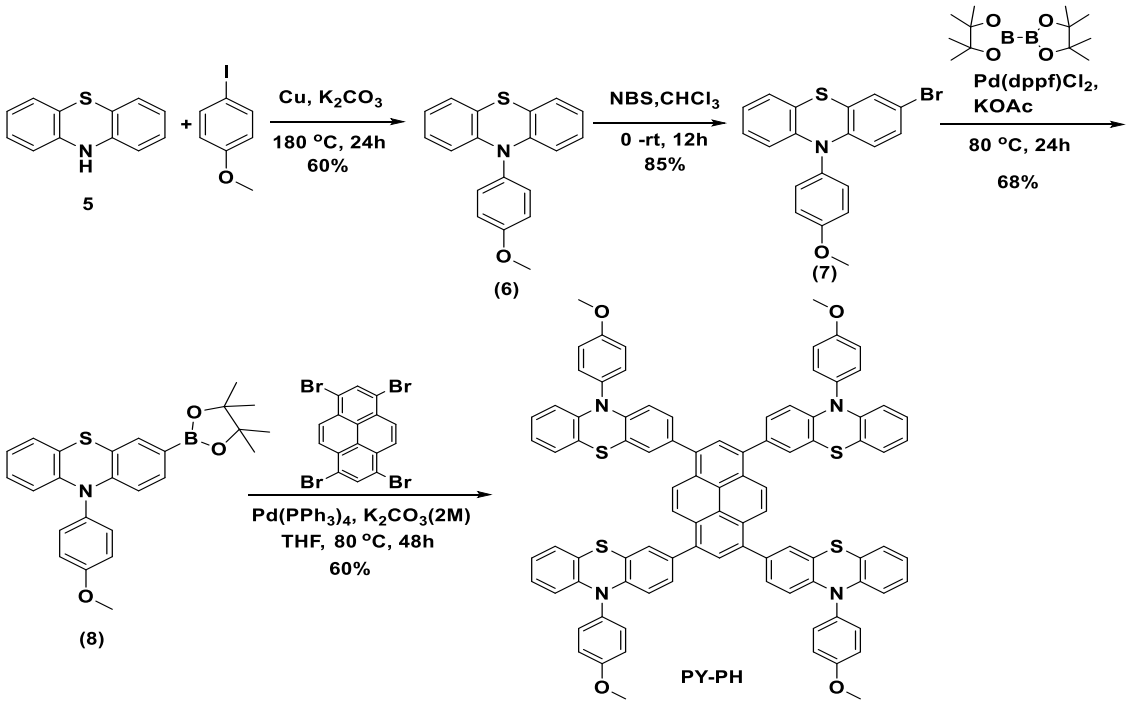

Scheme 4.2: Synthesis of 1,3,6,8-tetrakis(10-(4-methoxyphenyl)-10H-phenothiazin-3-yl)pyrene (**PY-PH)**

IR spectra of **PY-CA** and **PY-PH** are shown in **Figure 4.1** and **Figure 4.2**, respectively. In **Figure 4.1** the absorption band observed at 1316 cm^{-1} is attributed to C-N stretching while the band observed at 1225 cm^{-1} is due to C-O stretching of ether functional group. In **Figure 4.2**, the absorption bands appearing at 1295 cm^{-1} and 1234 cm^{-1} are attributed to the stretching of C-N and C-O bonds, respectively. The absorption band observed at 812 cm^{-1} is due to C-S stretching.

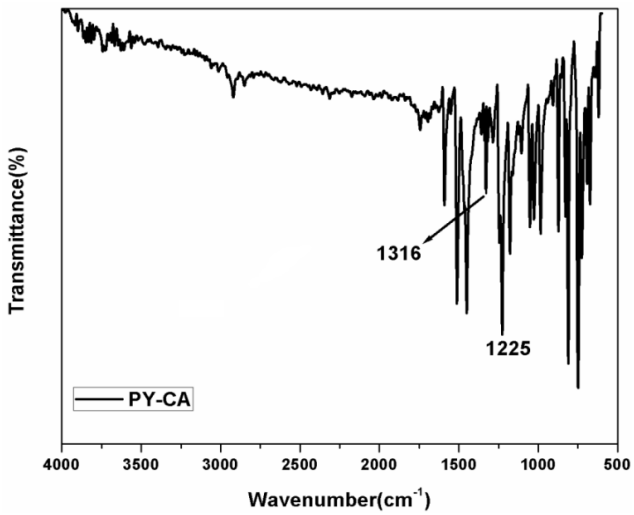

Figure 4.1: IR spectrum of **PY-CA**

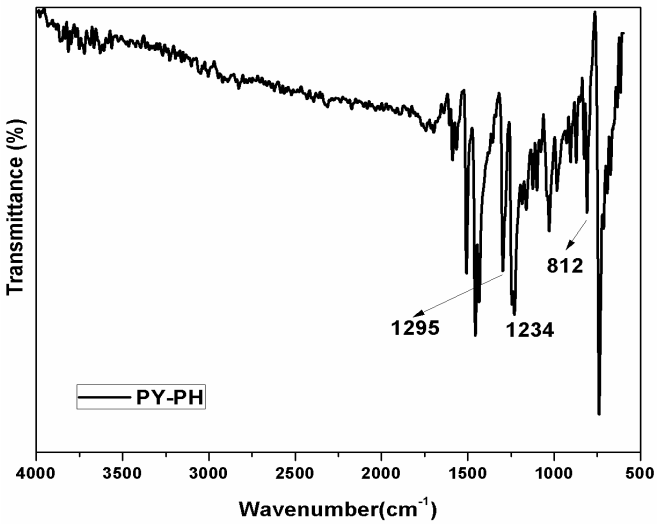

Figure 4.2: IR spectrum of **PY-PH**

^{1}H NMR spectrum of **PY-CA** with peak assignment is shown in **Figure 4.3.** Protons 'a' of methoxy group attached to aromatic ring exhibited a singlet at δ 3.95 ppm. Aromatic protons 'b' *ortho* to methoxy group exhibited a doublet at δ 7.17 ppm, whereas protons 'c' exhibited a signal at δ 7.44 ppm. NMR signals corresponding to protons 'm' and 'k' on pyrene core were observed at δ8.53 ppm and δ8.33 ppm, respectively. Protons on carbazole ring exhibited signals over the range of δ8.37- δ 7.29 ppm.

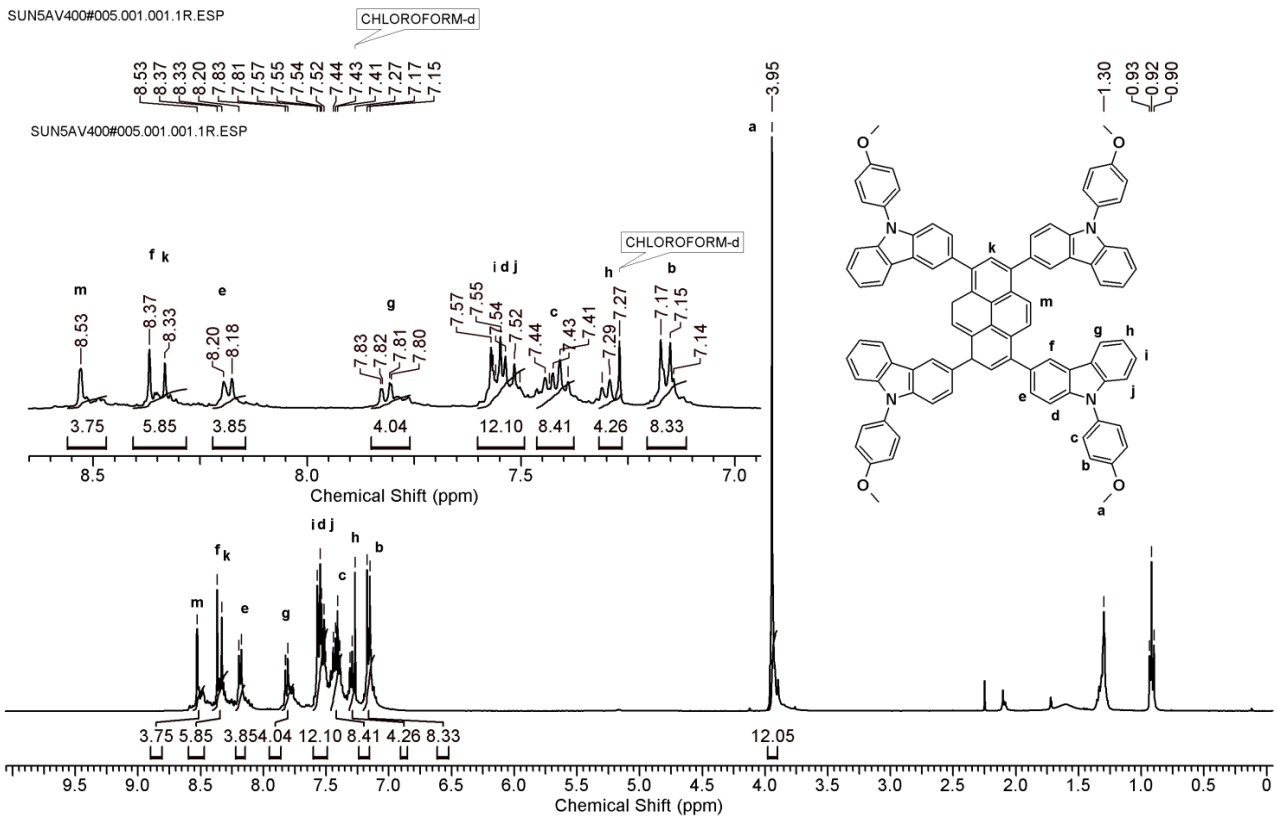

Figure 4.3: ^{1}H NMR spectrum (in $CDCl_3$) of 1, 3, 6, 8-tetrakis (9-(4-methoxyphenyl)-9H-carbazol-3-yl) pyrene (**PY-CA**)

^{13}C NMR spectrum of **PY-CA** with peak assignments is shown in **Figure 4.4** The carbon atom 'a' of methoxy group exhibited a signal at δ 55.59 ppm. The carbon atoms 'b' and 'e' of aromatic ring exhibited signals in the downfield region at δ 158.90 ppm and δ 140.70 ppm, respectively owing to inductive effect of heteroatoms attached to carbon. The signal for aromatic carbon 'c' was observed at δ115.12 ppm, whereas carbon 'd' exhibited a signal at 128.56 ppm. The signals corresponding to carbon atoms of central pyrene core and carbazole moiety were observed over the range δ 141.84- 109.49 ppm

^{1}H NMR spectrum of **PY-PH** with assignments is shown in **Figure 4.5.** A singlet at δ3.92 ppm was attributed to protons 'a' of methoxy group. The aromatic proton 'b' *ortho* to methoxy group was observed at δ 7.17 ppm, whereas proton 'c' *meta* to methoxy group was observed at δ 7.28 ppm. Protons 'm' and 'k' on pyrene core exhibited signals at δ 8.13 ppm and δ7.83 ppm, respectively. Protons on phenothiazine moiety exhibited signals over the range δ 7.41- δ 6.28.

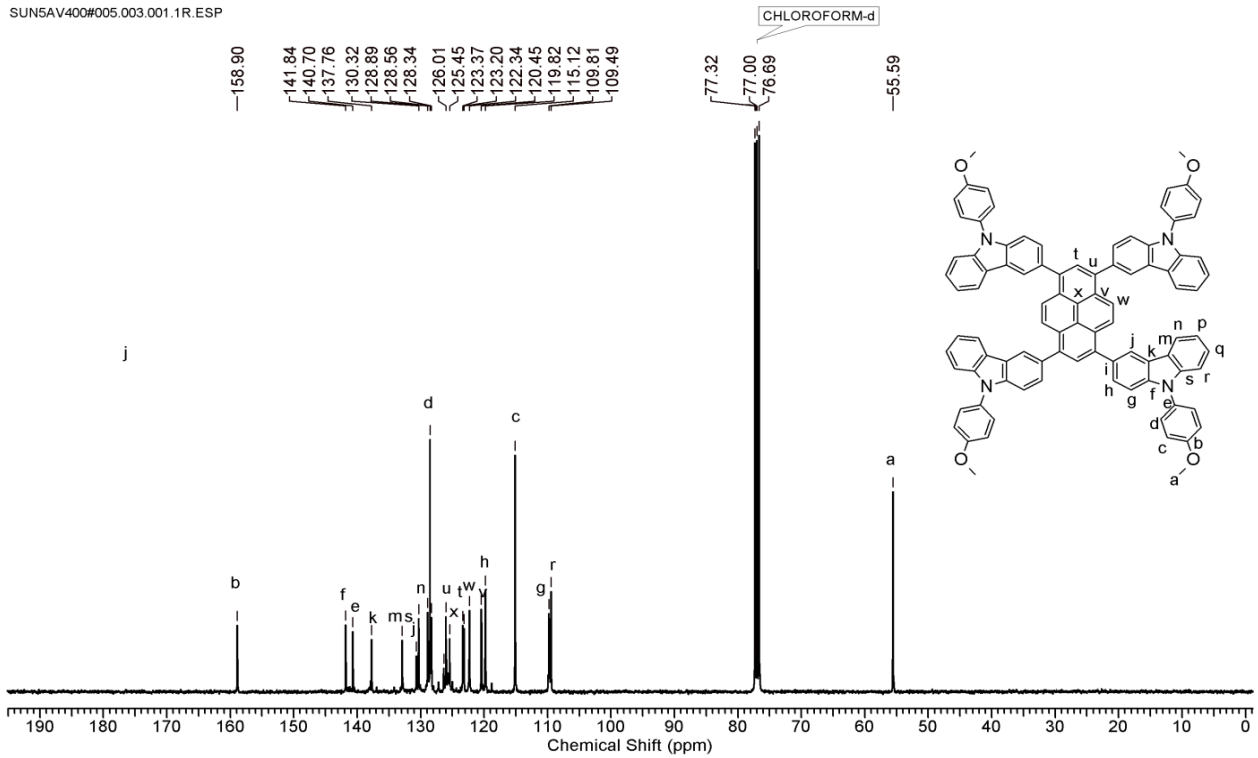

Figure 4.4: ^{13C} NMR spectrum (in $CDCl_3$) of 1, 3, 6, 8-tetrakis (9-(4-methoxyphenyl)-9H-carbazol-3-yl) pyrene (**PY-CA**)

^{13}C NMR spectrum of **PY-PH** with peak assignment is shown in **Figure 4.6.** The carbon atom 'a' of methoxy group was observed at δ 55.54 ppm. The carbon atoms 'b' and 'e' of aromatic ring exhibited signals in the downfield region at δ159.32 ppm and δ143.86 ppm, respectively due to inductive effect of oxygen and nitrogen atoms. The signal for aromatic carbon 'c' was observed at δ115.67 ppm, whereas carbon atom'd' exhibited signal at δ 132.25 ppm. The signals corresponding to carbon atoms of pyrene and phenothiazine moiety were observed over the range δ144.49- δ 115.44 ppm.

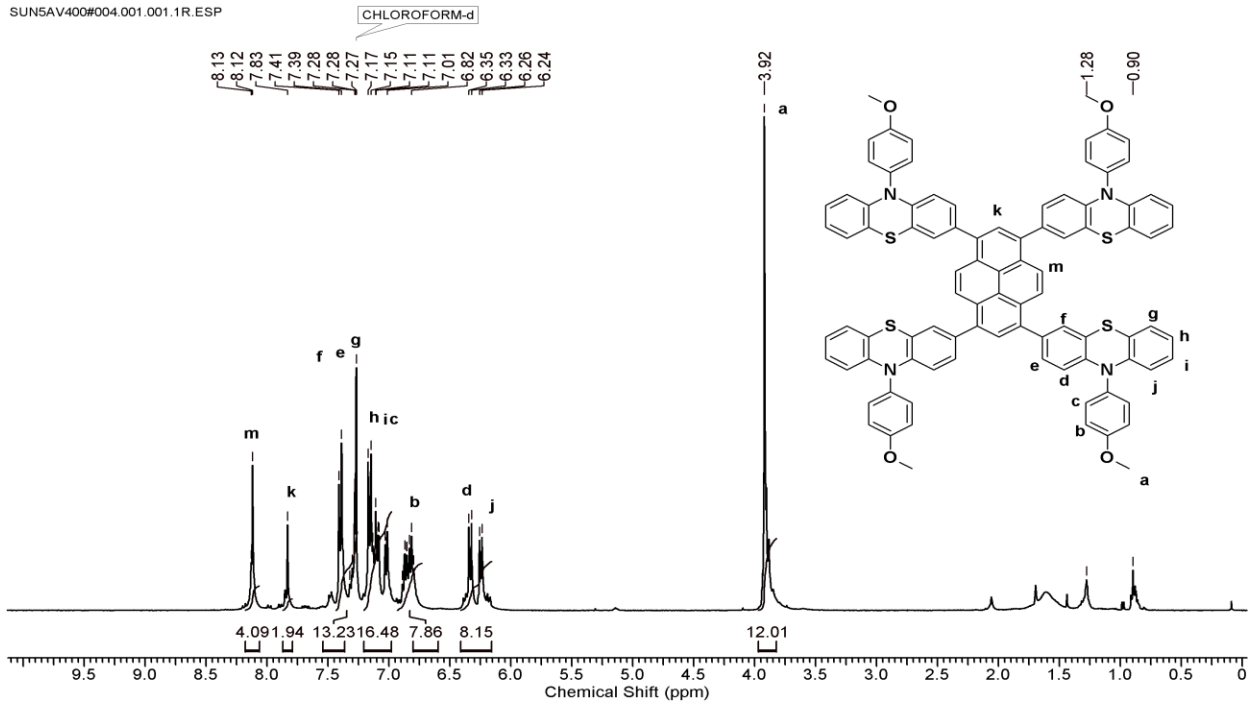

Figure 4.5: ^{1}H NMR spectrum (in $CDCl_3$) of 1, 3, 6, 8-tetrakis (10-(4-methoxyphenyl)-10H-phenothiazin-3-yl) pyrene (**PY-PH**)

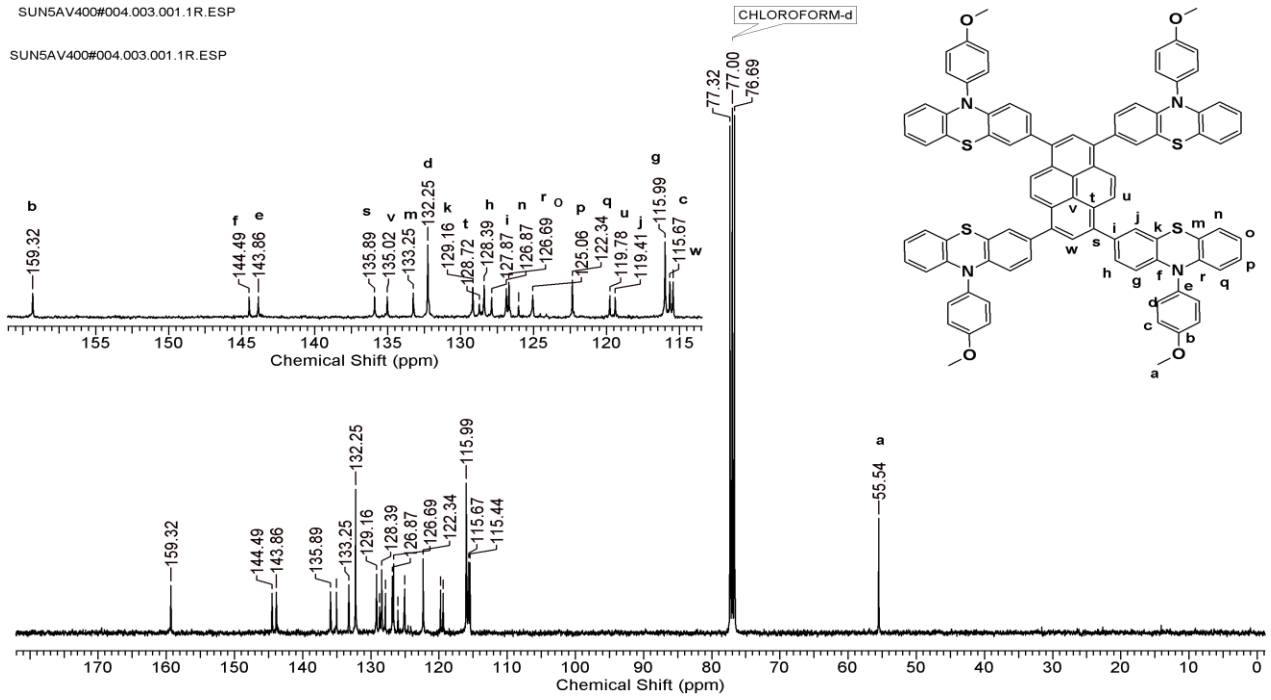

Figure 4.6: ^{13}C NMR spectrum (in $CDCl_3$) of 1, 3, 6, 8-tetrakis(10-(4-methoxyphenyl)-10H-phenothiazin-3-yl) pyrene (**PY-PH**)

MALDI-TOF of **PY-CA** and **PY-PH** were recorded using dithranol as a matrix and the spectra are shown in **Figure 4.7** MALDI-TOF spectrum for **PY-CA** showed a signal at 1286.04 (calculated for $C_{92}H_{62}H_4N_4$ =1286.48) and the signal for **PY-PH** was observed at 1415.04 (calculated for $C_{92}H_{64}N_4O_4S_4$=1416.38)

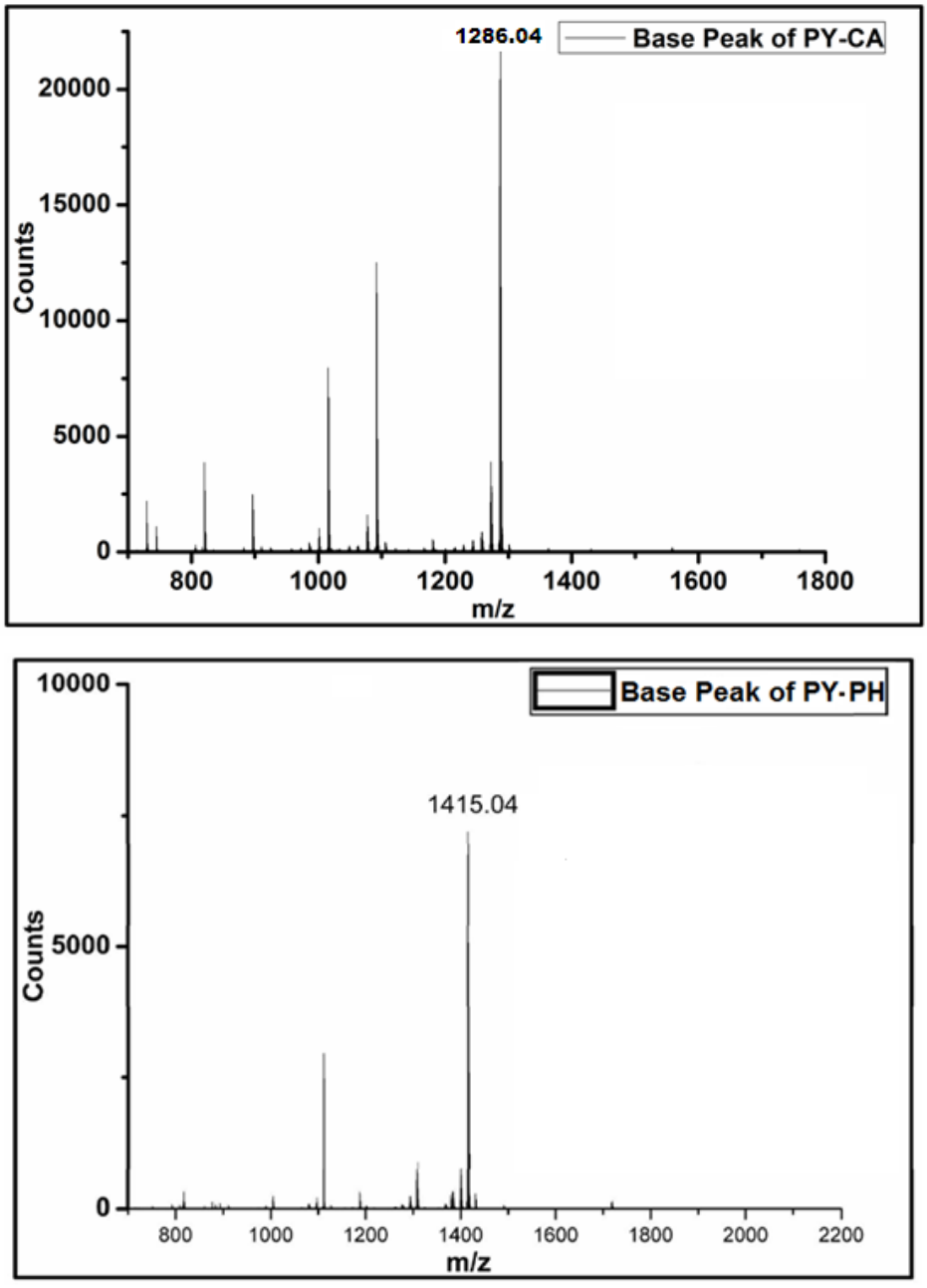

Figure 4.7: MALDI-TOF spectrum of **PY-CA** (top) and **PY-PH** (bottom)

4.3.2) Optical and electrochemical properties

The optical properties of **PY-CA** and **PY-PH** were characterized in solution (chloroform) as well as in thin film. Both UV-vis absorption (UV) and photoluminescence (PL) spectra of **PY-CA** and **PY-PH** in solution are shown in **Figure 4.8**

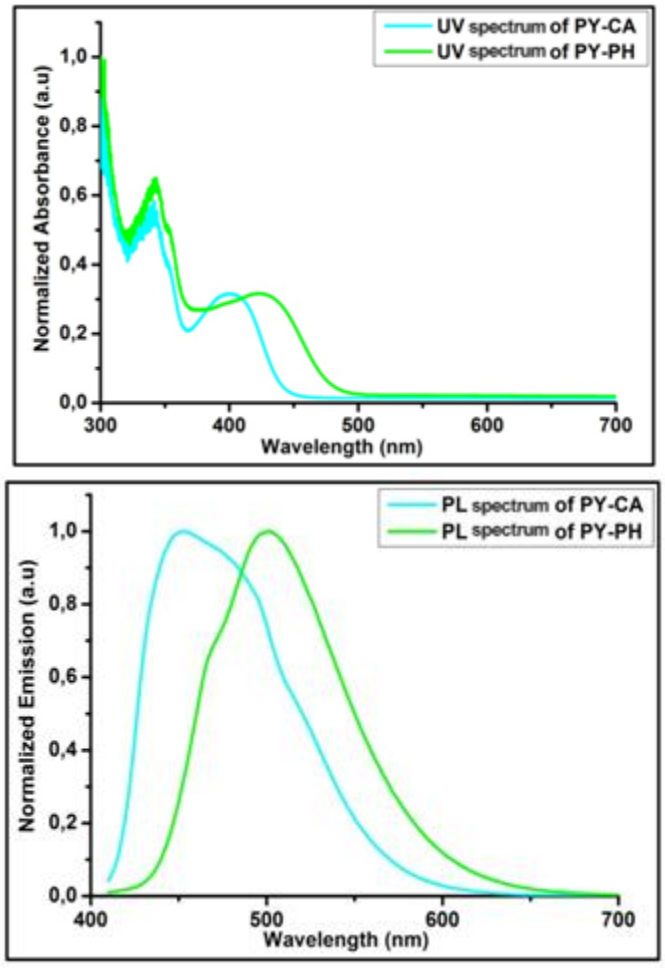

Figure 4.8: UV-vis absorption (top) and photoluminescence (bottom) spectra of **PY-CA** and **PY-PH** in chloroform

UV-vis spectra of both compounds exhibited two absorption peaks respectively at shorter and longer wavelengths. **PY-CA** exhibited absorbance peaks at 339 nm and 400 nm whereas **PY-PH** showed peaks at 340 nm and 430 nm, respectively. The absorption in the 300 nm to 500 nm region clearly indicated the wide band gap nature of the compounds. The near-identical peaks at 339 nm and 340 nm are the signature peaks for the central pyrene core and this is comparable with the absorbance of molecular pyrene (338 nm).[31, 32] Compared to the pyrene core, **PY-CA** and **PY-PH** exhibited the higher wavelength peaks at 400 nm and 430 nm, respectively, which

could be attributed to the enhanced conjugation between pyrene core and the attached carbazole/phenothiazine moiety. The 30 nm red shift in **PY-PH** compared to **PY-CA** is due to the more extended conjugation length of phenothiazine than carbazole. Both compounds showed a red shift of about 60 and 90 nm, respectively, in their absorption maxima compared to the base pyrene compound in the solution state. The plotoluminescence spectra of **PY-CA** and **PY-PH** in solution were recorded at 450 nm and 500 nm, respectively. The observed PL maxima were 57 nm and 107 nm red shifted compared to pyrene photoluminescence spectra (Pyrene PL_{max} 393 nm) [33]. The solution of **PY-CA** and **PY-PH** under a UV-lamp exhibited deep sky blue and green emission as shown in **Figure 4.9**

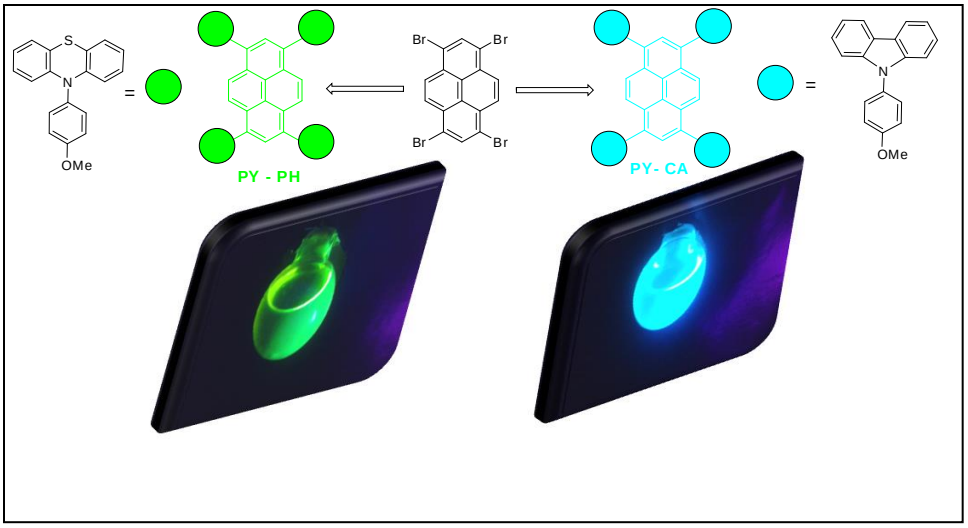

Figure 4.9: Emission of **PY-PH** and **PY-CA** solution under UV lamp

Thin films of **PY-PH** and **PY-CA** were spin coated on the separate quartz substrates and their UV-vis and PL spectra was measured (**Figure 2.10).** In the solid state, **PY-CA** exhibited absorbance maxima at 425 nm whereas **PY-PH** showed peak at 450 nm. The value of the solid **PY-CA** film is 25 nm red shifted compared to the solution measurement. Thin film PL measurement of **PY-CA** and **PY-PH** showed PL maxima at 485 nm and 520 nm, respectively.

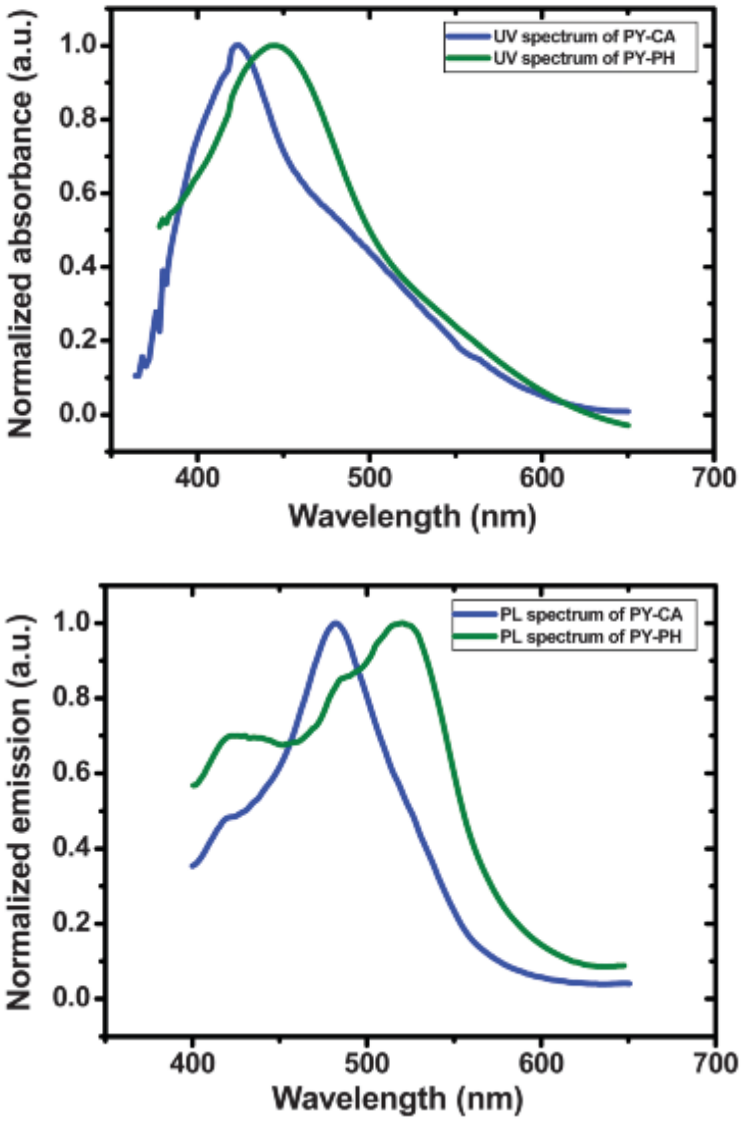

Figure 4.10: UV-vis absorption (top) and photoluminescence (bottom) spectra of **PY-CA** and **PY-PH** in thin films

The optical band gap of **PY-CA** and **PY-PH** were measured by using their spin coated thin films from chloroform solution directly on ITO coated glass. The thin film optical data on ITO coated glass for **PY-CA** and **PY-PH** are shown in **Figure 4.11**

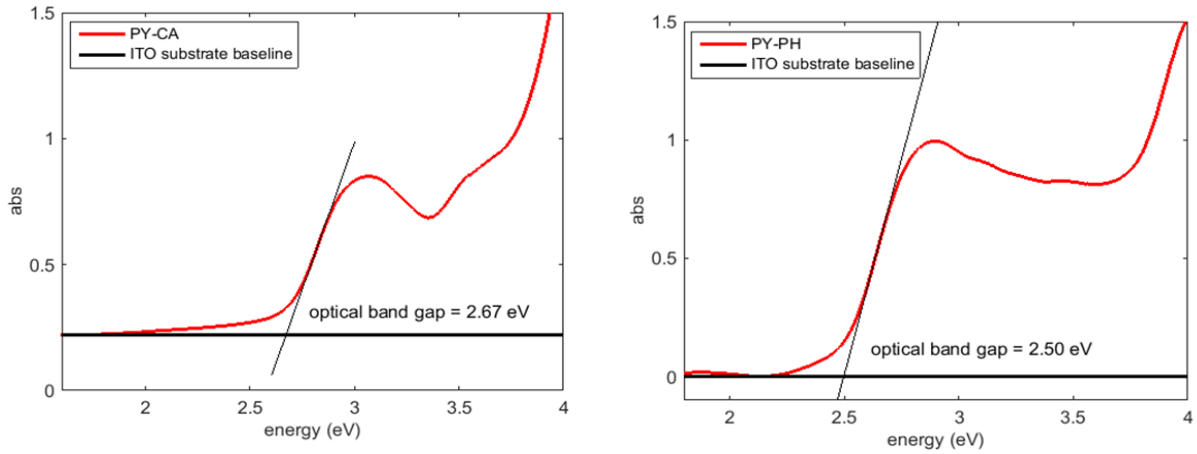

Figure 4.11: Optical band gap calculated using a thin film of **PY-CA** and **PY-PH** spin coated on the ITO coated glass substrates.

The optical band gap light absorption onset was determined by extrapolating the steepest slope to the intersection of the absorption baseline (substrate). The band gap of **PY-CA** and **PY-PH** was found to be 2.67 eV and 2.50 eV, respectively. The higher band gap value of **PY-CA** and **PY-PH** is a clear indication of blue/green emitters. The optical properties of **PY-CA** and **PY-PH** are summarized in **Table 4.1**

Table 4.1: Optical properties of **PY-CA** and **PY-PH**

Compound	**UV-Vis absorption in $CHCl_3$ (λ_{max} in nm)**	**UV-Vis absorption in thin film (λ_{max} in nm)**	**Photoluminescence (PL) spectrum in solution (λ_{max} in nm)**	**Photoluminescence (PL) spectrum in thin film (λ_{max} in nm)**	**Optical bandgap (eV)**
PY-CA	400	425	450	485	2.67
PY-PH	430	450	500	520	2.50

The energy levels of **PY-CA** and **PY-PH** organic semiconductors were characterized by the photoelectron spectroscopy in air (PESA) as shown in **Figure 4.12**

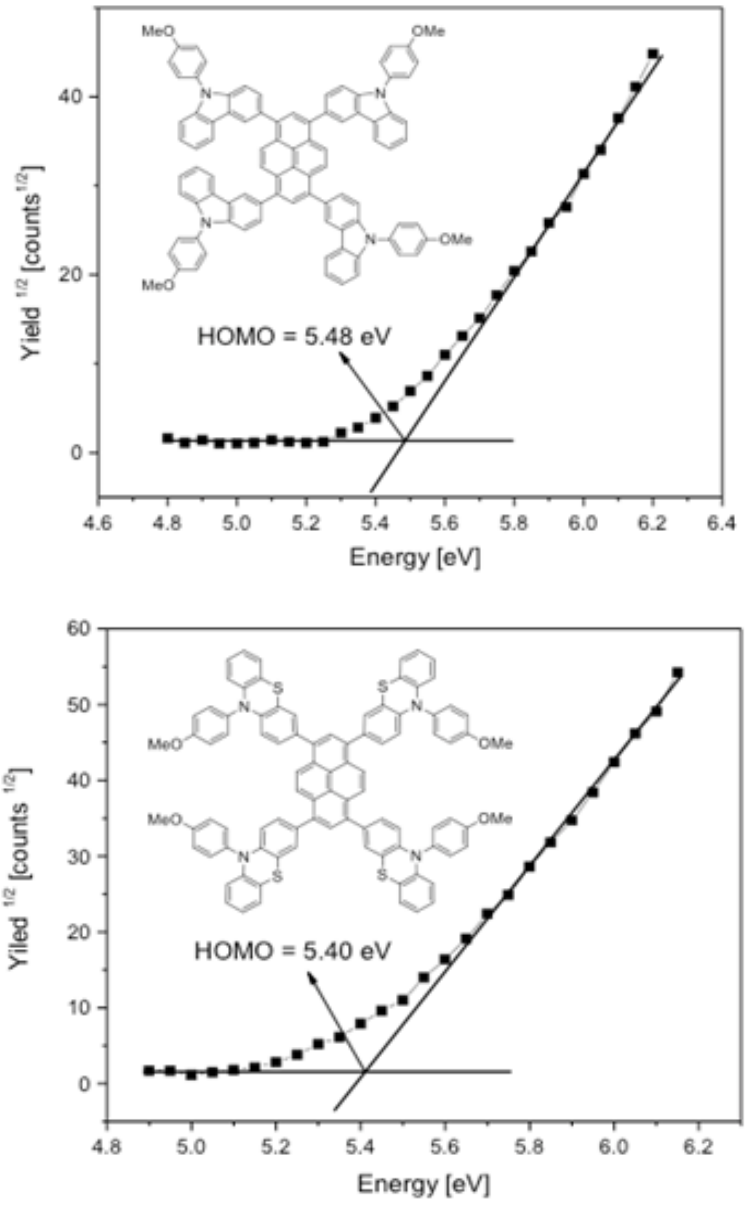

Figure 4.12: Photoelectron spectroscopy in air (PESA) analysis of **PY-CA** (top) and **PY- PH** (bottom) in thin film.

Thin films of **PY-CA** and **PY-PH** were deposited on ITO coated glass by spin coating, which were used for the determination the ionization potential. The photoelectron yield ratio was measured with respect to the applied UV-energy. The onset point or slope across this graph gave the HOMO value of these materials. [34] [35] The HOMO values for **PY-CA** and **PY-PH** are 5.48 eV

and 5.40 eV, respectively. The lower HOMO values **PY-CA** and **PY-PH** are significant for making the air stable organic electronic devices.[36] The higher HOMO of **PY-PH** compared to **PY-CA** is again attributed to the extended conjugated moiety and electron rich sulfur of phenothiazine. This observation is in good agreement with the optical red shift and the optical band gap measured for **PY-PH**.

4.3.3) Density functional theory (DFT) studies

Density functional theory (DFT) [37] calculations were performed to compute molecular structures, the energies of frontier orbitals and their localization as well as absorption and photoluminescence (PL) spectra. The B3LYP [38] and CAM-B3LYP [39] exchange-correlations functionals were used with the 6-31g (d, p) basis set. These B3LYP and CAM-B3LYP correlation functionals were used because B3LYP provides more reliable HOMO (highest occupied molecular orbital) and LUMO (lowest unoccupied molecular orbital) energies which can be compared to the measured redox levels, while the range-separated CAM-B3LYP is preferred for optical properties involving transitions with a significant degree of charge transfer.
The absorption and PL spectra were computed with time dependent DFT (TD-DFT)[40]. The PL spectra were computed by optimizing the first excited state. The calculations were performed in chloroform with the PCM (polarizable continuum model) model[41] of the solvent. All calculations were performed using Gaussian 09 [42]. The HOMO and LUMO of **PY-PH** and **PY-CA** are shown in **Figure 4.13** and **Figure 4.14** respectively. In both compounds, the HOMO is more delocalized than the LUMO and has appreciable amplitude on the phenothiazine and carbazole moieties, respectively, while the LUMO is more localized on the central fused pyrene core and partially on the fused backbone of the phenothiazine or carbazole units. This also means that there is an appreciable degree of charge transfer in the transition responsible for the first peak in the absorption and PL spectrum (which is mostly due to HOMO – LUMO interaction) which calls for the use of a range-separated hybrid functional in the analysis of optical properties [43] [44]. The calculated HOMO and LUMO energies of **PY-CA** are -4.82 eV and -1.63 eV whereas for **PY-PH**, values of energy levels are -4.79 eV and -1.79 eV, respectively. The higher HOMO value for **PY-PH** compared to **PY-CA** is related to the longer conjugation length of phenothiazine over carbazole.[8, 9] The HOMO–LUMO band gap for **PY-CA** and **PY-PH** was calculated to be 3.18 eV and 3.0 eV, respectively. The computed contraction of the band gap in **PY-PH** vs. **PY-CA** of

0.18 eV matches well with the experimentally measured difference in optical band gaps of 0.17 eV.

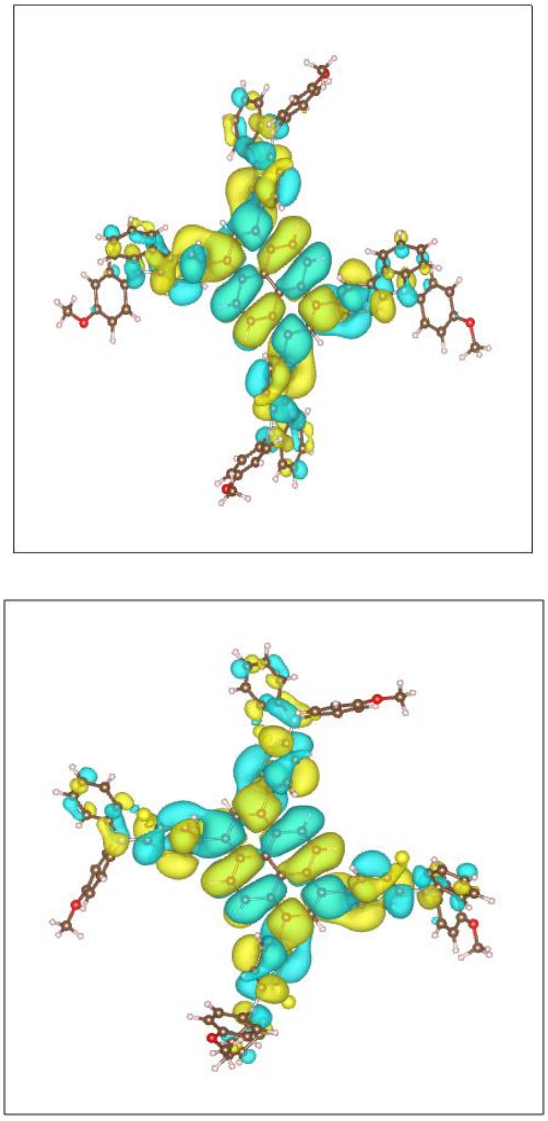

Figure 4.13: The electron density isocontours of HOMO and LUMO of **PY-CA** obtained at the CAM-B3LYP level

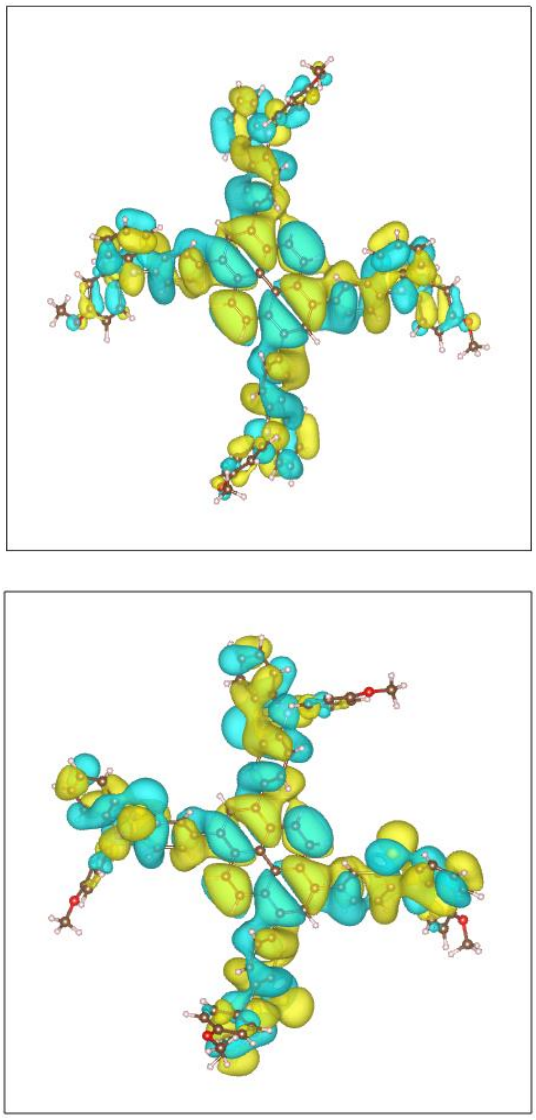

Figure 4.14: The electron density isocontours of HOMO and LUMO of **PY-PH** obtained at the CAM-B3LYP level

The absorption peak maximum computed by CAM-B3LYP/ B3LYP for **PY-CA** and **PY-PH** was observed at 379/437 nm and 389/471 nm, respectively. The absorption spectra are shown in **Figure 4.15**

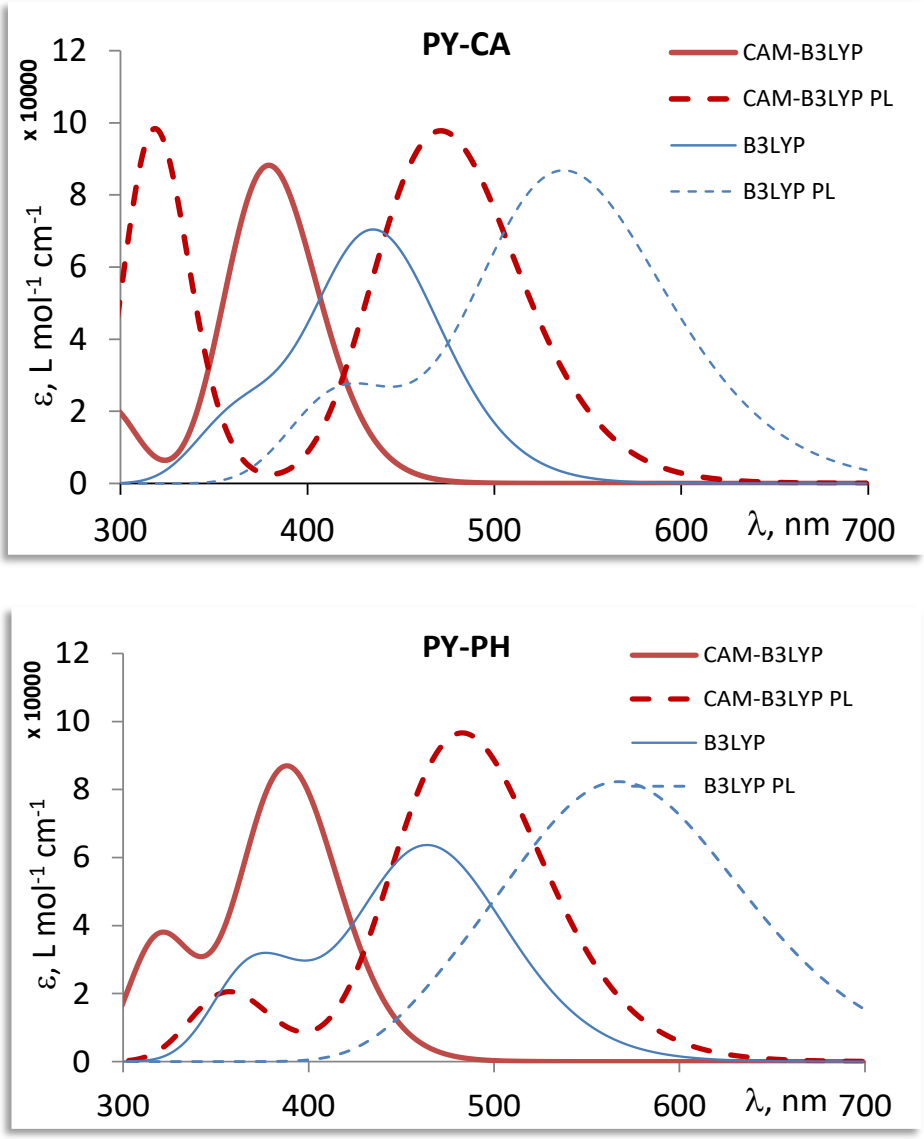

Figure 4.15: Theoretical UV-vis absorption spectra of **PY-CA** (top) and **PY-PH** (bottom) in chloroform computed with B3LYP and CAM-B3LYP functionals. Here and elsewhere, the extinction coefficient ϵ in L mol^{-1} cm^{-1} is calculated from the oscillator strengths f computed with DFT at excitation energies E_{exc}as $\epsilon = \frac{1.35\times10^4}{\sigma} f \exp\left[-2.7472\left(\frac{E-E_{exc}}{2\sigma}\right)\right]$ where σ =0.25 eV is the HWHM broadening.

The peaks computed using the two functionals therefore straddle the measured peaks at 400 and 430 nm of **PY-CA** and **PY-PH**, respectively (vide infra). This is expected, as B3LYP is known to underestimate the excitation energy for large conjugated systems and CAM-B3LYP often overestimates it.[40] These calculations confirm the red shift of the peak with phenothiazine vs. carbazole which is observed experimentally. The red shift was also confirmed for photoluminescence. The computed PL peaks were 471 and 538 nm for **PY-CA** and **PY-PH**, respectively (CAM-B3LYP, **Figure 4.16**).

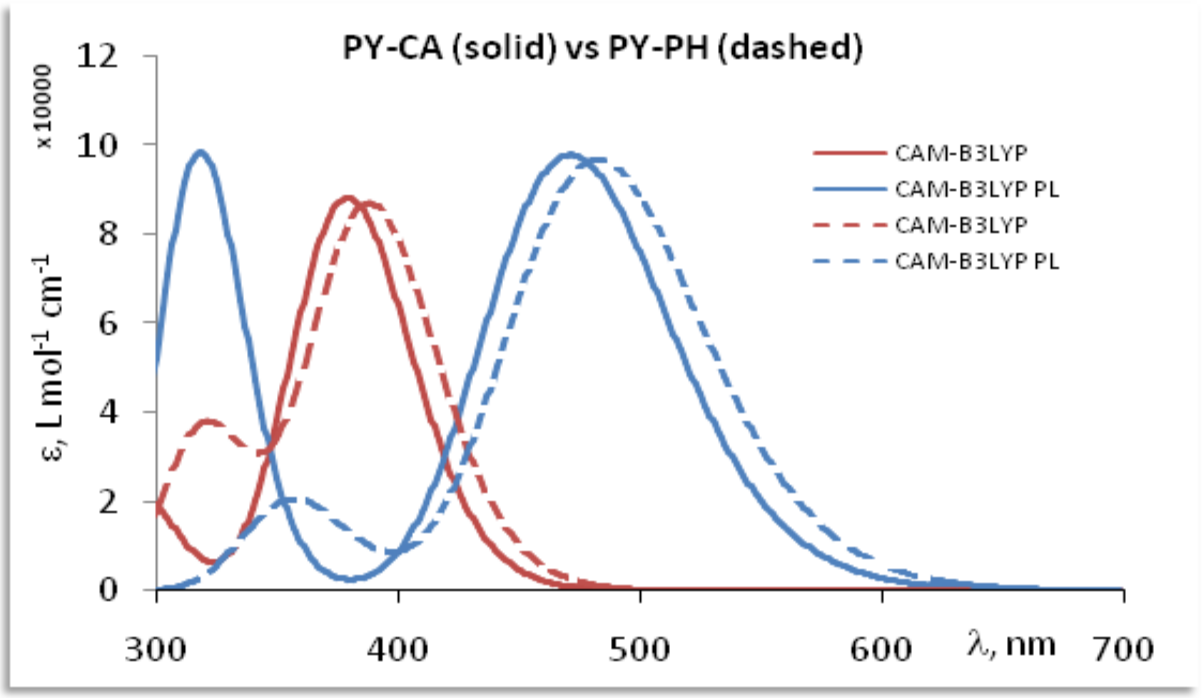

Figure 4.16: Comparative theoretical UV-vis absorption and photoluminescence spectra of **PY-CA** and **PY-PH** in chloroform computed with the CAM-B3LYP functional

In order to test the electroluminescence properties of the organic compounds synthesized, **PY-CA** and **PY-PH** were used as active emissive layer in OLED devices

4.3.4) OLED Device fabrication and studies

OLED devices were fabricated using **PY-CA** and **PY-PH** active emitting layer for evaluating the electroluminescence (EL) performance. The device configurations of compounds **PY-CA** and **PY-PH** are ITO/PEDOT:PSS (50 nm)/**PY-CA** (50 nm)/TPBi (20 nm)/Ca(20 nm)/Ag (100) and ITO/PEDOT:PSS (50 nm)/**PY-PH** (50 nm)/TPBi (20 nm)/Ca (20 nm)/Ag (100), respectively (**Figure 4.17**).

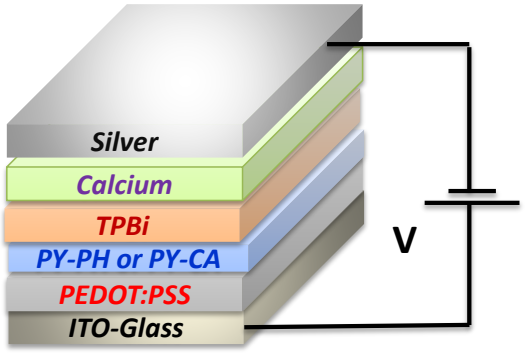

Figure 4.17: Device configuration of OLED device with **PY-CA** or **PY-PH** as emissive layer

ITO coated glass and calcium with silver act as the anode and the cathode, respectively whereas 2, 2', 2''-(1,3,5-benzinetriyl)-tris(1phenyl-1-H-benzimidazole) (TPBi) is an electron transporting layer. Patterned ITO glass substrates were routinely cleaned by detergent and deionized water, and then blown dry by nitrogen gas and kept in a 110 ^{o}C oven for 3 h before a 25 min ultra-violet ozone (UVO) surface treatment. Filtered poly (3, 4- ethylenedioxythiophene): polystyrene sulfonate (PEDOT:PSS) solution was spin-coated on the patterned ITO glass substrates and they were baked at 140 ^{o}C for 20 min The thickness of the PEDOT:PSS films were controlled to 150 nm. Then **PY-CA** and **PY-PH** solutions prepared in chloroform were separately spin-coated on the individual PEDOT:PSS coated ITO glass substrates. They were baked at 70 ^{o}C for 20 min. The thickness of both **PY-CA** and **PY-PH** films was controlled to 20 nm. All the spin-coat processes were performed in a nitrogen glove box environment. Both **PY-CA** and **PY-PH** coated substrates were then loaded into a thermal evaporation chamber at a vacuum pressure of below 3×10^{-6} Torr. 20 nm of 2,2 (1,3,5-benzinetriyl)-tris (1-phenyl-1-H-benzimidazole) (TPBi), 20 nm of calcium (Ca) and 100 nm of silver (Ag) were coated on the substrates. With the completion of the device, EL measurements were carried out. When a potential is applied, holes are injected from the anode and electrons injected from the cathode, respectively. Due to the recombination

of holes and electrons in the active emissive layer, blue and green photon emission was observed in OLED devices. The EL emission spectra were measured using the PR650 CCD camera with a computer controller power supply. The voltage–current–brightness (I–V–B) characteristics and the C.I.E. coordinates were also measured. The current and power efficiencies were calculated from the I–V–B data of the devices. The observed electroluminescence (EL) was recorded as shown in **Figure 4.18**, while the EL performance data are given in **Table 2.1**.

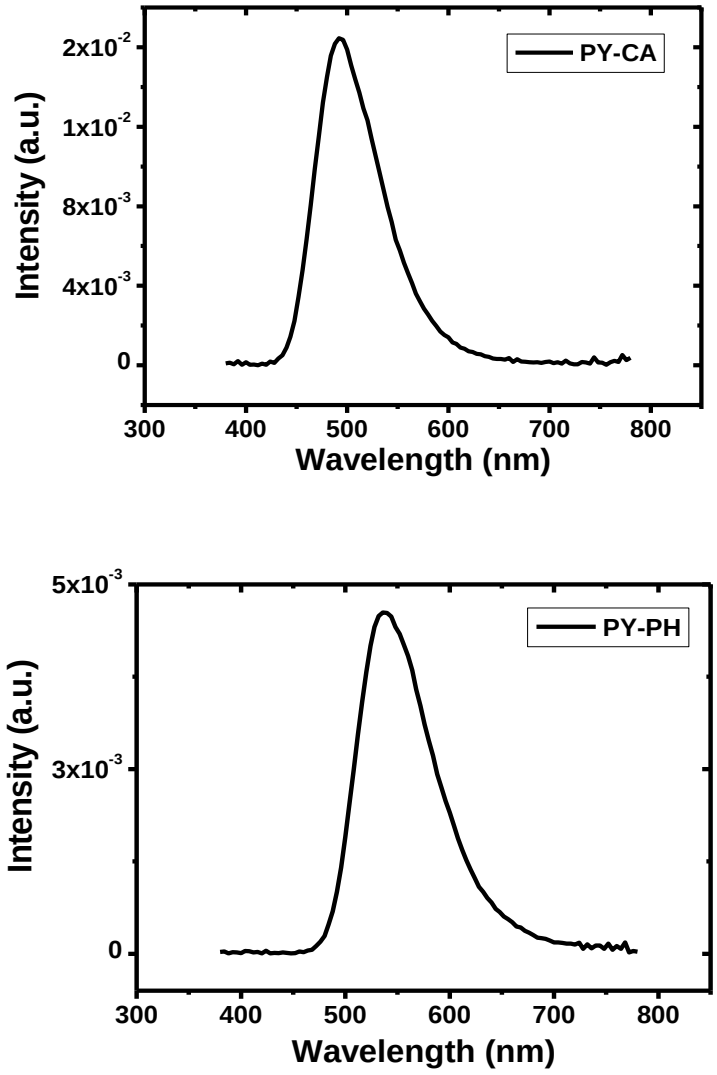

Figure 4.18: Electroluminescence spectrum of OLED device based on **PY-CA** (top) and **PY-PH** (bottom)

PY-CA device has an EL maximum of 493 nm emission peak in the visible blue region with a full wave half maximum (FWHM) of 80 nm and CIE coordinates of 0.19 and 0.42. While the

PY-PH device has an EL maximum of 540 nm in the visible green region with a FWHM of 85 nm and CIE coordinates of 0.37 and 0.59. **PY-CA** device shows a turn on-voltage (V_{on}), a maximum current efficiency (CE), a maximum power efficiency (PE_{max}), a maximum brightness (MB_{max}) of 3.3V,1.6 cd A^{-1},1.5 lm W^{-1} and 2500 cd m^{-2}, respectively. Whereas **PY-PH** device exhibits V_{on}, CE_{max} and MB_{max} 3.8 V, 1.1cd A^{-1}, 0.45 lmW^{-1} and 2116 cdm^{-2}. The power efficiency of the **PY-CA** device is three times higher (1.5 lm W-1) than **PY-PH** device (0.45 lm W-1). The CE and PE characteristics of **PY-CA** and the **PY-PH** device are shown in **Figure 4.19**

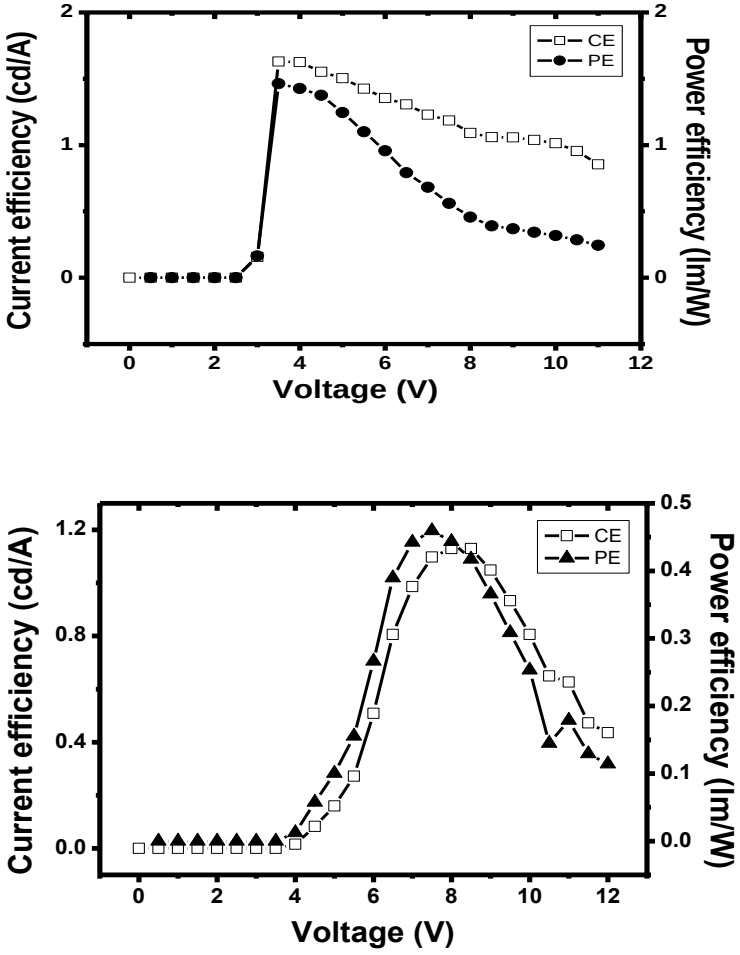

Figure 4.19: Current efficiency (CE) and power efficiency (PE) characteristics of **PY-CA** device (top) and **PY-PH** device (bottom)

The OLED device performance of PY-CA and PY-PH are summarized in **Table 4.**2. As the voltage increased from 3.3 V to 4 V, both the CE and PE of **PY-CA** device increased rapidly to the CE_{max} and the PE_{max} of 1.6 cdA^{-1} and 1.5 lmW^{-1} respectively. As the drive voltage further

increased, the CE and PE curves of **PY-CA** device rolled-off less rapidly. When voltage increased from 4V to 11V, the CE of **PY-CA** device remained at higher than one-half of CE_{max}, whereas when the drive voltage was increased from 4V to 7.5 V, PE values of **PY-CA** device still remained at higher than one-half of PE_{max}. In case of **PY-PH-** based OLED device as the voltage increased from 3.8 V to around 8 V, both the CE and PE of device increased gradually to the CE_{max} and the PE_{max} of 1.1 cd A^{-1} and 0.45 lm W-1, respectively. Unlike the case of **PY-CA** device, CE and PE curves of **PY-PH** device rolled-off more rapidly, CE and PE droped to one half of CE_{max} and PE when the drive voltage was increased from 8 V to 10 V. The overall higher performance of **PY-CA** than **PY-PH** was attributed to the appropriate energy levels for hole injection, better charge transporting and carrier mobility. The observed OLED performances for both compounds were much better than previously reported naphthalene substituted pyrene derivatives.[27] The stable blue color output additionally proves that **PY-CA** has high prospective to be a blue emitter in OLED applications. The turn on voltage of 3.3 V also made **PY-CA** based OLED device energy efficient.

Table 4.2: Electroluminescent performance summary of PY-PH and PY-CA based OLED device

Organic molecule	**Turn on Voltage (V_{on})**	**Current Efficiency (CdA^{-1})**	**Power Efficiency (lmW^{-1})**	**CIE coordinates**	**Electroluminescent Peak (nm)**	**Max. Brightness (cdm^{-2})**
PY-CA	3.3	1.6	1.5	(0.19,0.42)	493	2500
PY-PH	3.8	1.1	0.45	(0.37, 0.59)	540	2116

4.3.4) Atomic force microscopy (AFM) studies

The morphological behavior of **PY-CA** and **PY-PH** active layer thin film was characterized by atomic force microscopy (AFM) as shown in **Figure 2.20**. The measured root mean square (RMS) roughness of film samples was 2.32 nm for **PY-CA** and 1.06 nm for **PY-PH**. The pristine ITO coated glass showed high surface roughness with an RMS of 3.25 nm. The smooth film morphology of **PY-PH** film compared to **PY-CA** might be attributed to more bulky phenothiazine group compared to carbazole moiety. This is also one of the reasons why **PY-CA** exhibited better OLED performance than **PY-PH** counterpart.

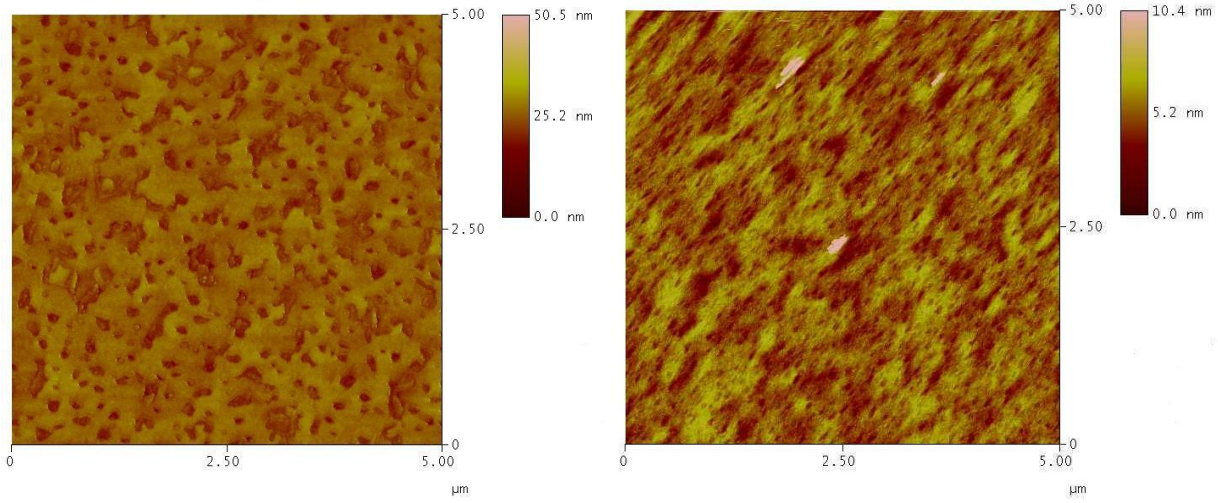

Figure 4.20: Atomic force microscopy images of **PY-CA** (left) and **PY-PH** (right) spin coated thin film on ITO coated glass.

The AFM images of **PY-CA** and **PY-PH** clearly demonstrated the amorphous nature of thin film with complete coverage of microstructure domains on thin film. The thin film morphology plays a crucial role for light emission in terms of transportation of holes and electrons in the recombination zone.

4.4) Conclusions

Two new solution processable 1,3,6,8- tetra substituted pyrene based electroluminescent small organic molecules, namely, 1, 3, 6, 8-tetrakis (9-(4-methoxyphenyl)-9H-carbazol-3-yl) pyrene **(PY-CA)** and 1,3,6,8-tetrakis(10-(4-methoxyphenyl)-10H-phenothiazin-3-yl)pyrene (**PY-PH)** were synthesized. **PY-CA** and **PY-PH** exhibited wide UV-vis absorption in the region 300 nm to 500 nm with an optical band gap of 2.67 eV and 2.50 eV, respectively. The HOMO values of **PY-CA** and **PY-PH** thin films were determined using PESA and were found to be 5.48 eV and 5.40 eV, respectively. **PY-CA** and **PY-PH** were used for OLED device applications and their electroluminescence properties were studied. The turn on voltage for both the devices was calculated in the range 3.3 V to 3.8 V. **PY-CA** exhibited blue emission with an electroluminescence peak at 493 nm, a maximum brightness at around 2500 cd m^{-1} and a power efficiency of 1.5 lmW^{-1}, whereas **PY-PH** showed green emission with an electroluminescence peak at 540 nm, a maximum brightness at around 2116 cd m^{-2} and a power efficiency of 0.45 lm W^{-1}. The reported OLED data clearly indicated that this class of functional materials hold a great promise for designing future cost effective and efficient light emitting materials for OLED devices. Further enhancements in the pyrene based small organic molecules with different substituents are expected to obtain improved performances with optimized molecular and device structure for OLED displays.

4.5) References

1. C. W. Tang and S. A. VanSlyke, *Appl. Phys. Lett.*, 1987, **51**, 913.
2. A. C. Grimsdale, K. Leok Chan, R. E. Martin, P. G. Jokisz and A. B. Holmes, *Chem. Rev.*, 2009, **109**, 897-1091.
3. L. S. Hung and C. H. Chen, *Mater. Sci. Eng.Rep.*, 2002, **39**, 143.
4. J. Kido and Y. Okamoto, *Chem. Rev.*, 2002, **102**, 2357-2368.
5. H. Uoyama, K. Goushi, K. Shizu, H. Nomura and C. Adachi, *Nature*, 2012, **492**, 234.
6. Y. H. Kim, H. C. Jeong, S. H. Kim, K. Yang and S. K. Kwon, *Adv. Funct. Mater.*, 2005, **15**, 1799.
7. Z. Zhao, S. Chen, J. W. Y. Lam, P. Lu, Y. Zhong, K. S. Wong, H. S. Kwok and B. Z. Tang, *Chem. commun.*, 2010, **46**, 2221.
8. X. Kong, A. P. Kulkarni and S. A. Jenekhe, *Macromolecules*, 2003, **36**, 8992.

9. K. R. Justin Thomas, M. Velusamy, J. T. Lin, Y. T. Tao and C. H. Chuen, *Adv.Funct. Mater.*, 2004, **14**, 387.
10. K. Mullen and U. Scherf, *Organic Light Emitting Devices: Synthesis, Properties and Applications*, John Wiley & Sons, New York, 2006.
11. Z. Ma, P. Sonar and Z.-K. Chen, *Curr. Org. Chem.*, 2010, **14**, 2034.
12. J. N. Moorthy, P. Natarajan, P. Venkatakrishnan, D.-F. Huang and T. J. Chow, *Org. Lett.*, 2007, **9**, 5215.
13. M. Y. Lo, C. Zhen, M. Lauters, G. E. Jabbour and A. Sellinger, *J. Am. Chem. Soc.*, 2007, **129**, 5808.
14. R. Xia, W. Y. Lai, P. A. Levermore, W. Huang and D. D. C. Bradley, *Adv. Funct. Mater.*, 2009, **19**, 2844.
15. Z. Zhao, J.-H. Li, X. Chen, X. Wang, P. Lu and Y. Yang, *J. Org. Chem.*, 2008, **74**, 383.
16. H. Zhang, Y. Wang, K. Shao, Y. Liu, S. Chen, W. Qiu, X. Sun, T. Qi, Y. Ma and G. Yu, *Chem.Ccommun.*, 2006, 755.
17. M. J. Sienkowska, J. M. Farrar, F. Zhang, S. Kusuma, P. A. Heiney and P. Kaszynski, *J. Mater. Chem.*, 2007, **17**, 1399.
18. F. Liu, W. Y. Lai, C. Tang, H. B. Wu, Q. Q. Chen, B. Peng, W. Wei, W. Huang and Y. Cao, *Macro. Rapid Commun.*, 2008, **29**, 659.
19. Y. Sagara, T. Mutai, I. Yoshikawa and K. Araki, *J. Am. Chem. Soc.*, 2007, **129**, 1520.
20. A. Mohr, P. Talbiersky, H.-G. Korth, R. Sustmann, R. Boese, D. Blaiser and H. Rehage, *J. Phys. Chem. B*, 2007, **111**, 12985.
21. R. Casier and J. Duhamel, *Macromolecules*, 2018, **51**, 3450.
22. N. J. Jeon, J. Lee, J. H. Noh, M. K. Nazeeruddin, M. Gratzel and S. I. Seok, *J. Am. Chem. Soc.*, 2013, **135**, 19087.
23. J. B. Birks, *Photophysics of Aromatic Molecules*, Wiley- Interscience, London, 1970.
24. S.I. Murata, P. Herman and J. R. Lakowicz, *J. Histochem. Cytochem.*, 2001, **49**, 1443.
25. T. M. Figueira-Duarte and K. Mullen, *Chem. Rev.*, 2011, **111**, 7260.
26. P. Sonar, M. S. Soh, Y. H. Cheng, J. T. Henssler and A. Sellinger, *Org. Lett.*, 2010, **12**, 3292.
27. J. K. Salunke, P. Sonar, F. L. Wong, V. A. L. Roy, C. S. Lee and P. P. Wadgaonkar, *Phys. Chem. Chem. Phys.*, 2014, **16**, 23320

28. K. N. Armarego and D. D. Perrin, *Purification of Laboratory Chemicals*, Butterworth-Heinemann, Oxford, 4th Edition, Butterworth Heinemann, 1996.
29. P. V. Ramachandran, D. Pratihar, D. Biswas, A. Srivastava and M. V. Ram Reddy, *Org. Lett.*, 2004, **6**, 481.
30. A. Suzuki, *J. Org.Chem.*, 1999, **576**, 147.
31. Y. Kusumoto, M. Shizuka and I. Satake, *Chem. Phys. Lett.*, 1986, **125**, 64.
32. O. A. Khakhel, *J. Appl. Spectrosc.*, 2001, **68**, 280.
33. F. H. Frimmel, *Refractory Organic Substances in the Environment*, John Wiley & Sons, New Jersey, 2008.
34. J. Jasieniak, M. Califano and S. E. Watkins, *ACS Nano*, 2011, **5**, 5888.
35. M. Onoda, K. Tada and H. Nakayama, *J. Appl.Phys.*, 1999, **86**, 2110.
36. S. Shinamura, I. Osaka, E. Miyazaki and K. Takimiya, *Heterocycles*, 2011, **83**, 1187.
37. E. K. U. Gross and R. M. Dreizler, *Density Functional Theory*, Springer Science & Business Media, New York, 2013.
38. A. D. Becke, *J. Chem. Phys.*, 1993, **98**, 5648.
39. T. Yanai, D. P. Tew and N. C. Handy, *Chem. Phys. Lett.*, 2004, **393**, 51.
40. D. Jacquemin, V. R. Wathelet, E. A. Perpete and C. Adamo, *J. Chem. Theor. Comput.*, 2009, **5**, 2420.
41. J. Tomasi, B. Mennucci and R. Cammi, *Chem. Rev.*, 2005, **105**, 2999.
42. M. J. Frisch, Gaussian 09, Gaussian Inc., Wallingford CT, 2009.
43. M. J. G. Peach, P. Benfield, T. Helgaker and D. J. Tozer, *J. Chem. Phys.*, 2008, **128**, 044118.
44. S. Manzhos, H. Segawa and K. Yamashita, *Chem. Phys. Lett.*, 2012, **527**, 51.

Supporting Information

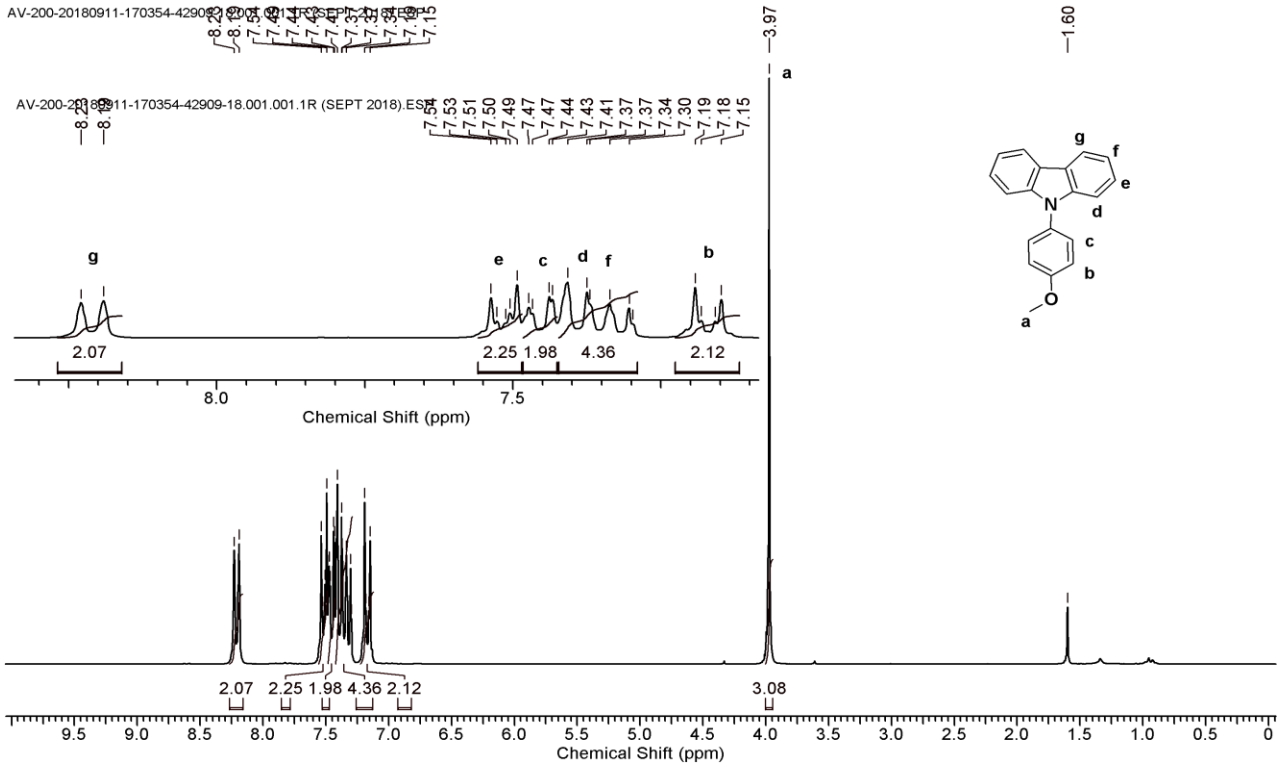

Figure S 4.1: ^{1}H NMR spectrum (in $CDCl_3$) of 9H-carbazole-9-(4-methoxyphenyl) (**2**)

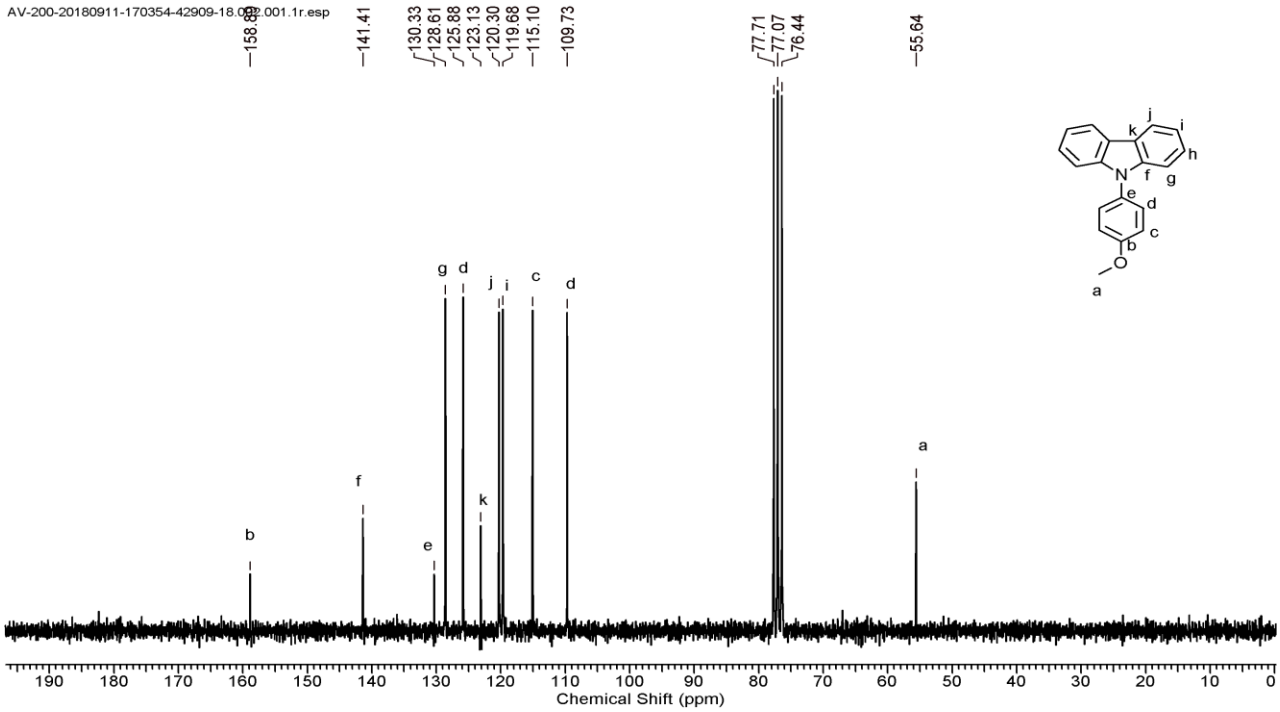

Figure S 4.2: ^{13}C NMR spectrum(in $CDCl_3$) of 9H-carbazole-9-(4-methoxyphenyl) (**2**)

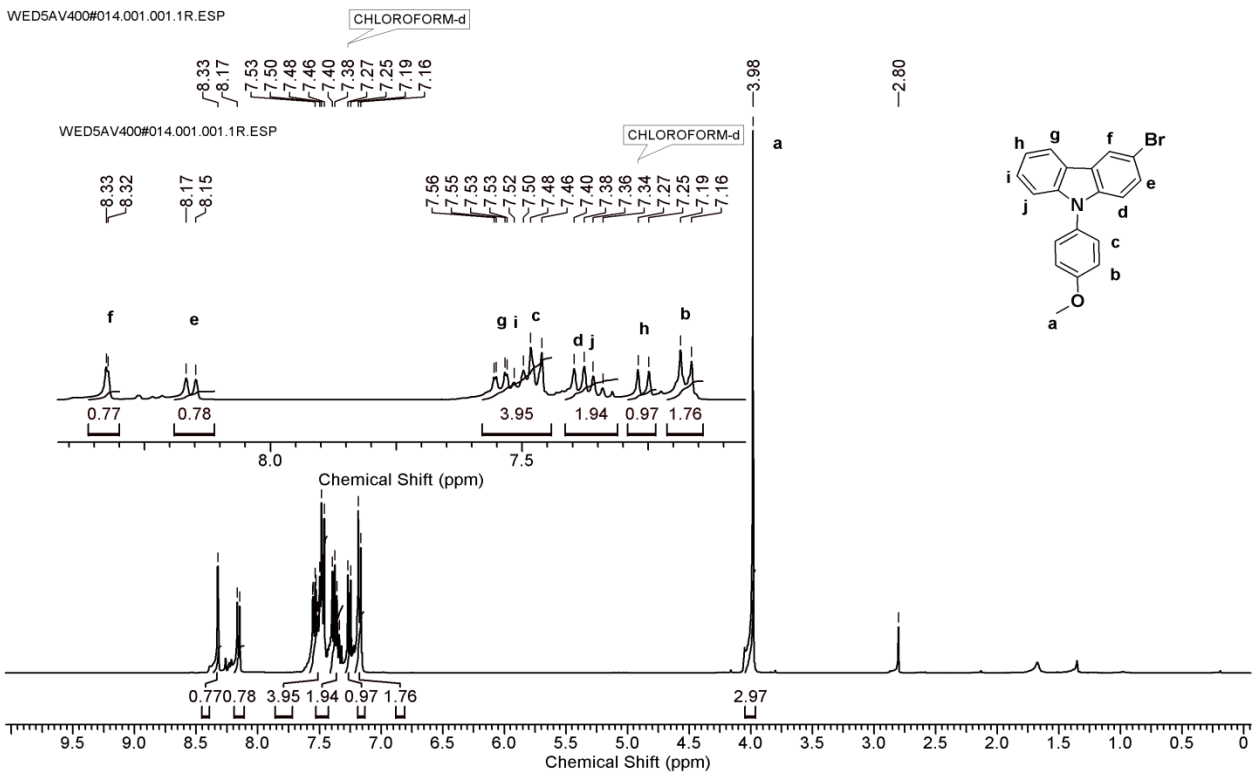

Figure S 4.3: ^{1}H NMR spectrum (in $CDCl_3$) of 3-bromo-9-(4-methoxyphenyl)-9H-carbazole (**3**)

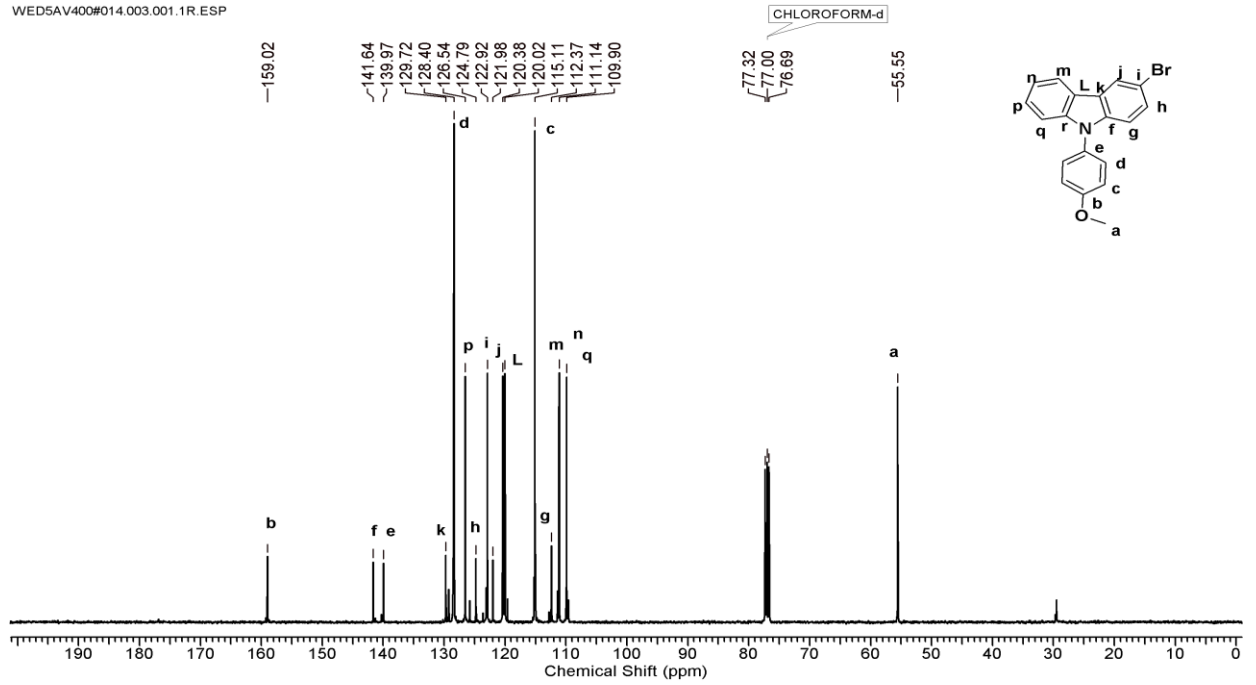

Figure S 4.4: ^{13}C NMR spectrum (in $CDCl_3$) of 3-bromo-9-(4-methoxyphenyl)-9H-carbazole (**3**)

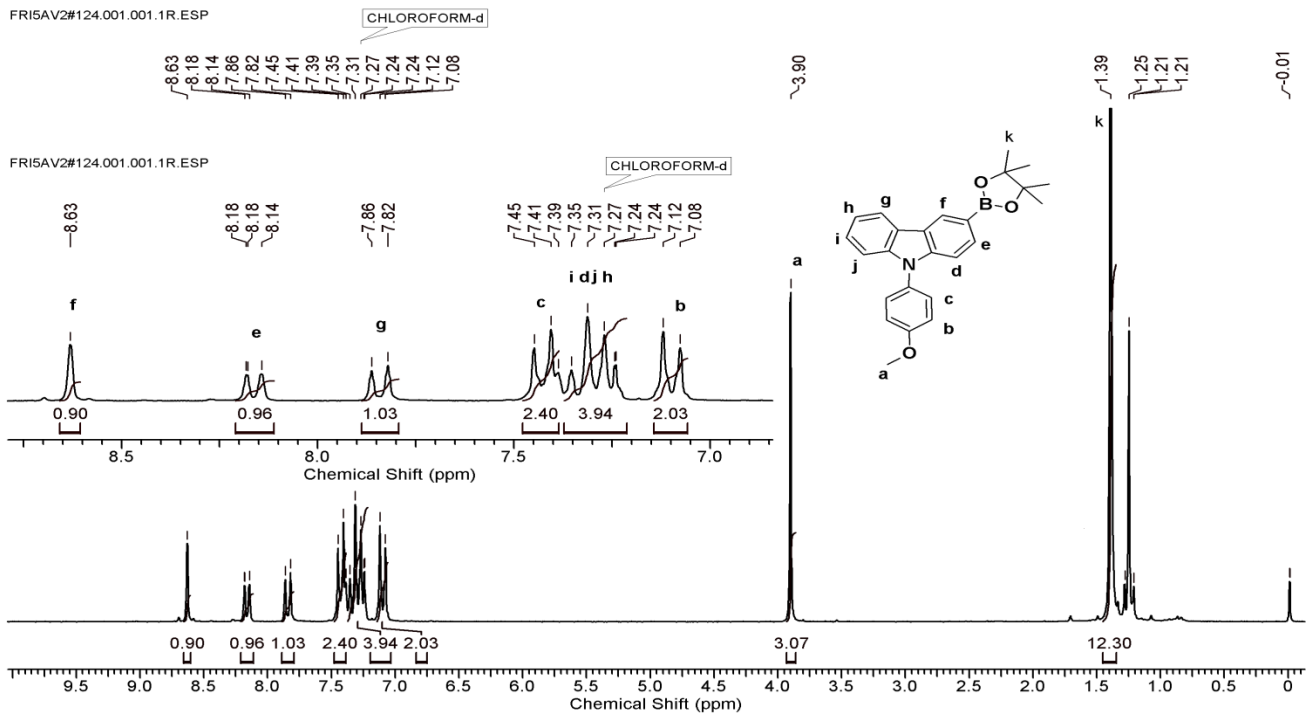

Figure S 4.5: ^{1}H NMR spectrum (in $CDCl_3$) of 9-(4-methoxyphenyl)-3-(4,4,5,5-tetramethyl-1,3,2-dioxaborolan-2-yl)-9H-carbazole (**4**)

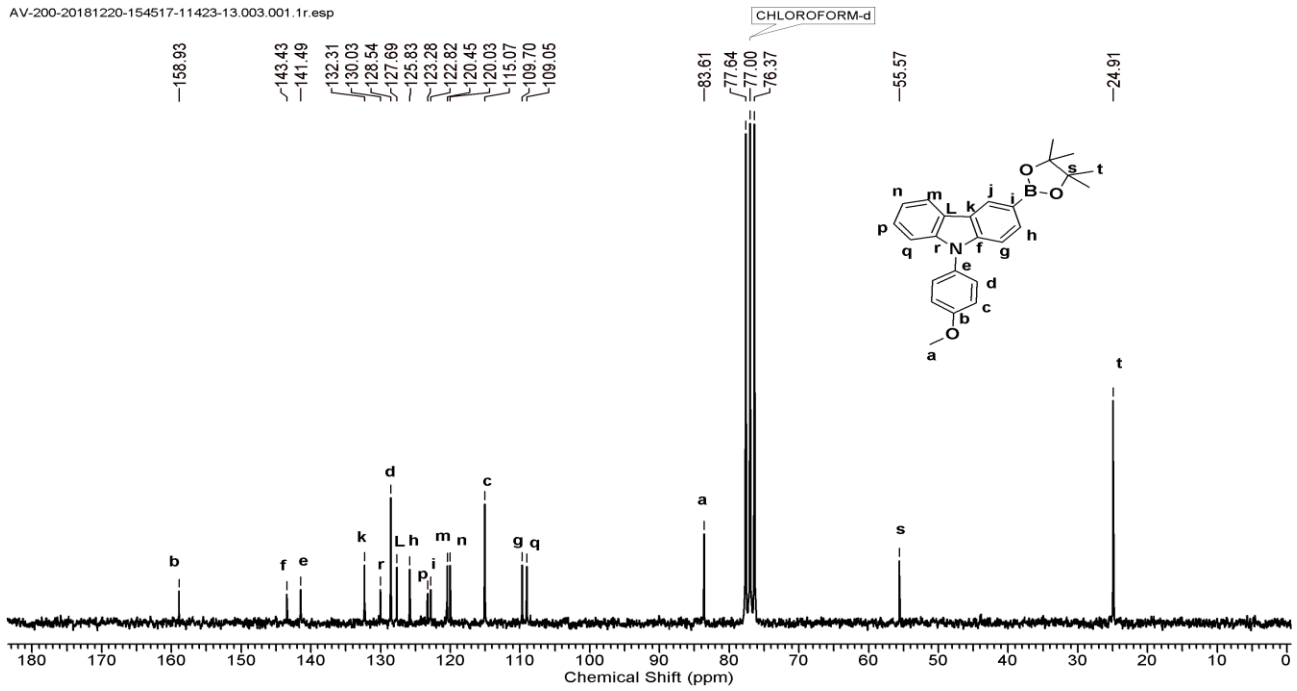

Figure S 4.6: ^{13}C NMR spectrum (in $CDCl_3$) of 9-(4-methoxyphenyl)-3-(4,4,5,5-tetramethyl-1,3,2-dioxaborolan-2-yl)-9H-carbazole (**4**)

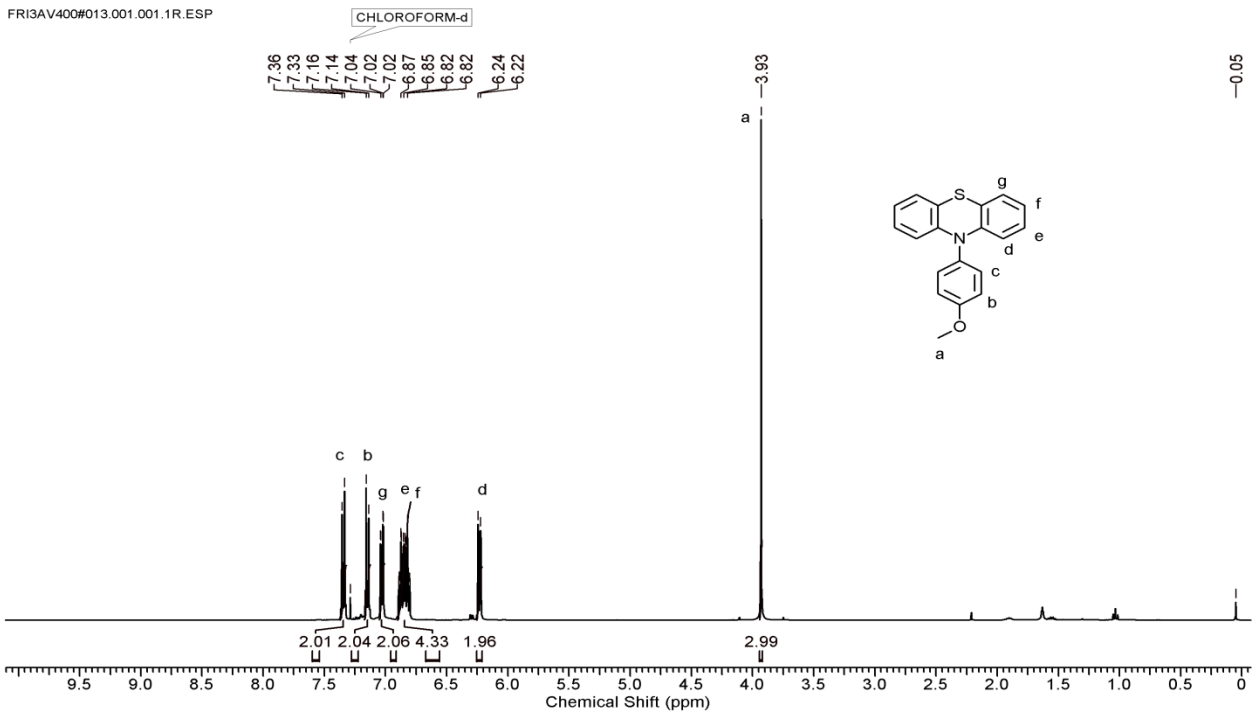

Figure S 4.7: ^{1}H NMR spectrum (in $CDCl_3$) of 10-(4-methoxyphenyl)-10H-phenothiazine (**6**)

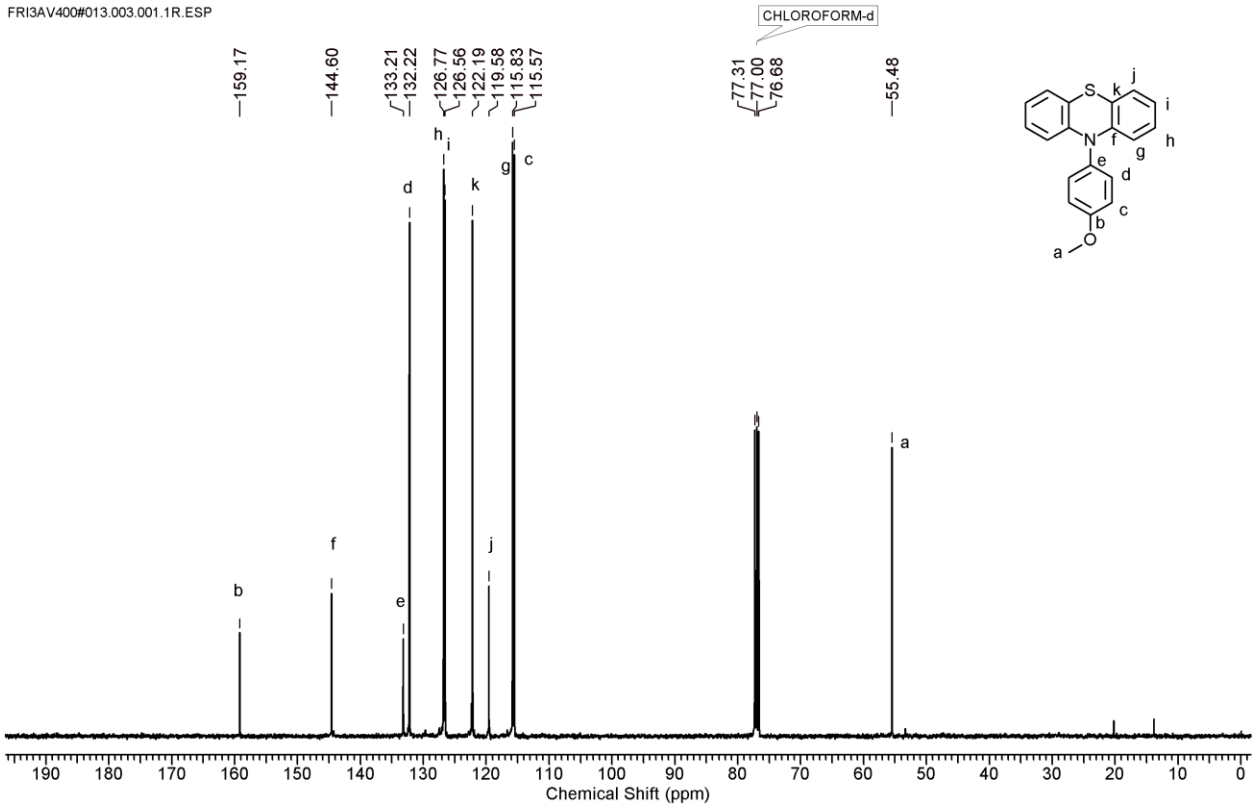

Figure S 4.8: ^{13}C NMR spectrum (in $CDCl_3$) of 10-(4-methoxyphenyl)-10H-phenothiazine (**6**)

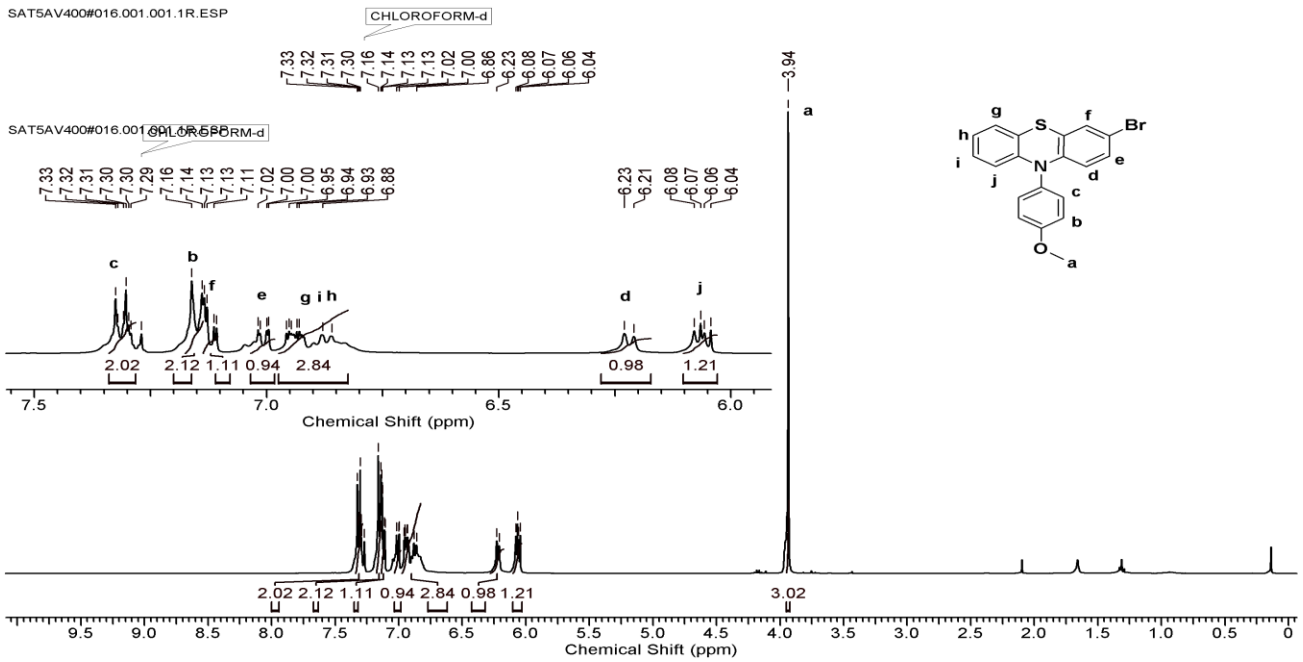

Figure S 4.9: ^{1}H NMR spectrum (in $CDCl_3$) of 3-bromo-10-(4-methoxyphenyl)-10H-phenothiazine(**7**)

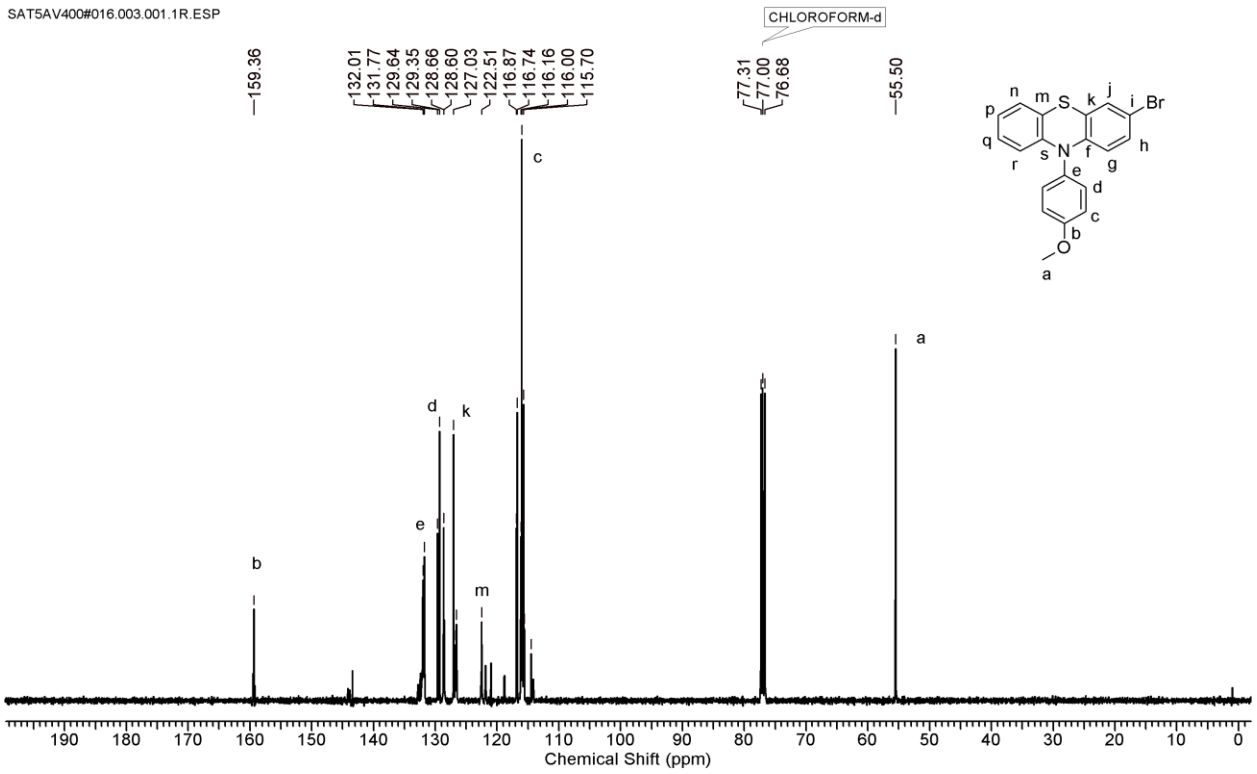

Figure S 4.10: ^{13}C NMR spectrum (in $CDCl_3$) of 3-bromo-10-(4-methoxyphenyl)-10H-phenothiazine (**7**)

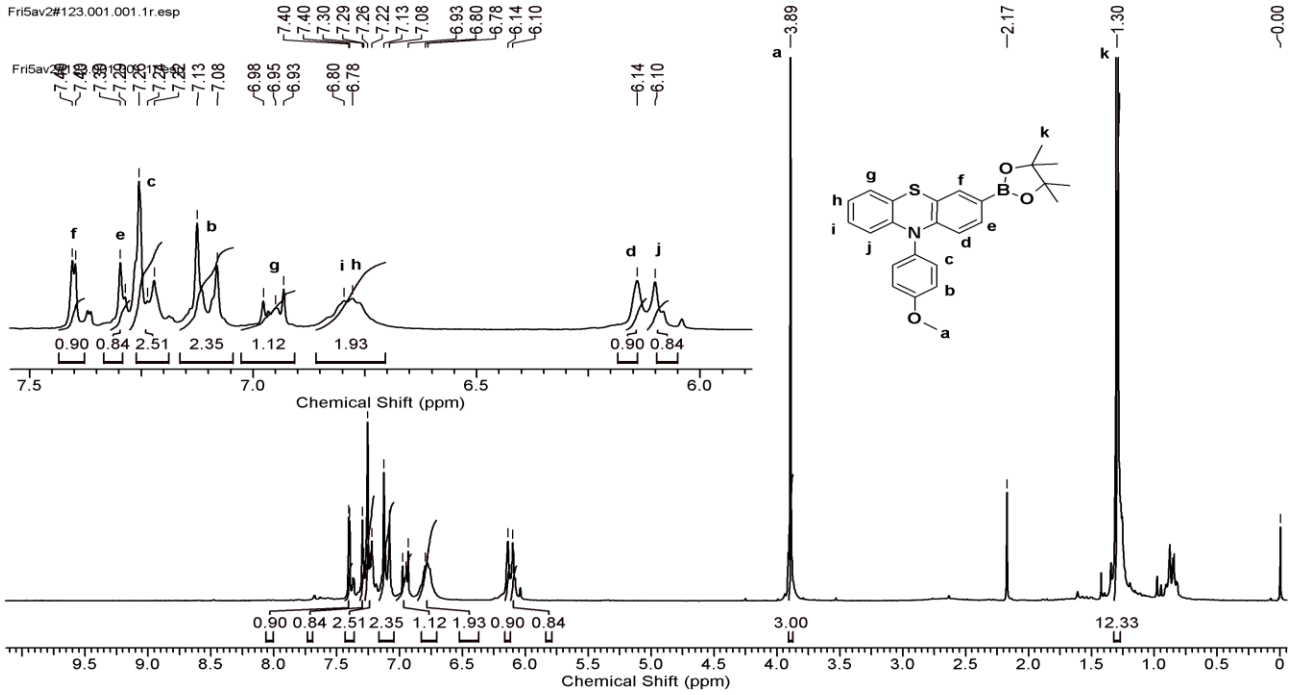

Figure S 4.11: ^{1}H NMR spectrum (in $CDCl_3$) of 10-(4-methoxyphenyl)-3-(4,4,5,5-tetramethyl-1,3,2-dioxaborolan-2-yl)-10H-phenothiazine (**8**)

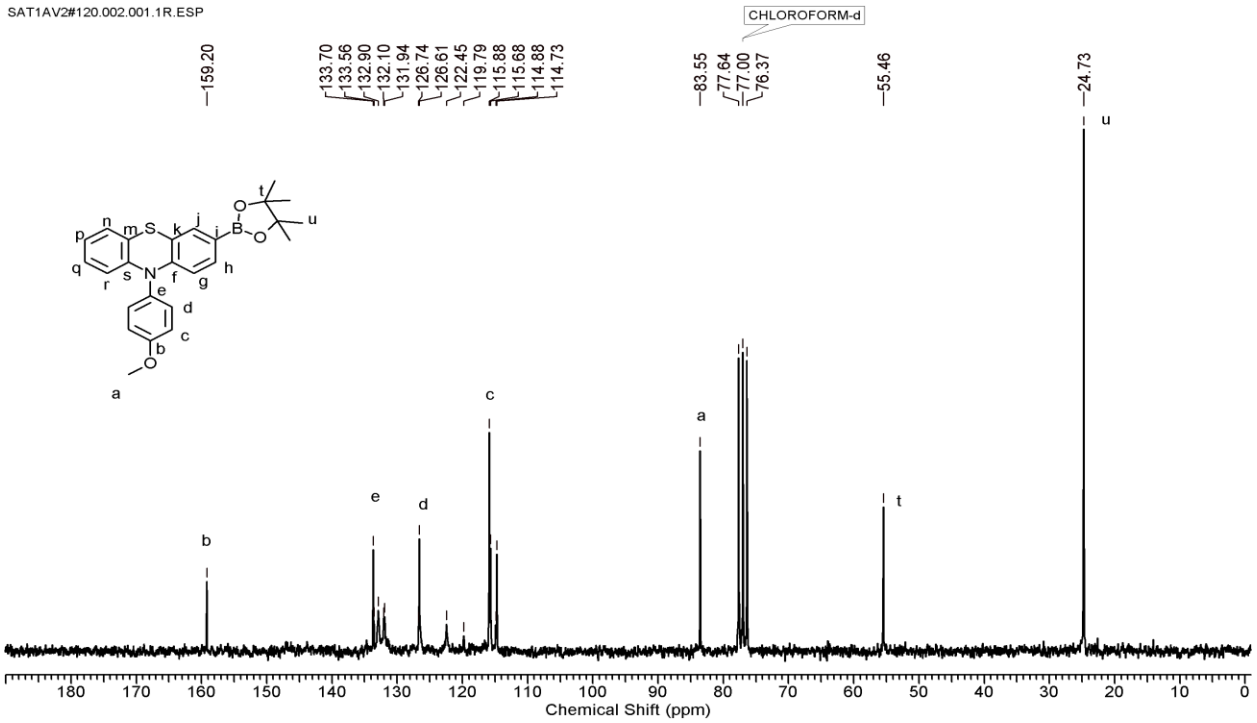

Figure S 4.12: ^{13}C NMR spectrum (in $CDCl_3$) of 10-(4-methoxyphenyl)-3-(4,4,5,5-tetramethyl-1,3,2-dioxaborolan-2-yl)-10H-phenothiazine (**8**)

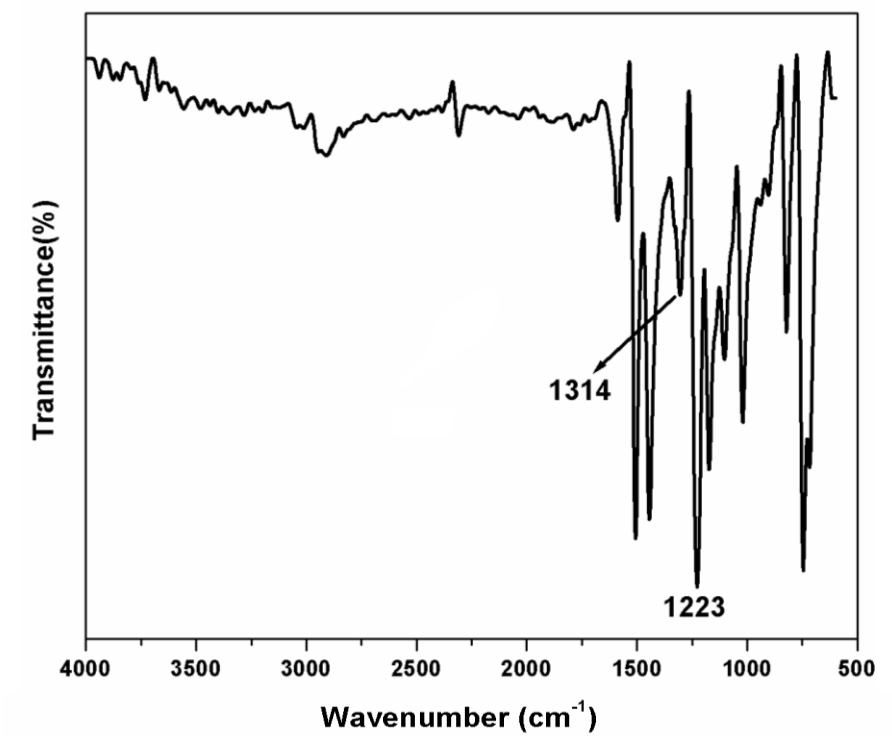

Figure S 4.13: IR spectrum of 9H-carbazole-9-(4-methoxyphenyl)

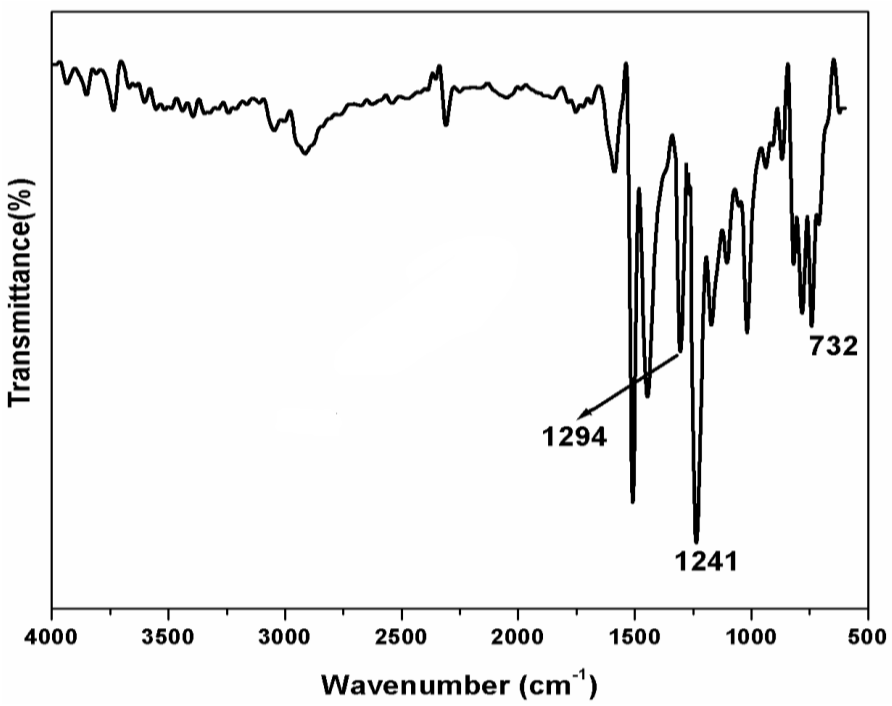

Figure S 4.14: IR spectrum of 3-bromo-9-(4-methoxyphenyl)-9H-carbazole

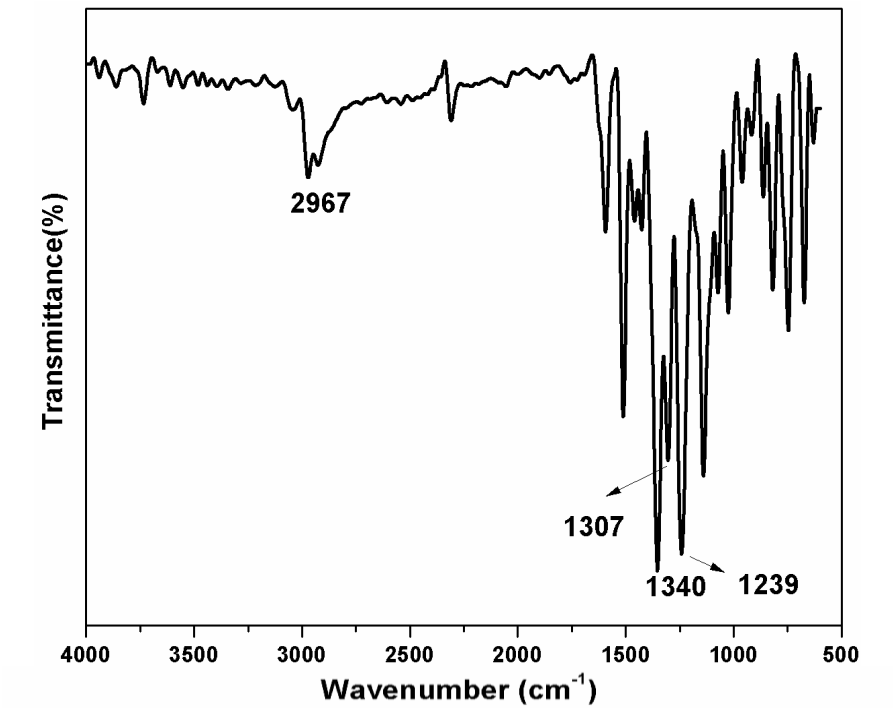

Figure S 4.15: IR spectrum of 9-(4-methoxyphenyl)-3-(4,4,5,5-tetramethyl-1,3,2-dioxaborolan-2-yl)-9H-carbazole

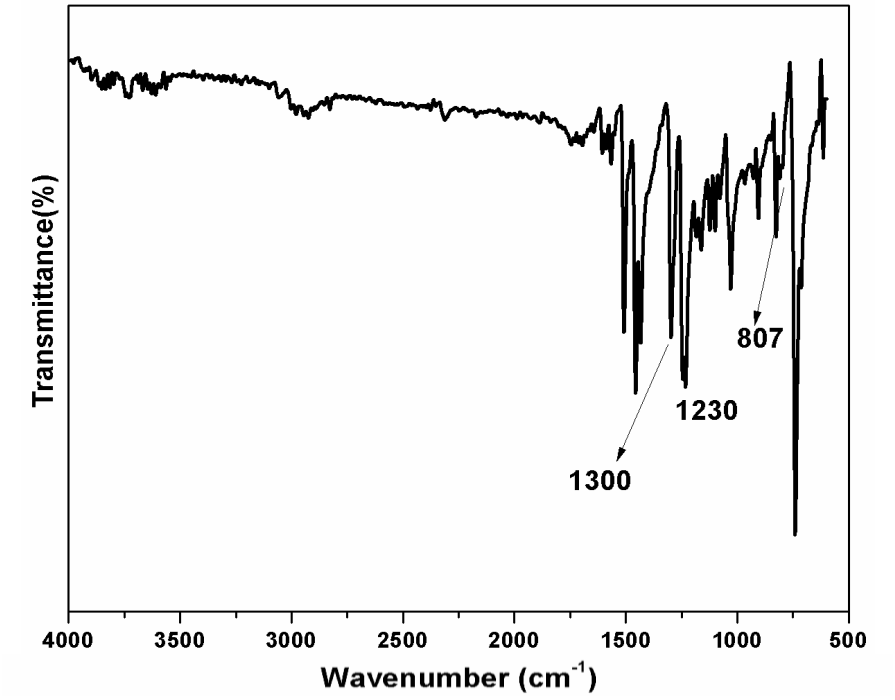

Figure S 4.16: IR spectrum of 10-(4-methoxyphenyl)-10H-phenothiazine

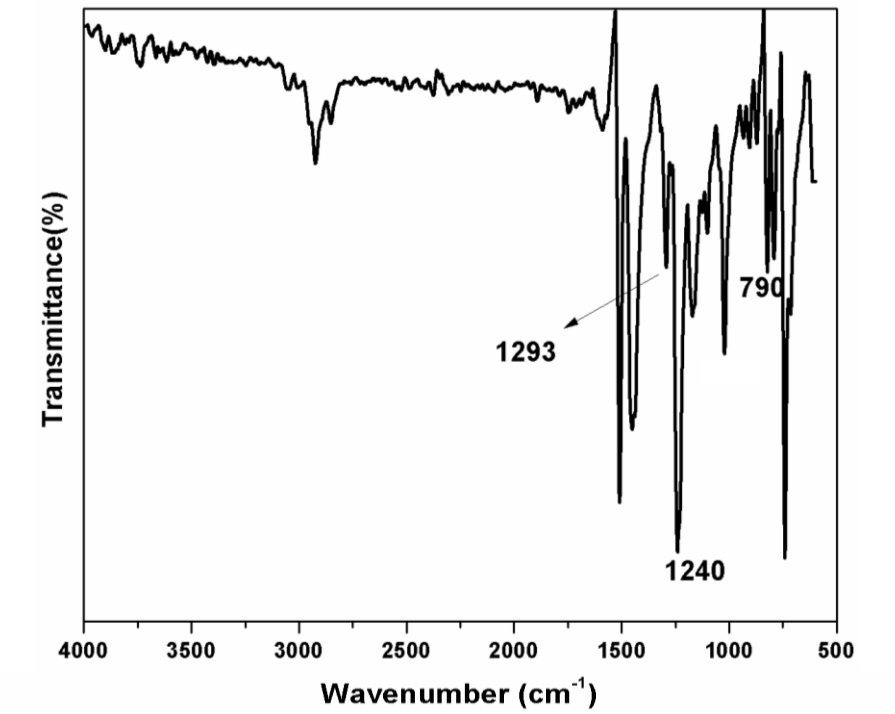

Figure S4.17: IR spectrum of 3-bromo-10-(4-methoxyphenyl)-10H-phenothiazine

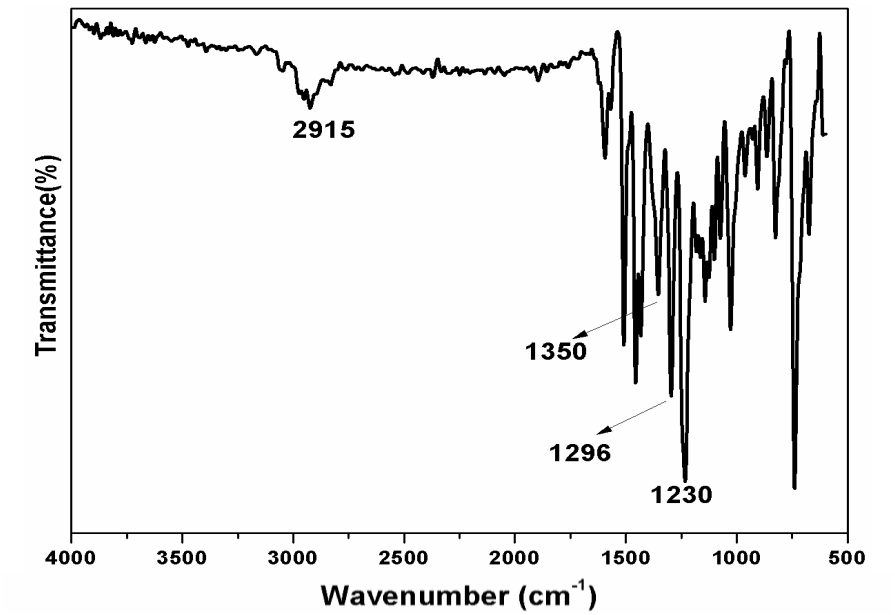

Figure S4.18: IR spectrum of 10-(4-methoxyphenyl)-3-(4,4,5,5-tetramethyl-1,3,2-dioxaborolan-2-yl)-10H-phenothiazine.

Table S 4.1: Atomic coordinates of **PY-CA**

opt B3LYP/6-31g(d,p) scrf (solvent-chloroform)

C	0.70802600	-3.46129500	-0.27827200
C	-0.57813400	-2.95760400	-0.28267300
C	-0.82009300	-1.59037600	-0.33294100
C	0.28355400	-0.68665200	-0.34461700
C	1.62268300	-1.18691200	-0.31916400
C	1.80709800	-2.59515500	-0.30617100
C	-2.15934900	-1.06946300	-0.34728500
C	0.02966900	0.74237400	-0.35360100
C	-1.31782000	1.21842400	-0.36983100
C	-2.39462200	0.25598800	-0.36591100
C	-1.54056500	2.60651400	-0.34686600
C	-0.47890100	3.50478900	-0.28939800
C	0.83598200	3.04270600	-0.28511300
C	1.12195300	1.66246400	-0.31629200
C	2.45853500	1.11486100	-0.25882800
C	2.69174700	-0.21421400	-0.26442300
H	3.69607500	-0.59070900	-0.20334800
H	3.27742400	1.81397900	-0.19371100
H	-2.96515300	-1.79239700	-0.32960100
H	0.87238400	-4.52968000	-0.25262600
H	-3.39983000	0.64434700	-0.35855400
H	-0.67545900	4.56808200	-0.27840100
C	-2.93315800	3.14626100	-0.37111400
C	-3.70903100	3.18384900	-1.51747200
C	-3.41231900	3.65798200	0.86970100
C	-5.03151100	3.72813900	-1.47326800
H	-3.33530300	2.81223800	-2.46263500
C	-4.70363000	4.17199000	0.87637400
H	-2.79729300	3.62790300	1.75729200
C	-5.49767200	4.20617900	-0.26628300
H	-5.62893200	3.75260500	-2.38161700
C	-5.55304600	4.76488300	1.92710200
N	-6.68224100	4.73709300	0.01302800
C	-6.74756900	5.08022500	1.28624900
C	-5.34719100	5.00766300	3.27082600
C	-7.67746100	4.90138500	-0.91194100
C	-7.79207000	5.65547400	1.97601800
C	-6.42190100	5.60024600	3.99531300
H	-4.41573900	4.75931200	3.76341400
C	-8.64298500	3.90811300	-1.13620400
C	-7.75326300	6.07419700	-1.68626000
C	-7.61506000	5.91670000	3.36694400
H	-8.73995000	5.90993800	1.50720100
H	-6.28565300	5.79910300	5.05522200
C	-9.67014700	4.08762400	-2.08368000
H	-8.60032300	2.99124700	-0.56168800

C	-8.76902200	6.24788600	-2.64535200
H	-7.01330300	6.85499200	-1.55522500
H	-8.43494300	6.36730000	3.91977800
C	-9.71944100	5.25717700	-2.81653000
H	-10.40107200	3.30164300	-2.23460200
H	-8.77882100	7.14746200	-3.23830500
C	1.92316800	4.05967000	-0.22521800
C	2.09473300	4.70042300	0.97550100
C	2.72294100	4.38051300	-1.37586100
C	3.10311100	5.70004900	1.12379500
H	1.47606300	4.44855800	1.82770400
C	3.68340600	5.36875400	-1.20414600
H	2.56179600	3.88078700	-2.32020700
C	3.87381200	6.00771000	0.02324000
H	3.23386300	6.19017000	2.08409600
C	4.67960200	5.99925200	-2.10176300
N	4.85346000	6.89689800	-0.07010400
C	5.34306800	6.92246700	-1.29673500
C	5.00702200	5.82759600	-3.43493400
C	5.29106900	7.67693700	0.96647500
C	6.36316600	7.70499900	-1.79438300
C	6.05826200	6.63702000	-3.96015700
H	4.49914400	5.11299700	-4.06791200
C	6.32325400	7.20754900	1.79435600
C	4.74942300	8.94621000	1.25435700
C	6.72175100	7.55271200	-3.16358200
H	6.90265100	8.42942900	-1.19040600
H	6.32978700	6.51570800	-5.00576800
C	6.82008300	7.99064300	2.85169200
H	6.76268200	6.23403500	1.61226100
C	5.23634400	9.72493100	2.32883300
H	3.93660100	9.33174900	0.64925200
H	7.52338300	8.16666500	-3.56496700
C	6.27922500	9.23423900	3.09560300
H	7.61795000	7.60670300	3.47383700
H	4.77559500	10.67952800	2.52898600
C	-1.76482900	-3.89289500	-0.21006800
C	-2.29452300	-4.16364200	1.02793800
C	-2.27987100	-4.48011600	-1.40327500
C	-3.40473800	-5.05228900	1.15466200
H	-1.88490600	-3.71353800	1.92429700
C	-3.36140000	-5.34734600	-1.24290300
H	-1.84713600	-4.26178000	-2.36876100
C	-3.90732100	-5.61979100	0.00778000
H	-3.81702600	-5.25920000	2.13877100
C	-4.18076700	-6.15418600	-2.17203200
N	-4.92057700	-6.46935300	-0.09641400
C	-5.11318600	-6.80279400	-1.35964900
C	-4.15252300	-6.32813200	-3.54296700
C	-5.63164900	-6.91183600	0.98865100
C	-6.05672500	-7.65341200	-1.89751500

C	-5.12380300	-7.20747300	-4.10668500
H	-3.43014600	-5.82522600	-4.17390000
C	-6.77130200	-6.22887100	1.44903700
C	-5.22939100	-8.05623400	1.69812800
C	-6.05250100	-7.85354200	-3.30845000
H	-6.79690200	-8.17496100	-1.29547900
H	-5.12064400	-7.35994000	-5.18320100
C	-7.49484400	-6.68682500	2.56761700
H	-7.10112400	-5.33692100	0.92931800
C	-5.94185400	-8.50783200	2.82536000
H	-4.34305100	-8.59546400	1.38526000
H	-6.79117800	-8.52250100	-3.74129100
C	-7.07544300	-7.82004100	3.23302000
H	-8.36594000	-6.13847200	2.90437500
H	-5.57873800	-9.37231200	3.35714300
C	3.14234400	-3.24174800	-0.29058100
C	4.00754300	-3.27448400	-1.37613800
C	3.47273700	-3.90067300	0.93416800
C	5.26144300	-3.95470800	-1.27963500
H	3.75484600	-2.79712200	-2.31357800
C	4.68900800	-4.56701600	0.98328400
H	2.78902000	-3.88443600	1.77086000
C	5.56769600	-4.59225700	-0.09580300
H	5.92777500	-3.96813600	-2.13780500
C	5.36650900	-5.36503500	2.02532600
N	6.65909600	-5.27839900	0.21731900
C	6.56410300	-5.76809100	1.44265100
C	5.01738400	-5.71606600	3.31386000
C	7.71997400	-5.46197200	-0.62613100
C	7.46375300	-6.54571700	2.13734600
C	5.94242600	-6.51846700	4.04360800
H	4.08293600	-5.40155400	3.76006900
C	8.80402300	-4.56993800	-0.61701200
C	7.75760500	-6.54223700	-1.52833800
C	7.13704000	-6.92480800	3.47193300
H	8.41017400	-6.87472000	1.71509300
H	5.68975600	-6.80656100	5.06073100
C	9.91216700	-4.76197800	-1.46463300
H	8.79418400	-3.72967000	0.06534900
C	8.85984900	-6.72233900	-2.39072400
H	6.92758000	-7.23821600	-1.56361500
H	7.84450500	-7.53437900	4.02778000
C	9.92149500	-5.83779300	-2.32950400
H	10.73625200	-4.05925900	-1.43807600
H	8.85365400	-7.54181200	-3.08888400
O	-10.72203900	5.30893400	-3.78561500
O	-7.81208500	-8.13254200	4.37731000
O	6.79205100	9.88683500	4.21624300
O	11.01851500	-5.90731600	-3.19004300
C	-11.56880200	6.44278900	-3.45867200
H	-11.06706400	7.36895000	-3.59035000

H	-12.40028600	6.40455200	-4.12191500
H	-11.90816900	6.36331600	-2.45224400
C	7.38358500	11.12180300	3.73424300
H	6.64896100	11.79526300	3.37250900
H	7.88562000	11.56675400	4.56031600
H	8.08122500	10.90542400	2.96072000
C	11.67928800	-7.17001500	-2.91351900
H	11.08980700	-8.00307200	-3.20953600
H	12.58502000	-7.17236000	-3.47272800
H	11.89625600	-7.23925800	-1.87322000
C	-8.39087600	-9.44933400	4.17263500
H	-7.65566700	-10.21201600	4.15333800
H	-9.04895800	-9.62684200	4.99049600
H	-8.93608800	-9.45975100	3.25997200

Table S 4.2: Atomic coordinates of **PY-PH**

opt B3LYP/6-31g(d,p) scrf(solvent-chloroform)

C	-4.05608768	-5.24678031	-0.00044900
C	-2.66323968	-5.24678031	-0.00044900
C	-1.95477668	-4.03829531	-0.00044900
C	-2.67188968	-2.81368631	-0.00041100
C	-4.09102368	-2.82302231	-0.00038100
C	-4.76783368	-4.04944031	-0.00048400
C	-0.51572168	-3.99621331	-0.00038400
C	-1.96310368	-1.56788131	-0.00019200
C	-0.54401568	-1.55855831	-0.00015700
C	0.15510232	-2.81707931	-0.00029500
C	0.13282732	-0.33206831	0.00000000
C	-0.57889568	0.86520269	0.00015100
C	-1.97181068	0.86520269	0.00017800
C	-2.68023668	-0.34323331	-0.00003000
C	-4.11932368	-0.38536231	-0.00024000
C	-4.79013968	-1.56448031	-0.00039500
H	-5.89070768	-1.59253431	-0.00091800
H	-4.65763068	0.57498569	-0.00015800
H	0.02244132	-4.95661331	-0.00068000
H	-4.60030568	-6.20326331	-0.00071200
H	1.25565132	-2.78913431	-0.00058200
H	-0.03477068	1.82176969	0.00012600
C	-2.74299882	2.19819514	0.00020319
C	-3.08259811	2.81272423	1.17034090
C	-3.09722610	2.78164505	-1.25160724
C	-3.80288419	4.05135207	1.16550252
H	-2.81553774	2.37258955	2.14294816
C	-3.78039311	3.96211877	-1.29572592
H	-2.80659371	2.26058553	-2.17573694
C	-4.15606996	4.63706284	-0.08893181
S	-4.16524584	4.69574776	2.35332409

H	-4.05804425	4.42378759	-2.25529506
N	-4.85801574	5.84711474	-0.11135808
C	-4.86948590	5.90451145	2.33092251
C	-5.22101531	6.49115835	1.07650992
C	-5.23155222	6.45644556	-1.39591498
C	-5.25022864	6.57660734	3.53767455
C	-5.94130874	7.72972996	1.07154849
C	-4.36873140	7.36046022	-2.01621260
C	-6.44848833	6.13079053	-1.99471667
H	-4.97432620	6.11397447	4.49730894
C	-5.93722592	7.75488803	3.49354232
C	-6.28734445	8.34067226	2.24172523
H	-6.20552727	8.17127186	0.09877389
C	-4.72314925	7.93915525	-3.23470420
H	-3.40973783	7.61757831	-1.54349344
C	-6.80272433	6.70882274	-3.21406301
H	-7.12856565	5.41816918	-1.50605046
H	-6.23183407	8.27338167	4.41787504
H	-6.84122312	9.29106637	2.24201936
C	-5.94037253	7.61298988	-3.83403733
H	-4.04339613	8.65219595	-3.72338115
H	-7.76210622	6.45155555	-3.68615860
O	-6.30344389	8.20643407	-5.08339844
C	-5.82717686	7.38958665	-6.15616589
H	-6.26402789	6.41550716	-6.08384481
H	-6.09918513	7.83397707	-7.09073994
H	-4.76195003	7.30806845	-6.09661268
C	1.67272200	-0.31405730	-0.00004479
C	2.37440077	-0.28500526	-1.17008701
C	2.35535757	-0.32805899	1.25164716
C	3.80717018	-0.27147204	-1.16528621
H	1.85952145	-0.27440694	-2.14260520
C	3.71917461	-0.31256137	1.29574655
H	1.75902596	-0.34997308	2.17571117
C	4.49121749	-0.28343925	0.08904183
S	4.54615110	-0.24662360	-2.35304108
H	4.25797538	-0.32118466	2.25523629
N	5.89005333	-0.26884391	0.11144006
C	5.94505157	-0.23465846	-2.33068339
C	6.62905747	-0.24472345	-1.07636562
C	6.60480483	-0.28642085	1.39585485
C	6.71723393	-0.21134648	-3.53738109
C	8.06178230	-0.23122600	-1.07144199
C	6.94122421	0.91337864	2.02336948
C	6.94658518	-1.50252891	1.98730690
H	6.17849776	-0.20471854	-4.49694813
C	8.08112244	-0.20026193	-3.49329476
C	8.76366575	-0.20953909	-2.24156767
H	8.57641960	-0.23866346	-0.09873737
C	7.61986678	0.89698495	3.24172790
H	6.67230824	1.87197460	1.55644360

C	7.62456511	-1.51911002	3.20651901
H	6.68135425	-2.44825339	1.49295199
H	8.67727928	-0.18307516	-4.41759029
H	9.86363970	-0.20016774	-2.24189685
C	7.96135514	-0.31963388	3.83370836
H	7.88562382	1.84264491	3.73609311
H	7.89355123	-2.47811220	3.67281884
O	8.65710034	-0.33611802	5.08293487
C	7.71166960	-0.35045147	6.15571410
H	7.09745260	-1.22316341	6.07818115
H	8.23273195	-0.36289989	7.09018672
H	7.09740433	0.52398387	6.10148303
C	-1.89192739	-6.57970091	-0.00058057
C	-1.52096031	-7.17621770	1.16935408
C	-1.57114220	-7.18235376	-1.25230997
C	-0.80069025	-8.41485389	1.16427358
H	-1.76203647	-6.72116245	2.14188257
C	-0.88904623	-8.36344205	-1.29655227
H	-1.88655034	-6.67552138	-2.17622801
C	-0.48101572	-9.01980754	-0.09001588
S	-0.40648691	-9.04096461	2.35173346
H	-0.63702783	-8.83982978	-2.25600141
N	0.22044150	-10.23013933	-0.11262416
C	0.29726404	-10.25000822	2.32906868
C	0.61528367	-10.85589736	1.07485964
C	0.55966065	-10.85917530	-1.39720351
C	0.71035666	-10.90352706	3.53538373
C	1.33555777	-12.09447922	1.06965509
C	-0.31917539	-11.77251720	-1.98023456
C	1.76004354	-10.54289401	-2.03328152
H	0.46008779	-10.42617461	4.49483650
C	1.39628051	-12.08242323	3.49099172
C	1.71295893	-12.68740977	2.23940145
H	1.57378905	-12.55094379	0.09705698
C	0.00269028	-12.36990387	-3.19873913
H	-1.26510175	-12.02223547	-1.47813307
C	2.08170435	-11.13963104	-3.25264576
H	2.45273728	-9.82292481	-1.57398995
H	1.71566763	-12.58668735	4.41496691
H	2.26693205	-13.63774886	2.23947561
C	1.20334585	-12.05312049	-3.83536386
H	-0.68967956	-13.09029256	-3.65804368
H	3.02803551	-10.88975416	-3.75413664
O	1.53304048	-12.66572980	-5.08472821
C	1.02799893	-11.86540737	-6.15679026
H	1.46633643	-10.89038039	-6.11115444
H	1.27504000	-12.32413409	-7.09137065
H	-0.03527776	-11.78286523	-6.07001764
C	-6.30772884	-4.06740132	-0.00101589
C	-7.00953969	-4.05345509	-1.17125646
C	-6.99022360	-4.09935324	1.25042331

C	-8.44230891	-4.06712178	-1.16679373
H	-6.49476976	-4.02834898	-2.14356622
C	-8.35403612	-4.11642760	1.29407821
H	-6.39378773	-4.11139818	2.17460137
C	-9.12621517	-4.10120356	0.08720525
S	-9.18142378	-4.04832353	-2.35457643
H	-8.89272899	-4.14302845	2.25329850
N	-10.52504889	-4.11657860	0.10921071
C	-10.58032205	-4.06106864	-2.33251490
C	-11.26418695	-4.09705100	-1.07859603
C	-11.23965580	-4.14615845	1.39348559
C	-11.35264044	-4.04003864	-3.53916748
C	-12.69691159	-4.11068644	-1.07400925
C	-11.57603796	-5.36818233	1.97656032
C	-11.58133617	-2.95257967	2.02923110
H	-10.81401210	-4.01144093	-4.49839173
C	-12.71652430	-4.05270243	-3.49536359
C	-13.39892692	-4.08937697	-2.24406275
H	-13.21143956	-4.13895812	-0.10162927
C	-12.25454340	-5.39652001	3.19477584
H	-11.30720089	-6.30899337	1.47472070
C	-12.25917885	-2.98076141	3.24830656
H	-11.31613454	-1.98934721	1.56990513
H	-13.31278530	-4.03592486	-4.41959944
H	-14.49890116	-4.09870405	-2.24461138
C	-12.59593169	-4.20245020	3.83106811
H	-12.52027112	-6.35968834	3.65411455
H	-12.52808614	-2.03952143	3.74953545
O	-13.29153628	-4.23183052	5.08013619
C	-12.34598480	-4.25691977	6.15261133
H	-11.73175236	-3.38196390	6.10710583
H	-12.86694196	-4.27877991	7.08696982
H	-11.73174981	-5.12878860	6.06623940

Chapter-5

Crystallization-Enhanced Bulk Hole Mobility in Phenothiazine-Based Organic Semiconductors

5.1) Introduction

The charge carrier mobility is of paramount importance in order to design new materials for organic electronic applications as it correlates with several key characteristics determining the performance of organic electronic devices. For instance, charge carrier transport directly affects the switching of organic field effect transistors (OFETs) and lower turn-on voltages are observed for organic light emitting diodes (OLEDs) based on materials with high mobility.[1,2] The mobility also influences charge carrier dynamics in organic photovoltaics (OPVs).[3,4] A large number of π-conjugated small molecules have been designed and synthesized for OPVs,[5-8] OLEDs[9,10] and OFETs.[11] In comparison to their polymeric counterparts, the benefits of solution-processable small-molecule-based organic semiconductors arise from their high structural flexibility, easy accessibility, simple preparation and purification, well-defined structure, and batch-to-batch reproducibility.[12- 14]

Phenothiazine is a well-known electron-rich heterocyclic molecule due to the presence of nitrogen and sulphur heteroatoms.[15] Phenothiazine is a good electron-donor in photo-excited charge transfer transitions, and exhibits a low and reversible oxidation potential for the generation of a stable radical cation.[16-21] Ability to suppress molecular aggregation due to butterfly conformation of phenothiazines,[22] together with their attractive hole-transport characteristics have resulted in their use in dye sensitized solar cells (DSSCs) as photosensitizers [23-31] as well as in organic thin film transistors and OLED.[32-35] Molecular aggregation and the degree of disorder in phenothiazine films have a strong impact on their optical properties[36] and better film-forming properties are usually observed in the systems for which aggregate formation is less likely to occur.[37, 38] However, the state-of-the- art phenothiazine molecules show fairly low bulk mobilities[32-35] which is one of the key reasons because of which scanty reports are available on phenothiazine molecules for application in organic photovoltaics.[39- 43]

The literature survey showed that, as the only exceptional example, high mobility values for charge-transfer complexes of iodine with N-methylphenothiazine (2:3 donor acceptor ratio) was reported by Matsunaga in 1960s, where a complex cation radical of phenothiazine was proposed as the conductive species.[44-50] Therefore, it is highly desirable to derive a phenothiazine derivative combining the properties such as high mobility, good film forming properties and high light harvesting capabilities which are necessary for different applications in the field of organic electronics. Based on previous mobility data for *para*-methoxyphenyl N-substituted

phenothiazines, the intramolecular charge transfer (ICT) character of phenothiazines can be improved by introducing substituents at C(3) and C(7) positions.[28] Extending the π -system of phenothiazine increases ICT and consequently improves its charge transport properties.[51 52] Even though there are several reports on such approach, the *para*-methoxyphenyl N-substituted phenothiazines usually bear a cyanoacrylic moiety at C(3) position.[53-57] Hence, we envisioned that substitution of such group with a stronger electron acceptor such as malononitrile would increase the ICT.

In the present work, phenothiazine based push-pull organic semiconducing molecules *viz* 2-((10-(4-methoxyphenyl)-10H-phenothiazin-3-yl) methylene) malononitrile (**O-1**), 2-((7,10-bis(4-methoxyphenyl)-10H-phenothiazin-3-) methylene) malononitrile (**O-2**) and 2-((7-(6-butoxynaphthalen-2-yl)-10-(4-methoxyphenyl)-10H-phenothiazin-3-yl)methylene) malononitrile (**O-3**) were designed and synthesized. In order to increase the electron density at the phenothiazine core, alkoxyaryl groups were appended at C(7) position; *para*-methoxyphenyl unit in **O-2** and 6-butoxynapthyl unit in **O-3**, which also helped to improve solution processability due to presence of bulkier molecular structure. **O-1, O-2** and **O-3** were characterized by IR, ^{1}H and ^{13}C spectroscopy, HRMS, DSC, TGA and X-ray diffraction analysis. The effect of substitution of electron donating group at C(7) position on the optical and electrochemical properties was studied. The charge transport properties of molecules were studied by impedance spectroscopy method.

5.2) Experimental

5.2.1) Materials

All the chemicals namely, phenothiazine, 4-iodoanisole, 6-bromo-2-naphthol, 1-bromobutane, N-bromosuccinimide, 4-methoxy phenylboronic acid, malononitrile, piperidine, bis(pinacolato) diboron, [1,1′-bis(diphenylphosphino)ferrocene] dichloropalladium(II)] ($Pd(dppf)Cl_2$), [tetrakis (triphenylphenylphosphine) palladium] ($Pd(PPh_3)_4$), copper powder, potassium carbonate, potassium acetate and phosphorous oxychloride were purchased from Sigma Aldrich and were used without further purification. Solvents namely, triethylene glycol dimethylether (TEGDME), N,N-dimethylformamide (DMF), 1,2-dichloroethane, chloroform and tetrahydrofuran (THF) were purchased from Aldrich and were purified according to the standard procedures.[58] All the reactions were carried out under argon or nitrogen atmosphere.

5.2.2) Instrumentation

Melting points were recorded on Electrothermal MEL-TEMP apparatus and are uncorrected. IR spectra were recorded on Perkin Elmer GX spectrophotometer in the range of 4000-500 cm^{-1} using ATR mode. ^{1}H and ^{13}C NMR spectra of compounds were recorded using chloroform-d ($CDCl_3$) as a solvent on Bruker AC spectrometer operating at 400 MHz for ^{1}H and 100 MHz for ^{13}C. HRMS characterization was performed on Thermo Scientific Q-Exacative with Accela 1250 pump. UV-Vis absorption spectra were measured with a Shimadzu UV-3600 UV/Vis/ NIR spectrophotometer, both in solution and thin film. Electrochemical measurements were performed by method of differential pulse voltammetry (DPV) using a potentiostat (Compact-Stat, Ivium Technologies). The charge carrier motility measurements were performed by impedance spectroscopy measurements using an Agilent 4294A impedance analyzer.

5.2.3) Synthesis

5.2.3.1) Synthesis of 10-(4-methoxyphenyl)-10H-phenothiazine (1)

Into a Schlenk tube equipped with a magnetic stirring bar were added phenothiazine (5 g, 25 mmol), 4-iodoanisole (7.04 g, 30 mmol), copper powder (1.6 g, 25 mmol), potassium carbonate (10.38 g, 75 mmol) and triethylene glycol dimethyl ether (50 mL) under argon flow and the reaction mixture was stirred at 180 ^{0}C for 24 h. After completion of reaction, the reaction mixture was quenched by pouring into ice cold water. The brown precipitate was collected by filtration and dried. The product was recrystallized from ethyl acetate to obtain compound **1** as a yellowish crystalline solid.

Yield: 5.74 g (75 %)

Melting point: 170 °C

IR (ATR, cm^{-1}): 1300 (C-N), 1230 (C-O-C), 807 (C-S-C) [**Figure S 5.15**]

^{1}H NMR (400 MHz, CDCl3) δ ppm = 7.34 (d, 2 H), 7.15 (d, 2 H), 7.03(d, 2 H), 6.88 - 6.80 (m, 4H), 6.23 (d, 2 H), 3.93 (s, 3 H). [**Figure S 5.1**]

^{13}C NMR (100 MHz, $CDCl_3$) δ ppm = 159.17, 144.6, 133.21, 132.22, 126.77, 126.56, 122.19, 119.58, 115.83, 115.57, 55.48. [**Figure S 5.2**]

HRMS: Calculated for $C_{19}H_{15}NOS$ 305.0869, found 305.0867

5.2.3.2) Synthesis of 10-(4-methoxyphenyl)-10H-phenothiazine-3-carbaldehyde (2)

Into a 100 mL two necked round bottom flask equipped with a magnetic stirring bar was added phosphorous oxychloride (3.65 mL) in dropwise manner into DMF (3.04 mL) at 0 ^{0}C. The reaction mixture was stirred at room temperature for 30 min, subsequently the solution of 10-(4-methoxyphenyl)-10H-phenothiazine **(1)** (4 g, 13 mmol) in 1,2-dichloroethane (30 mL) was added and the reaction mixture was heated to 80 ^{0}C for 12 h. After completion of reaction, the reaction mixture was poured into ice cold water (100 mL) and extracted with ethyl acetate (3×100 mL). The ethyl acetate solution was separated and washed with water (50 mL), brine solution (50 mL) and again with water (50 mL). The ethyl acetate layer was dried over anhydrous sodium sulfate and filtered. Removal of ethyl acetate on rotary evaporator afforded crude product which was purified by column chromatography using petroleum ether: dichloromethane (7:3, v/v) as an eluent to give the title compound **2** as a yellow solid.

Yield: 3.7 g (85 %)
Melting point: 176 °C

IR (ATR, cm^{-1}): 1678 (C=O, aldehyde) [**Figure S 5.16**]

^{1}H NMR (400 MHz, $CDCl_3$) δ ppm = 9.69 (s, 1 H), 7.46 (d, 1 H), 7.31 - 7.26 (m, 3 H), 7.15 (d, 2 H), 6.99-6.94 (dd, 1 H), 6.87 - 6.81 (m, 2 H), 6.20 (d, 1H), 6.18-6.13 (m, 1H) 3.92 (s, 3 H). [**Figure S 5.3**]

^{13}C NMR (100 MHz, $CDCl_3$) δ ppm = 189.7, 159.6, 149.51, 142.8, 132.24, 131.66, 130.84, 129.88, 127.38, 127.07, 126.58, 123.51, 119.98, 118.91, 116.36, 116.19, 114.92, 55.54.[**Figure S 5.4**]

HRMS: Calculated for $C_{20}H_{15}NO_2S$ 333.0823, found 333.0818.

5.2.3.3) Synthesis of 7-bromo-10-(4-methoxyphenyl)-10H-phenothiazine-3-carbaldehyde (3)

Into a two necked round bottom flask equipped with a magnetic stirring bar were added 10-(4-methoxyphenyl)-10H-phenothiazine-3-carbaldehyde (3 g, 8 mmol) and chloroform (50 mL). The mixture was cooled at 0^{o}C. Subsequently, the solution of N-bromosuccinimide (1.92 g, 10.7 mmol) in chloroform (15 mL) was added drop wise over a period of 15 minutes and the reaction mixture was stirred overnight at room temperature. After completion of reaction, the reaction mixture was poured into water and extracted with dichloromethane (3×50 mL). The

dichloromethane layer was washed with water (50 mL), brine solution (50 mL) and again with water (50 mL). The dichloromethane solution was dried over anhydrous sodium sulfate, filtered and evaporated on rotary evaporator to give a crude product, which was purified on silica gel chromatography using petroleum ether: ethyl acetate (9:1, v/v) as an eluent to afford title compound **3** as pale saffron solid.

Yield: 3.75 g (81%)

Melting point: 181 °C

IR (ATR, cm^{-1}): 1674 (C=O), 792 (C-Br). [**Figure S 5.17**]

^{1}H NMR (400 MHz, $CDCl_3$) δ ppm = 9.71 (s, 1 H), 7.43 (d, 1 H), 7.33-7.29 (dd, 1H), 7.27(d, 2 H), 7.15 (d, 2 H), 7.08 (d, *J* = 2.2 Hz, 1 H), 6.93-6.91 (dd, *J* = 2.4, 8.8 Hz,1 H), 6.21 (d, *J* = 8.6 Hz, 1 H), 6.01 (d, *J* = 8.8 Hz, 1 H), 3.93 (s, 3 H). [**Figure S 5.5**]

^{13}C NMR (100 MHz, CDCl3) δ ppm = 189.61, 159.75, 149.01, 142.08, 131.86, 131.46, 131.05, 130.07, 129.69, 128.68, 127.41, 121.13, 119.25, 117.53, 116.35, 115.67, 115.12, 55.57. [**Figure S 5.6**]

HRMS: Calculated for $C_{20}H_{14}BrNO_2S$ 410.9929, found 410.9923

5.2.3.4) Synthesis of 2-bromo-6-butoxynaphthalene (4)

Into a 250 mL two necked round bottom flask equipped with a magnetic stirring bar and an addition funnel were added 6-bromo-2-napthol (4 g, 18 mmol), potassium hydroxide (1.2 g, 21 mmol) and dimethyl sulfoxide (50 mL). The reaction mixture was stirred at room temperature for 30 minutes. Subsequently, 1-bromo butane (2.3 mL, 21 mmol) dissolved in dimethyl sulfoxide (10 mL) was added drop wise to the mixture *via* addition funnel and the reaction mixture was stirred overnight at room temperature. After completion of reaction, the mixture was poured into water (200 mL) and extracted with ethyl acetate (3× 50 mL). The ethyl acetate layer was separated and washed with water (50 mL), brine solution (50 mL) and again with water (50 mL). The ethyl acetate layer was dried over anhydrous sodium sulfate, filtered and evaporated on rotary evaporator. The obtained crude product was purified by column chromatography using petroleum ether as an eleunt to obtain the title product **4** as white solid.

Yield: 4.7 g (95 %)

Melting point: 141 °C

IR (ATR, cm^{-1}): 1254 (C-O-C) **[Figure S 5.18]**

^{1}H NMR (400 MHz, $CDCl_3$) δ ppm = 7.84 (s, 1 H), 7.57 - 7.48 (m, 2 H), 7.45 - 7.39 (m,1 H), 7.14-7.06 (dd, 1 H), 7.0 (d, 1 H), 3.98 (t,2 H), 1.85 -1.75 (m, 2 H), 1.59-1.40 (m,2 H), 0.97 (t, 3 H). [**Figure S 5.7**]

^{13}C NMR (100 MHz, $CDCl_3$) δ ppm = 157.34, 133.03, 129.83, 129.53, 129.41, 128.3, 128.26, 120.0, 116.79, 106.39, 67.66, 31.2, 19.26, 13.84. [**Figure S 5.8**]

HRMS: Calculated for $C_{14}H_{15}BrO$ 278.0306, found 278.0301

5.2.3.5) Synthesis of 2-(6-butoxynaphthalen-2-yl)-4, 4, 5, 5-tetramethyl-1, 3, 2-dioxaborolane (5)

Into a Schlenk tube equipped with a magnetic stirring bar were added 2-bromo-6-butoxynaphthalene (2 g, 7 mmol), bis(pinacolato)diboron (1.8 g, 7.8 mmol), $PdCl_2$(dppf) (0.523 g, 0.7 mmol) and potassium acetate (2.1 g, 21 mmol) under argon flow. The Schlenk tube was evacuated for 15 minutes. Dry 1,4-dioxane (20 mL) was added to the above mixture under argon flow and the reaction mixture was stirred at room temperature for 30 minutes. Once the color of reaction mixture turned black, it was heated at 80 °C for 24 h. After completion of reaction, the reaction mixture was quenched by addition into water (100 mL) and was extracted with ethyl acetate (3×50 mL). The ethyl acetate solution was separated and washed with water (50 mL), brine solution (50 mL) and again with water (50 mL). The ethyl acetate layer was dried over anhydrous sodium sulfate, filtered and evaporated on rotary evaporator. The crude obtained was purified by column chromatography using petroleum ether: ethyl acetate (8:2, v/v) to give title compound **5** as a white solid.

Yield: 1.68 g, (72 %)

Melting point: 135 °C

IR (ATR, cm^{-1}): 1360 (B-O), 1259 (C-O-C) [**Figure S 5.19**]

^{1}H NMR (400 MHz, $CDCl_3$) δ ppm = 8.29 (s, 1 H), 7.83 - 7.66 (m, 3 H), 7.14 - 7.07 (m, 2 H), 4.02 (t, , 2 H), 1.86-1.72 (m, 2H), 1.59 - 1.45 (m, 2 H), 1.36 (s, 12 H), 0.98 (t, 3H). [**Figure S 5.9**]

^{13}C NMR (100 MHz, $CDCl_3$) δ ppm = 158.0, 136.43, 135.9, 134.66, 131.0, 130.03, 128.20, 125.78, 118.91, 106.25, 83.62, 67.53, 31.18, 24.81, 19.21, 13.79. [**Figure S 5.10**]

HRMS: Calculated for $C_{20}H_{27}O_3B$ 326.2053, found 326.2049.

5.2.3.6) Synthesis of 7, 10-bis (4-methoxyphenyl)-10H-phenothiazine-3-carbaldehyde (6)

Into a Schlenk tube equipped with a magnetic stirring bar were added 7-bromo-10-(4-methoxyphenyl)-10 H-phenothiazine-3-carbaldehyde (1g, 2.4 mmol), 4-methoxy phenylboronic acid (0.405 g, 2.6 mmol), 2M aq. K_2CO_3 (3 mL) and tetrahydrofuran (15 mL) under argon flow and the reaction mixture was heated at 60 ^oC for 24 h. After completion of reaction, the mixture was poured into water and extracted with ethyl acetate (3× 50 mL). The ethyl acetate layer was separated and washed with water (50 mL), brine solution (50 mL) and again with water (50 mL). The ethyl acetate solution was separated and dried over anhydrous sodium sulfate, filtered and evaporated on rotary evaporator. The obtained crude product was purified using silica gel column chromatography with petroleum ether: ethy acetate (9:1, v/v) as an eluent to give the compound **4** as saffron solid.

Yield: 3.7 g (85 %)

Melting point: 188°C

IR (ATR, cm^{-1}): 1679 (C=O), 1243 (C-O-C). [**Figure S 5.20**]

^{1}H NMR (400 MHz, $CDCl_3$) δ ppm = 9.70 (s, 1 H), 7.47 (d, 1 H), 7.40 (d, 2 H), 7.33 - 7.26 (m, 3 H), 7.19 - 7.13 (m, 3 H), 7.01(dd, 1 H), 6.93 (d, 2H), 6.91 (dd, 2 H), 3.92 (s, 3 H), 3.83 (s, 3 H). [**Figure S 5.11**]

^{13}C NMR (100 MHz, $CDCl_3$) δ ppm =189.69, 159.63, 159.08, 149.28, 141.42, 136.28, 132.26, 131.90, 131.61, 130.79, 129.94, 127.41, 127.34, 125.09, 124.53, 119.68, 119.29, 116.63, 116.24, 114.89, 114.19, 55.55, 55.3.[**Figure S 5.12**]

HRMS: Calculated for $C_{27}H_{21}NO_3S$ 439.1242, found 439.1240

5.2.3.7) Synthesis of 7-(6-butoxynaphthalen-2-yl)-10-(4-methoxyphenyl)-10H-phenothiazine-3carbaldehyde (7)

Into a Schlenk tube equipped with a magnetic stirring bar were added 7-bromo-10-(4-methoxyphenyl)-10 H-phenothiazine-3-carbaldehyde (1 g, 2.4 mmol), 2-(6-butoxynaphthalen-2-

yl)-4,4,5,5-tetramethyl-1,3,2-dioxaborolane (0.950 g, 3 mmol), 2M aq. K_2CO_3 (3 mL), $Pd(PPh_3)_4$ (0.280 g) and tetrahydrofuran (15 mL) under argon flow and the reaction mixture was heated at 60 ^oC for 24 h. After completion of reaction, the reaction mixture was quenched by pouring into water and extracted with ethyl acetate (3× 50 mL). The ethyl acetate layer was washed with water (50 mL), brine solution (50 mL) and again with water (50 mL). The ethyl acetate layer was separated and dried over anhydrous sodium sulfate, filtered and evaporated on rotary evaporator. The crude product obtained was purified using silica gel column chromatography with petroleum ether: ethyl acetate (9:1, v/v) as an eluent to give title compound **7** as saffron solid.

Yield: 0.837 g (65 %)

Melting point: 153 °C

IR (ATR, cm^{-1}): 1689 (C=O), 1241(C-O-C) [**Figure S 5.21**]

^1H NMR (400 MHz, $CDCl_3$) δ ppm = 9.69 (s,1 H), 7.83 (d,1 H), 7.73 (d, 2 H), 7.58 - 7.53 (m, 1 H), 7.47 (d, 1 H), 7.33 - 7.25 (m, 4 H), 7.17 - 7.10 (m, 5 H), 6.21 (dd, 2 H), 4.08 (t, *J* = 6.5 Hz, 2 H), 3.92 (s, 3 H), 1.84 (dd, 2 H), 1.59 - 1.52(m, 2 H), 1.0 (t, 3H). [**Figure S 5.13**]

^{13}C NMR (100 MHz, $CDCl_3$) δ ppm = 189.69, 159.64, 157.24, 149.22, 141.72, 136.58, 134.28, 133.72, 132.22, 131.6, 130.83, 129.92, 129.48, 128.94, 127.41, 127.23, 125.55, 125.06, 124.92, 124.61, 119.7, 119.51, 119.4, 116.69, 116.25, 114.93, 106.26, 67.7, 55.55, 31.25, 19.27, 13.87. [**Figure S 5.14**]

HRMS: Calculated for $C_{34}H_{29}NO_3S$ 531.1868, found 531.1865

5.2.3..8) Synthesis of 2-((10-(4-methoxyphenyl)-10H-phenothiazin-3-yl) methylene) malononitrile (O-1)

Into a two necked round bottom flask equipped with a magnetic stirring bar were added 10-(4-methoxyphenyl)-10 H-phenothiazine-3-carbaldehyde (0.5 g, 1.5 mmol), malononitrile (0.148 g, 2.2 mmol) and chloroform (10 mL) under nitrogen flow. Two drops of piperidine were added into the reaction mixture and the reaction mixture was refluxed for 12 h. After completion of reaction, the reaction mixture was poured into water and extracted with dichloromethane (3 x 50 mL). The dichloromethane layer was separated and washed with water (50 mL), brine solution (50 mL) and again with water (50 mL). The dichloromethane solution was dried over anhydrous sodium sulphate, filtered, and solvent was removed on rotary evaporator. The crude product was

purified by column chromatography using petroleum ether: ethyl acetate (8:2, v/v) as an eluent to give the title compound (**O-1**) as a red solid.

Yield: 0.483 g, 87 %

Melting point: 199°C

IR (ATR, cm^{-1}): 2221 (CN) [**Figure 5.1**]

^{1}H NMR (500 MHz, $CDCl_3$) δ ppm = 7.43 (d, 1 H), 7.39-7.35 (m, 2 H), 7.25 (d, 2 H), 7.14 (d, 2 H), 6.96-6.91 (m, 1 H), 6.88 - 6.82 (m, 2 H), 6.16 - 6.12 (m, 2 H), 3.91 (s, 3 H). [**Figure 5.4**]

^{13}C NMR (100 MHz, $CDCl_3$) δ ppm = 159.9, 156.9, 149.6, 142.0, 131.6, 131.4, 131.3, 128.5, 127.3, 126.7, 125.2, 124.2, 120.5, 118.6, 116.8, 116.4, 115.3, 114.8, 113.6, 55.7. [**Figure 5.5**]

HRMS: calculated $[M+Na]^+$ for $C_{23}H_{16}N_3OSNa$= 404.0828; found 404.0824

5.2.3.9) Synthesis of 2-((7,10-bis(4-methoxyphenyl)-10H-phenothiazin-3-) methylene) malononitrile (O-2)

Into a two necked round bottom flask equipped with a magnetic stirring bar and a reflux condenser were added 7,10-bis(4-methoxyphenyl)-10 H-phenothiazine-3-carbaldehyde (0.5 g, 1.1 mmol), malononitrile (0.112 g, 1.7 mmol) and chloroform (10 mL). Two drops of piperidine were added into the reaction mixture and reaction mixture was refluxed for 12 h. After completion of reaction, the reaction mixture was poured into water and extracted using dichloromethane (3 x 50 mL). The dichloromethane solution was separated and washed with water (50 mL), brine solution (50 mL) and again with water. The dichloromethane layer was dried over anhydrous sodium sulfate, filtered and dichloromethane was removed on rotary evaporator. The crude product was purified by column chromatography using petroleum ether: ethyl acetate (8:2, v/v) as an eluent to obtain title compound (**O-2**) as a red solid.

Yield: 0.470 g, (85 %)

Melting point: 194°C

IR (ATR, cm^{-1}): 2217 (CN) [**Figure 5.2**]

^{1}H NMR (400 MHz, $CDCl_3$) δ ppm = 7.45 (s, 1 H), 7.42 - 7.36 (m, 4 H), 7.29 (d,2 H), 7.18 - 7.13 (m, 3 H), 7.03 (d, 1 H), 6.95 (d, 2 H), 6.16 (dd, 2 H), 3.93(s, 3 H), 3.84 (s, 3 H). [**Figure 5.6**]

^{13}C NMR (100 MHz, $CDCl_3$) δ ppm = 159.9, 159.2, 156.8, 149.3, 140.5, 136.9, 131.6, 131.5, 131.3, 131.2,128.5, 127.4, 125.2, 125.1, 124.5, 120.1, 119.0, 117.1, 116.4, 115.2, 114.8, 114.2, 113.6, 55.6, 55.3 [**Figure 5.7**]

HRMS: calculated $[M+Na]^+$ for $C_{30}H_{21}N_3O_2SNa$= 510.1247; found 510.1244

5.2.3.10) Synthesis of 2-((7-(6-butoxynaphthalen-2-yl)-10-(4-methoxyphenyl)-10H-phenothiazin-3-yl)methylene) malononitrile (O-3)

Into a two necked round bottom flask equipped with a magnetic stirring bar and a reflux condenser were added 7-(6-butoxynaphthalen-2-yl)-10-(4-methoxyphenyl)-10H-phenothiazine-3-carbaldehyde (0.5g, 0.94 mmol), malononitrile (93 mg, 1.4 mmol) and chloroform (10 mL). Two drops of piperidine were added into the reaction mixture and reaction mixture was refluxed for 12 h. After completion of reaction, the mixture was poured into water and extracted with dichloromethane (3 x 50 mL). The dichloromethane layer was separated and washed with water, brine solution and again with water. The dichloromethane solution was dried over anhydrous sodium sulfate, filtered and evaporated on rotary evaporator to afford a crude product which was purified by column chromatography using petroleum ether: ethyl acetate (8:2, v/v) to obtain **O-3** as a pale violet solid.

Yield: 0.455 g (81 %)

Melting point: 163 °C

IR (ATR, cm^{-1}): 2210 (CN, nitrile stretching) [**Figure 5.3**]

^{1}H NMR (400 MHz, $CDCl_3$) δ ppm = 7.85 (s, 1 H), 7.77 (dd, *J* = 2.1, 8.5 Hz, 2 H), 7.58 (dd, *J* = 1.5, 8.5 Hz, 1H), 7.48 (d, *J* = 2.1 Hz, 1 H), 7.41 (d, 2 H), 7.32 - 7.28 (m, 3 H), 7.21 - 7.17 (m, 4 H),7.15 (d, *J* = 2.1 Hz, 1 H), 6.25 (d, *J* = 8.5 Hz, 1 H), 6.19 (d, *J* = 8.9 Hz, 1 H), 4.11 (t, *J* = 6.6 Hz,2 H), 3.95 (s, 3 H), 1.90 - 1.84 (m, 2 H), 1.59 - 1.55(m, 2 H), 1.04 (t, *J* = 7.3 Hz, 3 H). [**Figure 5.8**]

^{13}C NMR (100 MHz, $CDCl_3$) δ ppm = 160.0, 157.4, 156.8, 149.3, 140.8, 137.3, 134.1, 133.9, 131.6, 131.3,129.5, 129.6, 129.0, 128.6, 127.3, 125.8, 125.2, 125.0, 125.0, 124.8, 120.2, 119.7, 119.1, 117.2,116.5, 115.3, 114.8, 113.6, 106.3, 67.8, 55.7, 31.3, 19.3, 13.9. [**Figure 5.9**]

HRMS: calculated $[M+Na]^+$ for $C_{37}H_{29}N_3O_2SNa$ =602.1873; found 602.1871

5.3) Results and discussion

5.3.1) Synthesis and characterization

The synthesis of 2-((10-(4-methoxyphenyl)-10H-phenothiazin-3-yl) methylene) malononitrile (**O-1**), 2-((7,10-bis(4-methoxyphenyl)-10H-phenothiazin-3-) methylene) malononitrile (**O-2**) and 2-((7-(6-butoxynaphthalen-2-yl)-10-(4-methoxyphenyl)-10H-phenothiazin-3-yl)methylene) malononitrile (**O-3**) is outlined in **Scheme 5.1**. 10-(4-Methoxyphenyl)-10H-phenothiazine (**1**) was prepared *via* Ullmann-coupling of 4-iodoanisole with commercially available phenothiazine. Vilsmeier-Haack formylation[59] reaction on (**1**) in 1,2-dichloroethane as solvent afforded monoformyl derivative of phenothiazine (**2**). The formyl derivative (**2**) on bromination using N-bromosuccinimide gave the corresponding bromo derivative (**3**). In another reaction, 2-bromo-6-butoxynaphthalene (**4**) was synthesized by O-alkylation of 6-bromo-2-naphthol using 1-bromobutane which was converted into boronic ester derivative *viz* 2-(6-butoxynaphthalen-2-yl)-4, 4,5,5-tetramethyl-1,3,2-dioxaborolane (**5**) by Miyaura borylation reaction.[60] Compound **3** on Suzuki coupling[61] using 4-methoxy phenyl bronic acid and boronic ester derivative **5** in the presence of tetrakis triphenylphosphine palladium catalyst afforded the corresponding derivatives *viz* 7, 10-bis (4-methoxyphenyl)-10 H-phenothiazine-3-carbaldehyde **(6)** and 7-(6-butoxynaphthalen-2-yl)-10-(4-methoxyphenyl)-10H-phenothiazine-3carbaldehyde **(7)**, respectively.

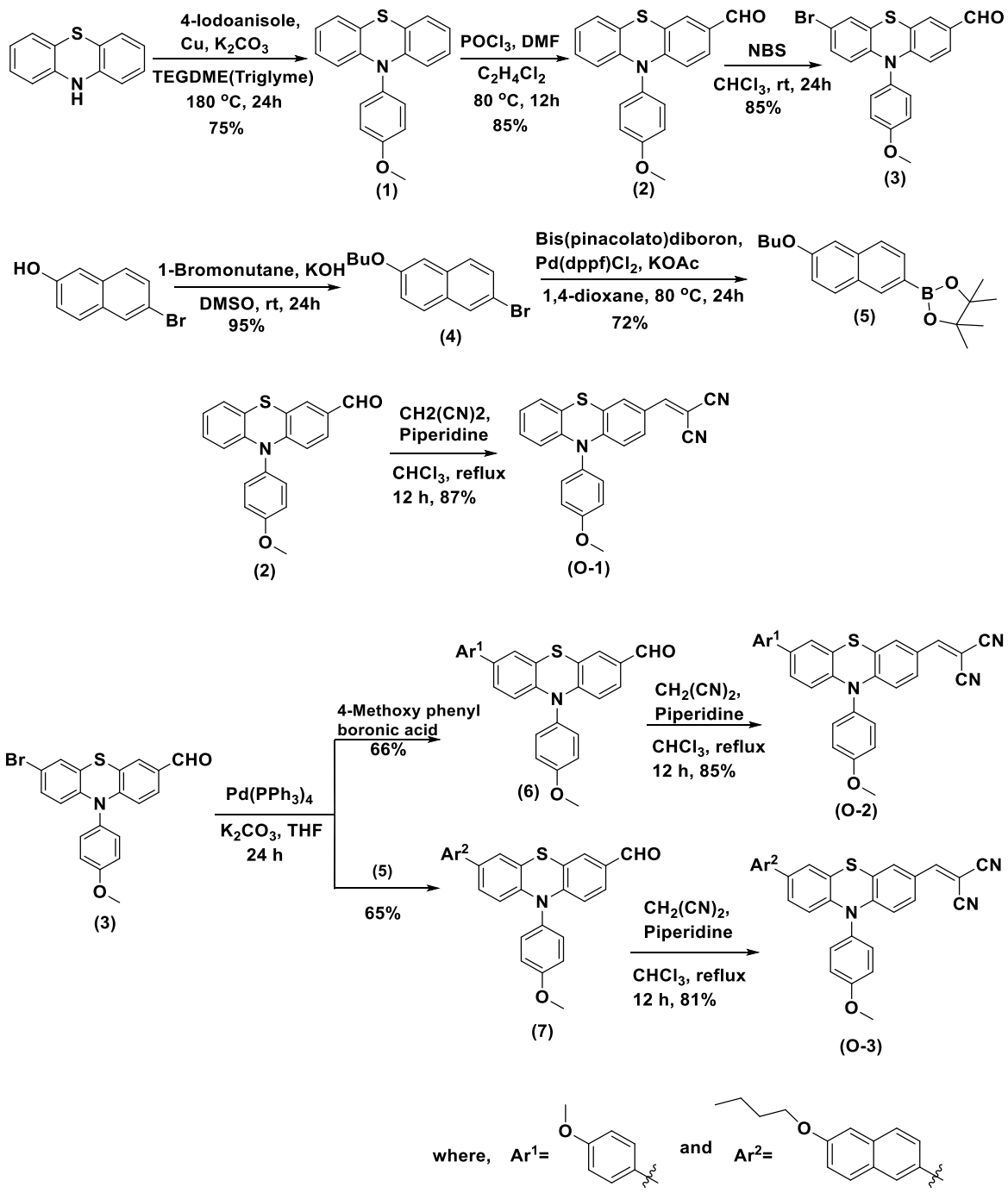

Scheme 5.1: Synthesis of phenothiazine based small organic molecules **O-1, O-2 and O-3**

The compounds **2, 6** and **7** on Knoevenagel condensation[62] using malononitile in the presence of piperidine yielded the corresponding cyanovinylene derivatives of phenothiazine compounds i.e. 2-((10-(4-methoxyphenyl)-10H-phenothiazin-3-yl) methylene) malononitrile (**O-1),** 2-((7,10-bis(4-methoxyphenyl)-10H-phenothiazin-3-) methylene) malononitrile (**O-2)** and 2-((7-(6-

butoxynaphthalen-2-yl)-10-(4-methoxyphenyl)-10H-phenothiazin-3-yl)methylene) malononitrile (**O-3**), respectively. **O-1**, **O-2** and **O-3** were soluble in common organic solvents such as chloroform, dichloromethane, tetrahydrofuran, acetonitrile, etc. This allowed purification of these compounds by column chromatography and solution processing while device fabrication.

IR spectrum of **O-1** is shown in **Figure 5.1**. The absorption band observed at 2221 cm^{-1} is attributed to the characteristic stretching of nitrile (CN) group which shows conversion of formyl group into cyanovinylene group. The bands observed at 1220 cm^{-1} and 1303 cm^{-1} are due to the stretching of C-O-C (ether) and C-N (amine) bonds, respectively.

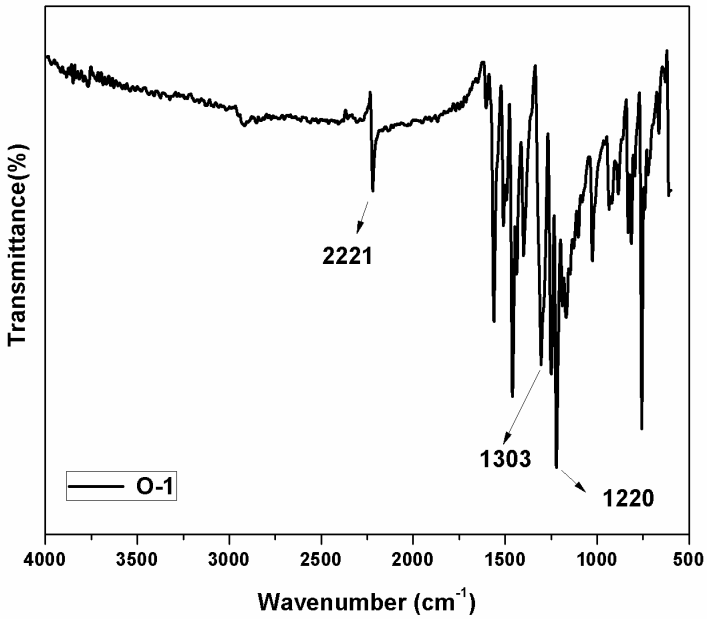

Figure 5.1: IR spectrum of 2-((10-(4-methoxyphenyl)-10H-phenothiazin-3-yl) methylene) malononitrile (**O-1**)

IR spectrum of **O-2** is shown in **Figure 5.2**.The absorption band exhibited at 2217 cm^{-1} is attributed to the stretching of nitrile (CN) group. The bands appearing at 1331 cm^{-1} and 1226 cm^{-1} are due to stretching of C-N (amine) and C-O-C (ether) bonds, respectively. IR spectrum of **O-3** is shown in **Figure 5.3**.The absorption band at 2210 cm^{-1} is attributed to stretching of nitrile group. The bands at 1221 cm^{-1} and 1296 cm^{-1} are attributed to the C-O-C (ether) and C-N (amine) linkages, respectively.

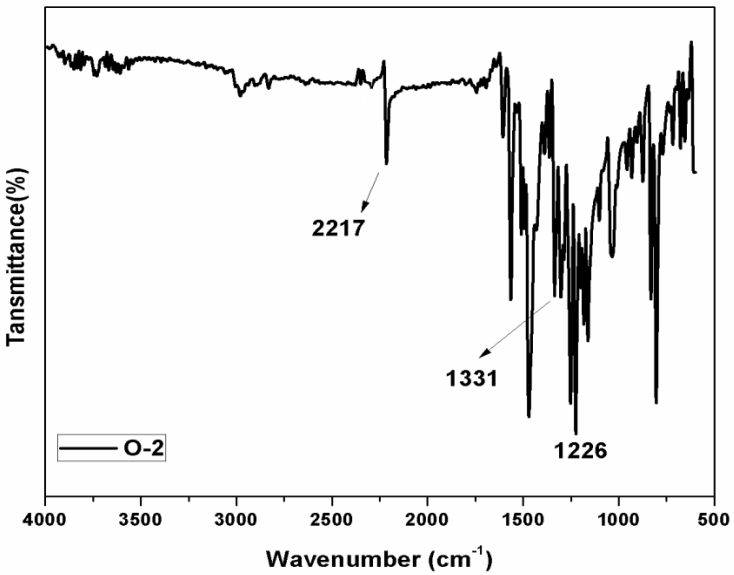

Figure 5.2: IR spectrum of 2-((7,10-bis(4-methoxyphenyl)-10H-phenothiazin-3-) methylene) malononitrile (**O-2**).

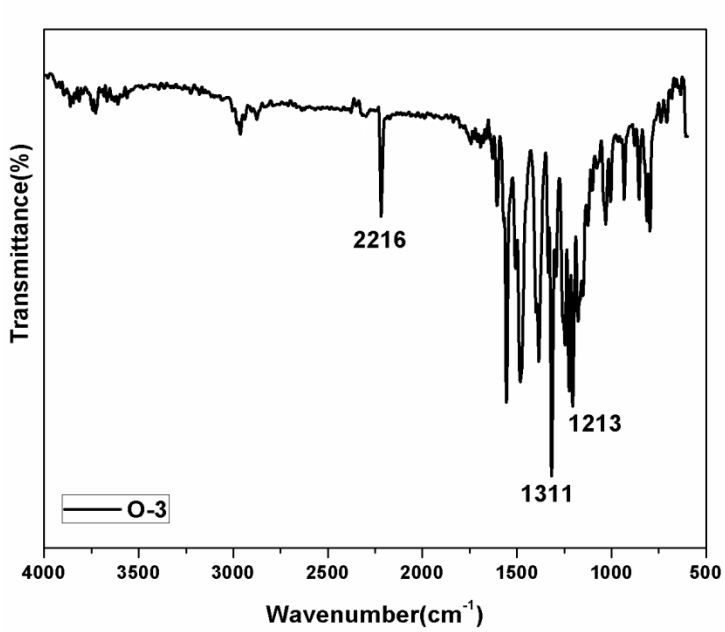

Figure 5.3: IR spectrum of 2-((7-(6-butoxynaphthalen-2-yl)-10-(4-methoxyphenyl)-10H-phenothiazin-3-yl)methylene) malononitrile (**O-3**)

^{1}H NMR spectrum of 2-((10-(4-methoxyphenyl)-10H-phenothiazin-3-yl) methylene) malononitrile (**O-1)** in $CDCl_3$ is shown in **Figure 5.4**. The proton 'a' of methoxy substituent exhibited a singlet at δ 3.91 ppm. Aromatic proton 'b' *ortho* to methoxy group exhibited a doublet at δ 7.15 ppm, whereas proton 'c' *meta* to methoxy group exhibited a doublet at δ 7.26

ppm. A signal at δ 7.26 ppm was exhibited by vinylic proton 'k'. The protons 'f' and 'g' of phenothiazine ring exhibited signals at δ7.43 ppm and δ 6.86 ppm. The protons 'd' and 'j' were observed in the range δ 6.16- δ 6.13 ppm. The proton 'e' exhibited a signal at δ7.37 whereas protons 'i' and 'h' were observed in the range δ 6.86 - δ6.84 ppm.

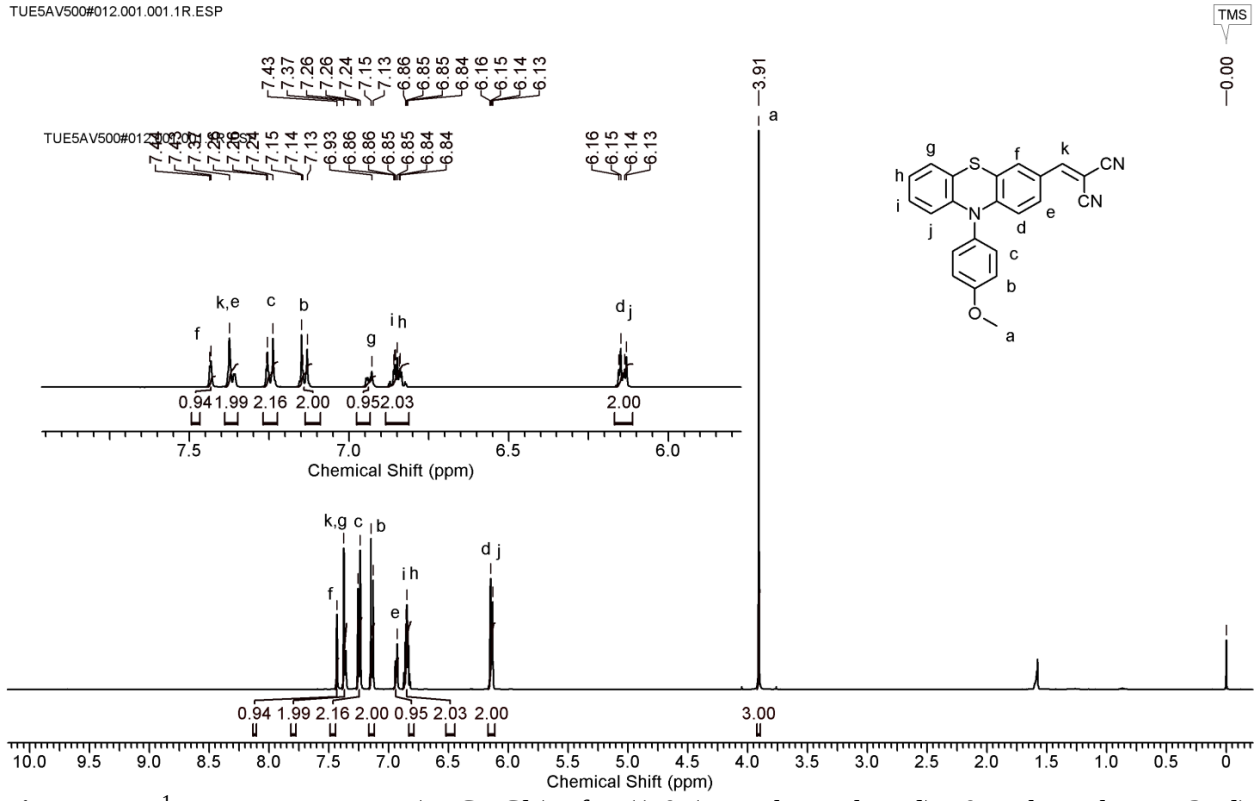

Figure 5.4: ^{1}H NMR spectrum (in $CDCl_3$) of 2-((10-(4-methoxyphenyl)-10H-phenothiazin-3-yl) methylene) malononitrile (**O-1**)

^{13}C NMR spectrum of 2-((10-(4-methoxyphenyl)-10H-phenothiazin-3-yl) methylene) malononitrile (**O-1)** in $CDCl_3$ is shown in **Figure 5.5**. The carbon atom 'a' of methoxy group exhibited a signal at δ 55.60 ppm. The carbon atoms 'b' and 'e' of aromatic ring exhibited signals in the downfield region at δ 159.86 ppm and δ 141.93, respectively due to inductive effect of oxygen. The carbon atoms 'c' and 'd' of aromatic ring exhibited signals at δ116.38 and δ131.30, respectively. A signal at δ 114.37 ppm is attributed to the carbon atom 'v' of nitrile group. Also the carbon atoms 't' and 'u' showed peaks at δ156.88 ppm and δ76.87 ppm, respectively. Carbon atoms of phenothiazine ring exhibited signals in the range δ131.58 – 115.23 ppm.

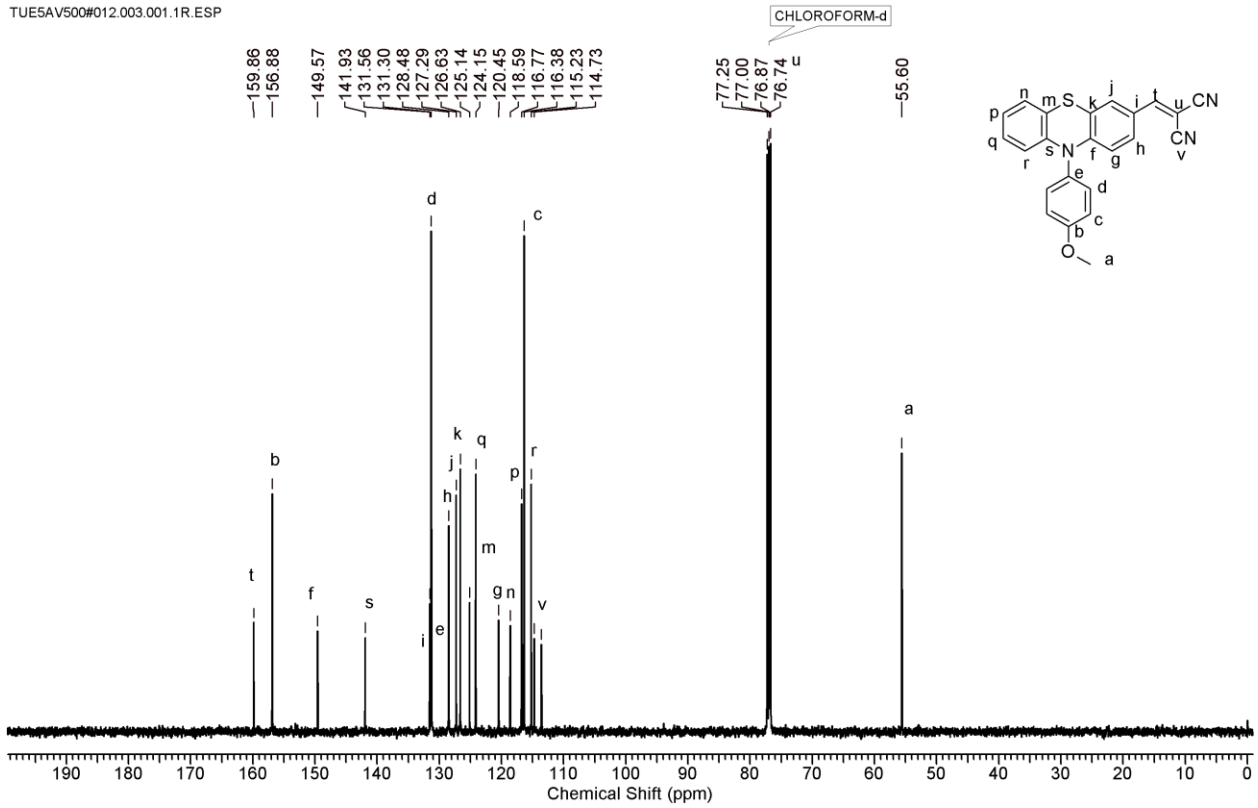

Figure 5.5: ^{13}C NMR spectrum (in $CDCl_3$) of 2-((10-(4-methoxyphenyl)-10H-phenothiazin-3-yl) methylene) malononitrile (**O-1**).

^{1}H NMR spectrum of 2-((7,10-bis(4-methoxyphenyl)-10H-phenothiazin-3-) methylene) malononitrile (**O-2**) is shown in **Figure 5.6**. The protons 'a' and 'n' of methoxy group exhibited signals at δ 3.93 ppm and δ3.84 ppm, respectively. The aromatic protons 'b' and 'm' *ortho* to methoxy substituent exhibited doublets at δ 7.18 ppm and δ 6.96 ppm, respectively. Whereas, the protons 'c' and 'k' *meta* to methoxy group exhibited signals at δ7.29 ppm and δ7.38 ppm, respectively. The vinylic proton 'j' was observed at δ7.41 ppm while the protons of phenothiazine ring were observed in the range δ7.45- δ6.14 ppm.

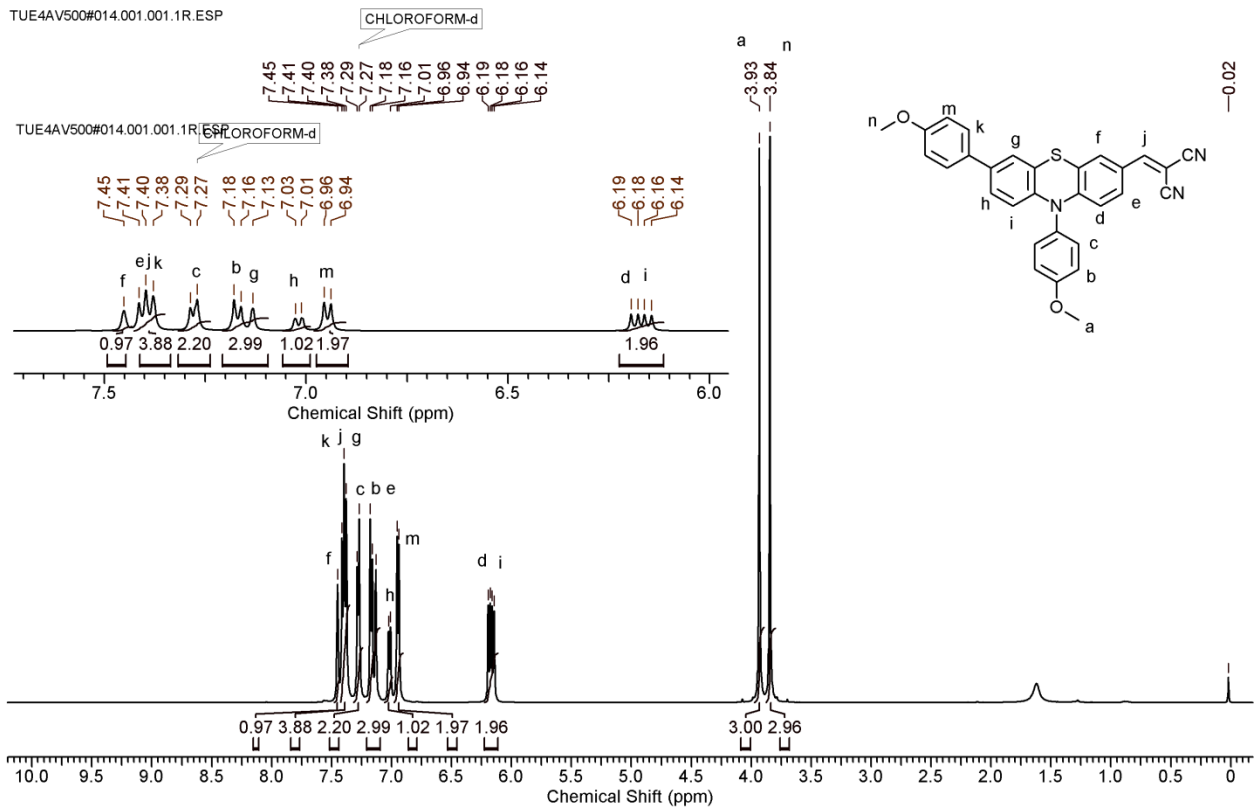

Figure 5.6: ^{1}H NMR spectrum (in $CDCl_3$) of 2-((7,10-bis(4-methoxyphenyl)-10H-phenothiazin-3-) methylene) malononitrile (**O-2**)

^{13}C NMR spectrum of 2-((7, 10-bis (4-methoxyphenyl)-10H-phenothiazin-3-) methylene) malononitrile (**O-2**) in $CDCl_3$ is shown in **Figure 5.7**. The carbon atoms 'a' and 'y' showed signals at δ 55.67 ppm and 55.38 ppm, respectively. Due to inductive effect of oxygen, the carbon atoms 'b' and 'x' of aromatic ring exhibited signals in the downfield region at δ 159.94 ppm and δ159.28 ppm, respectively. Carbon atoms denoted by 'c' and 'w' *ortho* to methoxy group exhibited signals at δ 114.31 ppm and δ116.48 ppm, whereas the carbon atoms 'd' and 'v' which are *meta* to the methoxy group exhibited peaks at δ131.28 ppm and 127.42 ppm, respectively. In case of cyanovinylene group, the carbon atom 'a_1' exhibited a peak at δ114.31 ppm while the carbon atoms 't' and 'z' showed peaks at δ156.86 ppm and 76.18 ppm. The carbon atoms of phenothiazine ring exhibited signals in the range δ 149.32- 115.25 ppm.

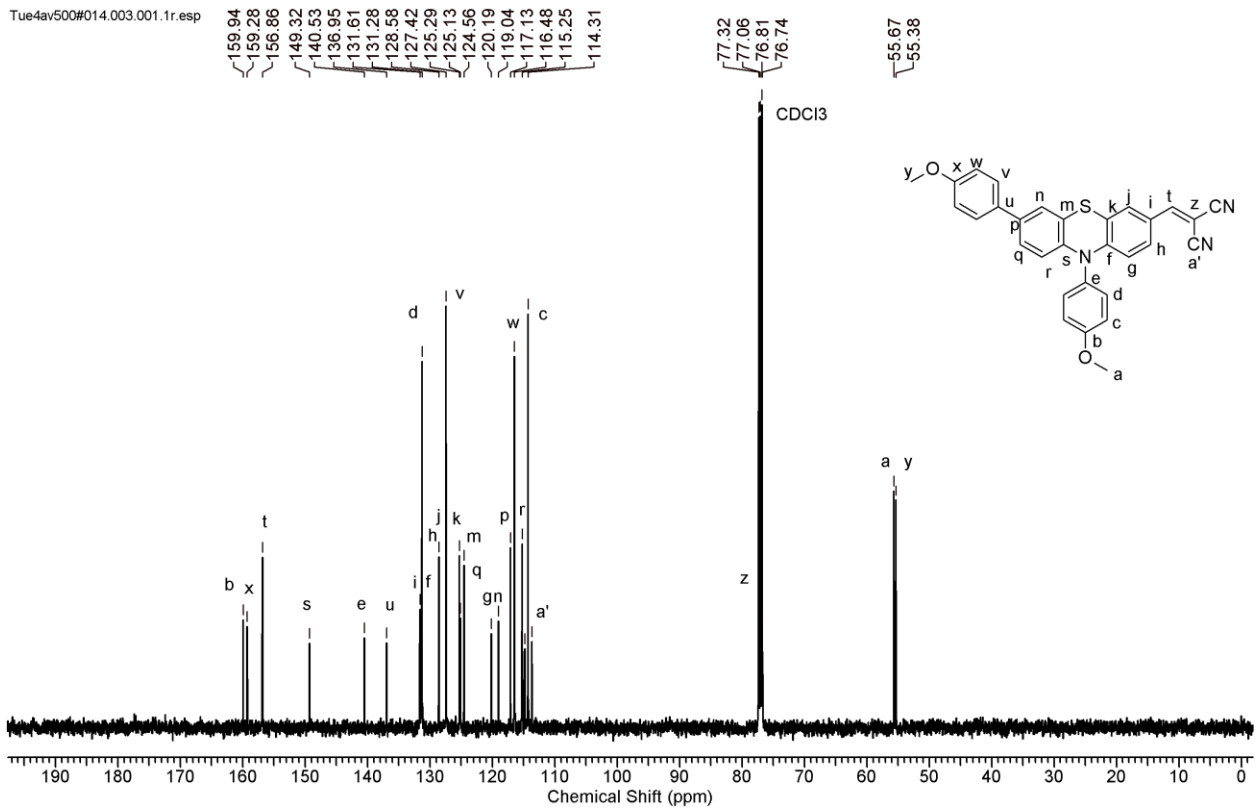

Figure 5.7: ^{13}C NMR spectrum (in $CDCl_3$) of 2-((7,10-bis(4-methoxyphenyl)-10H-phenothiazin-3-) methylene) malononitrile (**O-2**)

^{1}H NMR spectrum of 2-((7-(6-butoxynaphthalen-2-yl)-10-(4-methoxyphenyl)-10H-phenothiazin-3-yl)methylene) malononitrile (**O-3**) is shown in **Figure 5.8**. The proton 'a' of methoxy substituent showed a singlet at δ 3.95 ppm. The protons 'p' of methylene group attached to oxygen atom exhibited a triplet at δ 4.11 ppm while the protons 'k' of methyl group exhibited a triplet at δ 1.04 ppm. The methylene protons 'm' and 'n' exhibited peaks at δ1.58 ppm and δ1.87 ppm, respectively. The protons 'b' and 'c' showed signals at δ 7.18 ppm and δ 7.30 ppm, respectively. Two protons 'q' and 'v' of naphthalene unit *ortho* to butoxy substituent were observed at δ 7.20 ppm. The rest of the protons on naphthalene moiety were observed in the downfield range δ 7.85- δ7.57 ppm as singlet and doublet of doublet (dd) peaks. The proton 'j' was observed downfield at δ7.40 ppm while the protons on phenothiazine ring exhibited signals in the range δ 7.48- 7.15 ppm.

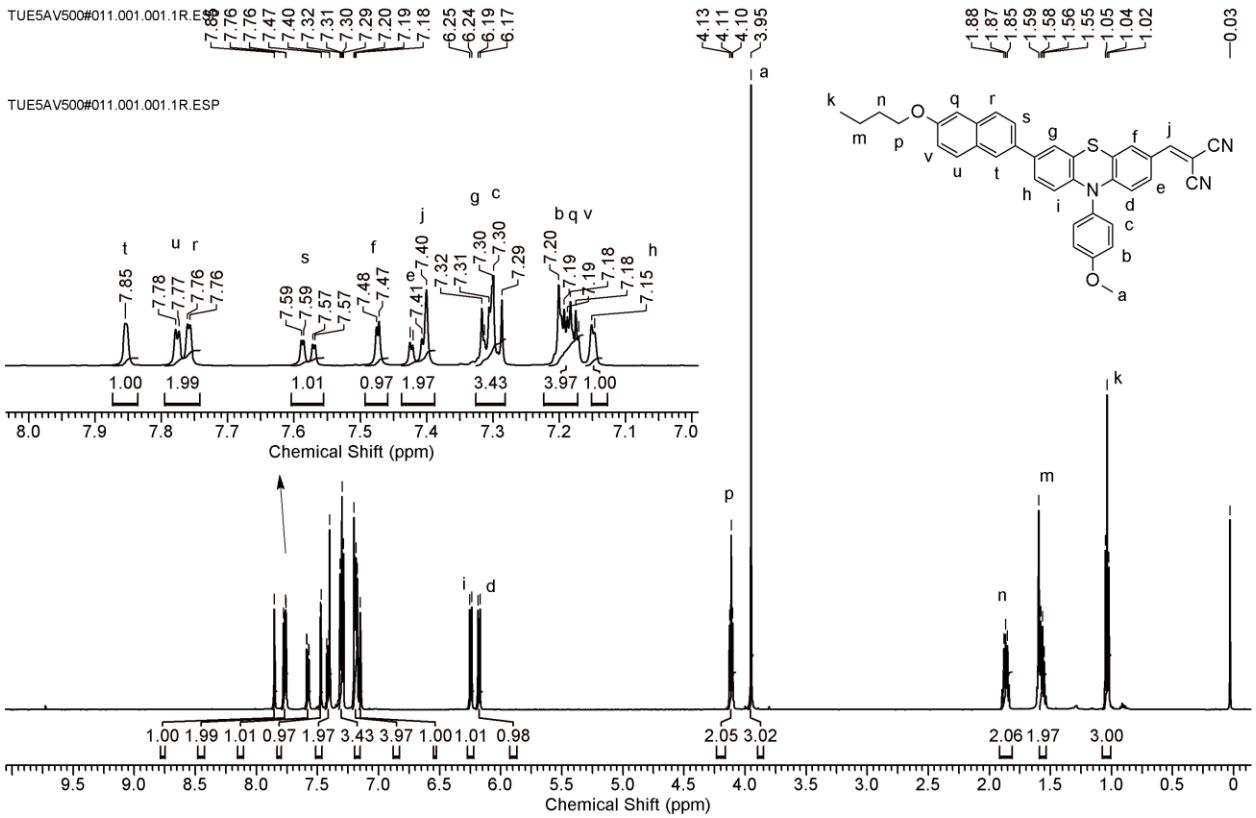

Figure 5.8: ^{1}H NMR spectrum (in $CDCl_3$) of 2-((7-(6-butoxynaphthalen-2-yl)-10-(4-methoxyphenyl)-10H-phenothiazin-3-yl)methylene) malononitrile (**O-3**) .

^{13}C NMR spectrum of 2-((7-(6-butoxynaphthalen-2-yl)-10-(4-methoxyphenyl)-10H-phenothiazin-3-yl)methylene) malononitrile (**O-3**) in $CDCl_3$ is shown in **Figure 5.9** The carbon atom '1' of methoxy group showed a signal at δ 55.38 ppm while the carbon atom '21' of methylene group exhibited a peak at δ 67.50 ppm. The carbon atoms labeled as '20', '19 and 18' exhibited the signals in the range δ31.01- δ13.63 ppm. In oxyphenylene unit, the carbon '2' and '5' exhibited signals at δ159.68 ppm and δ 140.57 ppm, respectively due to inductive effect of oxygen atom and nitrogen atom. The carbon '3' showed a peak at δ116.21 ppm while the carbon '4' on oxyphenylene unit exhibited a signal at δ 131.01 ppm. The carbon atom '34' of nitrile group showed a signal at δ114.51 ppm while the carbon atoms '33' and '32' exhibited peaks at δ 76.75 ppm and δ156.58 ppm, respectively. The carbon atoms of naphthalene and phenothiazine ring exhibited signals in the range δ 157.13- δ 106.06 ppm.

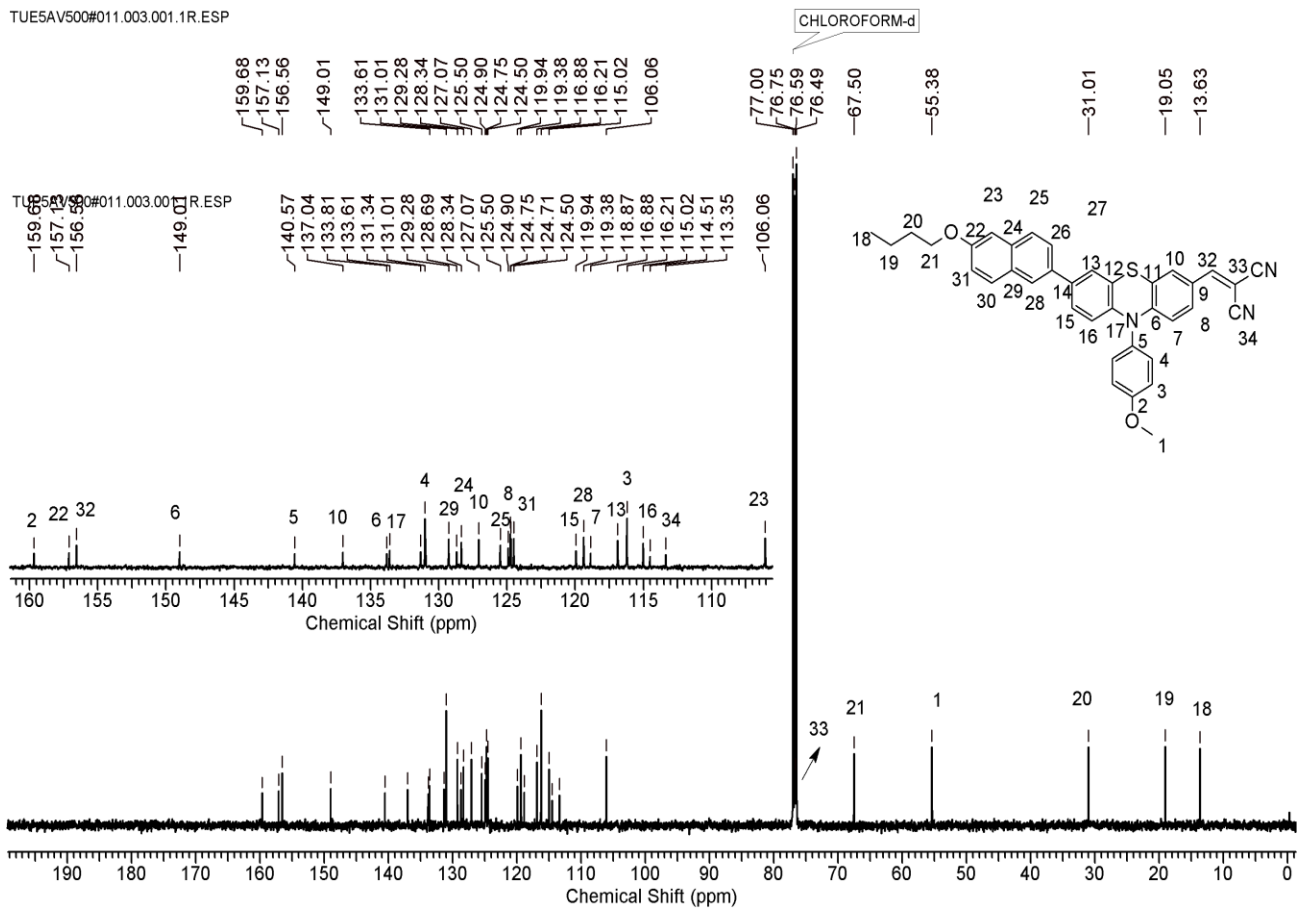

Figure 5.9: ^{13}C NMR spectrum (in $CDCl_3$) of 2-((7-(6-butoxynaphthalen-2-yl)-10-(4-methoxyphenyl)-10H-phenothiazin-3-yl)methylene) malononitrile (**O-3**).

The structure of **O-1**, **O-2** and **O-3** were further confirmed by **HRMS** ananlysis. In **Figure 5.10** HR-MS signal was observed at 404.0824 for $[M+Na]^+$ of **O-1** (calculated $[M+Na]^+$ for $C_{23}H_{16}N_3OSNa$= 404.0828). As observed in **Figure 5.11**, HR-MS signal at 510.1244 was observed for $[M+Na]^+$ of **O-2** molecule (calculated $[M+Na]^+$ for $C_{30}H_{21}\ N_3O_2SNa$= 510.1247). Also, in **Figure 5.12,** HR-MS signal for $[M+Na]^+$ of O-3 molecule was observed at 602.1871 (calculated $[M+Na]^+$ for $C_{37}H_{29}\ N_3O_2SNa$ =602.1873)

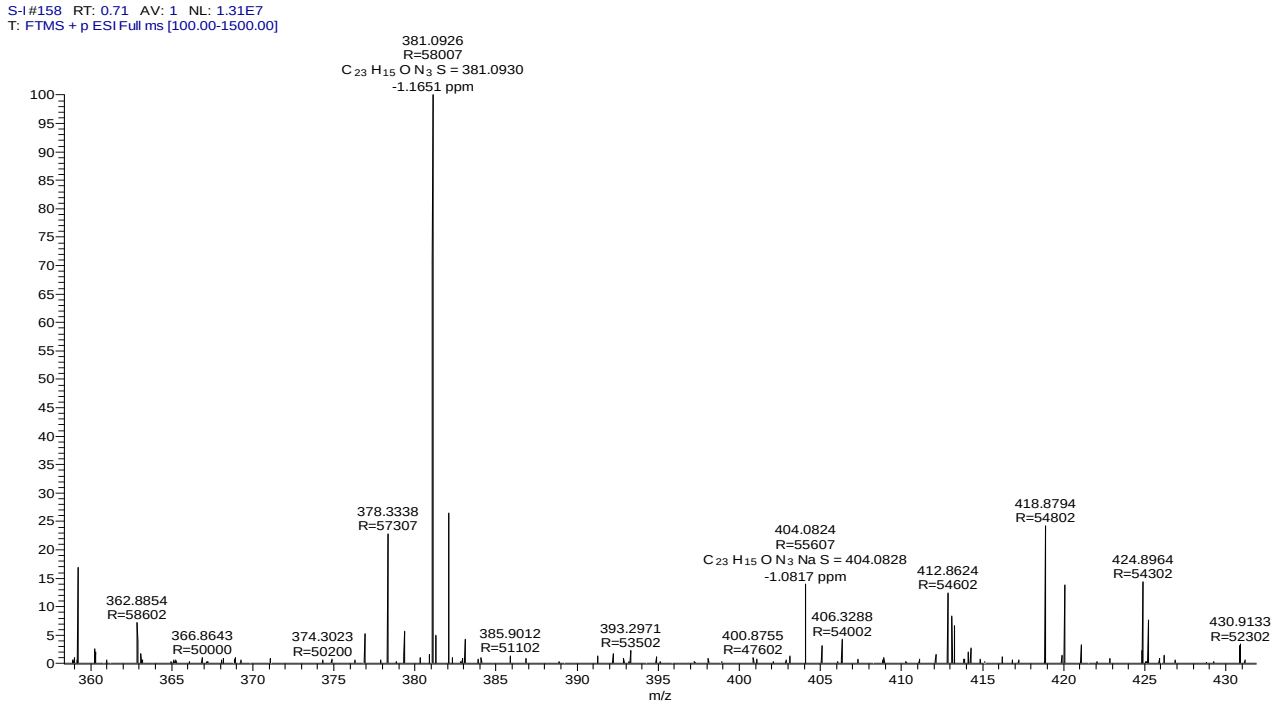

Figure 5.10: HRMS of 2-((10-(4-methoxyphenyl)-10H-phenothiazin-3-yl) methylene) malononitrile **(O-1)**

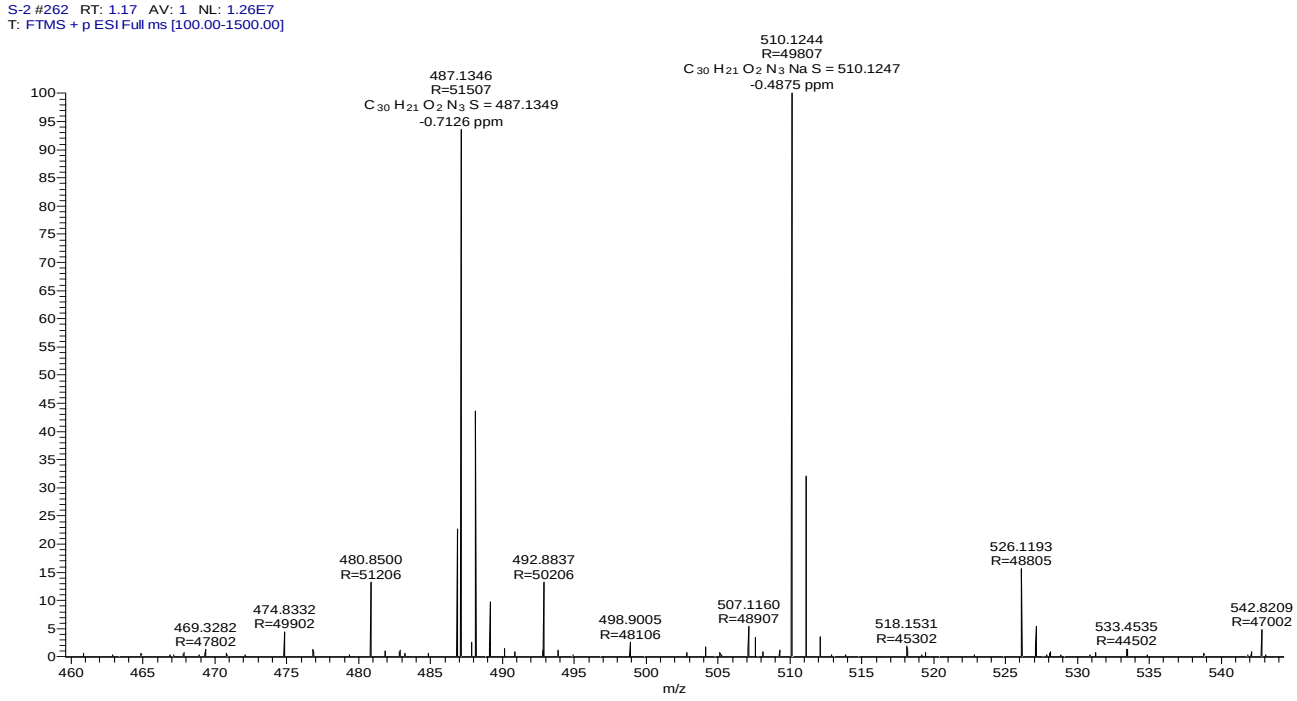

Figure 5.11: HRMS of 2-((7, 10-bis (4-methoxyphenyl)-10H-phenothiazin-3-) methylene) malononitrile (**O-2**)

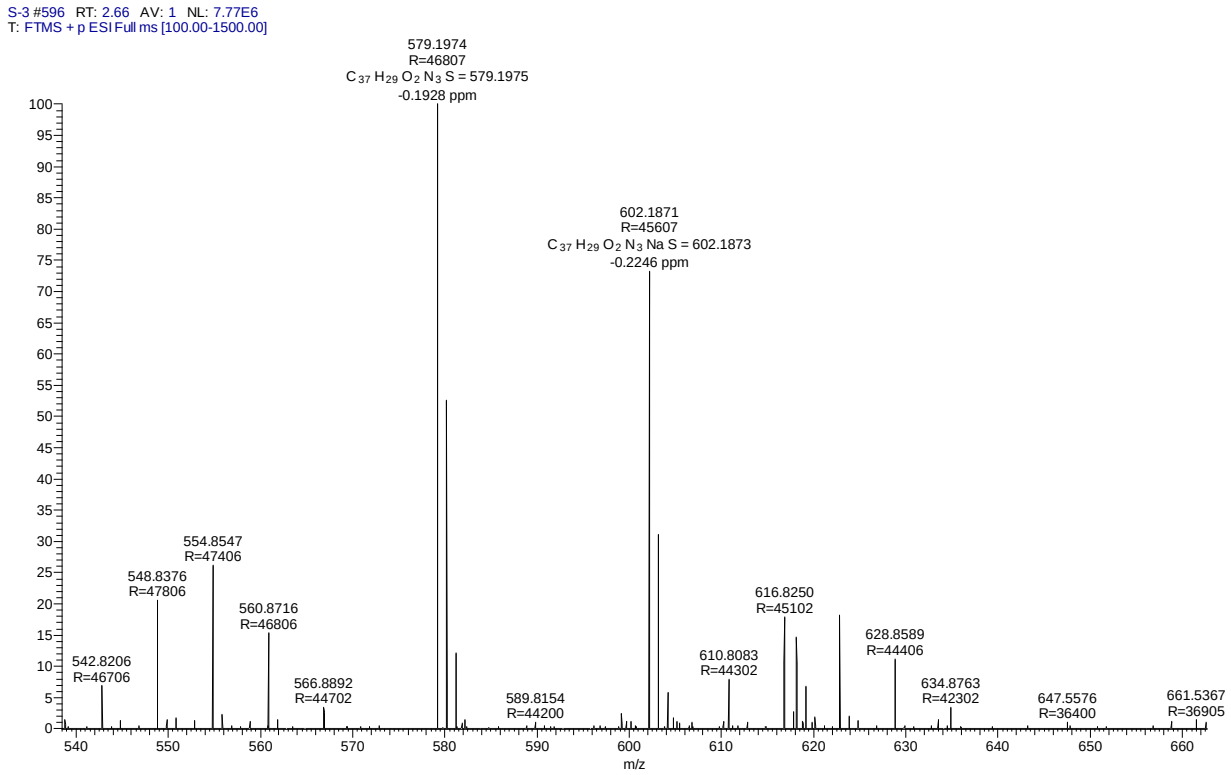

Figure 5.12: HRMS of 2-((7-(6-butoxynaphthalen-2-yl)-10-(4-methoxyphenyl)-10H-phenothiazin-3-yl)methylene) malononitrile (**O-3**)

The thermal properties of **O-1**, **O-2**, and **O-3** were investigated using DSC and TGA. Interestingly, given its lowest molecular weight in the series, DSC data in **Figure 5.13 (a)** showed a higher melting point (T_m) for **O-1** (199 °C) compared to **O-2** (194 °C) and **O-3** (163 °C). This can be attributed to its molecular packing and tendency towards crystallization, as detailed in subsequent section. In case of **O-3**, large drop in the melting point was observed as compared to **O-2**, probably due to the presence of the butoxy chain. **O-1**, **O-2** and **O-3** exhibited 5% weight loss at 302 ^oC, 386 ^oC and 404 ^oC, respectively as observed in **Figure 5.13 (b)** with an increasing trend with increasing molecular weight, i.e. **O-1<O-2<O-3**. The results of the thermal characterization are summarized in **Table 5.1** Thermal suitability of **O-1**, **O-2** and **O-3** is suitable for organic electronic device fabrication.[63]

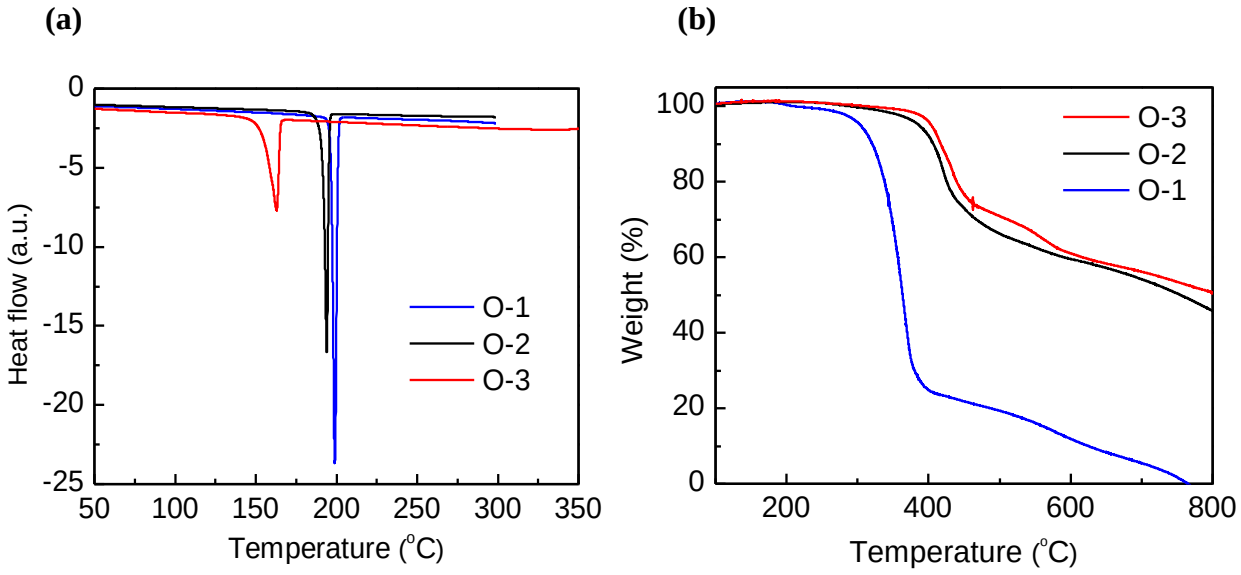

Figure 5.13: (**a**) DSC curves for **O-1**, **O-2** and **O-3**; (**b**) TG curves for **O-1**, **O-2** and **O-3**.

Table 5.1: Thermal properties of **O-1, O-2** and **O-3** by TGA and DSC

Compound	**T_d (in °C) for 5% weight loss (TGA)**	**Melting point in °C (by DSC)**
O-1	302	199
O-2	386	194
O-3	404	163

5.3.2) Optoelectronic studies

The UV-vis absorption spectra of **O-1**, **O-2**, and **O-3** in chloroform solution (concentration 10^{-5} M), together with the absorption spectra of thin films normalized at the Soret-transition (S0-S2) absorption maximum, are shown in **Figure 5.14** and data is summarized in **Table 5.2**. The absorption spectra of **O-1**, **O-2** and **O-3** showed two distinct bands: one at 320–330 nm and another at 490–510 nm. The former corresponds to π-π* electronic transition of the chromophores (Soret band).

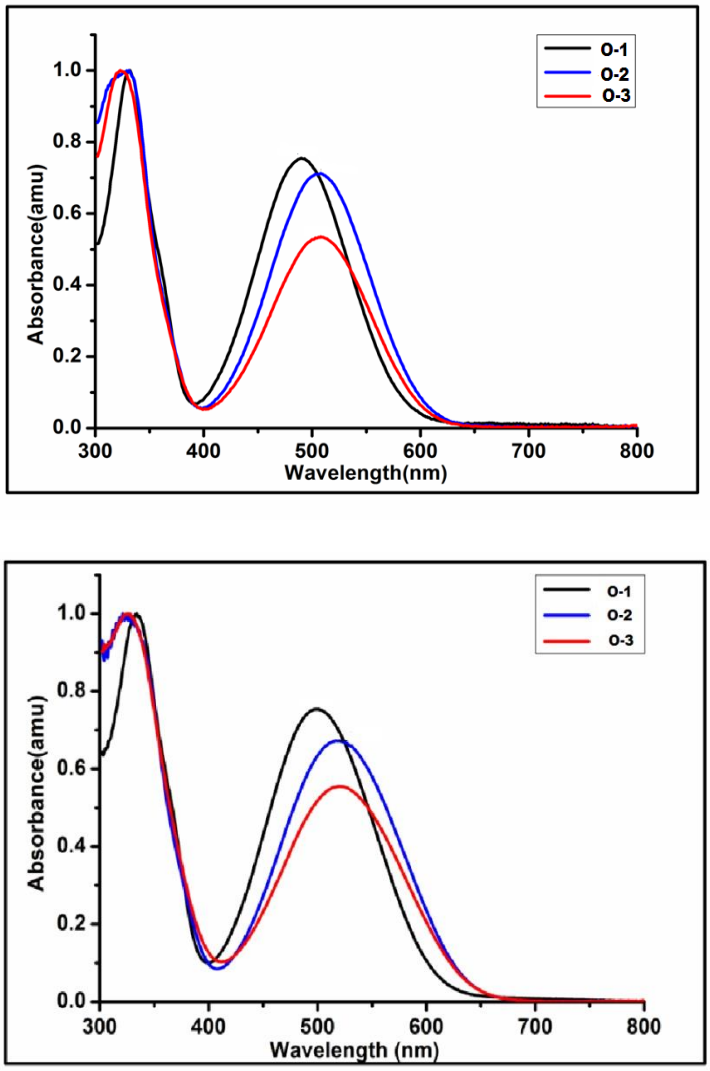

Figure 5.14: UV-vis absorption spectra of **O-1**, **O-2** and **O-3** in chloroform (top) and in thin film (bottom).

The latter is attributed to the intra- molecular charge transfer (ICT) from the donor to the acceptor moieties (Q band). As can be seen from **Fig. 5.14**, the Soret and Q bands are comparable, with slightly higher intensity for the Soret bands. Furthermore, in case of compounds **O-2** and **O-3**, the absorption maxima were separated by just 2 nm, while **O-1** absorption peaks were blue-shifted by 12–13 nm. The red-shift of the absorption maxima of **O-2** and **O-3** with respect to **O-1** was attributed to their extended conjugation. The absorption spectra of the films spin-coated onto glass substrates were bathocromically-shifted by 10–12 nm as

compared to the spectra measured in solution, likely due to chromophore-chromophore intermolecular interactions.[64]

Table 5.2: Optical properties of **O-1, O-2** and **O-3**

Compound	**λ_{max} (nm) (in $CHCl_3$)**	**λ_{max} (nm) (in thin film)**	**E_g^{opt} (eV)**
O-1	330,490	333,500	2.06
O-2	331,507	324,518	2.02
O-3	331, 509	325,521	2.0

In the experiment to investigate the hole mobility characteristics of phenothiazine compounds by impedance spectroscopy, thin films of **O-1, O-2** and **O-3** were deposited by spin coating using chlorobenzene as the solvent. Differently from **O-2** and **O-3**, the optical properties of **O-1** films underwent a clear and spontaneous variation even at room temperature, leading to a change of color observed by the naked eye. Moreover, the spectral variation of **O-1** films was greatly accelerated by the thermal treatment applied to remove the excess solvent. In **Figure 5.15**, the absorption spectrum of a freshly deposited **O-1** film is compared with that obtained after thermal annealing at 80 °C for 30 min (in an Ar-filled glove-box) and with that of a film stored at ambient temperature for around 10 h. In the latter two cases, the spectra are similar and broader compared to the spectrum of the freshly deposited **O-1** film, with an enhanced absorption toward lower energies. The spontaneous change in the spectral properties of **O-1** films at room temperature and upon thermal annealing indicated enhanced intermolecular electronic interactions, possibly due to development of a more ordered arrangement of **O-1** molecules in the solid state. The described behaviour was not observed for **O-2** and **O-3** films, which preserved to a large extent the original spectral features upon thermal treatment at 110°C for 30 min. (**Fig. 5.15 (a) and 5.15 (c))**.

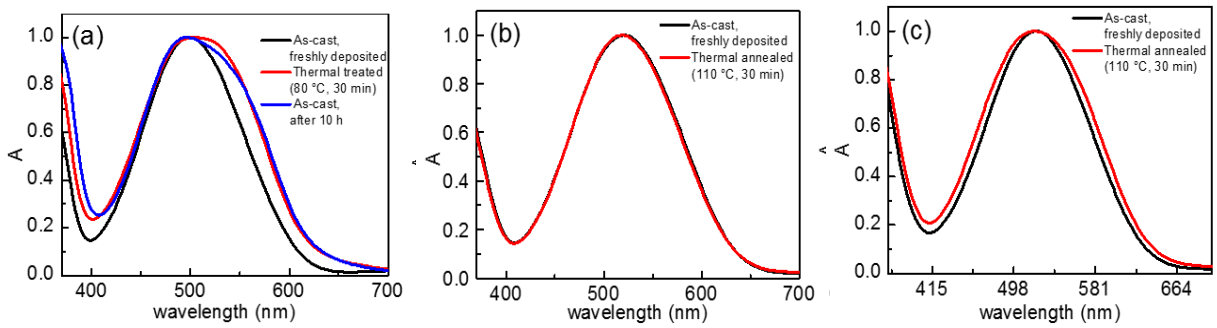

Figure 5.15: Normalised absorption spectra of **O-1** (**a**), **O-2** (**b**) and **O-3** (**c**) films, spin-coated from chlorobenzene solutions. Spectra of as-cast freshly deposited films, after 10 h at room temperature and thermally annealed films are shown.It should be noted that a lower temperature (80 °C), was applied for the thermal annealing of **O-1** films. That choice was motivated by the deterioration of **O-1** film compactness (appearance of pin-holes and cracks) upon heating above 80 °C, making them undesirable in the preparation of sandwich-type devices.

5.3.3) Electrochemical studies

The electrochemical properties of **O-1**, **O-2**, and **O-3** were determined by differential pulse voltammetry (DPV) in dichloromethane solution. The DPV was performed by employing a potentiostat and a three-electrode cell configuration. Dry tetrabutyl ammonium tetrafluoroborate in dichloromethane (0.1 M) was the supporting electrolyte, glass platinum electrode as the working electrode, Pt wire as the counter-electrode and Ag/AgCl wire as the pseudo-reference electrode. Ferrocene/ferrocenium (Fc/Fc^{+}) couple was used as an internal standard reference to scale the measured potentials against the vacuum level. All solutions were deoxygenated by bubbling of nitrogen gas prior to each experiment. The measurements were carried out between -2.2 V and 2.0 V, scanning in both directions with scan rate of 50 mV/s. The HOMO energy levels were calculated from the oxidation potentials observed from DPV curves according to the equation:

$$\mathbf{E_{HOMO}\,(eV) = -\,(E_{OX} - E_{Fc/Fc+}) - 4.80\ eV} \quad \text{…….. (eq.1)}$$

Where E_{ox} is the oxidation potential of sample and $E_{Fc/Fc+}$ the potential of ferrocene. E_{ox} and $E_{Fc/Fc+}$ are both referred against Ag/AgCl reference electrode. The value - 4.80 eV is energy level of ferrocene against vacuum.[65] The LUMO levels were derived from the optical band gap, since no clear reduction peaks could be appreciated from the DPV curves:

$$\mathbf{E_{LUMO}\,(eV) = E_g^{opt} - E_{HOMO}} \text{ ……(eq. 2)}$$

The voltammograms, i.e. changes in current-voltage curves, are presented in **Figure 5.16**, with respect to the ferrocene couple. The highest occupied molecular orbital (HOMO) levels, corresponding to the ionization potentials of the materials, were derived from DPV and are presented in **Table 5.3**. All the compounds exhibited similar electrochemical properties: the HOMO values lie in the range -5.24 to - 5.29 eV. Since no clear reduction peaks were appreciated from the voltammograms (**Figure 5.16)**, the LUMO values were derived from the optical band gap (E_g^{opt}) as summarized in **Table 5.3**.

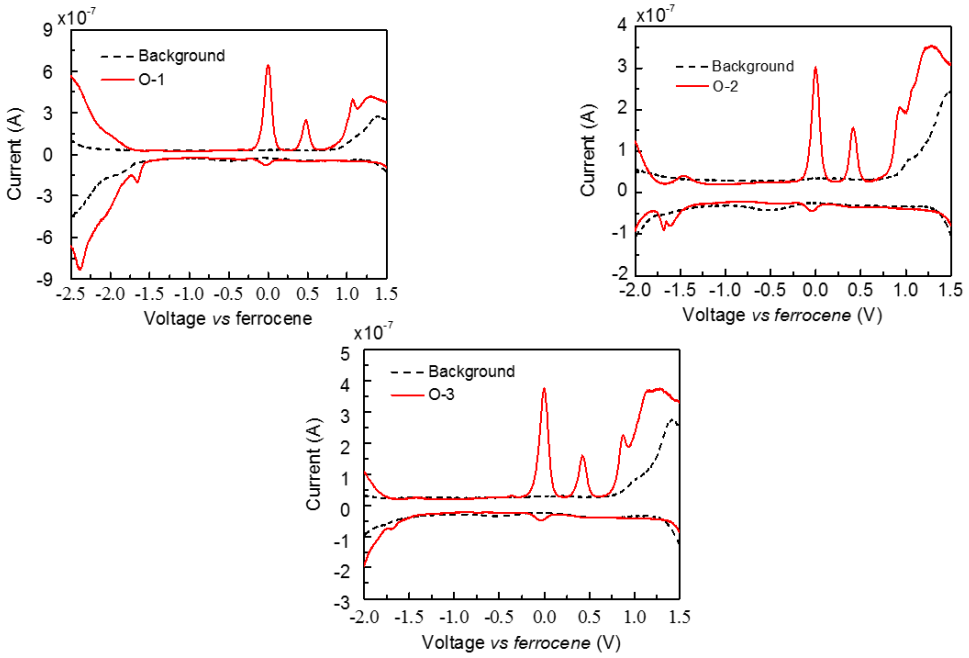

Figure 5.16: DPV voltammograms of **O-1**, **O-2** and **O-3**.

Table 5.3: HOMO and LUMO energy levels of **O-1**, **O-2** and **O-3**

Compound	**HOMO ^{DPV} (eV)**	**LUMO ^{opt} (eV)**
O-1	-5.29	-3.16
O-2	-5.24	-3.23
O-3	-5.24	-3.27

5.3.4) Hole mobility characterization

The bulk hole mobility in films of **O-1**, **O-2**, and **O-3** was investigated by means of impedance spectroscopy[66] applied to hole-only devices. Upon injecting charge carriers, by applying a dc bias superimposed to small harmonic voltage modulation, dramatic changes were observed in the impedance spectra.[67] The transit time of charge carriers "τ" can be inferred from the peak frequency of the negative differential subsceptance[68] or from the peak frequency of the imaginary part of impedance (ImZ). For dispersive charge transport, the latter method is considered more convenient. Indeed, even in high dispersion conditions, clear peaks are observed in the ImZ spectrum.[69]

Hole-only devices for charge carrier mobility investigations were prepared with thermally annealed films, at 80 °C for **O-1**, and at 110 °C for **O-2** and **O-3**. Hole-only devices were prepared in the sandwiched structure ITO/PEDOT:PSS/phenothiazine/MoO/Au, where ITO is indium tin oxide and PEDOT:PSS is poly(3,4-ethylenedioxythiophene)/polystyrene sulphonic acid (ITO-coated glass substrates were first cleaned in detergent and water, then ultrasonicated in acetone and isopropyl alcohol for 15 min each. The layer of PEDOT: PSS (~40 nm) was spin-coated at 4000 rpm onto the ITO-glass substrates, and baked in an oven at 120 °C for 10 min. The phenothiazine layers were deposited under ambient conditions by spin-coating (300 rpm) from chlorobenzene solutions (65–70 mg/mL). After the deposition, the films were transferred in an Ar-filled glove-box, where a thermal treatment was applied to remove the excess solvent before the top contact deposition. The MoO_3 layer (5 nm) and the Au top electrode (100 nm) were thermally evaporated at a base pressure of 4×10^{-6} mbar through a shadow mask defining a device active area of 8 mm^2. The electrical characterization of the devices was carried out at room temperature in glove-box. Impedance spectroscopy measurements were conducted in the frequency range 40 Hz–1.4 MHz, with an amplitude of the harmonic voltage modulation of 20 mV. The dc bias was varied in the range 0–14V.

Hole-only devices for charge carrier mobility investigations were prepared with thermally annealed films, at 80 °C for **O-1**, and at 110 °C for **O-2** and **O-3**. The frequency dependence of ImZ for typical hole-only devices is shown in **Figure 5.17**, for different values of the dc voltage. Clear peaks were observed for all molecules, shifting towards higher frequencies as the voltage increased. The transit time of charge carriers was obtained from the peak frequency through $\tau = k \times \tau_p$, where τ_p is the time constant corresponding to the peak frequency and k is a constant

depending on the dispersion degree.[69] The value of k was considered to be 0.44, as reported for a moderate degree of dispersion.[69] The hole mobility μ was calculated by using the well-known expression $\mu = d / (E\,\tau)$ [1,70] where d is the film thickness and E the electric field.

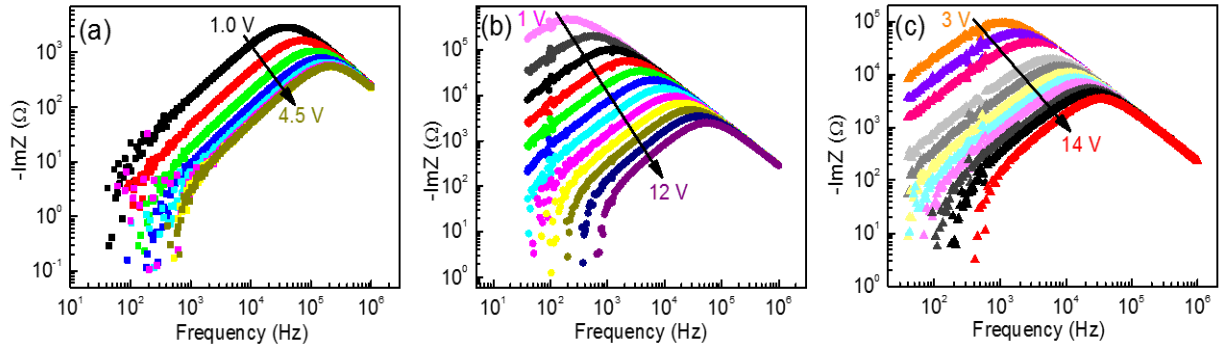

Figure 5.17: Imaginary part of impedance (ImZ) as a function of frequency for hole-only devices made of **O-1** (a), **O-2** (b) and **O-3** (c) films at different values of the dc voltage (the arrows indicates increasing voltage). Film thicknesses: 920 nm, 575 nm and 470 nm for **O-1**, **O-2** and **O-3**, respectively.

The obtained values are reproduced in **Figure 5.18** as a function of E. An outstanding bulk mobility of positive charge carriers was achieved for **O-1** films, with values of the order of 10^{-3}. For **O-2** and **O-3**, μ dropped dramatically, by three orders of magnitude, as compared to **O-1** films, with values on the order of 10^{-6} cm^2 V^{-1} S^{-1} in the same field range. The linear trend of mobility data for **O-2** and **O-3** shown in **Figure 5.18** indicates a Poole-Frenkel-type behavior of mobility.[71 72]

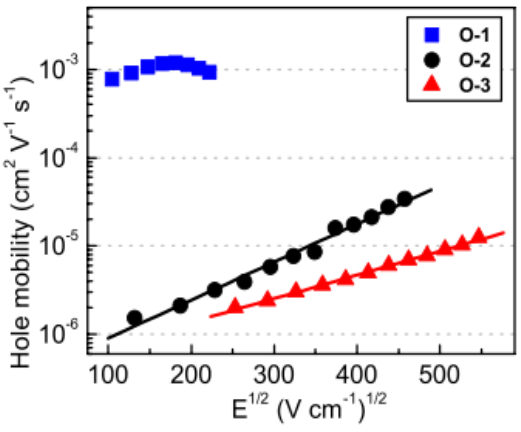

Figure 5.18: Bulk hole mobility of **O-1**, **O-2** and **O-3** as a function of the square root of electric field. For **O-2** and **O-3** the lines indicate the linear fit to the experimental data.

$$\boldsymbol{\mu = \mu_0 \exp(\gamma\sqrt{E})} \qquad \text{…….(eq. 1)}$$

Where, μ_0 denotes the mobility at zero field and γ is the parameter describing how strong the field dependence is. The parameters for the Poole-Frenkel fit to the mobility data of **O-2** film are $\mu_0 = 3.4 \times 10^{-7}$ cm^2 V^{-1} S^{-1} and $\gamma = 9.9\times 10^{-3}$ (V cm^{-1})$^{-1/2}$, while $\mu_0 = 4.0\times 10^{-7}$ cm^{2}V^{-1}S^{-1} and $\gamma = 6.2\times10^{-3}$ (V cm^{-1})$^{-1/2}$ were obtained for **O-3**.

5.3.5) Density functional theory (DFT) Studies

In order to get further insight into the electronic nature of the phenothiazine derivatives and to support our findings for the higher hole mobility of **O-1**, the compounds were studied by Density Functional Theory (DFT)[73] methods. Computational analysis for DFT study was performed as follows.

All the calculations were carried out using Gaussian 09 software package[74] without symmetry constraints. Solvent effects (chloroform) were considered in every calculation using the Polarizable Continuum Model (PCM) initially devised by Tomasi and coworkers[75,76,77] as implemented on Gaussian 09, with radii and non-electrostatic terms for Truhlar and coworkers' SMD solvation model.[78] Density Functional Theory (DFT) and Time-Dependent DFT (TDDFT) were used for computation of the ground and excited state properties, respectively. All calculations were performed using the PBE1PBE functional and 6-31G(d, p) basis set.[79,80,81,82,83] The functional uses a hybrid generalised gradient approximation (GGA), including 25% mixture of Hartree-Fock exchange[84] with DFT exchange-correlation,[85] given by Perdew, Burke and Ernzerhof functional (PBE).[86, 87]

Extensive TD-DFT calculations studies with different functionals have demonstrated that global hybrid methods containing between 22-25% of exact exchange provide better match with reference data.[88] Vertical excitation calculations of compound **O-1** with PBE1PBE, CAM-B3LYP and B3LYP functionals and 6-31G (d, p) basis set using PCM were compared with the experimental UV spectrum in chloroform. PBE1PBE was adopted for the computational study since the λ_{max} calculated (494 nm) was in better agreement with the experimental value (490 nm) than the one obtained with CAM-B3LYP (400 nm) or B3LYP (516 nm). Uses of PBE1PBE in the studies of vertical excitation systems have been reported for aromatic[89-91] and push-pull systems.[92] [93] The computational data described was obtained by using the following computational protocol: 1)The ground state geometry of each molecule was fully optimized with

default cut-offs on forces and step size to determine convergence. 2) The analytical calculation of the vibrational frequencies at the same level of theory verified the optimized structure by checking that they corresponded to true minima of the potential energy surface by the absence of imaginary frequencies. 3) The first six low-lying excited states were determined within the vertical TDDFT, with the default non-equilibrium solvation procedure. The less energetic allowed transition (S0→S1*) were mainly composed by HOMO→LUMO transitions. 4) The minimum energy point on the excited state potential energy surface was calculated by a TD-DFT geometry optimization of the first excited state in solution, with tight convergence criteria, with equilibrium, linear response solvation. 5) Natural Population Analysis (NPA) [94-101] was performed as implemented on Gaussian 09 to study the electronic structure of the optimized species.

The electronic nature of the phenothiazine derivatives **O-1** and **O-2** was explored by Density Functional Theory methods, as well as **O-3** simplified by replacement of the *n*-butyl chain with a methyl (**O-3(Me)**).

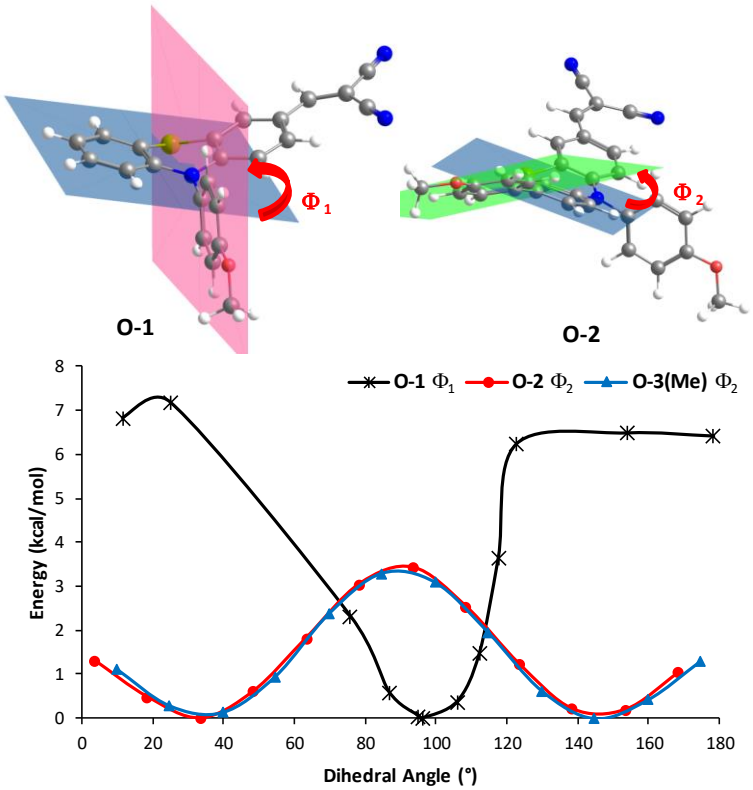

Figure 5.19: Plane figures of phenothiazine optimized structures, dihedral angles and energy profiles for substituent rotation.

In the ground state the geometries of the phenothiazines are slightly bent in the phenothiazine heterocyclic ring and adopt a butterfly shape. The presence of different substituents at the C(7) position of the phenothiazine has little or no effect on the dihedral angles made by the two aromatic rings, being about 19-20° for the three molecules studied. Although *N*- alkyl substituted phenothiazines present larger dihedral angles (*ca*. 41°), the presence of the *N*- methoxyphenyl substituent induces the heterocyclic moiety to adopt a geometry closer to planarity.[29] On the other hand, the methoxyphenyl *N*-substituent preferentially adopts a perpendicular position to the unsubstituted phenyl ring in **O-1** (ϕ_1) and its co-planarity demands for 7 Kcal/mol (**Figure 5.19**). Regarding rotation of substituents at C(7) position, these adopt a non-planar geometry having a dihedral angle (ϕ_2) of ca. 34° with the phenothiazine ring system in **O-2** and **O3(Me)** (**Figure 5.19**). Such slight distortion does not seem to encumber the resonance between the substituent at C(7) and the phenothiazine.

The distribution of electron density in HOMO and LUMO levels are presented in **Figure 5.20** and **Figure 5.21**

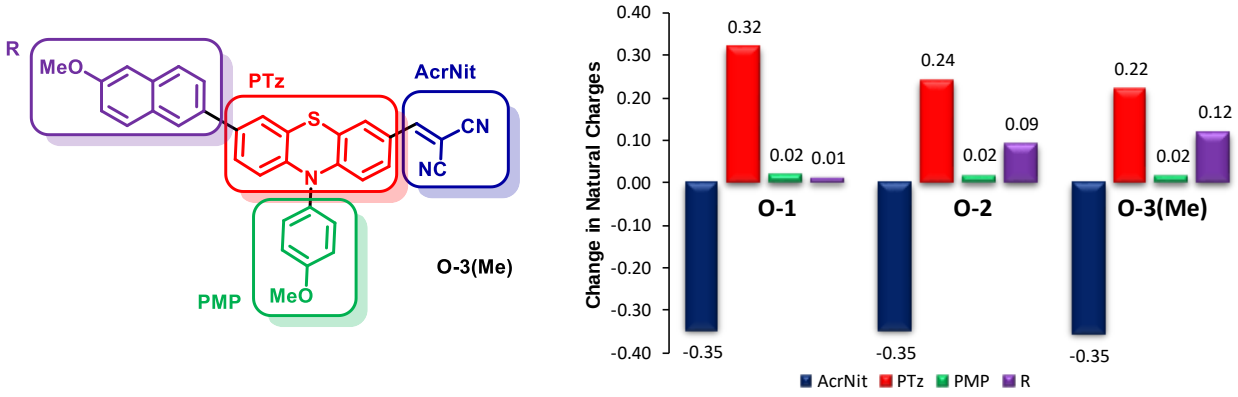

Figure 5.20: Differences in natural charges between ground state (S_0) and excited state (S_1), estimated by a time dependent DFT/PBE1PBE model.

The electron density distribution in the LUMO of phenothiazines was mainly localized on malononitrile end group and the adjacent phenyl ring, while in **O-2** and **O-3(Me)** HOMO orbitals were delocalized over phenothiazine moiety and its C(7) substituents, as shown in

Figure 5.20. Clearly, introduction of electron rich substituents in the C(7) position of phenothiazine derivatives increased the HOMO energy level while keeping the energy of LUMO orbitals localized on the acceptor end. The methoxyphenyl *N*-substituent was not involved in the electron density of the frontier orbitals, as would be expected due to its perpendicularity with the phenothiazine system. The strongest transition ((S0→S1*) was visibly dominated by HOMO→LUMO transitions for the three studied molecules, as determined by TDDFT (**Table S 5.1)** In the case of phenothiazine **O-3(Me)** a small contribution from HOMO-1→LUMO transition was found. The obtained values of absorption maxima (λ_{max}) reflected the observed experimental trends, although the absolute values for the excitation energies are overestimated by the method (by *ca.* 0.9-1.1eV). Further inspection into the S1 state and the distribution of natural charges in S0 as compared to the charges in S1 (**Figure 5.20**) showed that the three systems behave similarly concerning the acceptor moiety and the *N*- methoxyphenyl substituent. The acceptor moiety was electronically enriched by 0.35 upon excitation, while the *N*-substituent barely changed its natural charge. On the other hand, while most of the charge transfer occured from the phenothiazine ring into the malononitrile, the electron rich substituent at C(7) contributed to some extent to the internal charge transfer. In such instance the 6-methoxynaphtalene of **O-3(Me)** was slightly more electron donating than the 4-methoxyphenyl substituent in **O-2**, as demonstrated by the changes in natural charges (0.09 for **O-2** and 0.12 for **O-3(Me)**). As similar electronic features were determined for these three phenothiazine derivatives, the higher charge mobility of **O-1** should not be attributed to the modification of the electron density by introduction of substituents at C(7), but to the lower degrees of freedom of **O-1.**

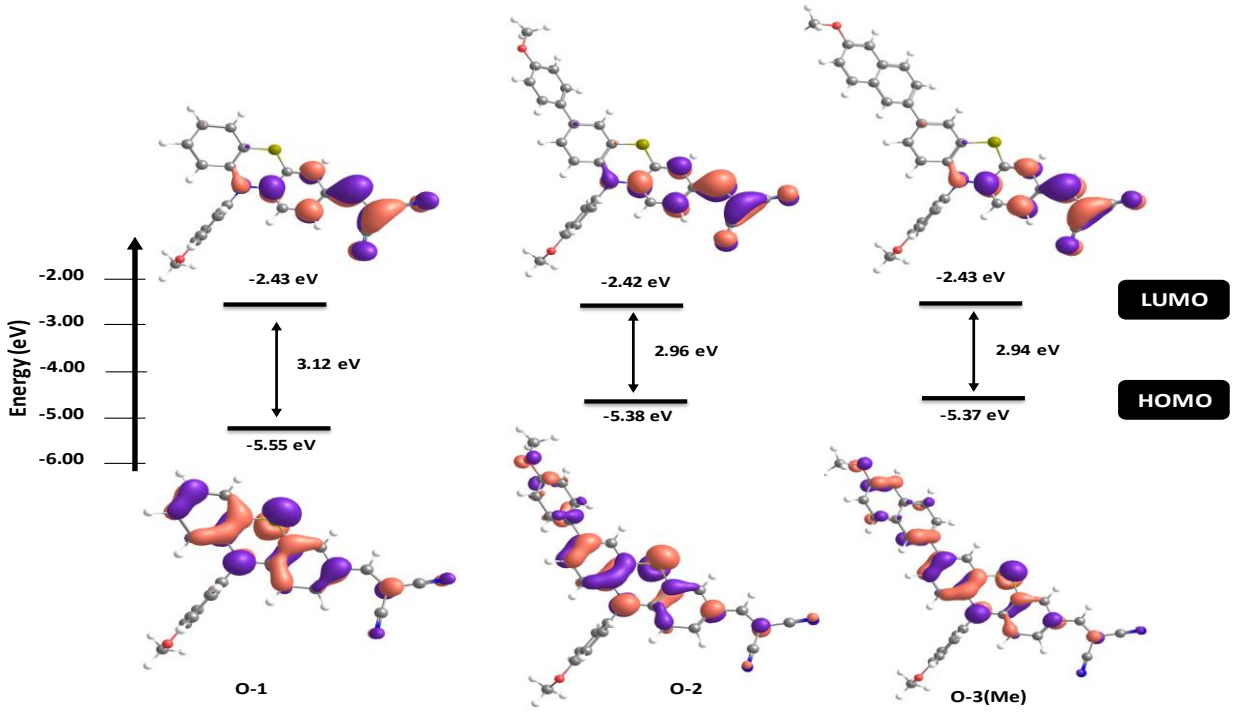

Figure 5.21: Energy levels and electron distribution for frontier molecular orbitals of **O-1**, **O-2** and **O-3(Me)** calculated with DFT at PBE1PBE/6-31G** level of theory (isosurface value = 0.04).

5.3.6) X-Ray diffraction (XRD) studies

To clarify the significant difference in charge transport properties of **O-1** with respect to **O-2** and **O-3**, powder X-ray diffraction (XRD) analysis was performed. XRD patterns recorded on (i) film samples, prepared and treated in the same conditions used for the preparation of hole-only devices, and (ii) powder samples are compared in **Figure 5.19**. The sharp peaks of XRD patterns of powder samples indicated a high degree of crystallinity for each of the three phenothiazine-based molecules. For film samples, on the other hand, the XRD pattern of **O-1** indicated the presence of crystalline material also in the film, in the same phase as in the powder, while amorphous patterns were obtained for the **O-2** and **O-3** films. The presence of crystalline phase is well in line with the annealing-induced spectral changes observed in **O-1** films (**Figure 5.15 (a)**) and the absence of such changes for **O-2** and **O-3**.

XRD investigations of the films confirm that the outstanding bulk hole mobility in **O-1** films can be ascribed to the presence of crystalline phases, completely absent in the layers deposited from the other two phenothiazines. The high degree of ordering of **O-1** is probably due to its more

compact and less twisted molecular structure as compared to **O-2** and **O-3.** The latter ones have bulkier substituents in the C(7) position, which are able to rotate freely (see the computational analysis), thereby decreasing the system order. Despite some exceptions on increased charge mobility with decreased π -π stacking[102] shorter π -π stacking distances typically result into higher charge carrier mobility.[103,104] Hence, a better π -π stacking in case of **O-1** could be responsible for its high hole mobility (*ca.* 10^{-3} $cm^2V^{-1}S^{-1}$) whereas the more twisted nature of **O-2** and **O-3** leads to poor motilities (*ca.* 10^{-6} $cm^2V^{-1}S^{-1}$). These low mobility values are comparable to those reported in the literature for other solution deposited[32,35,105] and thermally evaporated[106] phenothiazine derivatives. To the best of our knowledge, the mobility of **O-1** is the highest reported for phenothiazine-based small molecules, without complexation with iodine.

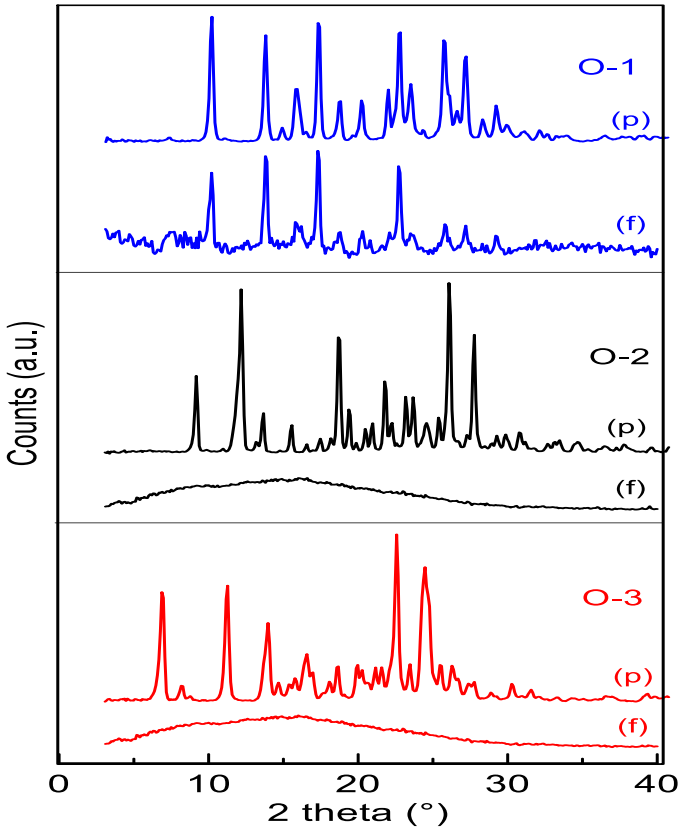

Figure 5.22: XRD patterns of powder samples (p) and film samples (f). All patterns are subtracted for background of substrates in order to enhance the presence of halos due to the amorphous component.

Table 5.4: Mobility data of **O-1, O-2** and **O-3**

Molecule	**Mobility ($cm^2V^{-1}s^{-1}$) (in the order of)**
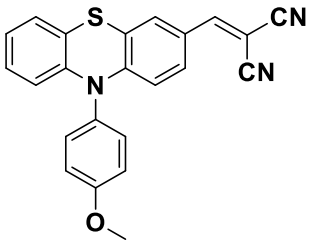 **(O-1)**	**10^{-3}**
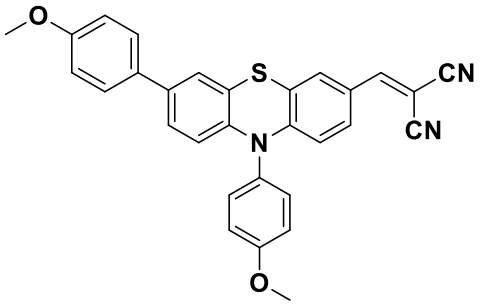 **(O-2)**	**10^{-6}**
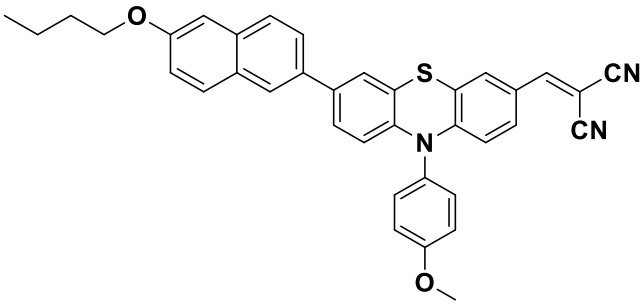	**10^{-6}**

5.4) Conclusions

Three new donor-acceptor systems based on C(7)-substituted phenothiazine derivatives *viz.* 2-((10-(4-methoxyphenyl)-10H-phenothiazin-3-yl) methylene) malononitrile **(O-1)**, 2-((7,10-bis(4-methoxyphenyl)-10H-phenothiazin-3-) methylene) malononitrile **(O-2)** and 2-((7-(6-butoxynaphthalen-2-yl)-10-(4-methoxyphenyl)-10H-phenothiazin-3-yl)methylene) malononitrile **(O-3)** were synthesised with good overall yields. The presence of crystalline phases in spin-

coated films prepared with the unsubstituted phenothiazine **O-1**, arising from the chemical structure of the compound, presumably led to excellent π- π stacking. While the introduction of bulky 4-methoxyphenyl and 6-butoxynaphthyl terminal groups in C(7) position of **O-2** and **O-3** showed a weak impact on the optical and electrochemical characteristics of the compounds, it exhibited strong influence on the structural properties of the related spin-coated thin films. In fact, disorder is introduced into **O-2** and **O-3** compounds, by making them more twisted, as the rotation of the bulky substituents requires as little as 3.4 Kcal/mol. This explains the observed amorphous nature of **O-2** and **O-3** films. The values of the bulk hole mobility of **O-2** and **O-3** samples (in order of 10^{-6} cm^2 $V^{-1}S^{-1}$) lie in the typical range of state-of-the-art phenothiazines, while **O-1** shows an outstanding mobility in the order of 10^{-3} cm^2 $V^{-1}S^{-1}$,the highest reported for phenothiazine-based materials. The achievements of this study provide a strong motivation to further design of phenothiazine-based donor-acceptor systems with high bulk mobility, to be adopted as hole-transport materials for organic electronics.

5.5) References

1. V. Coropceanu, J. R. M. Cornil, D. A. da Silva Filho, Y. Olivier, R. Silbey and J.L. Bredas, *Chem.Rev.*, 2007, **107**, 926.
2. H. Sirringhaus, N. Tessler and R. H. Friend, *Science*, 1998, **280**, 1741.
3. M. M. Mandoc, L. J. A. Koster and P. W. M. Blom, *Appl. Phys. Lett.*, 2007, **90**, 133504.
4. S. Yoshikawa, A. Saeki, M. Saito, I. Osaka and S. Seki, *Phys. Chem. Chem. Phys.*, 2015, **17**, 17778.
5. A. Mishra and P. Bauerle, *Angew. Chem. Int. Ed.*, 2012, **51**, 2020.
6. Y. Liu, C.C. Chen, Z. Hong, J. Gao, Y. M. Yang, H. Zhou, L. Dou, G. Li and Y. Yang, *Sci. Rep.*, 2013, **3**, 3356.
7. J. Roncali, P. Leriche and P. Blanchard, *Adv. Mater.*, 2014, **26**, 3821.
8. S. Mohamed, D. Demeter, J.-A. Laffitte, P. Blanchard and J. Roncali, *Sci. Rep.*, 2015, **5**, 9031.
9. H. Cao, Z. Chen, Y. Liu, B. Qu, S. Xu, S. Cao, Z. Lan, Z. Wang and Q. Gong, *Synth. Met.*, 2007, **157**, 427.
10. T. Yu, L. Liu, Z. Xie and Y. Ma, *Sci. Chi. Chem.*, 2015, **58**, 907.
11. W. Wu, Y. Liu and D. Zhu, *Chem. Soc. Rev.*, 2010, **39**, 1489.

12. H. Yan, Z. Chen, Y. Zheng, C. Newman, J. R. Quinn, F. Dotz, M. Kastler and A. Facchetti, *Nature*, 2009, **457**, 679.
13. G. Yu, J. Gao, J. C. Hummelen, F. Wudl and A. J. Heeger, *Science*, 1995, **270**, 1789.
14. G. Bazan and M. R. Bryce, *J. Mater. Chem. C*, 2016, **4**, 3675.
15. T.Y. Wu, M.H. Tsao, S.G. Su, H. P. Wang, Y.C. Lin, F.L. Chen, C.W. Chang and I. W. Sun, *J. Braz. Chem. Soc.*, 2011, **22**, 780.
16. C. S. Kramer, K. Zeitler and T. J. J. Muller, *Tetrahedron Lett.*, 2001, **42**, 8619.
17. M. Sailer, A. W. Franz and T. J. J. Muller, *Chem. Eur. J.*, 2008, **14**, 2602.
18. K. Memminger, T. Oeser and T. J. J. Muller, *Org. Lett.*, 2008, **10**, 2797.
19. H. Oka, *J. Mater. Chem.*, 2008, **18**, 1927.
20. B.C. Hong, N. S. Dange, C.-F. Ding and J.-H. Liao, *Org. Lett.*, 2011, **14**, 448.
21. T. Okamoto, M. Kuratsu, M. Kozaki, K. Hirotsu, A. Ichimura, T. Matsushita and K. Okada, *Org. Lett.*, 2004, **6**, 3493.
22. W. Wu, J. Yang, J. Hua, J. Tang, L. Zhang, Y. Long and H. Tian, *J. Mater. Chem.*, 2010, **20**, 1772.
23. M.J. Kim, Y.J. Yu, J.H. Kim, Y.S. Jung, K.Y. Kay, S.B. Ko, C.R. Lee, I.H. Jang, Y.U. Kwon and N.G. Park, *Dyes Pigm*, 2012, **95**, 134.
24. X. Qiu, R. Lu, H. Zhou, X. Zhang, T. Xu, X. Liu and Y. Zhao, *Tetrahedron Lett.*, 2008, **49**, 7446.
25. H. Tian, X. Yang, R. Chen, Y. Pan, L. Li, A. Hagfeldt and L. Sun, *Chem. Commun.*, 2007, **36**,3741.
26. M. Liang and J. Chen, *Chem. Soc. Rev.*, 2013, **42**, 3453.
27. S. H. Kim, H. W. Kim, C. Sakong, J. Namgoong, S. W. Park, M. J. Ko, C. H. Lee, W. I. Lee and J. P. Kim, *Org.Lett.*, 2011, **13**, 5784.
28. Z.S. Huang, H. Meier and D. Cao, *J. Mater. Chem. C*, 2016, **4**, 2404.
29. S. H. Kim, C. Sakong, J. B. Chang, B. Kim, M. J. Ko, D. H. Kim, K. S. Hong and J. P. Kim, *Dyes Pigm*, 2013, **97**, 262.
30. D. Cao, J. Peng, Y. Hong, X. Fang, L. Wang and H. Meier, *Org. Lett.*, 2011, **13**, 1610.
31. S. S. Park, Y. S. Won, Y. C. Choi and J. H. Kim, *Energy Fuels*, 2009, **23**, 3732.
32. J.H. Huang and K.C. Lee, *ACS Appl. Mater. Interfaces*, 2014, **6**, 7680.

33. Z. Li, Q. Dong, Y. Li, B. Xu, M. Deng, J. Pei, J. Zhang, F. Chen, S. Wen and Y. Gao, *J. Mater. Chem.*, 2011, **21**, 2159.
34. S. Kumar, M. Singh, J.H. Jou and S. Ghosh, *J. Mater. Chem. C*, 2016, **4**, 6769.
35. Y. Ahn, D. E. Jang, Y.B. Cha, M. Kim, K.H. Ahn and Y. C. Kim, *Bull. Korean Chem. Soc.*, 2013, **34**, 107.
36. H. Fidder, J. Knoester and D. A. Wiersma, *J.Chem. Phys.*, 1991, **95**, 7880.
37. F. C. Spano, *Acc. Chem. Res.*, 2009, **43**, 429.
38. J.F. Chang, J. Clark, N. Zhao, H. Sirringhaus, D. W. Breiby, J. W. Andreasen, M. M. Nielsen, M. Giles, M. Heeney and I. McCulloch, *Phys. Rev. B*, 2006, **74**, 115318.
39. X. Sun, Y. Liu, X. Xu, C. Yang, G. Yu, S. Chen, Z. Zhao, W. Qiu, Y. Li and D. Zhu, *J. Phys. Chem. B*, 2005, **109**, 10786.
40. G. Sang, Y. Zou and Y. Li, *J. Phys. Chem. C*, 2008, **112**, 12058.
41. C. H. Siu, L. T. L. Lee, S. C. Yiu, P. Y. Ho, P. Zhou, C. L. Ho, T. Chen, J. Liu, K. Han and W. Y. Wong, *Chem. Eur. J.*, 2016, **22**, 3750.
42. G. D. Blanco, A. J. Hiltunen, G. N. Lim, C. B. Kc, K. M. Kaunisto, T. K. Vuorinen, V. N. Nesterov, H. J. Lemmetyinen and F. D'Souza, *ACS Appl. Mater. Interfaces*, 2016, **8**, 8481.
43. Q. Tan, X. Yang, M. Cheng, H. Wang, X. Wang and L. Sun, *J. Phys. Chem. C*, 2014, **118**, 16851.
44. Y. Matsunaga, *Helv. Phys. Acta.*, 1963, **36**, 800.
45. Y. Matsunaga, *J. Chem.Phys.*, 1964, **41**, 1609.
46. K. Kan and Y. Matsunaga, *Bull. Chem. Soci. Jpn.*, 1972, **45**, 2096.
47. Y. Matsunaga and Y. Suzuki, *Bull. Chem. Soci. Jpn.*, 1972, **45**, 3375.
48. Y. Matsunaga and Y. Suzuki, *Bull. Chem. Soci. Jpn.*, 1973, **46**, 719.
49. F. Gutmann,, *Modern Bioelectrochemistry*, Springer, New York, 1st ed., 1986, pp. 177.
50. S. Doi, T. Inabe and Y. Matsunaga, *Bull. Chem. Soci. Jpn.*, 1977, **50**, 837.
51. A. A. Bakulin, A. Rao, V. G. Pavelyev, P. H. M. van Loosdrecht, M. S. Pshenichnikov, D. Niedzialek, J. r. m. Cornil, D. Beljonne and R. H. Friend, *Science*, 2012, **335**, 1340.
52. S. Shoaee, T. M. Clarke, C. Huang, S. Barlow, S. R. Marder, M. Heeney, I. McCulloch and J. R. Durrant, *J. Am. Chem. Soc.*, 2010, **132**, 12919.

53. Y. J. Chang, P.T. Chou, Y.Z. Lin, M. Watanabe, C.J. Yang, T.M. Chin and T. J. Chow, *J.Mater. Chem.*, 2012, **22**, 21704.

54. Z. Iqbal, W.Q. Wu, D.B. Kuang, L. Wang, H. Meier and D. Cao, *Dyes Pigm.*, 2013, **96**, 722.

55. Y. Hua, L. T. L. Lee, C. Zhang, J. Zhao, T. Chen, W.Y. Wong, W.K. Wong and X. Zhu, *J. Mater. Chem.A*, 2015, **3**, 13848.

56. R. Y.Y. Lin, F. L. Wu, C. T. Li, P. Y. Chen, K. C. Ho and J. T. Lin, *Chem Sus Chem*, 2015, **8**, 2503.

57. A. Bejan, S. Shova, M.D. Damaceanu, B. C. Simionescu and L. Marin, *Cryst. Growth Des.*, 2016, **16**, 3716.

58. K. N. Armarego and D. D. Perrin, *Purification of Laboratory Chemicals*, Butterworth-Heinemann, Oxford, 4th Edition, Butterworth Heinemann, 1996.

59. S. Kumar, P. Singh, P. Kumar, R. Srivastava, S. K. Pal and S. Ghosh, *J. Phys.Chem. C*, 2016, **120**, 12723.

60. P. V. Ramachandran, D. Pratihar, D. Biswas, A. Srivastava and M. V. Ram Reddy, *Org. Lett.*, 2004, **6**, 481.

61. A. Suzuki, *J.Organomet. Chem.*, 1999, **576**, 147.

62. G. Jones, *Org. React.*, 2004, **15**, 204.

63. A. J. Heeger, *Adv.Mater.*, 2014, **26**, 10.

64. F. Wurthner, T. E. Kaiser and C. R. Saha Moller, *Angew. Chem. Int. Ed.*, 2011, **50**, 3376.

65. B. W. D'Andrade and S. R. Forrest, *Adv. Mater.*, 2004, **16**, 1585.

66. J. R. Macdonald and E. Barsoukov, Impedance Spectroscopy : Theory, Experiment and . Applications, John Wiley & Sons, New Jersey, 2005, 1 st ed.,1.

67. C. Tanase, E. J. Meijer, P. W. M. Blom and D. M. De Leeuw, *Phys. Rev. Lett.*, 2003, **91**, 216601.

68. R. Kassing, *Phys. Status Solidi (a)*, 1975, **28**, 107.

69. D. C. Tripathi, A. K. Tripathi and Y. N. Mohapatra, *Appl. Phys.Lett.*, 2011, **98**, 14.

70. Y. Shirota and H. Kageyama, *Chem. Rev.*, 2007, **107**, 953.

71. J. Frenkel, *Phys. Rev.*, 1938, **54**, 647.

72. H. H. Poole, *The London, Edinburgh, and Dublin Philosophical Magazine and Journal of Science*, 1916, **32**, 112.

73. W. Kohn and L. J. Sham, *Phys.Rev.*, 1965, **140**, A1133.
74. M. J. Frisch, Gaussian 09, Gaussian Inc., Wallingford CT, 2009.
75. E. Cances, B. Mennucci and J. Tomasi, *J. Chem. Phys.*, 1997, **107**, 3032.
76. B. Mennucci and J. Tomasi, *J. Chem. Phys.*, 1997, **106**, 5151.
77. M. Cossi, V. Barone, B. Mennucci and J. Tomasi, *Chem. Phys. Lett.*, 1998, **286**, 253.
78. A. V. Marenich, C. J. Cramer and D. G. Truhlar, *J. Phys. Chem. B*, 2009, **113**, 6378.
79. R. Ditchfield, W. J. Hehre and J. A. Pople, *J. Chem. Phys.*, 1971, **54**, 724.
80. W. J. Hehre, R. Ditchfield and J. A. Pople, *J. Chem. Phys.*, 1972, **56**, 2257.
81. P. C. Hariharan and J. A. Pople, *Mol. Phys.*, 1974, **27**, 209.
82. M. S. Gordon, *Chem.Phys. Lett.*, 1980, **76**, 163.
83. P. C. Hariharan and J. A. Pople, *Theor. Chim. Acta.*, 1973, **28**, 213.
84. K. B. Wiberg, *Ab Initio Molecular Orbital Theory*, Wiley, New York, 1986.
85. R. G. Parr and W. Yang, *Density Functional Theory of Atoms and Molecules*, Oxford University Press, New York,1989.
86. J. P. Perdew, *Phys. Rev.B*, 1986, **33**, 8822.
87. J. P. Perdew, *Phys. Rev. Lett.*, 1996, **77**, 3865.
88. D. Jacquemin, V. R. Wathelet, E. A. Perpete and C. Adamo, *J. Chem. Theory Compt.*, 2009, **5**, 2420.
89. D. Jacquemin, E. A. Perpete, G. E. Scuseria, I. Ciofini and C. Adamo, *J. Chem. Theory Compt.*, 2008, **4**, 123.
90. D. Bousquet, R. Fukuda, P. Maitarad, D. Jacquemin, I. Ciofini, C. Adamo and M. Ehara, *J. Chem. Theory Compt.*, 2013, **9**, 2368.
91. Y. Xue, Y. Liu, L. An, L. Zhang, Y. Yuan, J. Mou, L. Liu and Y. Zheng, *Comput. Theor. Chem.*, 2011, **965**, 146.
92. C. A. Guido, P. Cortona, B. Mennucci and C. Adamo, *J. Chem. Theory Comput.*, 2013, **9**, 3118.
93. L. Zhang, K. Pei, M. Yu, Y. Huang, H. Zhao, M. Zeng, Y. Wang and J. Gao, *J. Phys. Chem.C*, 2012, **116**, 26154.
94. M. A. L. Marques and E. K. U. Gross, *Annu. Rev. Phys. Chem.*, 2004, **55**, 427.
95. J. E. Carpenter and F. Weinhold, *J. Mol. Struct.*, 1988, **169**, 41.
96. J. P. Foster and F. Weinhold, *J. Am.Chem. Soc.*, 1980, **102**, 7211.

97. A. E. Reed and F. Weinhold, *J.Chem.Phys.*, 1983, **78**, 4066.

98. A. E. Reed and F. Weinhold, *J. Chem. Phys.*, 1985, **83**, 1736.

99. A. E. Reed, R. B. Weinstock and F. Weinhold, *J.Chem.Phys.*, 1985, **83**, 735.

100. A. E. Reed, L. A. Curtiss and F. Weinhold, *Chem. Rev.*, 1988, **88**, 899.

101. F. Weinhold and J. E. Carpenter, *The Structure of Small Molecules and Ions*, Springer, New York, 1988, pp. 227.

102. J. H. Dou, Y. Q. Zheng, T. Lei, S. D. Zhang, Z. Wang, W. B. Zhang, J. Y. Wang and J. Pei, *Adv. Funct. Mater.*, 2014, **24**, 6270.

103. Z. Ma, H. Geng, D. Wang and Z. Shuai, *J. Mater. Chem. C*, 2016, **4**, 4546.

104. J. E. Anthony, *Chem. Rev.*, 2006, **106**, 5028.

105. R. Laurinaviciute, J. Ostrauskaite, E. Skuodis, J. V. Grazulevicius and V. Jankauskas, *Synth. Met.*, 2014, **192**, 50.

106. Y.J. Cheng, S.Y. Yu, S.C. Lin, J. T. Lin, L.Y. Chen, D.S. Hsiu, Y. S. Wen, M. M. Lee and S.-S. Sun, *J. Mater. Chem. C*, 2016, **4**, 9499.

Supporting Information

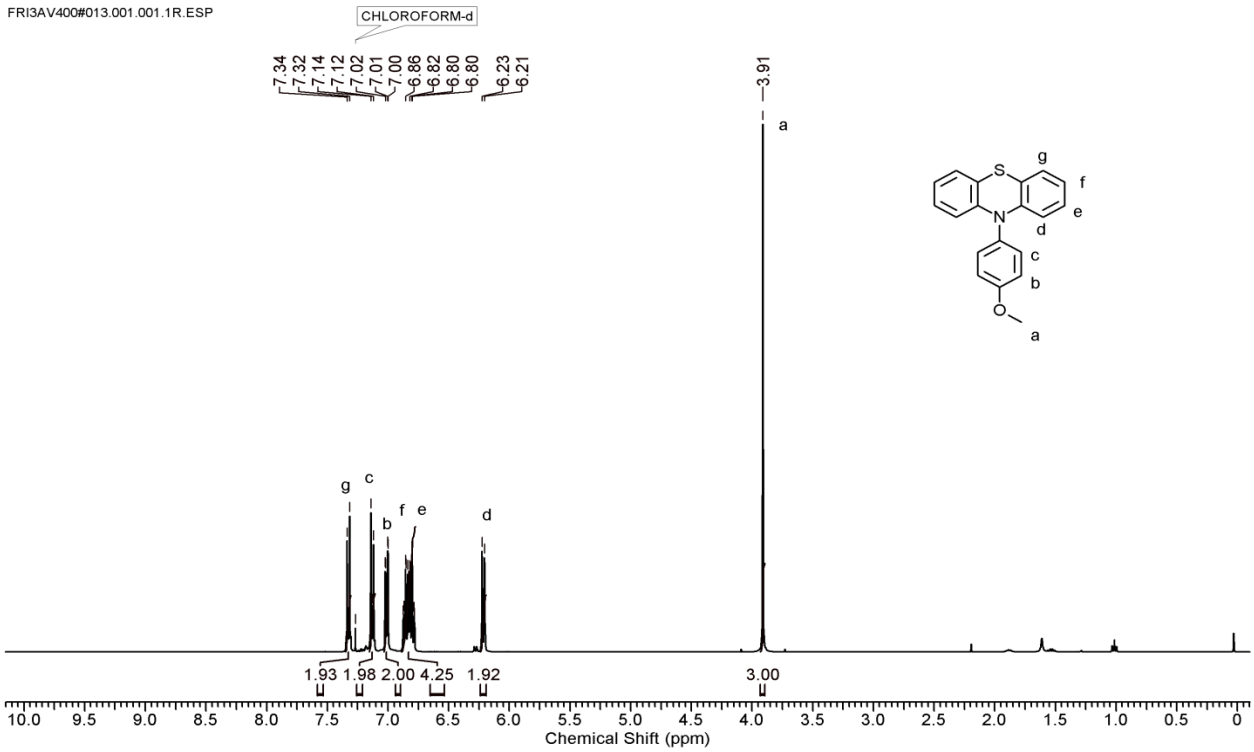

Figure S 5.1: ^{1}H NMR spectrum (in $CDCl_3$) of 10-(4-methoxyphenyl)-10H-phenothiazine (**1**)

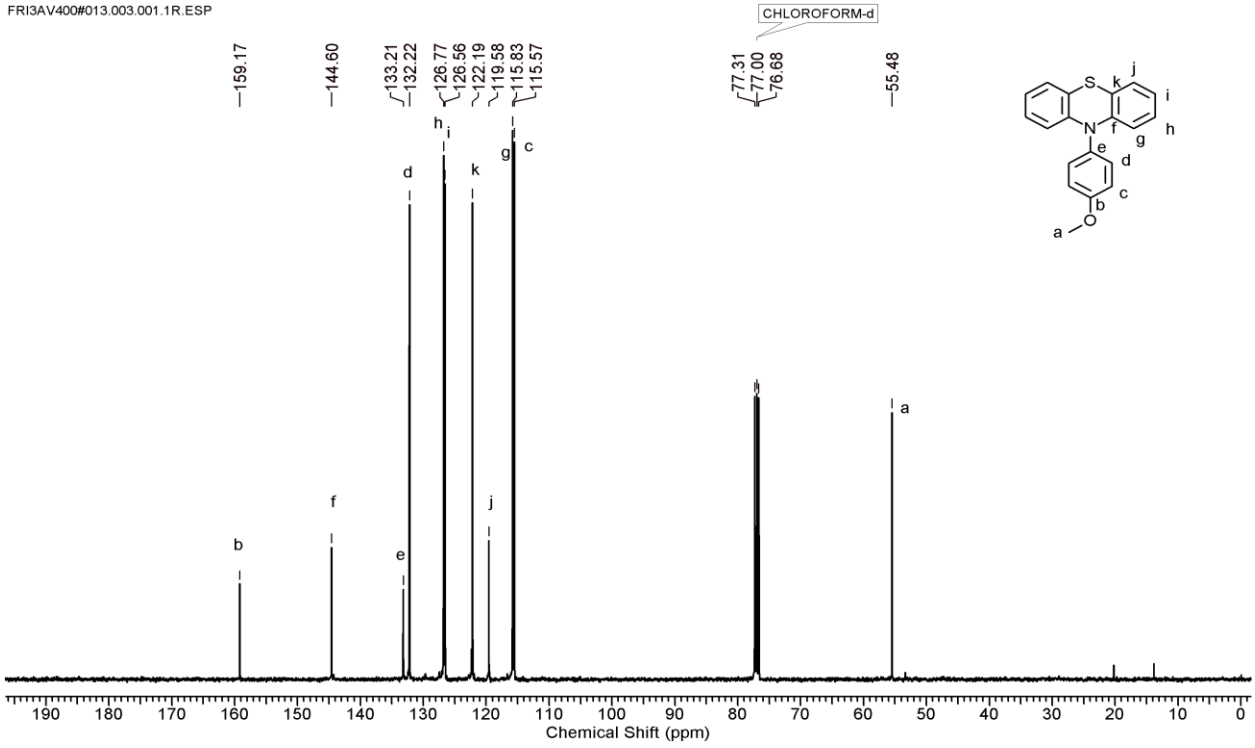

Figure S 5.2: ^{13}C NMR spectrum (in $CDCl_3$) of 10-(4-methoxyphenyl)-10H-phenothiazine (**2**)

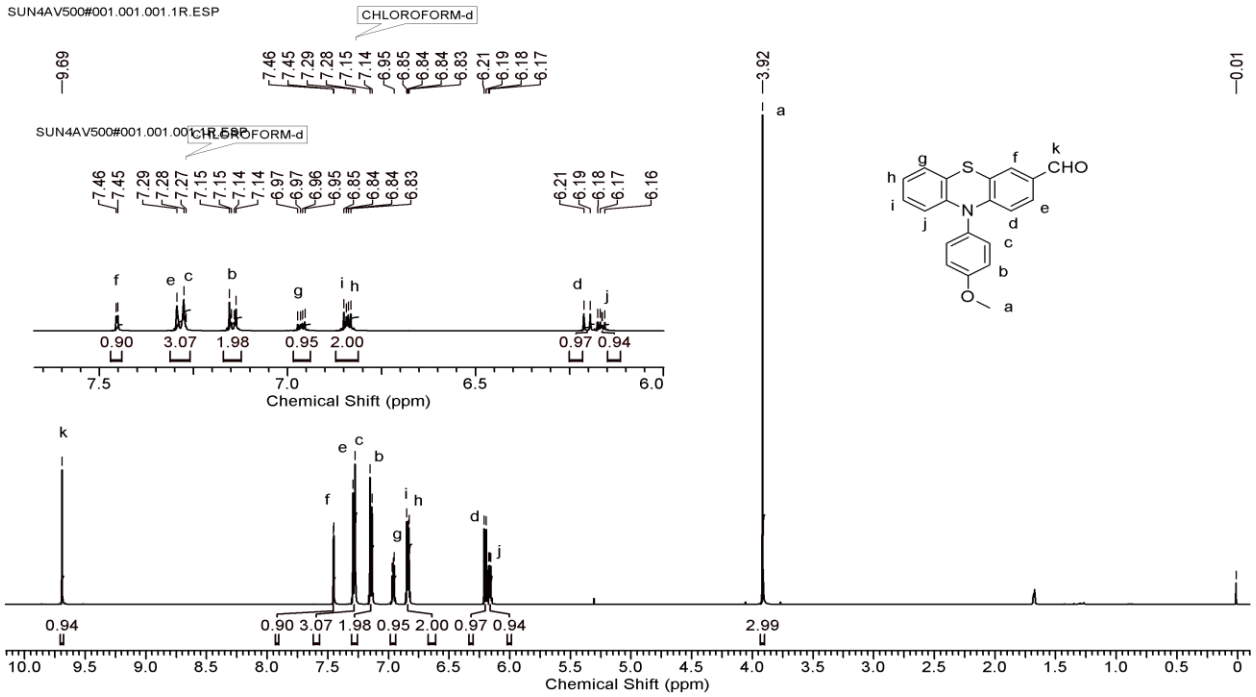

Figure S 5.3: ^{1}H NMR spectrum (in $CDCl_3$) of 10-(4-methoxyphenyl)-10H-phenothiazine-3-carbaldehyde (**2**)

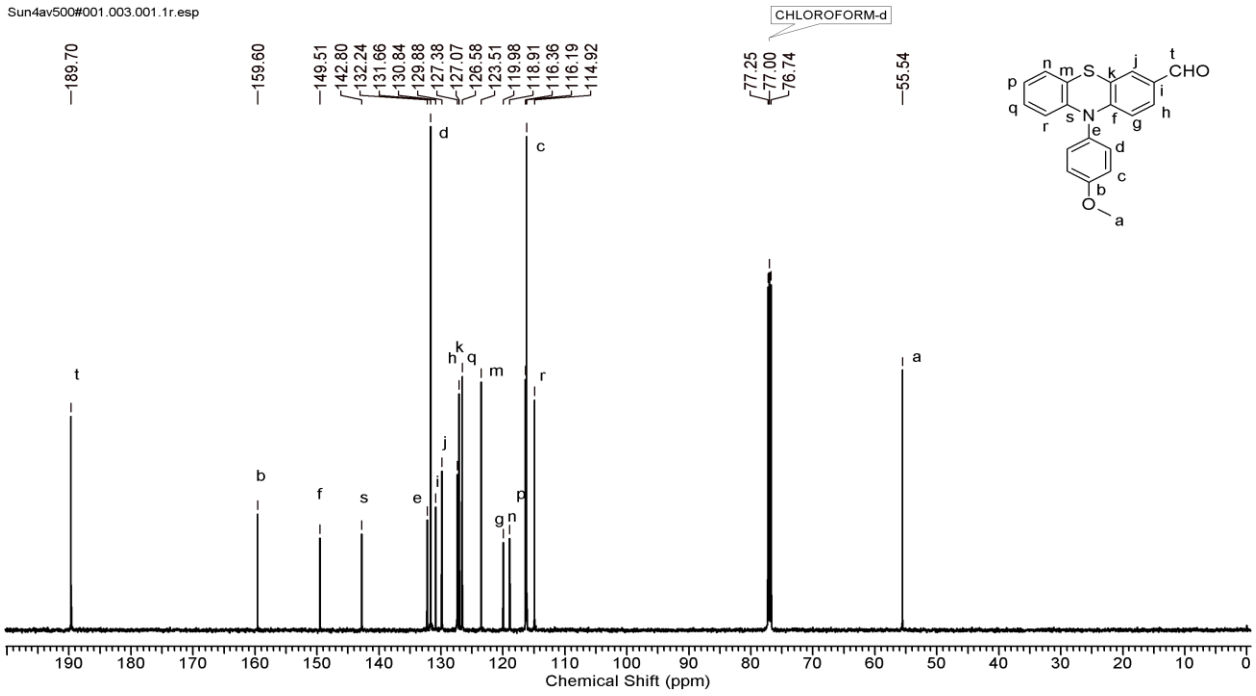

Figure S 5.4: ^{13}C NMR spectrum (in $CDCl_3$) of 10-(4-methoxyphenyl)-10H-phenothiazine-3-carbaldehyde (**2**)

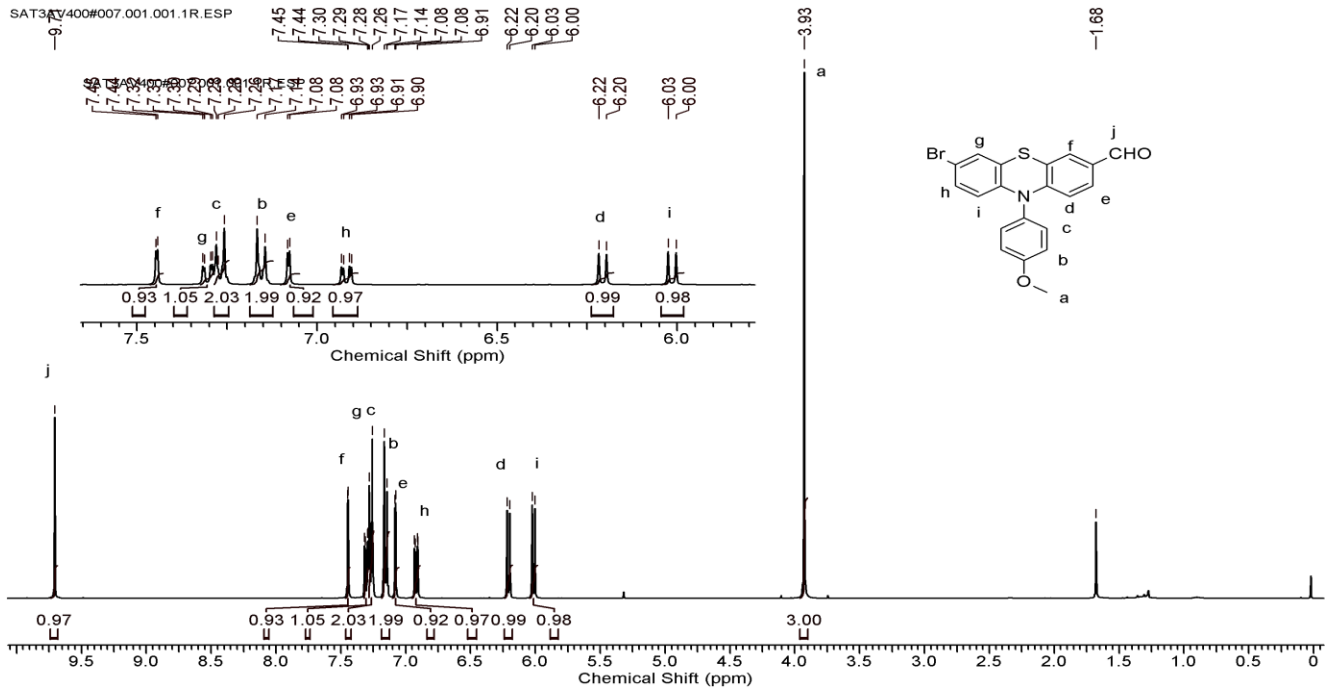

Figure S 5.5: ^{1}H NMR spectrum (in $CDCl_3$) of 7-bromo-10-(4-methoxyphenyl)-10H-phenothiazine-3-carbaldehyde (**3**)

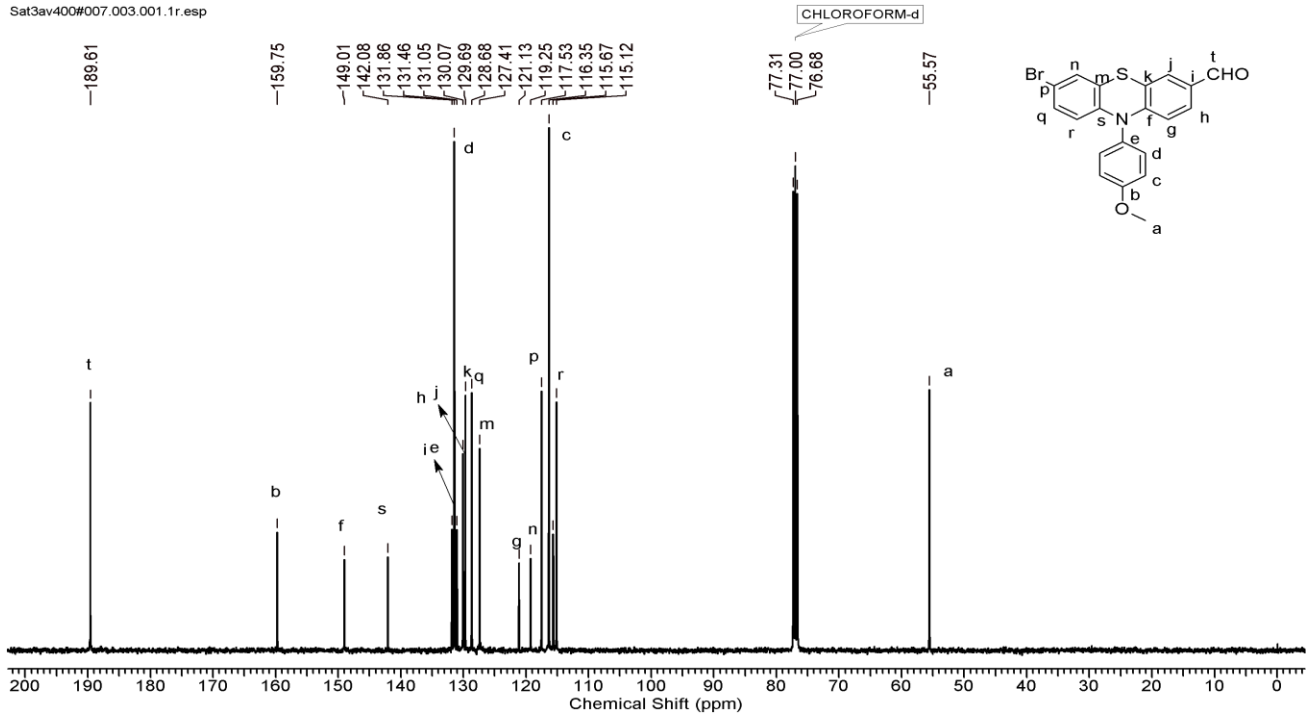

Figure S 5.6: ^{13}C NMR spectrum (in $CDCl_3$) of 7-bromo-10-(4-methoxyphenyl)-10H-phenothiazine-3-carbaldehyde (**3**)

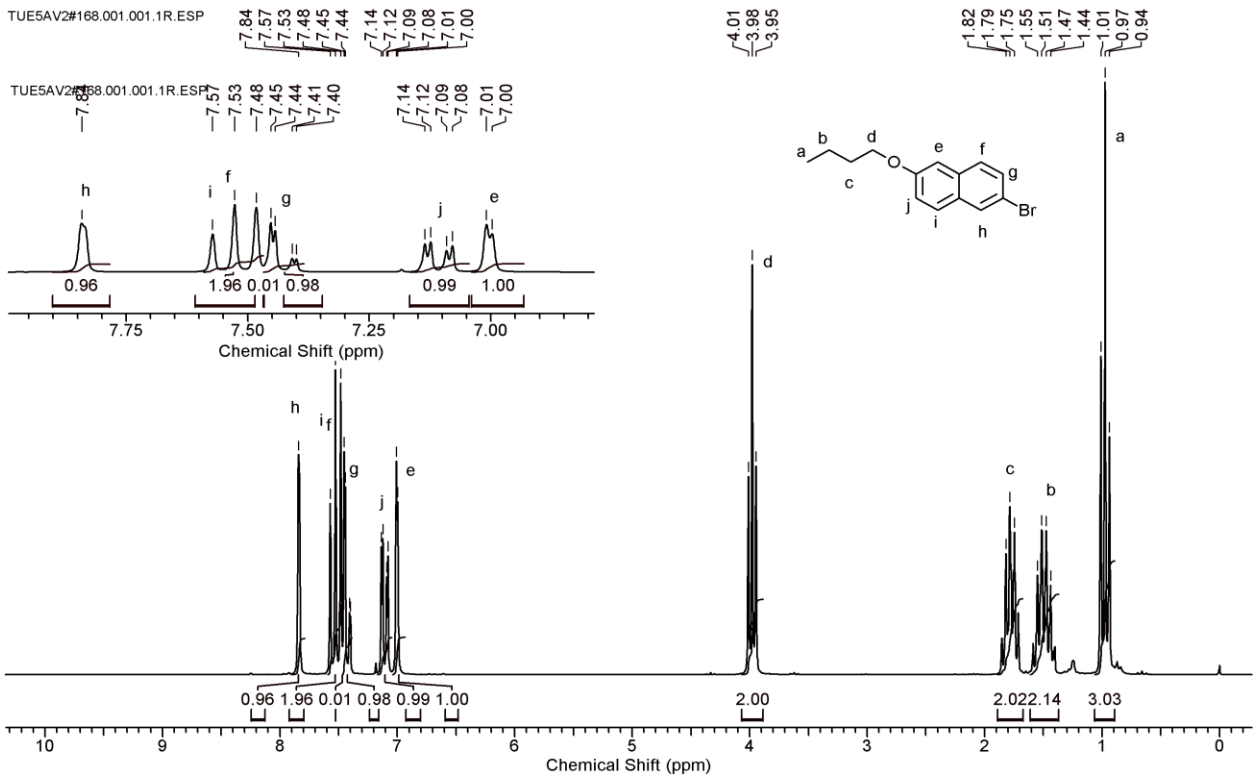

Figure S 5.7: ^{1}H NMR spectrum (in $CDCl_3$) of 2-bromo-6-butoxynaphthalene (**4**)

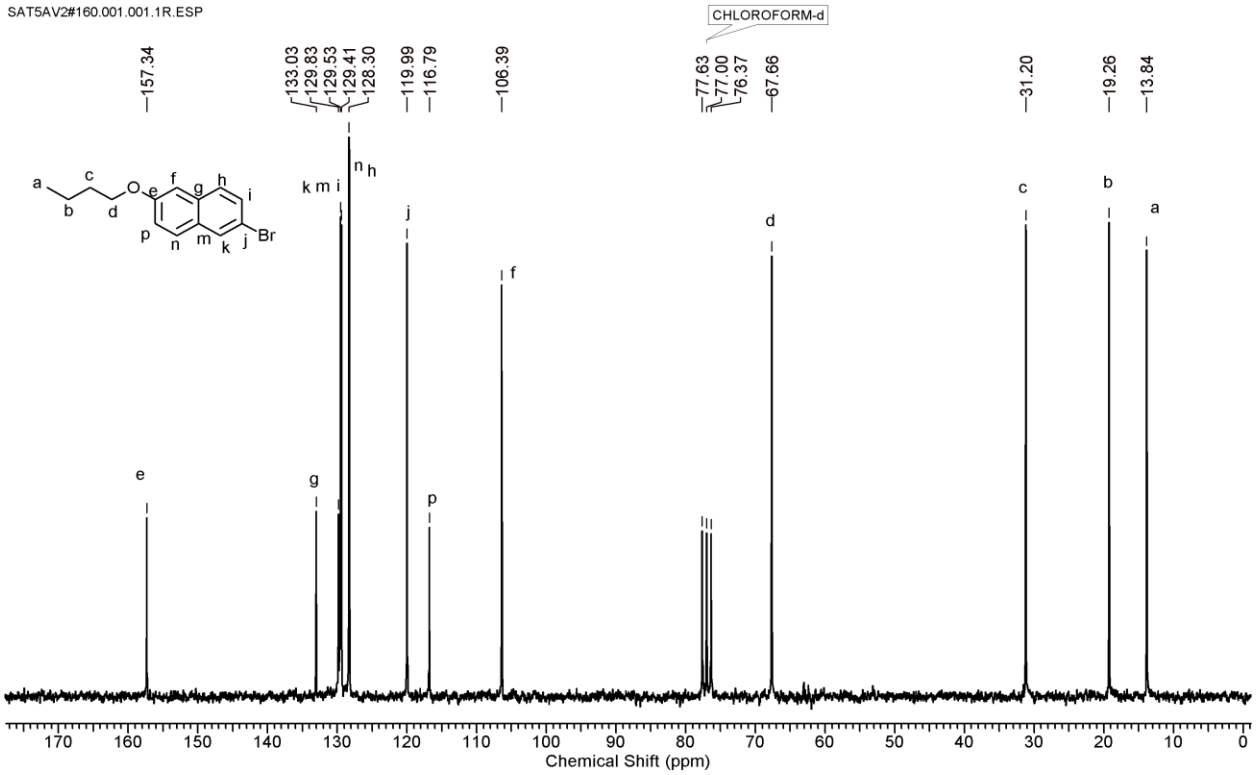

Figure S 5.8: ^{13}C NMR spectrum (in $CDCl_3$) of 2-bromo-6-butoxynaphthalene (**4**)

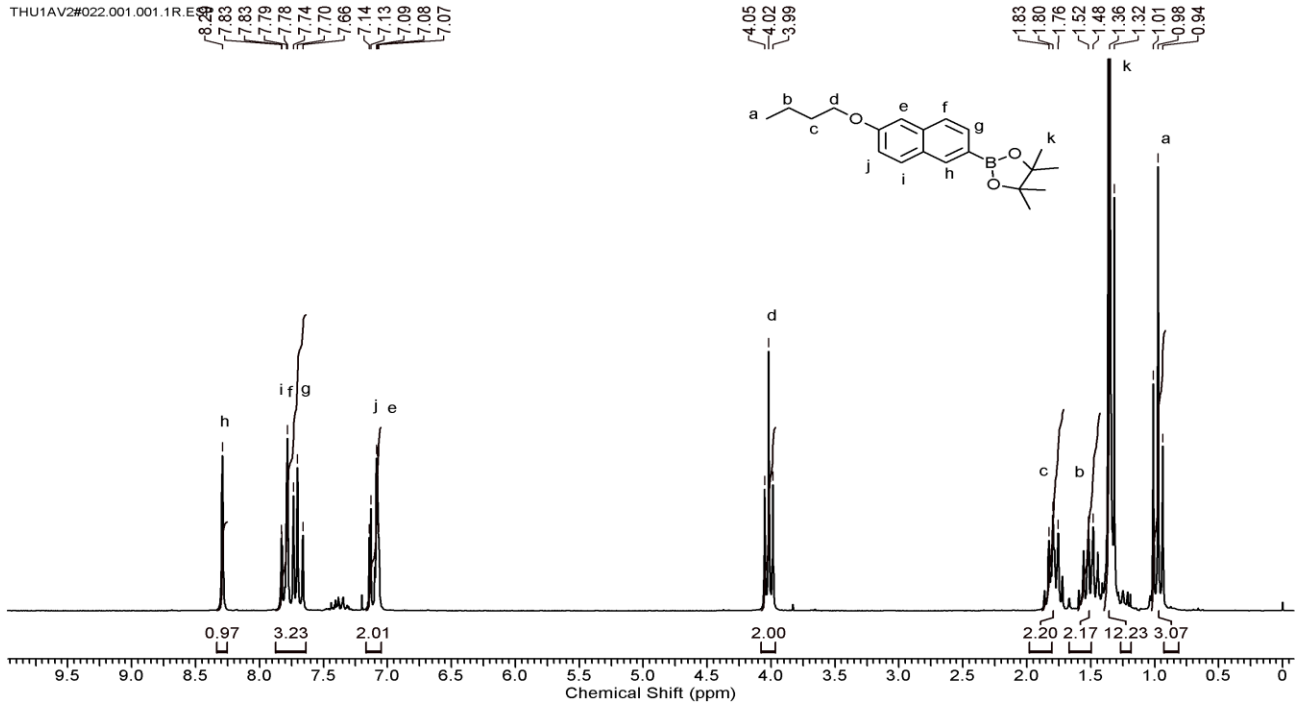

Figure S 5.9: ^{1}H NMR spectrum (in $CDCl_3$) of 2-(6-butoxynaphthalen-2-yl)-4,4,5,5-tetramethyl-1,3,2-dioxaborolane (**5**)

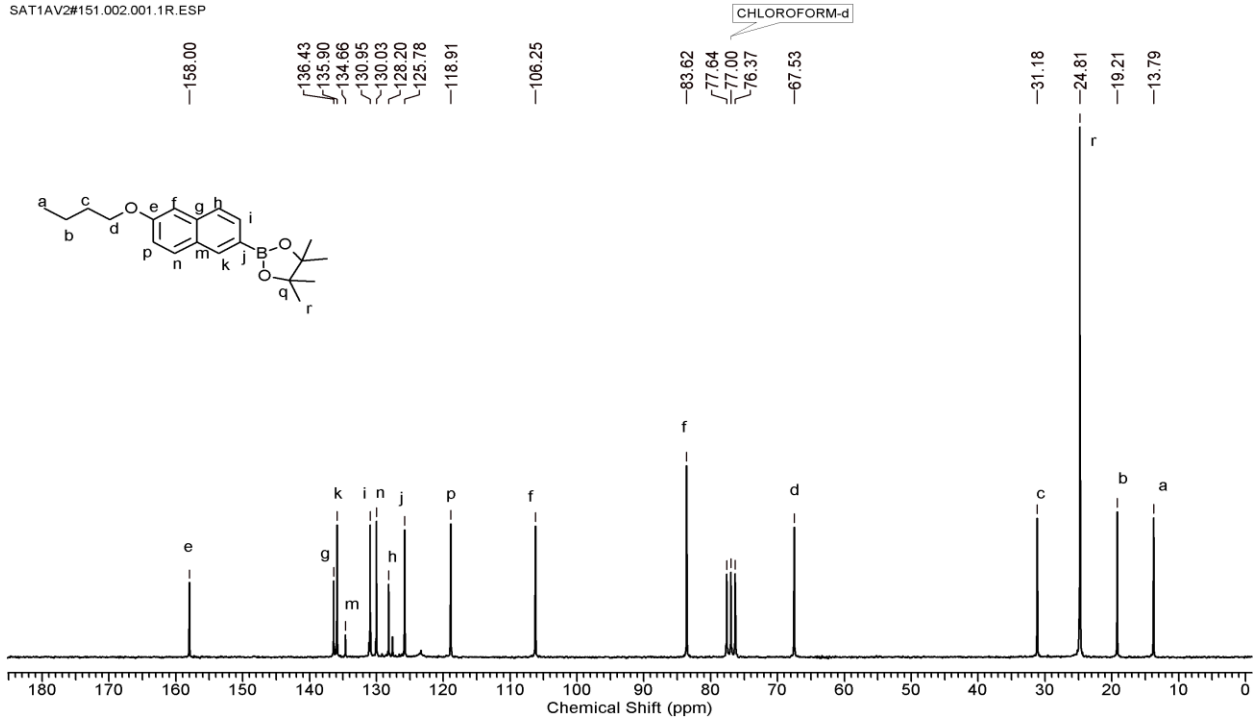

Figure S 5.10: ^{13}C NMR spectrum (in $CDCl_3$) of 2-(6-butoxynaphthalen-2-yl)-4, 4, 5, 5-tetramethyl-1,3,2-dioxaborolane (**5**)

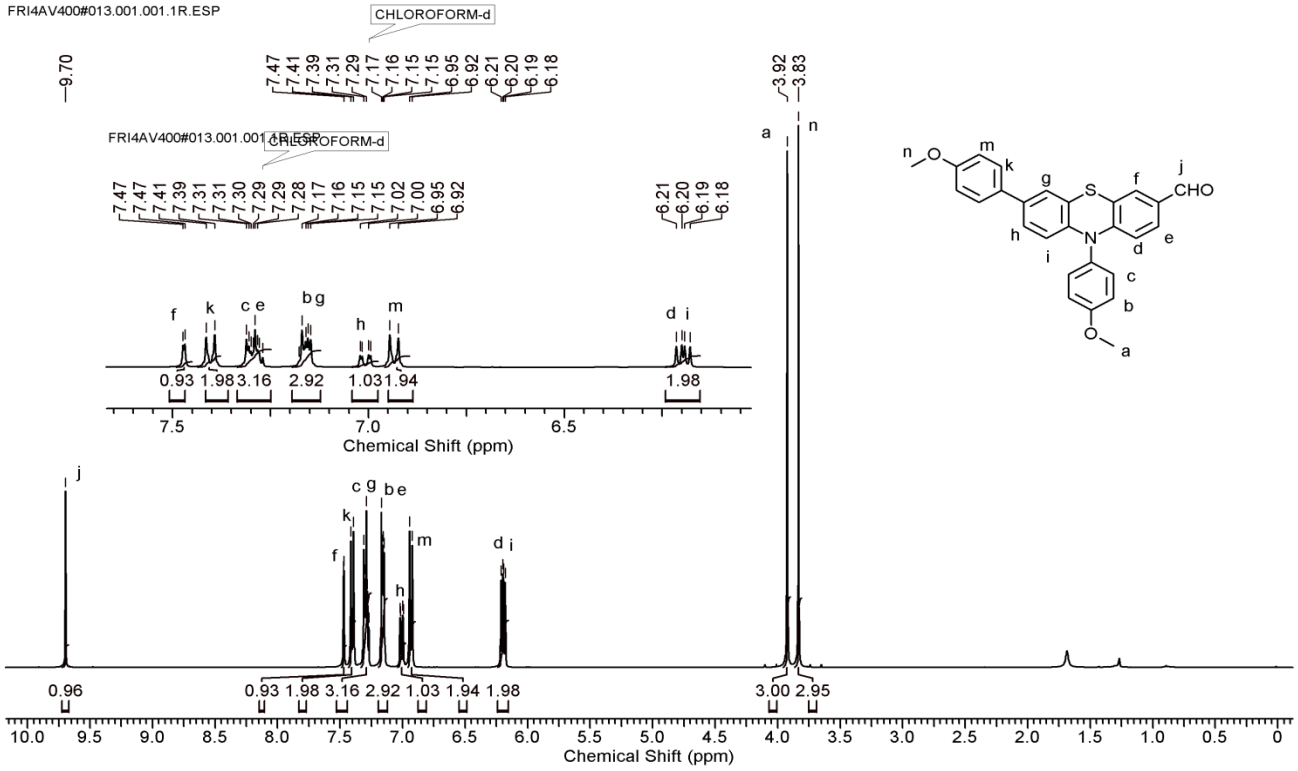

Figure S 5.11: ^{1}H NMR spectrum (in $CDCl_3$) of 7, 10-bis (4-methoxyphenyl)-10H-phenothiazine-3-carbaldehyde (**6**)

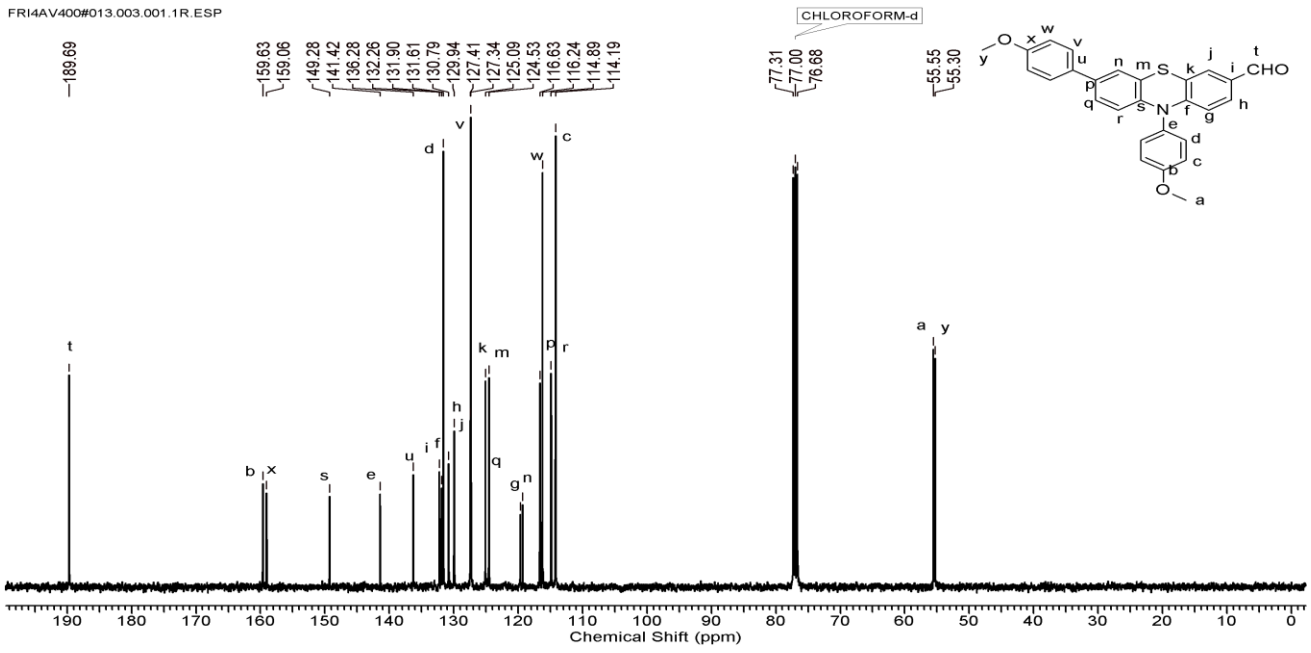

Figure S 5.12: ^{13}C NMR spectrum (in $CDCl_3$) of 7, 10-bis (4-methoxyphenyl)-10H-phenothiazine-3- carbaldehyde (**6**)

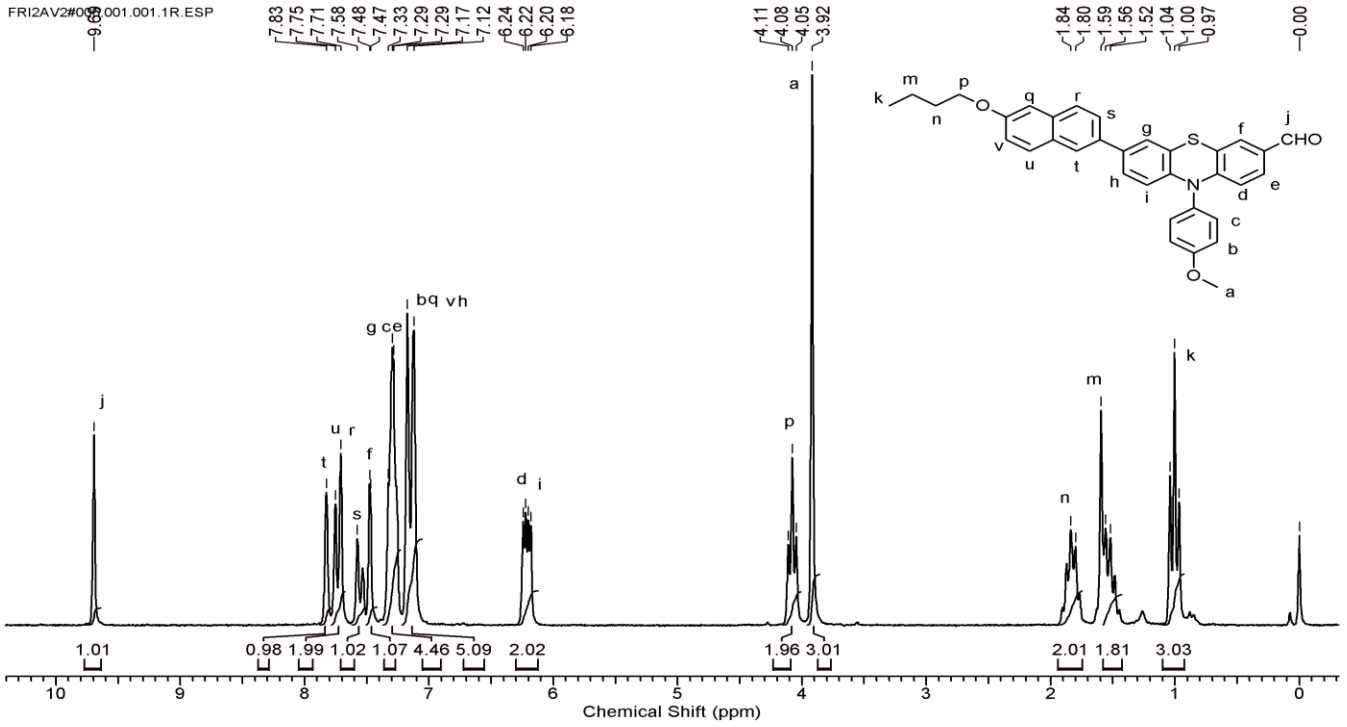

Figure S 5.13: ^{1}H NMR spectrum (in $CDCl_3$) of 7-(6-butoxynaphthalen-2-yl)-10-(4-methoxyphenyl)-10H-phenothiazine-3-carbaldehyde (**7**)

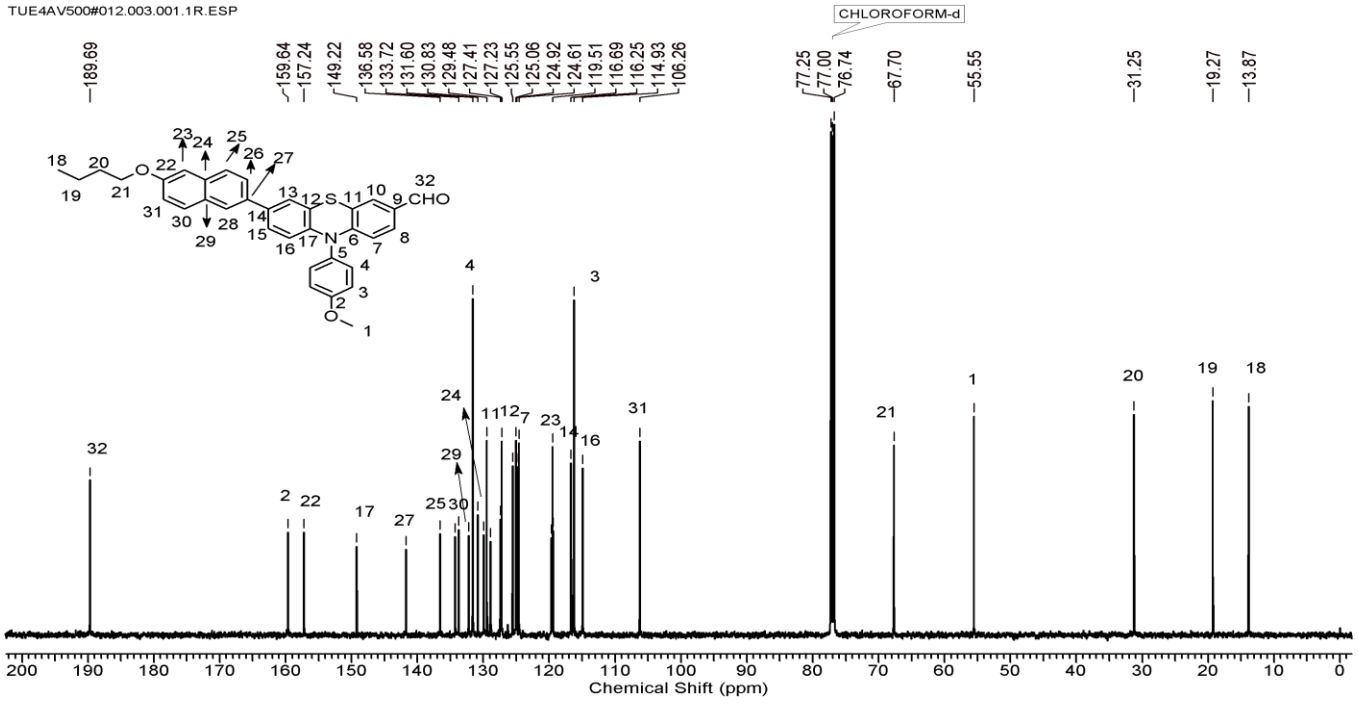

Figure S 5.14: ^{13}C NMR spectrum (in $CDCl_3$) of 7-(6-butoxynaphthalen-2-yl)-10-(4-methoxyphenyl)-10H-phenothiazine-3-carbaldehyde (**7**)

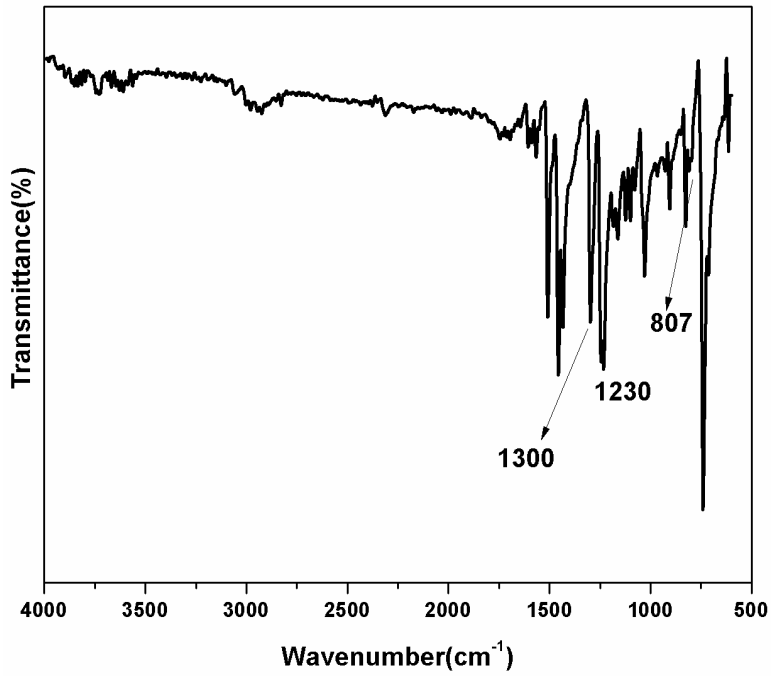

Figure S 5.15: IR spectrum of 10-(4-methoxyphenyl)-10H-phenothiazine (**1**)

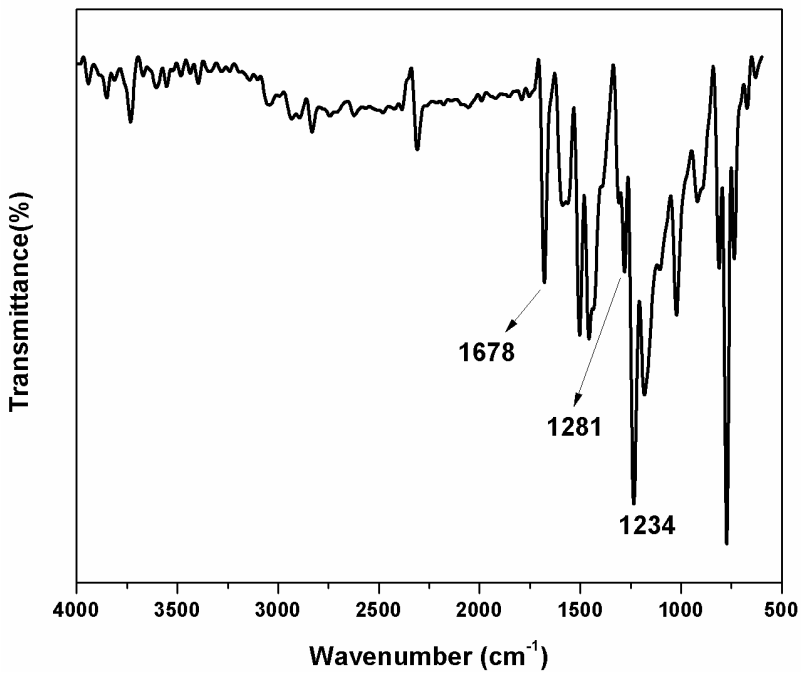

Figure S 5.16: IR spectrum of 10-(4-methoxyphenyl)-10H-phenothiazine-3-carbaldehyde **(2)**

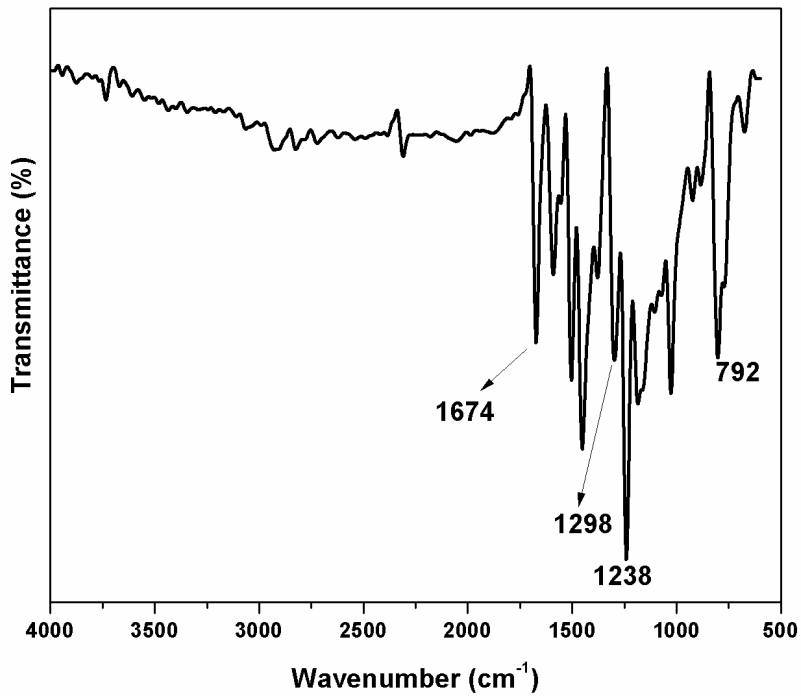

Figure S 5.17: IR spectrum of 7-bromo-10-(4-methoxyphenyl)-10H-phenothiazine-3-carbaldehyde **(3)**

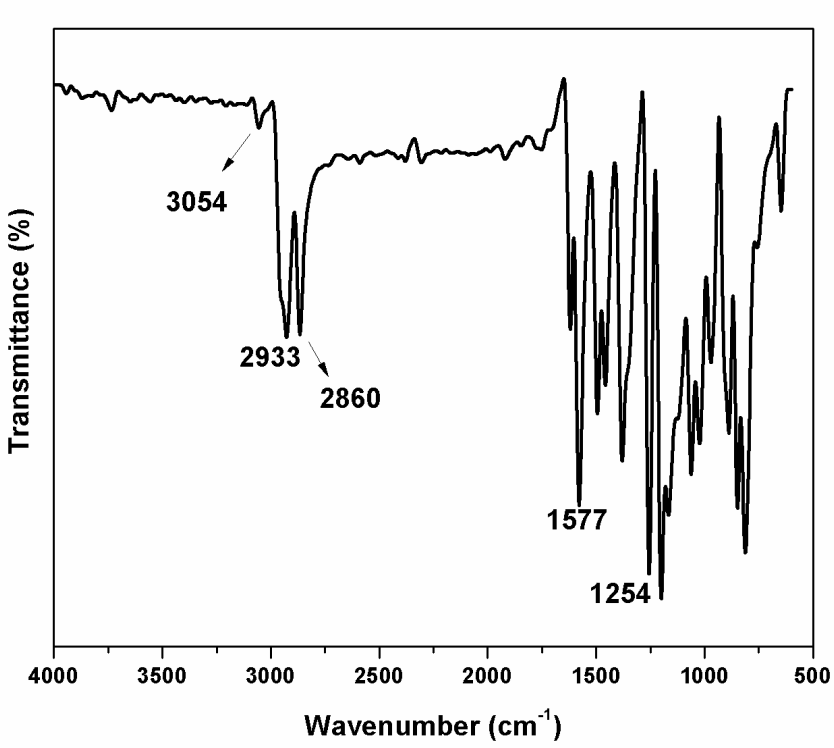

Figure S 5.18: IR spectrum of 2-bromo-6-butoxynaphthalene **(4)**

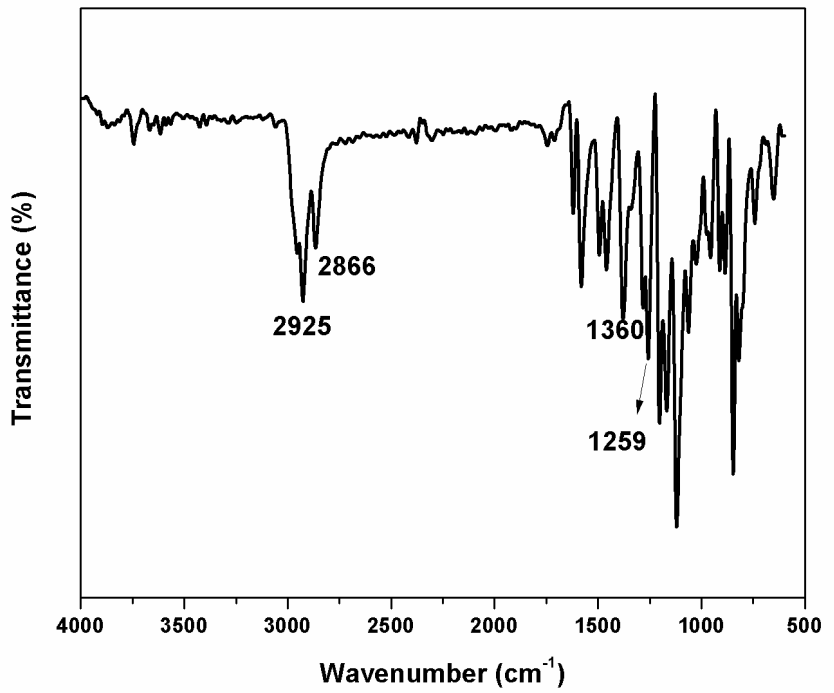

Figure S 5.19: IR spectrum of 2-(6-butoxynaphthalen-2-yl)-4,4,5,5-tetramethyl-1,3,2-dioxaborolane **(5)**

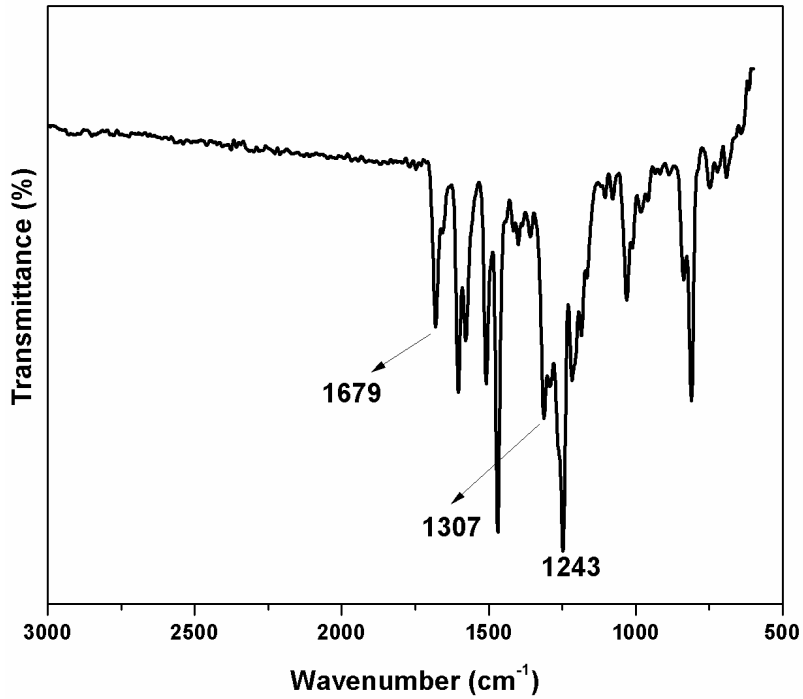

Figure S 5.20: IR spectrum of 7, 10-bis (4-methoxyphenyl)-10H-phenothiazine-3-carbaldehyde **(6)**.

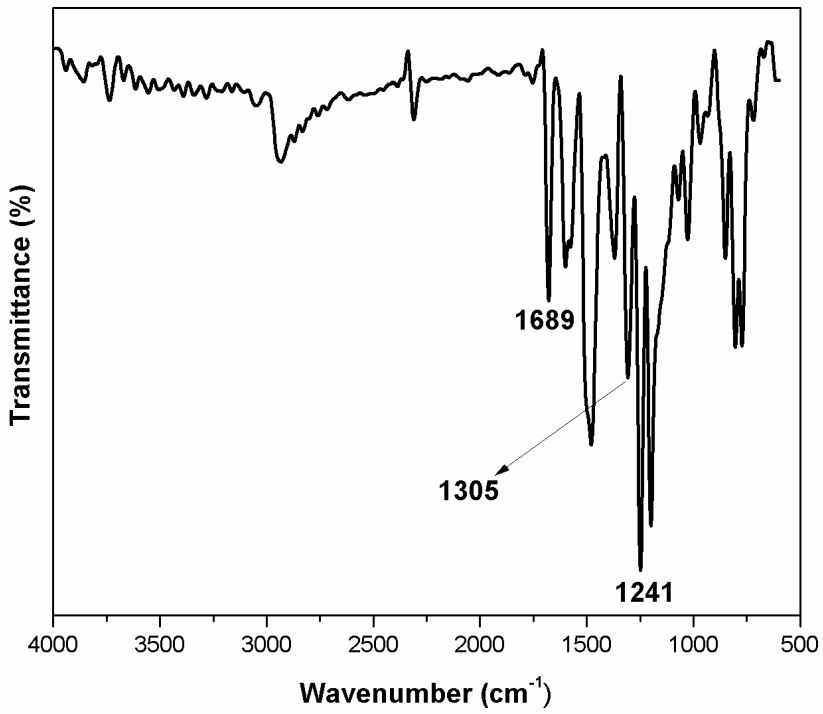

Figure S 5.21: IR spectrum of 7-(6-butoxynaphthalen-2-yl)-10-(4-methoxyphenyl)-10H-phenothiazine-3carbaldehyde (**7**)

Table S 5.1. Selected parameters for the vertical excitation of compounds **O-1**, **O-2** and **O-3(Me)** (only transitions with *f*> 0.1 are presented). Electronic excitation energies (eV), oscillator strengths (*f*) and configurations of the 6 low-lying excited states. Calculated by TDDFT//PBE1PBE/6-31G(d,p), based on the optimized ground state geometries (chloroform was employed as solvent in every calculations).

		TDDFT//PBE1PBE/6-31G(d,p)			
Compound	**Electronic Transition**[a]	**Excitation Energy**	***f***[b]	**Composition**[c]	**CI**[d]
O-1	$S_0 \rightarrow S_1$	2.51 eV (494 nm)	0.4296	H→ L	0.69897 (98 %)
	$S_0 \rightarrow S_3$	3.57 eV (348 nm)	0.4483	H−2→ L	0.67071 (90 %)
				H→ L+1	0.16637 (6 %)
	$S_0 \rightarrow S_4$	3.91 eV (317 nm)	0.3605	H→ L+1	0.65235 (85 %)
				H−2→ L	0.16726 (6 %)
				H→ L+3	0.13919 (4 %)
	$S_0 \rightarrow S_5$	4.24 eV (293 nm)	0.1968	H−3→ L	0.64701 (84 %)
				H→ L+2	0.22166 (10 %)
				H→ L+4	0.10537 (2 %)
O-2	$S_0 \rightarrow S_1$	2.39 eV (518 nm)	0.5523	H→ L	0.69641 (97 %)
	$S_0 \rightarrow S_4$	3.62 eV (342 nm)	0.3657	H−3→ L	0.57008 (65 %)
				H→ L+1	0.35145 (25 %)
				H−1→ L	0.16840 (6 %)
	$S_0 \rightarrow S_5$	3.82 eV (325 nm)	0.4415	H→ L+1	0.54958 (60 %)

				H−3→ L	0.35183 (25 %)
				H→ L+2	0.15250 (5 %)
				H−1→ L	0.10189 (2 %)
				H−1→ L+1	0.10135 (2 %)
	$S_0 \rightarrow S_6$	4.06 eV (305 nm)	0.2992	H→ L+3	0.61455 (76 %)
				H→ L+4	0.22405 (10 %)
				H→ L+2	0.14733 (4 %)
O-3(Me)	$S_0 \rightarrow S_1$	2.34 eV (520 nm)	0.5904	H→ L	0.68775 (94 %)
				H−1→ L	0.13211 (3 %)
	$S_0 \rightarrow S_3$	3.52 eV (352 nm)	0.3264	H−2→ L	0.47201 (45 %)
				H→ L+1	0.30403 (18 %)
				H−4→ L	0.28544 (16 %)
				H−3→ L	0.25604 (13 %)
				H→ L+2	0.13067 (3 %)
	$S_0 \rightarrow S_4$	3.55 eV (350 nm)	0.1908	H−2→ L	0.51881 (54 %)
				H−3→ L	0.29695 (18 %)
				H→ L+1	0.28020 (16 %)
				H−4→ L	0.20877 (9 %)
				H→ L+2	0.10212 (2 %)
	$S_0 \rightarrow S_5$	3.66 eV (339 nm)	0.1475	H→ L+1	0.53458 (57 %)
				H−3→ L	0.33839 (23 %)
				H−4→ L	0.26222 (14 %)
				H−1→ L	0.10157 (2 %)

[a] Only excited states with *f*>0.100 were considered. [b]Oscillator strength [c] H stands for HOMO and L stands for LUMO [d] Absolute CI coefficient of the wavefunction for each excitation. In parenthesis are indicated the percentage contribution of the configuration to excitation.

Table S5.2: Atomic coordinates for all the optimized species **O-1, O-2** and **O-3**

DFT-PBE1PBE/6-31G for ground state geometries

O-1

6	2.936421	-1.015454	0.805806
6	1.926595	-1.983083	0.973942
6	0.718709	-1.872942	0.317370
6	0.448309	-0.801959	-0.558518
6	1.480844	0.139102	-0.776542
6	2.673845	0.045488	-0.087063
7	-0.782368	-0.682440	-1.186531
6	-1.280289	0.560483	-1.650461
6	-0.413660	1.606778	-2.004461
16	1.332805	1.342232	-2.062057
6	-2.658101	0.780703	-1.759994
6	-3.153179	2.003008	-2.204395
6	-2.288115	3.041961	-2.525977
6	-0.916088	2.839439	-2.413420
1	2.072298	-2.830575	1.632804
1	-0.038102	-2.629458	0.483051
1	3.442096	0.795217	-0.258847
1	-3.350371	-0.011579	-1.502221
1	-4.227602	2.136855	-2.287214
1	-0.221050	3.635900	-2.663948
6	4.215328	-1.016469	1.453530
6	4.764093	-1.877957	2.369466
1	4.865161	-0.189478	1.175214
6	4.126982	-3.033366	2.904985
7	3.624876	-3.980879	3.355013
6	6.082799	-1.631015	2.853930
7	7.157654	-1.430840	3.249435
6	-1.803688	-2.691713	-2.117363
6	-1.710202	-1.773676	-1.078600
6	-2.518859	-1.921312	0.053144
6	-3.408663	-2.978308	0.136591
6	-3.505362	-3.904324	-0.912396
6	-2.696797	-3.758920	-2.043681
8	-4.403445	-4.895831	-0.735415
1	-2.751668	-4.464233	-2.865119
1	-1.172302	-2.571954	-2.992992
1	-2.445836	-1.203610	0.865259
1	-4.042632	-3.108477	1.008071
6	-4.542276	-5.860552	-1.763724
1	-5.309269	-6.556965	-1.421699
1	-4.867572	-5.401441	-2.704748
1	-3.607744	-6.409612	-1.929118
1	-2.669576	4.000259	-2.864106

O-2

6	2.825910	-0.749732	0.644215
6	1.926082	-1.808216	0.878333
6	0.685037	-1.833618	0.277437
6	0.268013	-0.814391	-0.603636
6	1.192592	0.216741	-0.891292
6	2.417762	0.257633	-0.256141
7	-0.995556	-0.832379	-1.171077
6	-1.623584	0.331453	-1.675364
6	-0.881309	1.440684	-2.107833
16	0.881348	1.363345	-2.198536
6	-3.017856	0.416617	-1.754045
6	-3.642622	1.554191	-2.248829
6	-2.908845	2.672434	-2.658924
6	-1.513720	2.592218	-2.561071
1	2.186689	-2.621372	1.545081
1	0.015723	-2.657276	0.492182
1	3.099194	1.074160	-0.480554
1	-3.625561	-0.425065	-1.443664
1	-4.725641	1.557688	-2.327371
1	-0.901454	3.443815	-2.844210
6	4.125929	-0.606598	1.230237
6	4.800955	-1.382549	2.138791
1	4.676391	0.272623	0.901405
6	4.310249	-2.579570	2.733797
7	3.928889	-3.558818	3.232032
6	6.108596	-0.989642	2.551585
7	7.175049	-0.670569	2.887417
6	-1.885387	-2.941057	-2.011117
6	-1.811041	-2.000976	-0.990607
6	-2.533828	-2.198342	0.190114
6	-3.314947	-3.331069	0.343168
6	-3.391448	-4.280443	-0.686334
6	-2.673543	-4.081286	-1.869476
8	-4.180684	-5.347007	-0.440636
1	-2.717297	-4.801678	-2.678303
1	-1.322409	-2.780626	-2.926019
1	-2.478006	-1.461263	0.986093
1	-3.879902	-3.502141	1.254184
6	-4.306752	-6.330329	-1.452823
1	-4.981854	-7.088363	-1.052820
1	-4.740015	-5.911745	-2.368928
1	-3.341617	-6.795858	-1.685074
6	-2.968652	4.662316	-4.182195
6	-3.568337	3.885097	-3.185288

6	-4.823777	4.298813	-2.707945
6	-5.445570	5.431187	-3.205427
6	-4.829069	6.195889	-4.204086
6	-3.579705	5.804593	-4.692079
8	-5.514798	7.282517	-4.626597
1	-3.081843	6.370653	-5.471358
1	-2.009807	4.360550	-4.594879
1	-5.312329	3.736310	-1.917115
1	-6.411676	5.750676	-2.825995
6	-4.926917	8.089300	-5.630331
1	-5.631740	8.901586	-5.815351
1	-3.971000	8.512675	-5.299046
1	-4.773311	7.529215	-6.560697

O-3(Me)

6	2.998071	-5.662209	6.368868
6	2.081092	-6.695072	6.646563
6	0.856216	-6.748635	6.014995
6	0.475688	-5.786555	5.057287
6	1.416055	-4.781810	4.731656
6	2.624298	-4.710067	5.396368
7	-0.770628	-5.832312	4.452702
6	-1.377411	-4.693952	3.872061
6	-0.615751	-3.616189	3.395952
16	1.147685	-3.718019	3.346778
6	-2.769111	-4.603890	3.757324
6	-3.372746	-3.490183	3.189039
6	-2.620182	-2.400794	2.737553
6	-1.227929	-2.486716	2.865438
1	2.313793	-7.463379	7.373987
1	0.172358	-7.550496	6.263805
1	3.319286	-3.914776	5.139626
1	-3.390206	-5.423749	4.098039
1	-4.453402	-3.481765	3.083934
1	-0.601716	-1.658400	2.546344
6	4.285942	-5.496226	6.976158
6	4.940922	-6.234927	7.929165
1	4.845710	-4.632937	6.621842
6	4.440222	-7.410791	8.557516
7	4.050734	-8.372986	9.081929
6	6.239833	-5.825143	8.353346
7	7.299057	-5.492581	8.698712
6	-1.661551	-7.967338	3.686135
6	-1.598881	-6.985965	4.667847
6	-2.354587	-7.122678	5.836553
6	-3.156537	-8.236745	6.016729
6	-3.222507	-9.226881	5.025633
6	-2.470346	-9.089144	3.855004
8	-4.037414	-10.268823	5.292609
1	-2.503678	-9.842719	3.076367
1	-1.074701	-7.852411	2.779443
1	-2.309638	-6.352431	6.601330
1	-3.747547	-8.360764	6.918795
6	-4.161476	-11.284636	4.312794
1	-4.869225	-12.009065	4.718648
1	-4.555176	-10.888147	3.369484
1	-3.203471	-11.784892	4.127941
6	-2.614214	-0.490404	1.095048
6	-3.260447	-1.209746	2.141444
6	-4.495579	-0.766738	2.575311
6	-5.120734	0.366418	2.002867
6	-4.463835	1.077658	0.952030
6	-3.193217	0.610807	0.521170
6	-5.088476	2.202913	0.377244
1	-2.686621	1.136155	-0.284476
1	-1.653623	-0.839515	0.726562
1	-5.003898	-1.277930	3.389435
6	-6.384541	0.831278	2.438960
6	-6.327064	2.626729	0.821004
6	-6.981100	1.930587	1.868575
1	-6.891482	0.301144	3.241406
1	-4.599132	2.748809	-0.424531
8	-6.848697	3.714526	0.206200
6	-8.128544	4.168205	0.606692
1	-7.951201	2.258176	2.225148
1	-8.349617	5.031732	-0.023101
1	-8.138801	4.481772	1.657294
1	-8.899312	3.404617	0.446419

Chapter-6

Summary, Conclusions and Future Perspectives

6.1) Summary and conclusions

The emergence of organic electronics in the last century has brought a revolution in the field of electronics technology. With its widening applications in different areas such as energy generation (OPVs), energy storage (batteries) displays and lightning (OLEDs), actuators, sensors (biosensors/ chemosensors), etc. and its ability to compete with the conventional inorganic electronics technology, there is high urge for the development of new organic semiconducting materials with tuned properties to enhance the optoelectronic applications. In line with such requirements, overall objective of the present work was to design and synthesize solution processable small organic molecules and evaluate their applications in the field of organic electronics.

In the first working chapter, a pyrene-based 1,3,6,8- tetrasubstituted small molecule containing carbazole moiety attached through alkyl spacer, namely, 1,3,6,8-tetrakis(4-((5-(9H-carbazol-9-yl) pentyl)oxy)phenyl)pyrene (**PY-II**) was synthesized and characterized by FT-IR, ^{1}H, ^{13}C NMR and MALDI-TOF spectroscopy. With 5% weight loss at 435 ^{o}C, **PY-II** exhibited good thermal stability. **PY-II** exhibited absorption over the wide range 275 nm to 500 nm with optical band gap of 2.76 eV making it a wide band gap blue light emitting material. Fluorescence emission of **PY-II** was observed at 434 nm and 450 nm in solution and solid state, respectively. Photoluminescence quantum yield (PLQY) of 0.9 in solution and 0.33 in solid state was obtained. Time resolved PL decay measurements were carried out both in solution and as a thin film to understand the lower value of PLQY in solid state. **PY-II** exhibited lower HOMO value of -5.71 eV (PESA study) which was attributed to the presence of non conjugated aliphatic linker in the molecule. Non-doped OLED device was fabricated by solution processing of **PY-II** as an emissive layer and device performance was evaluated. OLED device showed turn-on voltage of 4.5 V, current efficiency of 0.41 cdA^{-1}, power efficiency of 0.17 lmW^{-1}, CIE coordinates of (0.16, 0.16) and maximum brightness of 202 cdm^{-2}. EL spectrum of OLED device was measured over the range 5 to 11V and it was observed that device showed two emission peaks at 445 nm and 470 nm. It was observed that as the voltage was increased from 4.5 to 7 V, current efficiency reached to its maximum value (CE_{max}) of 0.45cdA^{-1}, whereas maximum power efficiency (PE_{max}) of 0.17 lmW^{-1} was observed at 8.5 V. When the voltage was increased beyond 10V, the values of CE and PE rolled off but remained at values higher than half of CE_{max} and PE_{max}. The

results point towards use of pyrene-based material as promising blue emitting material in optoelectronic applications.

In the second working chapter, two solution processable pyrene-based small organic molecules bearing carbazole and phenothiazine substituents appended at 1,3,6,8 positions on pyrene core were synthesized. The small molecules namely, 1,3,6,8-tetrakis(9-(4-methoxyphenyl)-9H-carbazol-3yl)pyrene (**PY-CA**) and 1,3,6,8-tetrakis(10-(4-methoxyphenyl)-10Hphenothiazin-3-yl)pyrene (**PY-PH**) were evaluated as blue and green emitters, respectively. UV-vis absorption of **PY-CA** and **PY-PH** over the range 300 -500 nm showed the wide band gap nature of organic materials with an optical band gap of 2.67 eV and 2.50 eV for **PY-CA** and **PY-PH**, respectively. In UV-vis absorption spectroscopy **PY-CA** and **PY-PH** exhibited absorption maxima (in solution) at 400 nm and 430 nm, respectively. Higher value of λ_{max} for **PY-PH** was attributed to the more extended conjugation length in phenothiazine compared to carbazole. Absorption spectra of **PY-CA** and **PY-PH** in solid state exhibited peaks (λ_{max}) at 425 nm and 450 nm, respectively. Photoluminescence peaks for **PY-CA** and **PY-PH** in solution state were observed at 450 nm and 500 nm, respectively whereas PL peaks in solid state for **PY-CA** and **PY-PH** were observed at 485 nm and 520 nm, respectively. The red shifted values in solid state were attributed to the intermolecular π-π interactions. The HOMO energy levels in **PY-CA** and **PY-PH** determined by PESA were found to be 5.48 eV and 5.40 eV, respectively. The lower HOMO levels were significant for the fabrication of air stable organic electronic devices. OLEDs were fabricated by solution processing of **PY-CA** and **PY-PH** as emissive layer and the device performance was evaluated. For **PY-CA** and **PY-PH**-based devices, the turn-on voltage of 3.3V and 3.8 V , current efficiency of 1.6 cdA^{-1} and 1.1 cdA^{-1}, power efficiency of 1.5 lmW^{-1} and 0.5 lmW^{-1} were observed, respectively. The CIE coordinates of (0.19, 0.42) and (0.37, 0.59), maximum brightness of 2500 cdm^{-2} and 2116 cdm^{-2} and electroluminescent peaks of 493 nm and 543 nm were exhibited by **PY-CA** and **PY-PH** devices, respectively. The results obtained for **PY-CA** and **PY-PH** devices indicated pyrene-based materials as the promising ones for applications in organic electronic devices and their properties can be tuned by structural modification of pyrene-based small organic molecules.

In the third working chapter, a series of phenothiazine-based donor-acceptor type molecules bearing substituents at C-7 position on phenothiazine ring were synthesized. Phenothiazine derivatives, namely, 2-((10-(4-methoxyphenyl)-10H-phenothiazin-3-yl) methylene)

malononitrile (**O-1**), 2-((7,10-bis(4-methoxyphenyl)-10H-phenothiazin-3-yl) methylene) malononitrile(**O-2**) and 2-((7-(6-butoxynaphthalen-2-yl)-10-(4-methoxyphenyl)-10Hphenothiazin-3-yl) methylene) malononitrile (**O-3**) were characterized by FT-IR, ^{1}H, ^{13}C NMR spectroscopy and HRMS. **O-1**, **O-2** and **O-3** exhibited good thermal stability with 5% weight loss at 302 ºC, 386 ºC and 404 ºC, respectively. UV-vis absorption spectra of phenothiazine-based small molecules exhibited two bands in the region 320-330 nm and 490-510 nm. The bands in the former region were observed due to π-π* transition of chromophore while bands observed in the latter region were attributed to the intramolecular charge transfer (ICT). **O-1**, **O-2** and **O-3** exhibited λ_{max} at 490 nm, 507 nm and 509 nm, respectively in the solution. In the solid state red shifted λ_{max} was observed at 500 nm, 518 nm and 521 nm for **O-1**, **O-2** and **O-3**, respectively. The observed red shift in solid state was attributed to the intermolecular interactions. The optical band gap was found to be in the range 2.0 eV-2.06 eV. The HOMO energy levels of molecules were determined by differential pulse voltammetry (DPV) method and were found to be -5.29 eV, -5.24 eV and -5.24 eV for **O-1**, **O-2** and **O-3**, respectively. This showed that introduction of substituent at C-7 position on phenothiazine raised the HOMO level (**O-1** to **O-2**) but no effect on HOMO level was observed for change of substituent at C-7 position (**O-2** to **O-3**). The hole mobility characteristics of phenothiazine-based molecules were evaluated by impedance spectroscopy and the hole only devices were fabricated by spin coating and the hole mobility values observed were of the order of 10^{-3} cm^2 $V^{-1}S^{-1}$ for **O-1** based device, whereas hole mobility values in the order of 10^{-6} cm^2 $V^{-1}S^{-1}$ were found for **O-2** and **O-3** based devices. To understand the difference in mobility values, XRD study of **O-1**, **O-2** and **O-3** was performed both for coated films as well as powder samples. It was observed that **O-1** exhibited crystalline nature in film as well as in powder sample. However, **O-2** and **O-3** exhibited amorphous behavior in the films. This phenomenon of crystallization observed in the film of **O-1** could be attributed as the reason behind high charge carrier mobility for **O-1** as compared to **O-2** and **O-3**.

5.2) Future perspectives

The work covered in the thesis was primarily focused on design and synthesis of solution processable small organic molecules for applications in the field of organic electronics. This work has opened many possibilities for the future work.

- The high brightness along with high photoluminescence quantum yield (PLQY) in solution are important requirements for different applications such as bioimaging and sensors. **PY-II** with high PLQY in solution is, therefore, a potential candidate to serve in these applications.
- The introduction of bulky groups on pyrene helps to reduce π-π interactions and excimer formation. Hence, it will be worthwhile to append higher generations of carbazole dendrons on pyrene core in **PY-II** and study their effects on the optical properties and OLED device performance of modified molecules.
- It would be interesting to replace carbazole moieties appended on pyrene core in **PY-II** molecule with other chromophores such as fluorene, phenothiazine, etc. and study their effects on optoelectronic properties of modified molecules.
- There is a scope to study effects of systematic variations in alkyl chain length of spacer in **PY-II** on film forming properties and isolation effect.
- It would be worthwhile to introduce single, double and triple bonds between pyrene core and appended substituents in **PY-CA** and **PY-PH** and study their effects on OLED performance.
- The higher charge carrier mobility value demonstrated by **O-1** qualifies it to be a potentially useful candidate in OFET devices.

List of Publications

1. Nitin G. Valsange, F. L. Wong, **Durgaprasad Shinde**, C. S. Lee, V. A. L. Roy, Sergei Manzhos, K. Feron, Samuel Chang, Ryuzi Katoh, Prashant Sonar and Prakash P. Wadgaonkar, "A new pyrene cored small organic molecule with a flexible alkyl spacer: a potential solution processable blue emitter with bright photoluminescence"
   New J. Chem., **2017**,41, 11383.

2. Jagadish K. Salunke, F. L. Wong, Krishna Feron, Sergei Manzhos, Ming Fai Lo, **Durgaprasad Shinde**, Abhijeet Patil, C. S. Lee, V. A. L. Roy, Prashant Sonar and Prakash P. Wadgaonkar, "Phenothiazine and carbazole substituted pyrene-based electroluminescent organic semiconductors for OLED devices"
   J.Mater. Chem. C, **2016**, 4, 1009.

3. **D. B. Shinde**, Jagadish K. Salunke, Nuno R. Candeias, Francesca Tinti,Massimo Gazzano, Prakash P. Wadgaonkar, Arri Priimagi, Nadia Camaioni and Paola Vivo **,** "Crystallisation-enhanced bulk hole mobility in phenothiazine-based organic semiconductors"
   Sci. Reports, 2017, 7, 46268.